

# Reversible physical network stabilised nematics : soft solids for new liquid crystal displays

**Citation for published version (APA):**

Boxtel, van, M. C. W. (2002). *Reversible physical network stabilised nematics : soft solids for new liquid crystal displays*. [Phd Thesis 1 (Research TU/e / Graduation TU/e), Chemical Engineering and Chemistry]. Technische Universiteit Eindhoven. <https://doi.org/10.6100/IR552211>

**DOI:**

[10.6100/IR552211](https://doi.org/10.6100/IR552211)

**Document status and date:**

Published: 01/01/2002

**Document Version:**

Publisher's PDF, also known as Version of Record (includes final page, issue and volume numbers)

**Please check the document version of this publication:**

- A submitted manuscript is the version of the article upon submission and before peer-review. There can be important differences between the submitted version and the official published version of record. People interested in the research are advised to contact the author for the final version of the publication, or visit the DOI to the publisher's website.
- The final author version and the galley proof are versions of the publication after peer review.
- The final published version features the final layout of the paper including the volume, issue and page numbers.

[Link to publication](#)

**General rights**

Copyright and moral rights for the publications made accessible in the public portal are retained by the authors and/or other copyright owners and it is a condition of accessing publications that users recognise and abide by the legal requirements associated with these rights.

- Users may download and print one copy of any publication from the public portal for the purpose of private study or research.
- You may not further distribute the material or use it for any profit-making activity or commercial gain
- You may freely distribute the URL identifying the publication in the public portal.

If the publication is distributed under the terms of Article 25fa of the Dutch Copyright Act, indicated by the "Taverne" license above, please follow below link for the End User Agreement:

[www.tue.nl/taverne](http://www.tue.nl/taverne)

**Take down policy**

If you believe that this document breaches copyright please contact us at:

[openaccess@tue.nl](mailto:openaccess@tue.nl)

providing details and we will investigate your claim.

# **Reversible Physical Network Stabilised Nematics**

Soft Solids for New Liquid Crystal Displays

**CIP-DATA LIBRARY TECHNISCHE UNIVERSITEIT EINDHOVEN**

Boxtel, Marysia C.W. van

Reversible physical network stabilised nematics : soft solids for new liquid crystal displays / by Marysia C.W. van Boxtel. - Eindhoven : Technische Universiteit Eindhoven, 2002.

Proefschrift. - ISBN 90-386-2723-8

NUGI 813

Trefwoorden: vloeibare kristallen / vloeibare kristalschermen ; LCD's / elektro-optische schakelaars / polymeren ; reologie / dendrimeren / dispersies / colloïden

Subject headings: liquid crystals / liquid crystal displays ; LCD's / electro-optical switches / polymers ; rheology / dendrimers / dispersions / colloids

An electronic copy of this thesis is available on the web site of the Eindhoven University of Technology in PDF-format (<http://www.tue.nl/bib>)

© 2002, M.C.W. van Boxtel

Cover design: Marysia van Boxtel, Paul Verspaget

Printed by University Press Facilities, Eindhoven, The Netherlands

# **Reversible Physical Network Stabilised Nematics**

Soft Solids for New Liquid Crystal Displays

PROEFSCHRIFT

ter verkrijging van de graad van doctor aan de Technische  
Universiteit Eindhoven, op gezag van de Rector Magnificus,  
prof.dr. R.A. van Santen, voor een commissie aangewezen door  
het College voor Promoties in het openbaar te verdedigen  
op woensdag 13 februari 2002 om 16.00 uur

door

**Marysia Cornelia Wilhelmina van Boxtel**

geboren te Sint-Oedenrode

Dit proefschrift is goedgekeurd door de promotoren:

prof.dr.ing. D.J. Broer

en

prof.dr. P.J. Lemstra

Copromotor:

dr.ing. C.W.M. Bastiaansen

The research described in this thesis was financially supported by the Netherlands Organisation for Scientific Research (NWO).

# Contents

## Chapter 1 Introduction

1.1	Displays operating on linearly polarised light.....	1
1.2	Light-scattering electro-optical switches .....	2
1.2.1	Polymer dispersed liquid crystal displays.....	3
1.2.2	Anisotropic gels .....	5
1.2.3	Silica filled nematics .....	6
1.2.4	Thermoreversible gels.....	6
1.3	Challenges in the field of liquid crystal displays .....	7
1.4	Aims of the thesis.....	8
1.5	Scope of the thesis.....	10
1.6	References .....	11

## Chapter 2 Synthesis of polymer colloids

2.1	Introduction .....	13
2.2	Experimental .....	14
2.2.1	Materials.....	14
2.2.2	Dispersion polymerisation .....	15
2.2.3	Emulsion polymerisation .....	16
2.2.4	Techniques .....	17
2.3	Results and discussion.....	19
2.3.1	The homopolymerisation reaction of methyl methacrylate .....	20
2.3.2	The homopolymerisation reaction of divinylbenzene.....	22
2.3.3	The copolymerisation reaction of methyl methacrylate and divinylbenzene....	23
2.3.4	Effect of polymerisation parameters on particle size and conversion.....	26
2.3.5	Examples of the particle morphology .....	30
2.3.6	Emulsion polymerisation .....	32
2.4	Conclusions .....	32
2.5	References .....	33

## Chapter 3 Colloidal dispersions in a liquid crystal

### Phase behaviour, morphology and rheological properties

3.1	Introduction .....	35
3.2	Theoretical background.....	36
3.3	Experimental .....	40

3.3.1	Materials.....	40
3.3.2	Preparation of the LC colloidal dispersions.....	40
3.3.3	Electro-optical cell construction .....	41
3.3.4	Techniques .....	42
3.4	Results and discussion.....	44
3.4.1	Phase behaviour .....	44
3.4.2	Morphology formation.....	48
3.4.3	Influence of colloid concentration on morphology.....	51
3.4.4	Influence of colloid size on morphology .....	52
3.4.5	Thermal stability .....	54
3.4.6	Rheological properties .....	55
3.5	Conclusions .....	58
3.6	References .....	58

## **Chapter 4 Colloidal dispersions in a liquid crystal**

### **Dielectric and electro-optical properties**

4.1	Introduction.....	61
4.2	Experimental .....	62
4.2.1	Materials and sample preparation .....	62
4.2.2	Techniques .....	62
4.3	Results and discussion.....	64
4.3.1	Determination of the director order parameter.....	64
4.3.2	The interlayer model .....	67
4.3.3	Quasi-static field-induced changes of the director order .....	69
4.3.4	Temperature- and time-dependent orientational order.....	72
4.3.5	Electro-optical properties of the LC colloidal dispersions in TN displays .....	76
4.3.5.1	Transmittance-voltage characteristics.....	76
4.3.5.2	Switching kinetics.....	78
4.3.6	Electro-optical properties of the LC colloidal dispersions for light-scattering electro-optical switches.....	81
4.3.6.1	Transmittance-voltage characteristics.....	81
4.3.6.2	Switching kinetics.....	83
4.4	Conclusions .....	84
4.5	References .....	85

## **Chapter 5 Dendrimer filled nematics**

5.1	Introduction.....	87
5.2	Experimental .....	88

5.2.1	Materials.....	88
5.2.2	Preparation of the dendrimer filled nematics.....	89
5.2.3	Electro-optical cell construction.....	89
5.2.4	Techniques.....	90
5.3	Results and discussion.....	91
5.3.1	Phase behaviour.....	91
5.3.2	Morphology.....	93
5.3.3	Rheological properties.....	94
5.3.4	Dielectric behaviour.....	95
5.3.5	Electro-optical properties of the dendrimer filled nematics for light-scattering electro-optical switches.....	99
5.3.5.1	Transmittance-voltage characteristics.....	99
5.3.5.2	Switching kinetics.....	101
5.4	Conclusions.....	103
5.5	References.....	103

## **Chapter 6 Anisotropic thermoreversible gels**

6.1	Introduction.....	105
6.2	Experimental.....	106
6.2.1	Materials.....	106
6.2.2	Preparation of the thermoreversible gels.....	106
6.2.3	Electro-optical cell construction.....	106
6.2.4	Techniques.....	106
6.3	Results and discussion.....	107
6.3.1	Phase behaviour.....	107
6.3.2	Morphology.....	110
6.3.3	Dynamic mechanical properties.....	112
6.3.4	Electro-optical properties of the thermoreversible gels for light-scattering electro-optical switches.....	114
6.3.4.1	Transmittance-voltage characteristics.....	114
6.3.4.2	Switching kinetics.....	116
6.4	Conclusions.....	117
6.5	References.....	118

## **Chapter 7 A continuous process for the production of liquid crystal displays**

7.1	Introduction.....	119
7.2	Experimental.....	121
7.2.1	Materials.....	121



7.2.2	Sample preparation .....	121
7.2.3	Techniques .....	121
7.3	Results and discussion.....	122
7.3.1	Influence of processing parameters.....	122
7.4	Conclusions .....	126
7.5	References .....	126
<b>Technology assessment .....</b>		<b>127</b>
<b>Summary.....</b>		<b>131</b>
<b>Samenvatting.....</b>		<b>135</b>
<b>Dankwoord .....</b>		<b>139</b>
<b>Curriculum Vitae .....</b>		<b>141</b>

# Chapter 1

## Introduction

### 1.1 Displays operating on linearly polarised light

Flat panel displays have become essential devices in modern electronic systems, such as mobile phones and laptop computers, as a means to visualise information. In the production of flat panel displays polymers are indispensable materials because of their low density and easy processability and are nowadays used to fulfil a number of functions as integrated display components. Among the flat panel displays, especially the liquid crystal displays (LCD's)<sup>1</sup> are reputed to excel in overall performance and have found a variety of applications in both professional and private environments. The ongoing tendency to improve the performance of displays and to make displays larger, flatter, and more flexible keeps on stimulating the development of new or improved LCD approaches with respect to processing and/or properties.

In the early 1970s a flat panel LCD, based on a twisted nematic (TN) liquid crystal (LC) mode, was introduced, which became initially widely used in small area applications like digital watches, calculators and automotive displays.<sup>2</sup> This TN-LCD consists of two parallel glass substrates, each coated with a transparent electrode layer, usually indium tin oxide (ITO). On the inner side of the cell both substrates are provided with rubbed polyimide layers in order to induce unidirectional orientation of the LC molecules, which are in direct contact with the substrates. As the direction of the two orientation layers is chosen to be mutually perpendicular, the LC in the cell is forced into a 90° twist (Figure 1.1).

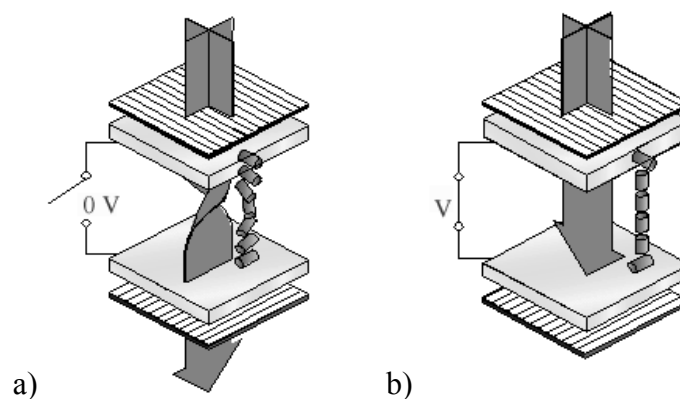


**Figure 1.1:** Schematic representation of a twisted nematic liquid crystal display (TN-LCD) in the normally white mode: (a) Transparent off-state; (b) light-blocking, dark on-state.

The exterior of the electro-optical cell is equipped with a polariser, which converts the incident light into linearly polarised light. Electrical addressing is employed to switch the polarisation direction of the propagating linearly polarised light through switching of the LC between a 90° twisted (planar) state and a vertically aligned (homeotropic) state. The switching voltages are in the order of 3-5 V ( $\sim 0.5 \text{ V}\cdot\mu\text{m}^{-1}$ ). In case of transmissive displays visual perception of this switching is generated by the presence of an analyser. In the normally white mode the polarisers are applied in a crossed manner, so that the electro-optical cell is electrically switched between a transparent off- and a dark on-state.

Since the introduction of the first TN display, tremendous research efforts were directed towards the improvement of the display performance. In order to realise high-multiplex operation for high-information content applications super twisted nematic (STN) displays were developed.<sup>3</sup> Here, the layer twist angle was increased from 90° to 180°-270° in order to achieve a critical increase of the steepness of the electro-optical curve. The use of compensation foils, which mimic the twist of the LC layer in the opposite sense, substantially reduced colouration effects and improved viewing angle characteristics, thus allowing the development of full-colour STN displays.<sup>4</sup> Alternative TN display designs with improved viewability include vertically aligned nematic (VAN),<sup>5,6</sup> in-plane switching (IPS),<sup>7</sup> and axially symmetric-aligned microcell (ASM) displays<sup>8</sup> and are switched from a perfectly oriented homeotropic or planar (dark) state to a 90° twisted (transparent) state. Via smart design of the inner surface of the display cell, multidomain pixelation is achieved in the addressed state, thus averaging optical retardation effects over all directions. Although the performance of the (S)TN displays is currently such, that they are incorporated in laptop computers, a major drawback of the TN display principle remains the required presence of the polarisers, which severely restrain the brightness and energy efficiency of these portable computer devices.

## 1.2 Light-scattering electro-optical switches

The limitations of the TN displays with respect to their performance have stimulated extensive research activities concerning the development and performance optimisation of light-scattering display devices that utilise two-phase mixtures based on an organic, low molecular weight LC phase and a polymer<sup>9-12</sup> or inorganic phase.<sup>13-15</sup> While with the TN devices the optical contrast is gained through modulation of the polarisation direction of the light, with these two-phase materials the optical contrast is gained through light scattering. In principle, this light scattering can originate from two sources. The first contribution comes from the difference in refractive index between the two phases, while the second contribution comes from the refractive index mismatches in the LC matrix itself. Due to a strong

perturbation of the LC orientation by the presence of the additional phase, the LC resembles a multidomain structure (Figure 1.2).

As the light-scattering display technique employs non-polarised light, light-scattering materials offer great potential for enhanced light-throughput in the addressed state and thus higher display brightness. As a result, the energy costs of the backlight will be significantly reduced and higher energy efficiencies can be obtained, which prolongs the lifetime of batteries in portable electronic devices.

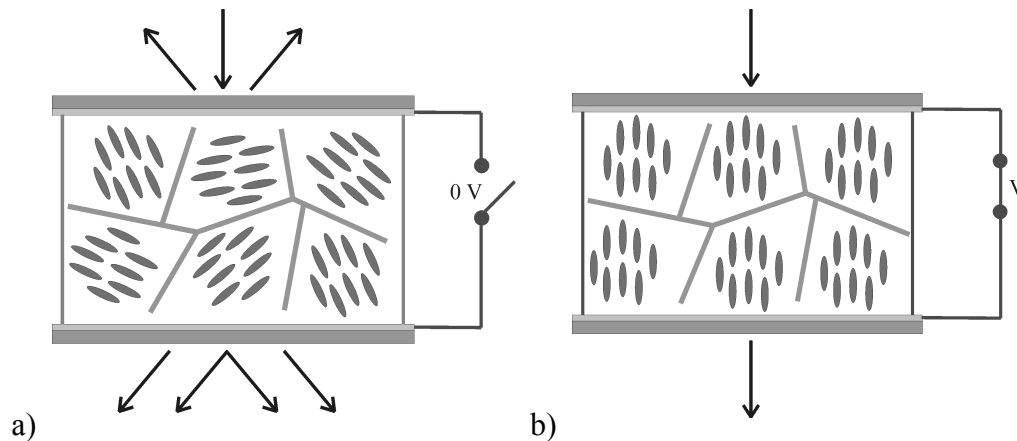


**Figure 1.2:** Schematic drawing of a light-scattering display based on a two-phase material: (a) Light-scattering off-state; (b) transparent on-state.

### 1.2.1 Polymer dispersed liquid crystal displays

Several light shutter technologies were proposed based on two-phase mixtures of LC and polymer in which the polymer forms the (co-)continuous phase.<sup>9,10,16,17</sup> For instance, in the mid 1980s the so-called polymer dispersed liquid crystal (PDLC) display was introduced, which consists of nematic LC droplets or domains with diameters in the range of 1-3  $\mu\text{m}$  embedded in a continuous polymer matrix (Figure 1.3).<sup>9,11,18,19</sup>

The refractive index of the polymer phase,  $n_p$ , is matched to the ordinary refractive index,  $n_o$ , of the liquid crystal. In the absence of an electric field, the directors of the nematic LC domains are randomly oriented with respect to each other. Consequently, the incident light is multiply scattered as it experiences a refractive index mismatch between the LC and the polymer phase and, additionally, between neighbouring LC droplets. In case the LC molecules have positive dielectric anisotropy, in the presence of an electric field they are macroscopically aligned with their director along the electric field lines, which generates a refractive index match between the two phases. As a result, the incident light propagates through the PDLC film without being scattered, and a transparent state is gained.

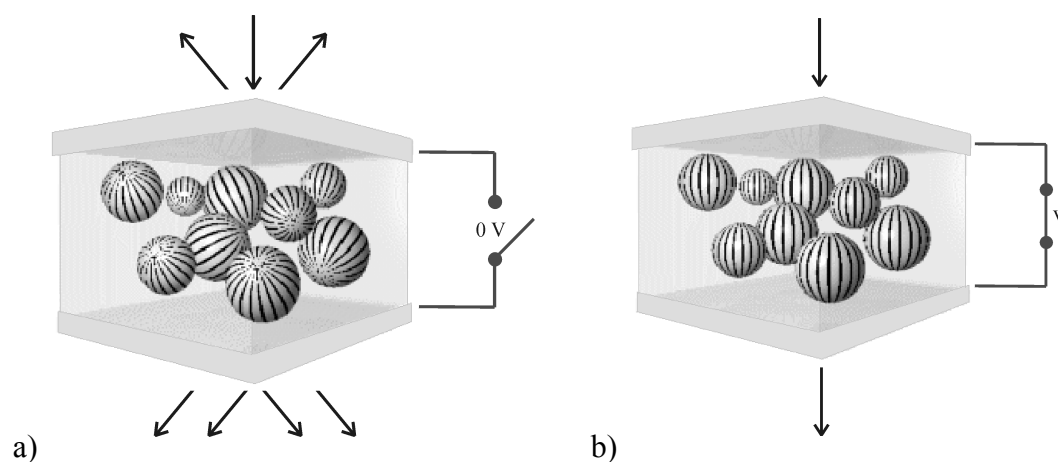


**Figure 1.3:** Operation principle of a polymer dispersed liquid crystal (PDLC) light shutter: (a) Light-scattering off-state with randomly oriented nematic LC droplets; (b) transparent on-state with the director of the LC droplets aligned by an applied electric field.

In this way, the PDLC's are electrically switched between a white light-scattering and a transparent state, which makes these polymer/LC composites particularly interesting for use in e.g. large-area switchable privacy windows, light shutters or projection displays. Compared to TN operation, these PDLC's offer a higher light transmittance in the on-state, an improved viewing angle, and fast switching kinetics.<sup>20</sup> However, due to additional surface interactions between the LC and polymer phase, the switching voltages are significantly increased up into the 10-200 V ( $\sim 1\text{-}10 \text{ V}\cdot\mu\text{m}^{-1}$ ) range and hysteresis is generally observed in the transmittance-voltage characteristic.<sup>11</sup>

Conventional routes for the production of light-scattering polymer/LC composites employ a phase separation process (Figure 1.4). Within such a process, phase separation is induced through cooling of a homogeneous LC/polymer system (thermally induced phase separation, TIPS), through evaporation of the solvent of a solution containing an LC and a polymer (solvent induced phase separation, SIPS), or, usually, via photopolymerisation of a reactive monomer that is homogeneously mixed with an LC (polymerisation induced phase separation, PIPS).<sup>20-24</sup> In the latter case, during polymerisation the LC material becomes immiscible with the polymer formed and starts to phase separate into nematic LC-rich droplets that become finally encapsulated into a solid polymer matrix. Here, initial composition, cure temperature and curing rate show a significant influence on the final size, shape and packing of the LC domains, which in turn determine the electro-optical properties.<sup>20,23,24</sup>

Recently, a reversed PDLC morphology was observed, the so-called polymer ball morphology.<sup>25-29</sup> By properly adjusting photopolymerisation parameters the polymer formed is precipitated from the mixture rather than the LC, which gives rise to the formation of interconnected polymer particles dispersed in an LC continuum.

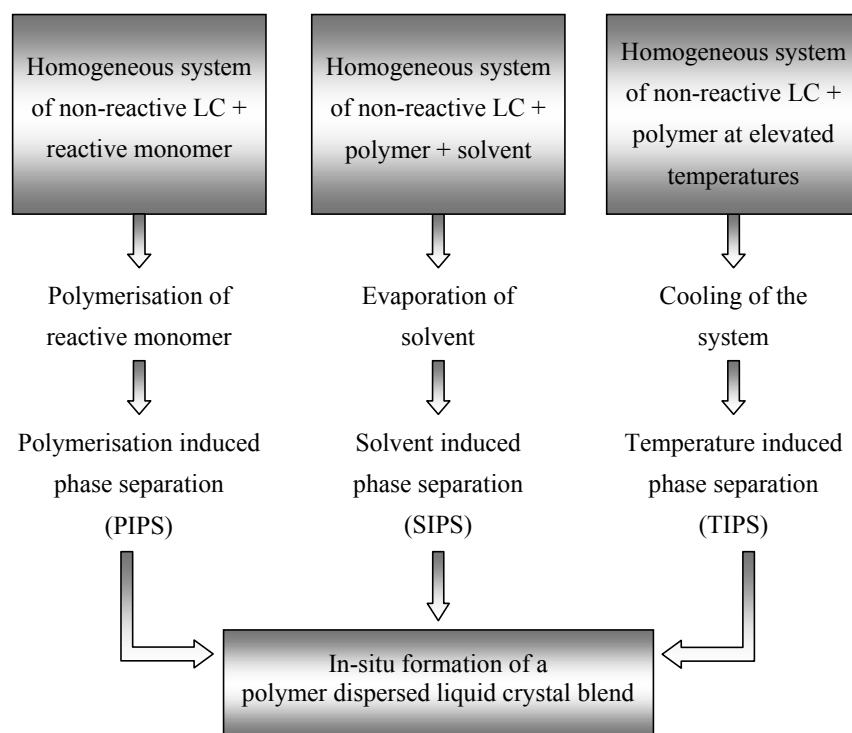


**Figure 1.4:** Schematic representation of three types of phase separation processes that are commonly employed for the in-situ formation of a PDLC blend.

The polymer ball morphology shows a pronounced memory effect, i.e. after removal of the voltage a highly transparent state is preserved for months. As the initial light-scattering state is restored upon application of a thermal treatment, these materials have been exploited in thermally addressed displays, which are operated either in normal or in reverse mode.<sup>26</sup>

### 1.2.2 Anisotropic gels

A variation on the PDLC approach is the liquid crystal dispersed polymer (LCDP) system, which contains only a small amount of polymer (1-10 wt %) that is present in the LC in the form of a continuous chemical network.<sup>12,17,30</sup> In order to manipulate the orientation of the LC in a more profound way, LC reactive monomers were employed in the preparation of either permanently stable anisotropic networks<sup>31-35</sup> or anisotropic chemical gels<sup>10,36-39</sup> by utilising in-situ photopolymerisation in the macroscopically oriented state. In the former case, the mesogenic order is permanently fixed and is stable against thermal and mechanical fluctuations, while in the latter case also non-reactive LC molecules are present which do not participate in the network formation process and therefore can still be oriented by external fields. The function of the anisotropically oriented, crosslinked network is to stabilise the initial macroscopic orientation of the free LC and, hence, to provide the LC molecules with a

memory state in order to facilitate the reorientation process after removal of the electric field. Here, one can distinguish between uniaxial planar<sup>10,36,38</sup> and homeotropic gels<sup>37</sup> that operate in reverse and normal mode, respectively, and chiral gels that are reversibly switched between a reflective and a transparent state.<sup>39</sup> The uniaxial planar gels selectively scatter only one polarisation direction of the light. With polymer-stabilised cholesteric LC's both normal and reverse mode light-shutters can be realised, where both polarisation directions of the light are scattered. These chiral gels are electrically switched between a transparent, macroscopically aligned and a light-scattering, focal conic state, where the polymer network provides the stabilisation of the focal conic structure and its domain size.<sup>17</sup> An advantage of the polymer-stabilised LC approach with respect to the PDLC concept is that in the clear state haze is almost absent for all viewing angles, due to the low fraction of polymer network.<sup>17</sup>

### 1.2.3 Silica filled nematics

Another class of light-scattering electro-optical switches was developed, comprising an LC continuum in combination with dispersed, spherical silica particles with small diameter (< 20 nm) which associate into larger 3-D agglomerates.<sup>13,15</sup> Because of the small size of the dispersed particles, these so-called silica filled nematics exhibit no light scattering through refractive index mismatches between the two phases. However, due to surface interactions between the silica particle network and the surrounding LC molecules, the orientation of the LC is highly disturbed. Hence, a multidomain structure is formed (domain size ~ 100 nm) which causes the strong light scattering in the off-state.<sup>15,40</sup> Presumably, because of rearrangement of the silica agglomerates under application of an electric field, the transparency of the homeotropic on-state is retained after removal of the electric field and, consequently, a bistable device is obtained. These memory effects can be adjusted by altering the driving voltage/frequency, the aerosil content, or by chemically modifying the particle surface in a way to change the aerosil interparticle interaction and, more important, the LC-aerosil anchoring energy.<sup>41-43</sup> A few options to erase the memory state are e.g. thermal writing, dual frequency addressing or by applying mechanical distortions.<sup>14,15,44,45</sup>

### 1.2.4 Thermoreversible gels

A new approach in the field of LCD's is the addition of small amounts of low molecular weight, organic compounds to the LC solvents.<sup>46-50</sup> These functionalised organic additives are able to associate into 3-D finely dispersed, supramolecular structures, primarily through intermolecular hydrogen bonding interactions.<sup>46,47,51-54</sup> Thus, while in the case of the anisotropic chemical gels a covalently crosslinked, permanent polymer network is formed, in the case of these anisotropic physical gels non-covalent interactions are employed to generate

a thermo-reversible network. This self-assembly generates a microphase-separated structure, where the LC molecules are confined within the small spaces that are defined by the physical network. Through strong surface anchoring interactions between the LC and the network, the confined LC molecules are immobilised which causes physical gelation of the LC phase. During the last years these materials have been explored for their potential use in electro-optical devices. In spite of their light-scattering power,<sup>51</sup> these thermoreversible gels have mainly been applied in TN-LCD's in an attempt to accelerate the response speed of the LC molecules.<sup>46-50</sup>

### 1.3 Challenges in the field of liquid crystal displays

In general, the electro-optical performance of LCD's based on two-phase mixtures strongly depends on the morphological characteristics of the functional material e.g. the degree of phase separation between the two phases, the interfacial interaction and the shape and dimensions of the two phases. Consequently, it is essential to have a good control over the final morphology of the functional mixture. This becomes a complicated issue due to the fact that the morphology of polymer/LC systems, like PDLC's, is formed in-situ during the phase separation. Although the derivation of phase separation conditions-morphology relationships might be a useful aspect in controlling the final structure of the polymer/LC blend to some extent, it is very commonly experienced that, as the phase separation process proceeds, the LC becomes partly entrapped in the polymer-rich phase and vice versa.<sup>55-58</sup> These intermixing phenomena intervene with the morphology tuning process and lead to considerable deviations of desired electro-optical properties.

Apart from the performance of both the light-scattering and TN systems, the conventional production process of display devices also needs to be considered. At the moment, LCD's are manufactured via batch-wise processes. However, the LCD cell construction is rather complex (see Figure 1.5), which makes the batch-wise fabrication of these devices both laborious and expensive. This, in turn, impedes the development of large-area displays.

These issues might be settled by (1) the development of materials with a well-defined morphology and by (2) the introduction of novel continuous manufacturing processes for flat panel displays, that are significantly more cost-effective than the established batch-wise technologies and which make the production of large-area displays feasible. In addition, in the near future multiple display applications are being anticipated, and a proper design of the new continuous processing technology would enable its universal applicability to a variety of electro-optical switches.



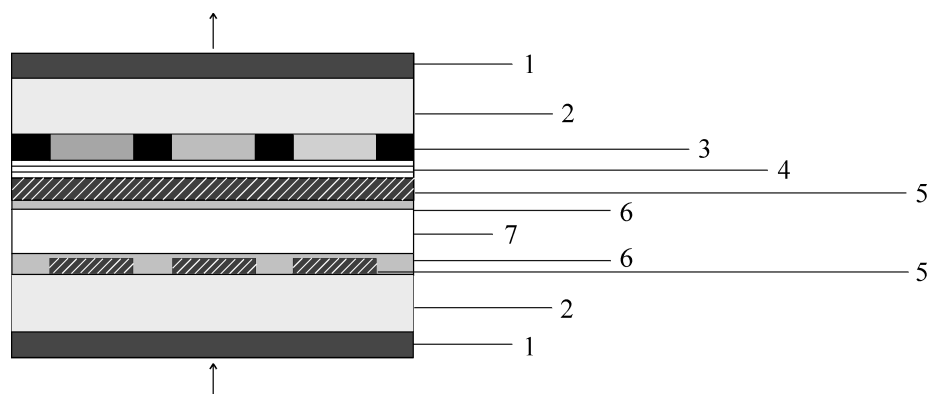


**Figure 1.5:** Schematic representation of a display cell design concept: (1) Polariser; (2) glass substrate; (3) pixelated colour filter + black mask; (4) planarisation layer; (5) ITO electrode (pattern); (6) polyimide orientation layer; (7) liquid crystal component.

## 1.4 Aims of the thesis

The first objective of this thesis is to explore novel experimental routes, as an alternative for phase separation processes, for the preparation of polymer/LC composites with an accurately controlled morphology. For this purpose, polymer/LC composites are developed based on (sub-)micron-sized, internally crosslinked polymer colloids dispersed in a low molecular weight liquid crystal.

The experimental route that is followed for the generation of these so-called LC colloidal dispersions includes two separate steps, i.e. in a first step the colloids are synthesised via dispersion or emulsion polymerisation and in a second step the colloids are mixed with an LC (Figure 1.6). Via an appropriate choice of polymerisation parameters the morphological features of the polymer colloids are tuned with respect to chemical and physical properties, such as surface modification, dimension and composition. Also, in view of the electro-optical application, it is attempted to match the refractive index of the polymer colloids to the  $n_o$  of the LC by properly selecting the composition of the monomer mixture for the polymerisation reaction. By including a crosslinking agent in the monomer feed, it is attempted to avoid the occurrence of intermixing phenomena during dispersion of the resulting polymer colloids in the organic LC solvent. The preservation of a well-defined colloid and LC phase during the mixing step enables the derivation of morphology-property relationships for the corresponding two-phase systems and a subsequent optimisation of their performance.

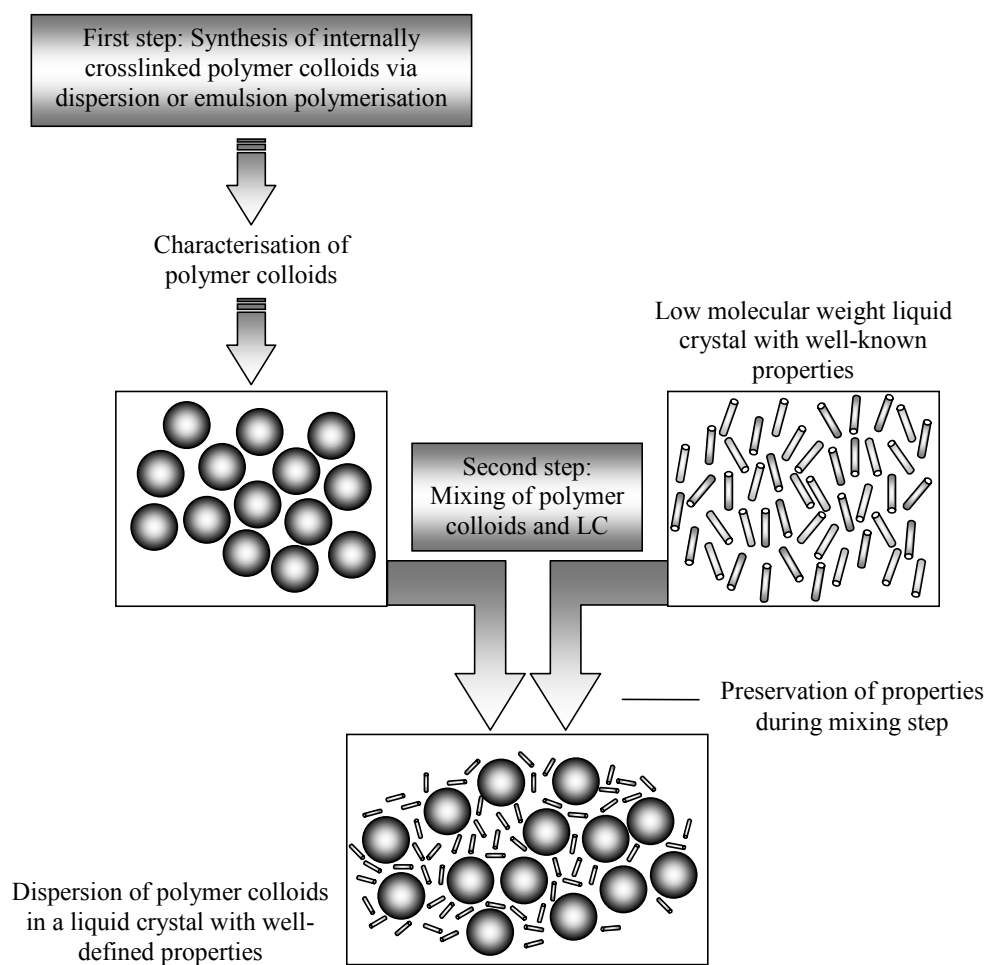


**Figure 1.6:** Schematic representation of a novel experimental route for the generation of polymer/LC model systems.

A second objective of this thesis is to make the introduction of continuous processing technologies for the manufacturing of electro-optical switches feasible. A continuous production process for displays is envisaged as is schematically shown in Figure 1.7 for in-plane switches. In this process the glass substrate conventionally used is replaced by, for instance, a flexible polyester foil which is provided with an (interdigital) ITO electrode pattern. The polarisers are installed via the use of coatable materials. In order to mechanically stabilise and chemically protect the various coatings a polymer top layer is applied by starting from e.g. a coatable polymer solution or a polymerisable monomer mixture. Alternatively, a lamination process is employed to cover the layers with a solid foil. A significant problem that is encountered in the realisation of this process concerns the application of the LC, since it lacks in rheological stability. Therefore, in this thesis new materials are designed based on LC's and functional organic or polymeric additives, where the additives are employed to introduce, as a whole, new or improved combinations of rheological and electro-optical properties with regard to conventional electro-optical switches.

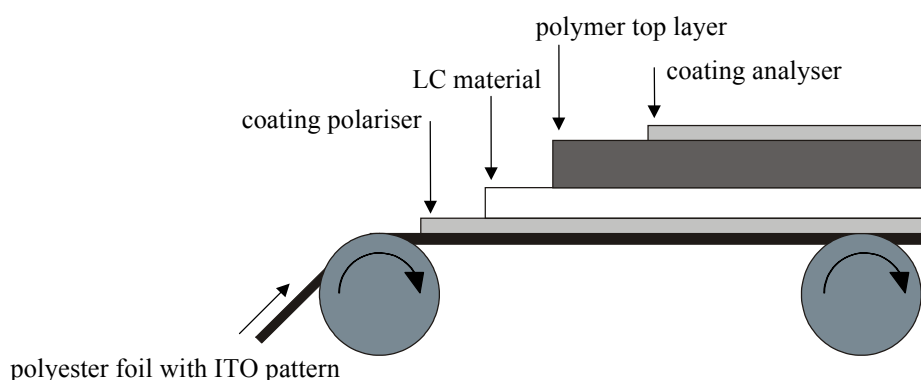


**Figure 1.7:** *Schematic representation of the envisaged continuous process for electro-optical switches.*

## 1.5 Scope of the thesis

In **Chapter 2** the monomers methyl methacrylate and divinylbenzene are selected for the generation of polymer colloids via free-radical polymerisation by use of the dispersion or, in a few cases, the emulsion polymerisation method. In order to gain more insight into the reaction kinetics of the dispersion polymerisation and the composition of the polymer colloids formed the consumption of the monomers during their homo- and copolymerisation is studied via the use of several off-line and on-line sampling techniques. Additionally, the influence of several dispersion polymerisation parameters on particle size and monomer conversion is investigated. Via an appropriate combination of polymerisation parameters uniform colloidal particles are prepared with a broad range of particle sizes.

The polymer colloids obtained are used in **Chapter 3** for the production of colloidal dispersions in an LC. The phase behaviour of the polymer/LC blends is evaluated with respect to the degree of phase separation between the LC and colloid phase. The morphology of the two-phase materials is studied in three dimensions by use of a confocal laser scanning technique. The peculiar behaviour and resulting morphology of the LC colloid systems are explained in more detail from a theoretical point of view. Furthermore, the materials are evaluated for their use in continuous processes by looking into their rheological properties.

In **Chapter 4** the LC colloidal materials are tested for their application as electro-optical switches. Electro-optical cells with a TN configuration are filled with dispersions based on rather low fractions of colloids and characterised with respect to their electro-optical behaviour. Dispersions based on rather high colloid fractions are examined for their use as light-scattering electro-optical switches. The orientation, relaxation behaviour and electrical switching of the LC molecules in the presence of the colloids is investigated in more detail by the performance of a dielectric analysis.

In **Chapter 5** dendrimers are used as additives for the LC in order to extend the range of available particle sizes down to the nanometer scale. Within this study three types of dendrimers are used, which differ from each other in the length of the covalently bonded alkyl endchains. The dendrimer filled nematics are evaluated on their application as light-scattering electro-optical switches. For a better understanding of the effect of the dendrimer additive on the orientation of the LC molecules, dielectric relaxation spectroscopy experiments are conducted. In addition, the change in flow behaviour upon addition of dendrimers to the LC is studied via rheological measurements.

Next to the LC colloidal dispersions and the dendrimer filled LC's, a third type of soft solid-like, two-phase material is described in **Chapter 6** and is referred to as thermo-reversible gels. These gels are based on the addition of low molecular weight, organic molecules to an LC. The gels are used for the design of light-scattering electro-optical switches via an appropriate tuning of their phase behaviour. The mechanical strength of the anisotropic physical gels is evaluated via a dynamic mechanical analysis.

In **Chapter 7** the practical realisation of a film-based continuous process is briefly discussed in some more detail for the LC colloidal dispersions.

Finally, the different materials are evaluated in a **Technology assessment** for their potential use in the production of new liquid crystal displays with respect to both properties and production method.

## 1.6 References

- (1) Goodman, L.A. *Introduction to liquid crystals*, edited by Priestley, E.B., Wojtowicz, P.J., Sheng, P., Plenum Press, New York, **1975**.
- (2) Schadt, M., Helfrich, W. *Appl. Phys. Lett.*, **1971**, *18*, 127-128.
- (3) Scheffer, T.J., Nehring, J. *Appl. Phys. Lett.*, **1984**, *45*, 1021-1023.
- (4) Heynderickx, I., Broer, D.J. *Mol. Cryst. Liq. Cryst.*, **1991**, *202*, 113-126.
- (5) Ohmuro, K., Kataoka, S., Sasaki, T., Koike, Y. *SID Int. Symp.: Dig. Tech. Pap.*, Boston, **1997**, *XXVIII*, 845.
- (6) Takeda, A., et al. *SID Int. Symp.: Dig. Tech. Pap.*, California, **1998**, *XXIX*, 1077.
- (7) Oh-e, M., Yoneya, M., Kondo, K. *J. Appl. Phys.*, **1997**, *82*, 528-535.
- (8) Yamada, N., Kohzaki, S., Funada, F., Awane, K. *Sharp Tech. J.*, **1995**, 14-17.
- (9) Doane, J.W., Vaz, N.A., Wu, B.G., Zumer, S. *Appl. Phys. Lett.*, **1986**, *48*, 269-271.
- (10) Hikmet, R.A.M. *J. Appl. Phys.*, **1990**, *68*, 4406-4412.
- (11) Coates, D. *Displays*, **1993**, *14*, 94-103.
- (12) Dierking, I. *Adv. Mater.*, **2000**, *12*, 167-181.
- (13) Eidenschink, R., De Jeu, W.H. *Electron. Lett.*, **1991**, *27*, 1195-1196.
- (14) Kreuzer, M., Tschudi, T., Eidenschink, R. *Mol. Cryst. Liq. Cryst.*, **1992**, *222*, 219-227.
- (15) Kreuzer, M., Tschudi, T., De Jeu, W.H., Eidenschink, R. *Appl. Phys. Lett.*, **1993**, *62*, 1712-1714.
- (16) Craighead, H.G., Cheng, J., Hackwood, S. *Appl. Phys. Lett.*, **1982**, *40*, 22-24.
- (17) Yang, D.K., Chien, L.C., Doane, J.W. *Appl. Phys. Lett.*, **1992**, *60*, 3102-3104.
- (18) Drzaic, P.S. *Liq. Cryst.*, **1988**, *3*, 1543-1559.

- (19) Erdmann, J., Doane, J.W., Zumer, S., Chidichimo, G. *Proc. SPIE-Int. Soc. Opt. Eng.*, **1989**, 1080, 32-40.
- (20) Amundson, K., Van Blaaderen, A., Wiltzius, P. *Phys. Rev. E*, **1997**, 55, 1646-1654.
- (21) Doane, J.W., Golemme, A., West, J.L., Whitehead, J.B., Wu, B.G. *Mol. Cryst. Liq. Cryst.*, **1988**, 165, 511-532.
- (22) Kim, B.K., Kim, S.H., Choi, C.H. *Mol. Cryst. Liq. Cryst. Sci. Technol., Sect. A*, **1995**, 261, 605-616.
- (23) Grand, C., Achard, M.F., Hardouin, F. *Liq. Cryst.*, **1997**, 22, 287-296.
- (24) Carter, S.A., LeGrange, J.D., White, W., Boo, J., Wiltzius, P. *J. Appl. Phys.*, **1997**, 81, 5992-5999.
- (25) Yamaguchi, R., Sato, S. *Jpn. J. Appl. Phys., Part 2*, **1991**, 30, L616-L618.
- (26) Yamaguchi, R., Ookawara, H., Sato, S. *Jpn. J. Appl. Phys., Part 2*, **1992**, 31, L1093-L1095.
- (27) Yamaguchi, R., Sato, S. *Liq. Cryst.*, **1993**, 14, 929-935.
- (28) Chang, S.J., Lin, C.M., Fuh, A.Y.G. *Liq. Cryst.*, **1996**, 21, 19-23.
- (29) Chang, S.J., Lin, C.M., Fuh, A.Y.G. *Jpn. J. Appl. Phys., Part 1*, **1996**, 35, 2180-2183.
- (30) Fung, Y.K., et al. *Liq. Cryst.*, **1995**, 19, 797-801.
- (31) Broer, D.J., Gossink, R.G., Hikmet, R.A.M. *Angew. Makromol. Chem.*, **1990**, 183, 45-66.
- (32) Broer, D.J., Heynderickx, I. *Macromolecules*, **1990**, 23, 2474-2477.
- (33) Broer, D.J. *Mol. Cryst. Liq. Cryst. Sci. Technol., Sect. A*, **1995**, 261, 513-523.
- (34) Heynderickx, I., Broer, D.J. *Mol. Cryst. Liq. Cryst. Sci. Technol., Sect. A*, **1995**, 263, 415-427.
- (35) Broer, D.J., Mol, G.N., Van Haaren, J., Lub, J. *Adv. Mater.*, **1999**, 11, 573-578.
- (36) Hikmet, R.A.M. *Mol. Cryst. Liq. Cryst.*, **1991**, 198, 357-370.
- (37) Hikmet, R.A.M. *Mol. Cryst. Liq. Cryst.*, **1992**, 213, 117-131.
- (38) Hikmet, R.A.M., Boots, H.M.J. *Phys. Rev. E*, **1995**, 51, 5824-5831.
- (39) Hikmet, R.A.M., Kemperman, H. *Liq. Cryst.*, **1999**, 26, 1645-1653.
- (40) Kreuzer, M., Tschudi, T. *SPIE*, **1993**, 1983, 458.
- (41) Guba, G., et al. *Mol. Cryst. Liq. Cryst. Sci. Technol., Sect. A*, **1994**, 251, 303-309.
- (42) Glushchenko, A.V., et al. *Mol. Cryst. Liq. Cryst. Sci. Technol., Sect. A*, **1995**, 262, 111-118.
- (43) Glushchenko, A.V., Kresse, H., Reznikov, Y.A., Yaroshchuk, O.V. *Liq. Cryst.*, **1997**, 23, 241-246.
- (44) Abraham, M., et al. *Proc. SPIE-Int. Soc. Opt. Eng.*, **1994**, 2175, 143-146.
- (45) Yaroshchuk, O., Glushchenko, A., Kresse, H. *Cryst. Res. Technol.*, **1995**, 30, 32-36.
- (46) Kato, T., Kutsuna, T., Hanabusa, K. *Mol. Cryst. Liq. Cryst. Sci. Technol., Sect. A*, **1999**, 332, 2887-2892.
- (47) Mizoshita, N., Hanabusa, K., Kato, T. *Adv. Mater.*, **1999**, 11, 392-394.
- (48) Kato, T., Mizoshita, N., Katsuna, T., Kondo, G., Hanabusa, K. *Abstr. Pap. Am. Chem. Soc.*, **1999**, 218, 364-365.
- (49) Kato, T., Mizoshita, N., Kutsuna, T., Kondo, G., Hanabusa, K. *Macromol. Symp.*, **2000**, 154, 15-24.
- (50) Mizoshita, N., Hanabusa, K., Kato, T. *Displays*, **2001**, 22, 33-37.
- (51) Kato, T., Kutsuna, T., Hanabusa, K., Ukon, M. *Adv. Mater.*, **1998**, 10, 606-608.
- (52) Kato, T., Kondo, G., Hanabusa, K. *Chem. Lett.*, **1998**, 193-194.
- (53) Kato, T., et al. *Abstr. Pap. Am. Chem. Soc.*, **1999**, 218, 301-302.
- (54) Mizoshita, N., Kutsuna, T., Hanabusa, K., Kato, T. *Chem. Commun.*, **1999**, 781-782.
- (55) Vaz, N.A., Smith, G.W., Montgomery, G.P. *Mol. Cryst. Liq. Cryst.*, **1987**, 146, 17-34.
- (56) Smith, G.W., Vaz, N.A. *Mol. Cryst. Liq. Cryst. Sci. Technol., Sect. A*, **1993**, 237, 243-269.
- (57) Carpaneto, L., Ristagno, A., Stagnaro, P., Valenti, B. *Mol. Cryst. Liq. Cryst. Sci. Technol., Sect. A*, **1996**, 290, 213-226.
- (58) Roussel, F., Buisine, J.M., Maschke, U., Coqueret, X. *Phys. Rev. E*, **2000**, 62, 2310-2316.

# Chapter 2

## Synthesis of polymer colloids

### 2.1 Introduction

As discussed in the previous chapter, it is attempted to generate a new experimental procedure for the design of polymer/LC model systems. Within this experimental route the synthesis of polymeric colloids precedes the preparation of polymer/LC dispersions. The aim of the particle synthesis step is to prepare colloidal particles with specific and well-defined properties, which are preserved during the post-processing step.

Various types of polymerisation methods are nowadays available for the production of polymer particles with a reasonably controlled size. For instance, with suspension polymerisation rather large polymer beads can be produced with sizes ranging from 50-1000  $\mu\text{m}$ .<sup>1</sup> Smaller polymer colloids with diameters ranging from 0.05-0.8  $\mu\text{m}$  can be obtained by emulsion polymerisation.<sup>2</sup> These methods generally employ an aqueous polymerisation medium that poorly dissolves the monomers, and so the reaction proceeds in a heterogeneous manner comprising separate phases.

The preparation of monodisperse particles with a size intermediate to the ones obtained by emulsion and suspension polymerisation has received a lot of attention. For the preparation of micron-sized particles of uniform size seeded polymerisation methods were proposed based on single-step or multi-step swelling procedures.<sup>3-9</sup> These polymerisation methods use seed particles that are swollen with monomers and, in some cases, with an inert diluent to enhance the swelling process. Subsequently, a repolymerisation step is carried out, which results in a growth of the initial seed particles to sizes in the 1-100  $\mu\text{m}$  range.

In the past decade, considerable interest has been directed towards the free-radical dispersion polymerisation technique due to its inherent simplicity.<sup>10,11</sup> With this method polymer dispersions with uniform sizes in the 0.1-20  $\mu\text{m}$  range are directly prepared in a single polymerisation step. Furthermore, this polymerisation method allows the use of an organic medium. The dispersion polymerisation principle relies on the fact that the monomers are soluble in the (organic) medium, while the formed polymers are insoluble and thus precipitate. An essential component of the dispersion polymerisation is the stabiliser. The function of the stabiliser is to impart colloidal stability to the precipitate, thus allowing further growth into well-defined, sterically stabilised latex particles. Previous studies have mainly addressed the preparation of sub-micron to micron-sized, monodisperse polystyrene

(PS) and poly(methyl methacrylate) (PMMA) particles by use of the dispersion polymerisation technique.<sup>12-18</sup> For the polymerisation of methyl methacrylate and styrene in most cases the use of a hydrocarbon, alcohol or aqueous mixture was reported as the medium and various (precursor) graft or diblock copolymers were proposed as the stabiliser.<sup>17,19-28</sup> For instance, for the preparation of sub-micron sized PMMA particles a poly(styrene-*b*-[ethylene-*co*-propylene]) copolymer proved to be suitable in combination with *n*-heptane<sup>29-31</sup> or decane.<sup>32,33</sup> Although the PS block of the copolymeric stabiliser is virtually immiscible with PMMA, the PS block copolymers were surprisingly found to be very well capable of stabilising a PMMA dispersion in a hydrocarbon solvent. This phenomenon was related to the entrapment of the PS chains within the growing particle.<sup>33,34</sup>

Later, also reports appeared about the incorporation of a crosslinking agent in latex particles. Usually, significant difficulties like instability problems or irregular particle shapes were encountered in the preparation of polyvinylpyrrolidone (PVP) stabilised, highly crosslinked dispersions based on divinylbenzene (DVB).<sup>35-37</sup> These peculiarities were thought to originate from the irreversible anchoring of poly(vinylpyrrolidone-*g*-divinylbenzene) stabiliser molecules within the particles. These grafted stabilisers are formed in-situ during the polymerisation reaction via abstraction of hydrogen from the PVP backbone, followed by the addition of DVB.<sup>24,35,38,39</sup>

In this chapter, the generation of poly(methyl methacrylate-*co*-divinylbenzene) colloids with a controlled size via the dispersion polymerisation method is evaluated. This method was used because of its inherent simplicity, the possibility to utilise an organic medium and the ability to obtain monodisperse colloidal latex particles within the desired size range. A poly(styrene-*b*-[ethylene-*co*-propylene]) block copolymer was chosen as the stabilising component in combination with *n*-heptane as the medium. Within this combination, the poly(ethylene-*co*-propylene) block is highly compatible with the apolar medium and therefore acts as the soluble block, while the polystyrene block preferentially anchors onto the particle surfaces. The reaction kinetics of the free-radical dispersion polymerisation is studied by recording monomer conversion in time by off-line and/or on-line sampling techniques. In addition, in an attempt to extend the range of generated particle sizes to smaller sizes, the emulsion polymerisation method was employed in a few cases. In this procedure a non-ionic surfactant was used because of its compatibility with organic media.

## 2.2 Experimental

### 2.2.1 Materials

The monomers selected are methyl methacrylate (MMA; 99%, Aldrich) and a technical-grade divinylbenzene (DVB55, Aldrich), a mixture containing two divinylbenzene

isomers (*p*-DVB: 17.7 wt %; *m*-DVB: 38.2 wt %), two ethylvinylbenzene isomers (*p*-EVB: 10.9 wt %; *m*-EVB: 32.0 wt %) and some minor impurities like diethylbenzene (0.2 wt %) and naphthalene (0.5 wt %).<sup>40</sup> The divinylbenzene fraction of this mixture (55 wt %) provides the chemical crosslinks. This DVB grade is well known from literature and is commonly used as a crosslinker blend, since a 100% divinylbenzene grade is not commercially available and since purification procedures for the isolation of the divinylbenzene isomers are very laborious.<sup>41,42</sup> The monomers were purified with an inhibitor adsorption column (Aldrich, inhibitor remover for hydroquinone and tert-butylcatechol).

For the dispersion polymerisation *n*-heptane (extra pure) was purchased from Merck and was used as received. The steric stabiliser, a poly(styrene-*b*-[ethylene-*co*-propylene]) copolymer containing 38.5-42 wt % of styrene units was obtained from Shell (Kraton G-1701x,  $M_w = 1.1 \cdot 10^5 \text{ g.mole}^{-1}$ ,  $M_w/M_n \approx 1.1$ ). As a radical initiator dibenzoyl peroxide was used, containing approximately 25 wt % water (DBP, Fluka). The initiator was recrystallised from ethanol with average yields of approximately 33 %.

For the emulsion polymerisation deionised water was used. The pH buffer sodium hydrogen carbonate ( $\text{NaHCO}_3$ , 99 %) and the initiator 4,4'-azobis(4-cyanovaleric acid) (ABCA, 25 % water) were purchased from Aldrich and used as received. The NaOH was purchased from Janssen Chemica and used as received. A non-ionic, steric stabiliser, a polyoxyethylene(40)nonylphenyl ether (4-( $\text{C}_9\text{H}_{19}$ ) $\text{C}_6\text{H}_4(\text{OCH}_2\text{CH}_2)_{40}\text{OH}$ , Igepal CO-890,  $M_n = 1,982 \text{ g.mole}^{-1}$ ) was obtained from Aldrich.

## 2.2.2 Dispersion polymerisation

The components and the amounts of components that were used in a typical dispersion polymerisation experiment are shown in Table 2.1.

**Table 2.1:** *Typical recipe for the preparation of highly crosslinked, refractive index matched poly(methyl methacrylate-co-divinylbenzene) colloids via dispersion polymerisation.*

Component	Amount [g]
<i>n</i> -heptane	138.9
MMA	11.47 (7.4 wt %)
DVB55	3.96 (2.6 wt %)
DBP (75 % pure)	0.1 (0.5 g.l <sup>-1</sup> )
Kraton G-1701x	0.817 (4 g.l <sup>-1</sup> )



The dispersion polymerisation reactions were performed under nitrogen in a sealed, water thermostated, double-walled glass reaction vessel equipped with a mechanical stirrer at a temperature of 60-90 °C. The organic solvent *n*-heptane was added to the reactor together with the steric stabiliser Kraton G-1701x. The nitrogen purging was started in the reactor and the reactor was heated to reaction temperature under continuous stirring in order to dissolve the stabiliser. After a clear solution was obtained, the monomers MMA and DVB55, containing the dissolved initiator DBP, were added to the organic medium and the reactor was sealed off. In Table 2.2 the recipes are listed for the dispersion polymerisations that were monitored by Raman spectroscopy, gas chromatography (GC) and/or gravimetric analysis.

**Table 2.2:** *Recipes that were used for the monitored dispersion polymerisations: (a) The homopolymerisation of MMA; (b) the homopolymerisation of DVB55; (c) the copolymerisation of MMA and DVB55.*

Component	<sup>a)</sup> Amount [g]	<sup>b)</sup> Amount [g]	<sup>c)</sup> Amount [g]
<i>n</i> -heptane	138.9	138.9	138.9
MMA	15.43 (10 wt %)	-	11.47 (7.4 wt %)
DVB55	-	15.43 (10 wt %)	3.96 (2.6 wt %)
DBP (recryst.)	0.1 (0.5 g.l <sup>-1</sup> )	0.1 (0.5 g.l <sup>-1</sup> )	0.1 (0.5 g.l <sup>-1</sup> )
Kraton G-1701x	1.634 (8 g.l <sup>-1</sup> )	1.634 (8 g.l <sup>-1</sup> )	0.817 (4 g.l <sup>-1</sup> )

### 2.2.3 Emulsion polymerisation

The components and the amounts of components that were used in a typical emulsion polymerisation experiment are listed in Table 2.3.

**Table 2.3:** *Typical recipe for the preparation of highly crosslinked, refractive index matched poly(methyl methacrylate-co-divinylbenzene) colloids via emulsion polymerisation.*

Component	Amount [g]
Water	700
NaHCO <sub>3</sub>	1.30
MMA	26.02 (3.4 wt %)
DVB55	8.98 (1.2 wt %)
ABCA (75 % pure)	0.97 (1.3 g.l <sup>-1</sup> )
Igepal CO-890	10 (14 g.l <sup>-1</sup> )
1 M NaOH	7.6

The emulsion polymerisation reaction was performed in a sealed, water thermostated, double-walled glass reaction vessel equipped with a mechanical stirrer and a cooling device at elevated temperature of 70 °C. The deionised water was added to the reactor together with the sodium hydrogen carbonate and the non-ionic steric stabiliser Igepal CO-890. The argon purging was started in the reaction vessel and mechanical stirring was initiated in order to dissolve the stabiliser. After 30 minutes, the monomers MMA and DVB55 were added to the aqueous medium, after being purged with argon for 20 minutes. Next, the reactor was heated up to 70 °C while the argon purging was continued. After 30 minutes the initiator ABCA was added to the reactor content, after being dissolved in a small amount of sodium hydroxide solution. The argon purging was continued during reaction. The emulsion obtained was purified from stabiliser residues by use of repeating washing procedures.

#### 2.2.4 Techniques

##### *Gas chromatography (GC)*

The conversions of the separate monomers during or after dispersion polymerisation were determined by analysing the concentrations of unreacted monomer in the dispersion by means of GC. The samples were quenched in ice water, directly after sampling. A Hewlett Packard 5890 A gas chromatograph was utilised, equipped with a Hewlett Packard capillary column (AT-WAX, length = 30 m, internal diameter = 0.53 mm, film = 1.0 µm), a flame ionisation detector and an autosampler. A GC program was chosen where the initial oven temperature was maintained for 7 minutes at 28 °C. Next, the temperature was increased with a rate of 5 °C.min<sup>-1</sup> to a final temperature of 180 °C. Isopropanol served as an internal standard for normalisation of the monomer peaks.

##### *Raman spectroscopy*

The conversions of the various vinyl bonds of the monomers during polymerisation were monitored on-line using Raman spectroscopy. The Raman spectrometer (Dilor Labram) was equipped with a Millennia II doubled Nd:YVO<sub>4</sub> laser (Spectra Physics). The laser was operated at 0.2 W and generated a 532 nm line that was used for excitation of the molecules. The laser light was guided to the reactor set-up by means of 10 m glass fibre. The end of the glass fibre was connected to a Dilor Superhead<sup>®</sup> provided with a 20x long working distance objective in order to focus the monochromatic laser bundle into the reaction mixture. The scattered laser light was collected with the same objective, thus under an angle of 360°, and guided back to the spectrometer. By use of a 1800 grooves/mm grating in the spectrometer in combination with a 1024x256 pixel CCD detector spectral resolutions of 0.14 nm (corresponding to 1.5 cm<sup>-1</sup>) were realised.

The polymerisation reactions were carried out in a special thermostated (double-walled) glass reaction vessel provided with a small single-wall window through which the laser light was transmitted. The reactor was equipped with a cooler and a PT-100 thermocouple. Mixing was ensured by use of a magnetic stirrer bar. The monomers were added to the reaction medium together with the stabiliser and initiator at room temperature. Next, the probe position was optimised by positioning the objective in such a way that the intensity of the measured Raman bands was approximately maximal.<sup>43</sup> Subsequently, the monitoring was started and the system was heated up to the desired polymerisation temperature. Next, the polymerisation mixture was purged with argon. Before and during reaction, samples were taken from the reactor through a flexible Teflon tube, which was also used for the argon purging. Directly after sampling, the samples were quenched in ice water. The spectra recorded were smoothed using the Savitsky Golay procedure, baseline corrected and further analysed by use of a Labview program. The Raman spectra obtained were normalised with respect to a properly chosen solvent band in order to account for possible changes in light-scattering intensity and probe position during reaction monitoring.<sup>43</sup>

#### *Electron microscopy (EM)*

The size and polydispersity of the particles formed was estimated with scanning electron microscopy (SEM, Cambridge Stereoscan 200), environmental scanning electron microscopy (ESEM, Philips XL30 FEG, operated at 1-10 kV) or transmission electron microscopy (TEM, JEOL 2000 FX, operated at 80 kV). For the TEM samples carbon coated grids were used. The (E)SEM samples were prepared by applying the (diluted) colloidal dispersions directly on a sample holder, which was provided with double-sided tape. The organic medium of the dispersion was evaporated overnight under vacuum at room temperature. The dried latex samples were coated with a gold/palladium layer.

#### *Particle sizing*

The size and polydispersity of colloids with sizes larger than ~150 nm (according to EM) were measured by laser light scattering via the use of a Coulter LS apparatus. This particular technique transforms scattered light intensities, measured as a function of the scattering angle and the wavelength of the light, into particle sizes. With this laser light scattering technique particles are detected with diameters in the 0.14-3000  $\mu\text{m}$  range and measurements are automatically converted into volume or surface area distributions. Unless mentioned otherwise, the data were taken from the volume distributions.

The size and polydispersity of colloids with sizes smaller than ~150 nm were measured by photon correlation spectroscopy (PCS) via the use of a Coulter N4 Plus apparatus. The PCS technique sizes particles by characterising the exact time scale of the random intensity fluctuations in the interference pattern of the scattered light caused by the

motion of the Brownian particles. In this way, particles are detected with sizes in the 0.001-2  $\mu\text{m}$  range. The measurements were converted by the PCS software into weight distributions.

Via the particle sizing measurements the peaks of the weight, volume and surface area distributions were characterised by a mean particle diameter and a standard deviation, defined as:  $\bar{d} = \sum d_i f(d) = \sum d_i x_i / \sum x_i$  and  $S.D.(d) = [\sum (d_i - \bar{d})^2 f(d)]^{1/2} = [\sum x_i (d_i - \bar{d})^2 / \sum x_i]^{1/2}$ , where  $d_i$  is the diameter corresponding to the  $i^{\text{th}}$  histogram bin,  $f(d)$  is the probability function, and  $x_i$  is the relative weight, volume or surface area of particles with diameter  $d_i$ .

## 2.3 Results and discussion

The selection of the monomers for the polymerisation reaction relies on a few criteria. Firstly, after mixing the polymer colloids with an LC material, a complete phase separation between the polymer and the LC phase has to be accomplished. Previously, it was shown that with dispersions of thermoplastic polymer colloids in LC the intended phase separation between the LC and the polymer phase could not be achieved due to the occurrence of intermixing phenomena.<sup>44</sup> As opposed to this, the utilisation of internally crosslinked poly(methyl methacrylate-*co*-divinylbenzene) colloids appeared to be very promising in this respect. Therefore, this particular colloid system was used for this study.

Secondly, the refractive index of the synthesised polymer colloids has to match the ordinary refractive index of the LC material used in order to gain optimum optical properties of the LC colloidal systems in the electrically addressed state. In the copolymerisation reaction, the ratio of the two monomers, MMA and DVB, was therefore chosen such that at equal conversions of the individual monomers an average refractive index of the polymer colloids,  $n_p$ , is obtained, which equals the ordinary refractive index of LC E7,  $n_o$  ( $= 1.5216$ ). This particular ratio was calculated via a mixing rule, as given by the Lorentz-Lorenz equation<sup>45</sup> and was found to be equal to 2.896:1 wt/wt MMA/DVB.

In the following sections GC, Raman spectroscopy and gravimetric analysis were used as experimental tools in the monitoring of the individual monomer or vinyl bond conversions during the homopolymerisation reactions of both MMA and DVB55 and, subsequently, their copolymerisation reaction. The reaction mixtures of these monitored polymerisation reactions were composed according to the recipes of Table 2.2. Next, starting from the recipe of Table 2.1, the influence of several polymerisation parameters on the particle size (and particle size distribution) and total monomer conversion was investigated: (i) the monomer concentration, (ii) the stabiliser concentration, (iii) the initiator concentration, and (iv) the polymerisation temperature. In all cases the average particle size was estimated from (E)SEM or TEM photographs of particles that were formed within 47 hours of polymerisation. The corresponding total monomer conversion after 47 hours of polymerisation was determined via gravimetric analysis.

### 2.3.1 The homopolymerisation reaction of methyl methacrylate

For the homopolymerisation of MMA (see Table 2.2a for recipe), the integrated area (intensity) of the vinyl-stretch vibration band of MMA at  $1630\text{ cm}^{-1}$  in the Raman spectrum was related to the conversion of the vinyl bonds of MMA. For this purpose, the spectrum was normalised on the  $900\text{ cm}^{-1}$  aliphatic C-C stretching band of the solvent *n*-heptane. This band was chosen as the internal standard as it appeared to be unaffected by the disappearance of the vinyl bonds upon polymerisation. Moreover, by comparing Figures 2.1a and b it is seen that this band shows no significant overlap with monomer bands.

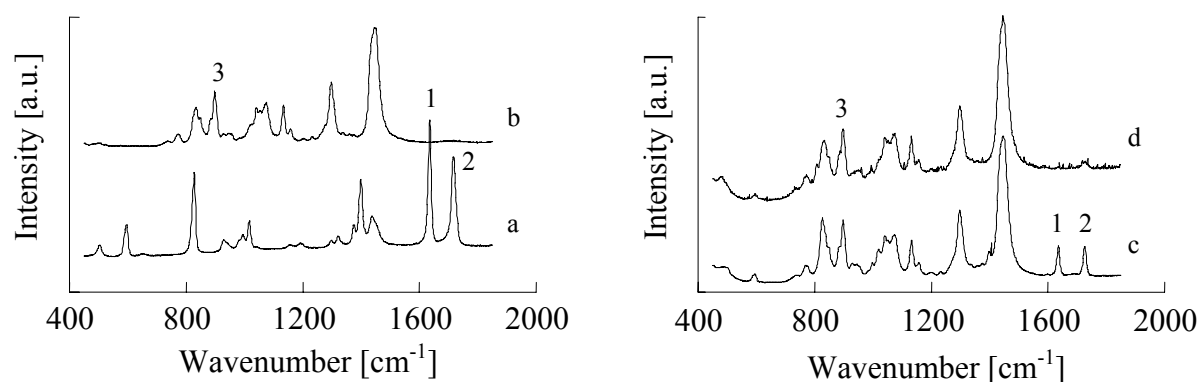


**Figure 2.1:** Raman spectra for (a) MMA, (b) *n*-heptane, (c) complete reaction mixture at the start of the reaction, (d) complete reaction mixture at the end of the reaction: (1) Vinyl-stretch vibration; (2) carbonyl-stretch vibration; (3) internal standard.

Accordingly, the relative intensity of the normalised vinyl-stretch vibration band of MMA at  $1630\text{ cm}^{-1}$  during polymerisation was related to the monomer conversion as follows:

$$X = \left[ 1 - \frac{I_{1630\text{ cm}^{-1}}^{\text{norm}}(t)}{I_{1630\text{ cm}^{-1}}^{\text{norm}}(t=0)} \right] \cdot 100\% \quad (2.1)$$

where  $X$  is the conversion of the vinyl bonds,  $I_{1630\text{ cm}^{-1}}^{\text{norm}}(t)$  is de instantaneous normalised intensity of the vinyl-stretch band, and  $I_{1630\text{ cm}^{-1}}^{\text{norm}}(t=0)$  is de normalised intensity of the vinyl-stretch band at the start of the polymerisation. The results are displayed in Figure 2.2 and are in good agreement with gravimetric and GC data. The conversion-time curve exhibits features that are typical for a dispersion polymerisation, like an initial acceleration in the polymerisation rate shortly after the inhibition period together with a tailing-off at rather high conversions.<sup>10</sup> Here, the inhibition period was deliberately introduced in order to prolong the time for equilibration of the spectrum at reaction temperature (see experimental section).

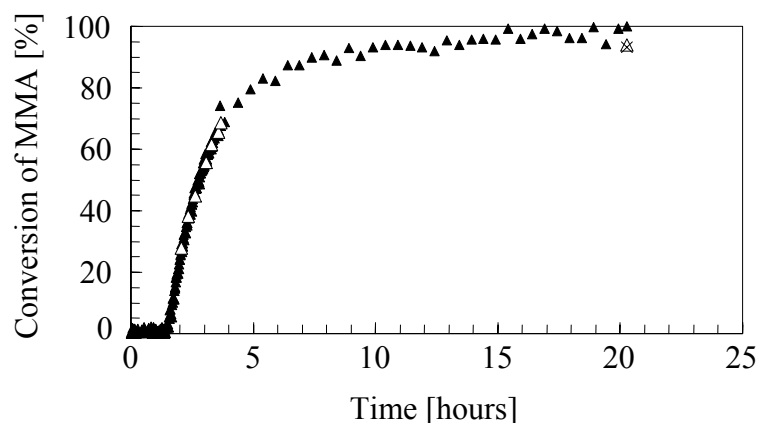


**Figure 2.2:** Total monomer conversion as a function of time for the homopolymerisation of MMA: (▲) On-line Raman data; (△) off-line gravimetric data; (x) off-line GC data.

The fast rate of the dispersion polymerisation of MMA is in agreement with models for the dispersion polymerisation of linear polymers like MMA, proposing competition between solution polymerisation in the continuous phase and micro-bulk polymerisation within the monomer-swollen particles.<sup>11,18,46</sup>

From Figures 2.1c and d it is deduced that during the homopolymerisation of MMA the intensity of the normalised carbonyl-stretch band at  $1730\text{ cm}^{-1}$  decreases with the intensity of the normalised vinyl-band stretch vibration. The spectra reveal that no noticeable shift of this band takes place during reaction. Therefore, apart from the vinyl band itself, also the  $1730\text{ cm}^{-1}$  band can be related to monomer conversion.<sup>47</sup> This might be useful in the copolymerisation of MMA and another monomer. In Figure 2.3 the instantaneous intensity of the normalised carbonyl-stretch band divided by the intensity at zero conversion is depicted as a function of the conversion.

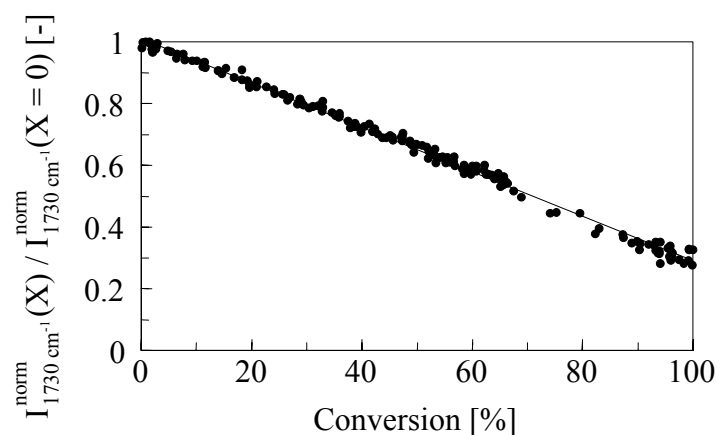


**Figure 2.3:** Relative normalised area of the MMA carbonyl-stretch band as a function of the monomer conversion (●). The solid line is a linear fit of the experimental data.

A linear relationship is found between the relative normalised integrated band area and the monomer conversion, which can be written in the following form:

$$\frac{I_{1730\text{ cm}^{-1}}^{\text{norm}}(X)}{I_{1730\text{ cm}^{-1}}^{\text{norm}}(X=0)} = 1 - A \cdot X \quad (2.2)$$

where  $I_{1730\text{ cm}^{-1}}^{\text{norm}}(X)$  is the instantaneous normalised intensity of the carbonyl band,  $I_{1730\text{ cm}^{-1}}^{\text{norm}}(X=0)$  is the normalised intensity of the carbonyl band at the start of the polymerisation, and  $A$  is a linear fit constant. The interpretation of Figure 2.3 is, that the C=O stretching vibration of the carbonyl bond of the MMA monomer becomes strongly restricted when the monomeric block becomes incorporated into the polymer chain. The linear fit constant  $A$  is a measure for this restriction and is found to be equal to 0.719.

### 2.3.2 The homopolymerisation reaction of divinylbenzene

The polymerisation of technical-grade DVB was initially monitored by Raman spectroscopy and performed in dioxane, as the DVB spectrum showed too much overlap with the spectrum of *n*-heptane (see Figure 2.4). The C-O-C stretching band of dioxane at 1100  $\text{cm}^{-1}$  was chosen as the internal standard.

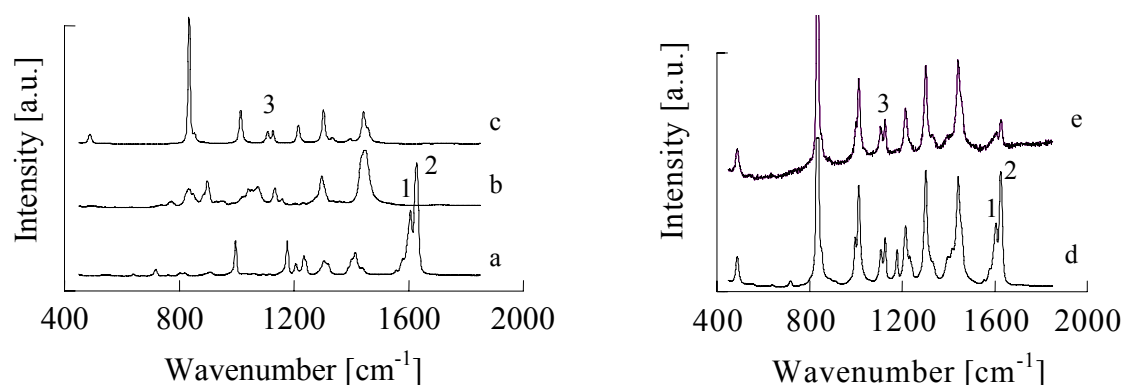


**Figure 2.4:** Raman spectra for (a) DVB mixture, (b) *n*-heptane, (c) dioxane, (d) complete reaction mixture at the start of the reaction, (e) complete reaction mixture at the end of the reaction: (1) Aromatic ring stretch vibration; (2) vinyl-stretch vibration; (3) internal standard.

During polymerisation the normalised vinyl-stretch band of the aromatic monomers at 1630  $\text{cm}^{-1}$  was monitored. Again, a decrease of this band was observed during polymerisation. However, in this case the decrease of the vinyl band could not be appropriately related to conversions, as the DVB mixture contains different types of vinyl

bonds with probably different absorption coefficients. Therefore, alternative techniques were employed to detect monomer conversion during polymerisation of the crosslinker mixture.

Accordingly, another homopolymerisation of DVB55 was performed in *n*-heptane, using a recipe similar to the one that was used for the MMA homopolymerisation (Table 2.2a and b). The total monomer conversion was determined by use of gravimetric analysis (Figure 2.5).

In the next section GC is utilised as an alternative experimental technique to trace the conversions of the individual monomeric components during the copolymerisation reaction between MMA and DVB55.

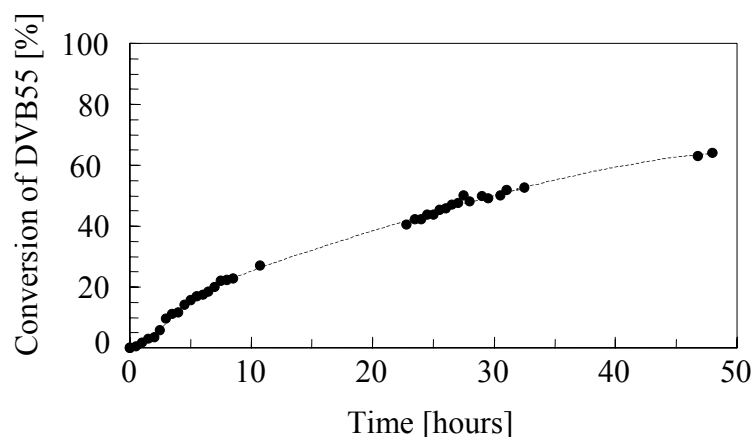


**Figure 2.5:** Total monomer conversion as a function of time for the homopolymerisation of DVB55: (●) Off-line gravimetric data. The broken line is drawn to guide the eye.

When comparing Figure 2.5 (homopolymerisation DVB55) with Figure 2.2 (homopolymerisation MMA) it is obvious that the polymerisation kinetics is significantly slower for the DVB homopolymerisation. The polymerisation kinetics as shown in Figure 2.5 points to only a very weak initial autoacceleration effect. Summarising, the polymerisation rate decreases in time and the conversion asymptotically reaches a plateau, which is consistent with solution polymerisation kinetics. This supports the model, which proposes that for highly crosslinked, non-swellable particles the locus of polymerisation is primarily within the continuous phase and that, consequently, growth of the dense particles mainly occurs through deposition of oligomeric or polymeric chains onto the existing particle surfaces.<sup>35,48</sup>

### 2.3.3 The copolymerisation reaction of methyl methacrylate and divinylbenzene

The copolymerisation reaction between MMA and DVB55 is very complex as each individual component of the multi-monomer system has its own particular reactivity towards



the other reagents. For instance, MMA has different reactivities towards the two DVB isomers *m*-divinylbenzene and *p*-divinylbenzene.<sup>49</sup>

In Figure 2.6 the conversions of MMA and DVB55 are displayed as a function of polymerisation time (see Table 2.2c for recipe). In Figure 2.7 the DVB55 conversion is resolved into the conversions of the individual compounds. Here, it has to be noted that it was not possible to completely separate the peaks of the para and meta isomers in the gas chromatograph. The small partial overlapping of the peaks might have caused some experimental deviations.

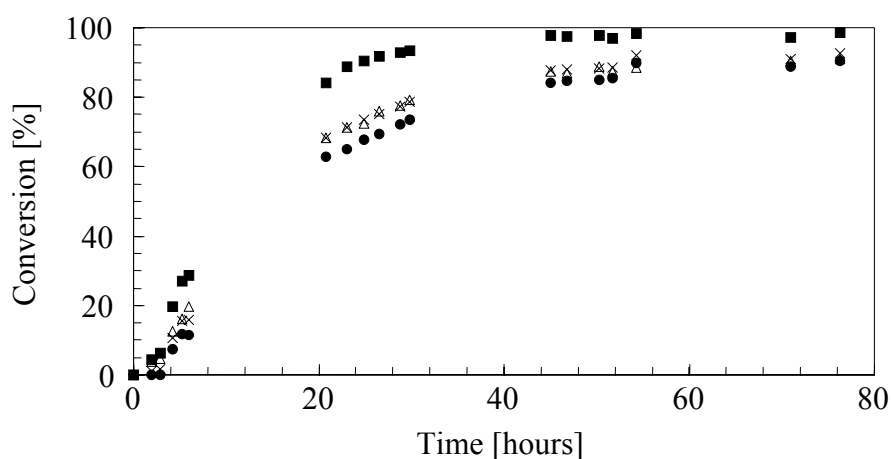


**Figure 2.6:** Monomer conversion as a function of polymerisation reaction time according to GC and gravimetric analysis: (●) MMA conversion; (■) DVB55 conversion; (x) total monomer conversion according to GC; (Δ) total monomer conversion according to gravimetric analysis.

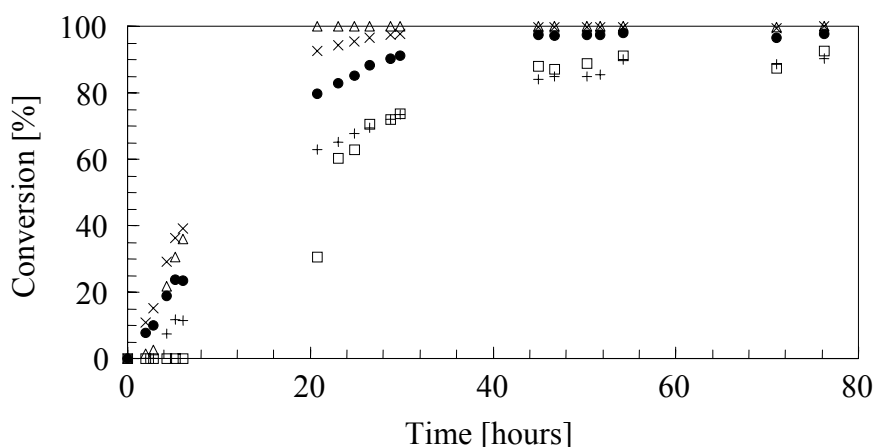


**Figure 2.7:** Conversion of the DVB55 components and MMA as a function of polymerisation reaction time according to GC: (Δ) *p*-DVB; (x) *m*-DVB; (●) *m*-EVB; (□) *p*-EVB; (+) MMA.

Figure 2.6 shows that the GC results are in fairly good agreement with the gravimetric data. The conversion versus time profile is indicative of a polymerisation rate that is intermediate to the polymerisation rates of the individual MMA and DVB55 homopolymerisations (see Figures 2.2 and 2.5). From this it is concluded that, with respect to the MMA homopolymerisation, particle growth via solution polymerisation becomes more pronounced upon participation of DVB55 in the polymerisation reaction.

According to the individual conversion curves of MMA and the DVB and EVB isomers in Figure 2.7, the most reactive monomer is *p*-DVB, followed by *m*-DVB, *m*-EVB and *p*-EVB. This is consistent with previous findings.<sup>37,40</sup> The reactivity of MMA is found to be approximately comparable to the reactivity of the latter EVB isomer. As the two DVB isomers exhibit higher radical reactivities than the EVB isomers and MMA, it is anticipated that the crosslinkers will predominantly exist in the particle cores, while the particle surfaces will contain less crosslinking agent and primarily consist of precipitated linear chains.<sup>37,50</sup>

Figure 2.7 is in agreement with expectations that arise from a theoretical analysis of the reaction between MMA and DVB isomers (Figure 2.8). For high levels of MMA in the starting monomer mixture a composition drift will occur, which leads to the formation of polymers with an increasing level of MMA building blocks.

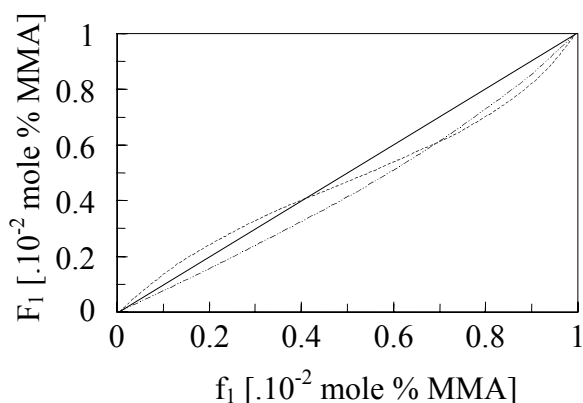


**Figure 2.8:** Fraction of MMA in the copolymer,  $F_1$ , as a function of the fraction of MMA in the monomer feed,  $f_1$ , for the copolymerisation of MMA and *p*-DVB (---) and the copolymerisation of MMA and *m*-DVB (- -), as calculated from the corresponding reactivity ratios. The straight solid line fits the equation  $F_1 = f_1$ .

Elsewhere, it has been reported that the reactivity of the vinyl groups of divinylbenzene decreases when they become pendant vinyl groups.<sup>42</sup> This would give a strongly decreasing crosslinking rate in time, which is in line with other experimental observations.<sup>40</sup> This feature was previously explained in terms of local concentration of pendant groups and accessibility. At the start of the reaction the consumption of the second double bonds of DVB is favoured, due to their relatively high, local concentrations within the zone of the growing chain. At higher conversion, the pendant vinyl groups become less

accessible due to the densification of the surrounding network and, consequently, their consumption will be restricted.<sup>40,42,51,52</sup>

Figures 2.6-2.8 clearly suggest the presence of a composition gradient within the polymer colloids. For the purpose of obtaining perfectly refractive index-matched copolymer particles, it would be preferred for the composition of the copolymer to be identical to the composition of the monomer feed. Perhaps the desired copolymer composition is more closely approached by a more appropriate tuning of the composition of the monomer feed, thereby compensating for the composition drift. To what extent the presence of a composition gradient affects the optical properties of colloidal dispersions in an LC will be illustrated later in Chapter 4.

Furthermore, it is seen from Figure 2.6 that unequal and incomplete monomer conversions were obtained of 98.5 % and 90.4 % for DVB55 and MMA, respectively. Under the present circumstances, higher and more similar monomer conversions would probably be more readily achieved via an extension of the polymerisation reaction time. Another option is a change in polymerisation conditions, as is dealt with in the next section.

### 2.3.4 Effect of polymerisation parameters on particle size and conversion

The influence of the monomer concentration on the average diameter of the particles and monomer conversion, obtained after 47 hours of polymerisation, is displayed in Figure 2.9. From Figure 2.9b it is seen that the conversion after 47 hours of polymerisation increases somewhat with monomer concentration. This is consistent with the general kinetics of a free-radical dispersion polymerisation, which predicts an increase in polymerisation rate with increasing monomer concentration.<sup>10</sup>

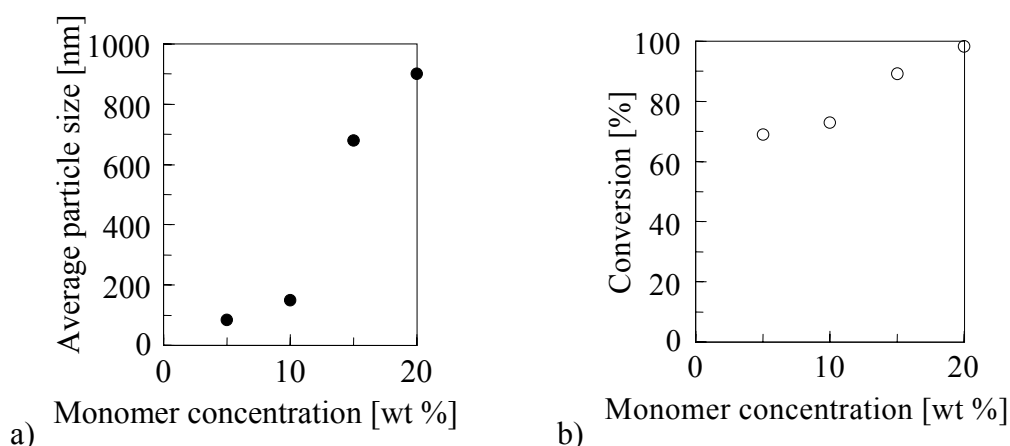


**Figure 2.9:** (a) Average particle size and (b) monomer conversion as a function of monomer concentration for dispersion polymerisation reactions performed according to the recipe of Table 2.1 (stabiliser concentration = 2 g.l<sup>-1</sup>).

Figure 2.9a clearly shows that the average particle size sharply increases with increasing monomer concentration. This is in agreement with previous reports concerning the dispersion polymerisation of methyl methacrylate or styrene<sup>12,20</sup> and arises from an increased solution polymerisation rate and, thus, an increased precipitation rate of oligomer chains.<sup>24</sup> Also, the amount of monomer in the medium has a strong effect on particle size via the solubilising power of the medium. Firstly, at higher levels of monomer, the solubilising power of the medium for the polymer formed is significantly improved.<sup>12,13</sup> This ensures that the oligomeric nuclei or radicals grow to a larger critical size before precipitation occurs via a self- and/or aggregative nucleation process, thereby favouring the formation of less numerous and larger particles.<sup>11</sup> Secondly, as also the stabiliser becomes more soluble, the affinity for the particle nuclei is reduced, and the nuclei can grow via coalescence into larger particles.<sup>24</sup>

When sufficient mature particles are formed which can capture all the radicals and nuclei in the continuous phase, no more particles will be formed and the particle nucleation stage is completed. This implies that larger particles with a lower surface to volume ratio promote secondary nucleation, as the oligomer radicals have more potential to form nuclei themselves than being captured by existing particles.<sup>11</sup> This extension of the particle formation stage thus allows a significant broadening of the particle size distribution. Indeed, it was observed that at high monomer concentrations of 15 and 20 wt % the particle size distribution was pronouncedly broader and smaller particles existed next to the larger particles. When 5 or 10 wt % monomer was used, smaller particles resulted of more uniform size. In Table 2.4 the results are listed of particle sizing measurements conducted with the particle dispersions in *n*-heptane.

**Table 2.4:** Characteristics of the weight and volume distributions obtained by use of particle size measurements for particles that were prepared via dispersion polymerisations started from various monomer concentrations.

Monomer concentration [wt %]	5	15	20
$\bar{d}$ [nm]	164 <sup>a</sup>	789 <sup>b</sup> (737) <sup>c</sup>	938 <sup>b</sup> (879) <sup>c</sup>
S.D. [nm]	17.0 <sup>a</sup>	203 <sup>b</sup>	458 <sup>b</sup>
C.V. <sup>d</sup> [%]	10.4 <sup>a</sup>	25.7 <sup>b</sup>	48.8 <sup>b</sup>

<sup>a</sup> Photon correlation spectroscopy

<sup>b</sup> Laser light scattering

<sup>c</sup> Surface area-weighted mean particle diameter (laser light scattering)

<sup>d</sup> C.V. (coefficient of variation) = S.D./  $\bar{d}$

For the larger particles in particular the surface area-weighted average particle diameter was found to be in good agreement with the particle diameter obtained via (E)SEM investigations (Table 2.4 and Figure 2.9a). For the smallest particles a much larger average

diameter was obtained via the particle sizing measurements in comparison to the electron microscopy results, which points to the occurrence of agglomeration.

Apart from monomer concentration, the stabiliser concentration also affects the course of the polymerisation reaction. An increase in stabiliser concentration can cause the following changes: (1) the adsorption rate of the stabiliser is increased, and (2) the viscosity of the continuous phase is increased.<sup>24</sup> These two factors contribute to a reduction of the extent of aggregation, resulting in the formation of more numerous, smaller particles with narrowed particle size distributions. As is shown in Figure 2.10a, especially in the low stabiliser concentration range the effect of stabiliser on particle size is very strong. However, a too drastic lowering of the stabiliser concentration down to 0.5 g.l<sup>-1</sup> was found to lead to instability phenomena. Figure 2.10a shows a reciprocal relation between particle size and stabiliser concentration, which fits the equation  $d = Kc^{-0.6}$ , where  $c$  is the stabiliser concentration,  $d$  the particle diameter and  $K$  a constant equal to 274. This experimental relationship with a coefficient  $c^{-0.6}$  has been found before.<sup>11</sup>

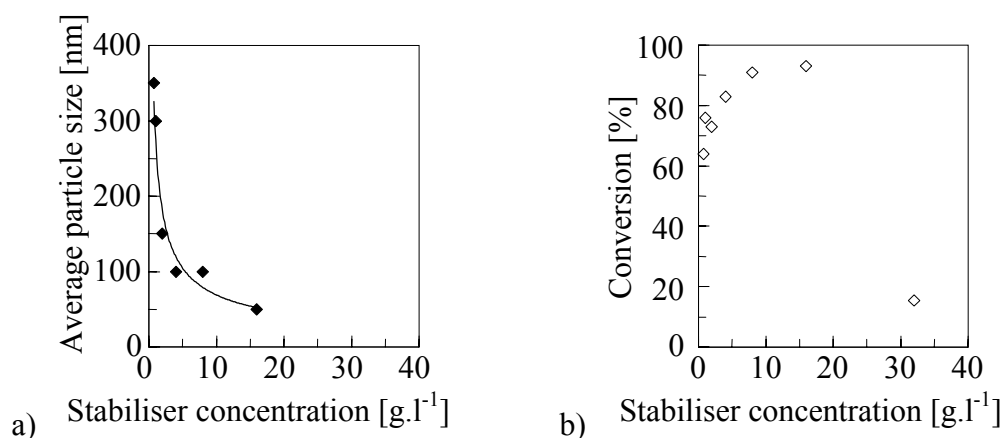
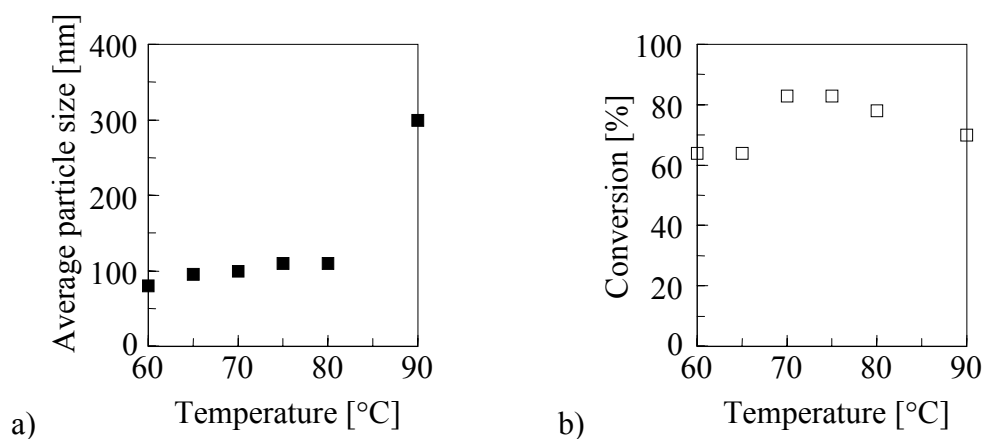


**Figure 2.10:** (a) Average particle size and (b) monomer conversion as a function of stabiliser concentration for dispersion polymerisation reactions performed according to the recipe of Table 2.1. The data of Figure 2.10a are fitted with the equation  $d = Kc^{-0.6}$ .

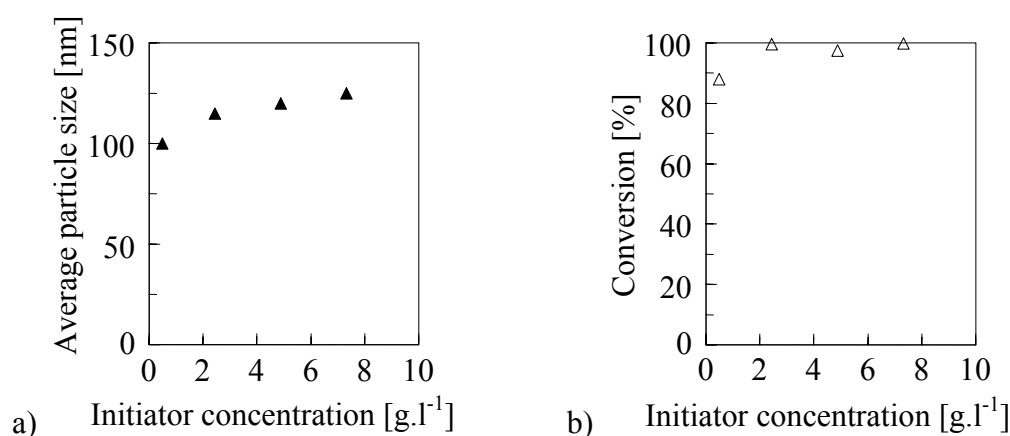
The larger particles obtained at lower stabiliser concentration were found to exhibit somewhat broader particle size distributions than the smaller particles that were obtained at higher levels of stabiliser. Furthermore, the conversion is found to increase with increasing stabiliser concentration (Figure 2.10b). This phenomenon might be attributed to the dependence of medium viscosity on stabiliser concentration. In case of a higher medium viscosity, caused by higher levels of stabiliser, the termination reaction between growing chains might be hampered, resulting in an increased polymerisation rate. At the extremely high stabiliser concentration of 32 g/l the viscosity of the dispersion was observed to be extremely high, thus hampering all mixing phenomena and explaining the outlying data point.

An increase in the polymerisation temperature can cause the following changes leading to larger particles: (1) the solubilising power of the medium is increased, (2) the concentration of precipitated oligomer chains is increased due to an increase in both the decomposition rate of the initiator and the propagation rate of oligomeric radicals, (3) the solubility of the stabiliser in the medium is increased and (4) the viscosity of the continuous phase is decreased.<sup>13,24,27</sup>

That the effect of temperature is not so pronounced can be extracted from Figure 2.11a. Only at a rather high polymerisation temperature of 90 °C, a significant increase in particle size is observed. With respect to monomer conversion, optimum reaction temperatures of 70-80 °C are found (Figure 2.11b). Probably, at lower and higher temperatures problems arise due to a too low or too high decomposition rate of the initiator.

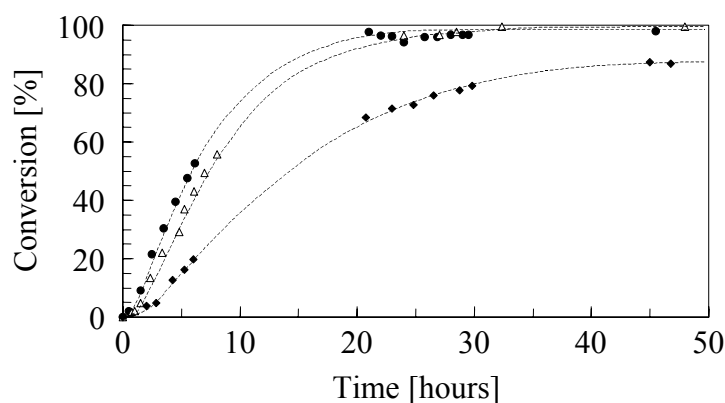


**Figure 2.11:** (a) Average particle size and (b) monomer conversion as a function of temperature for dispersion polymerisation reactions performed according to the recipe of Table 2.1.



**Figure 2.12:** (a) Average particle size and (b) monomer conversion as a function of initiator concentration for dispersion polymerisation reactions performed according to the recipe of Table 2.1.

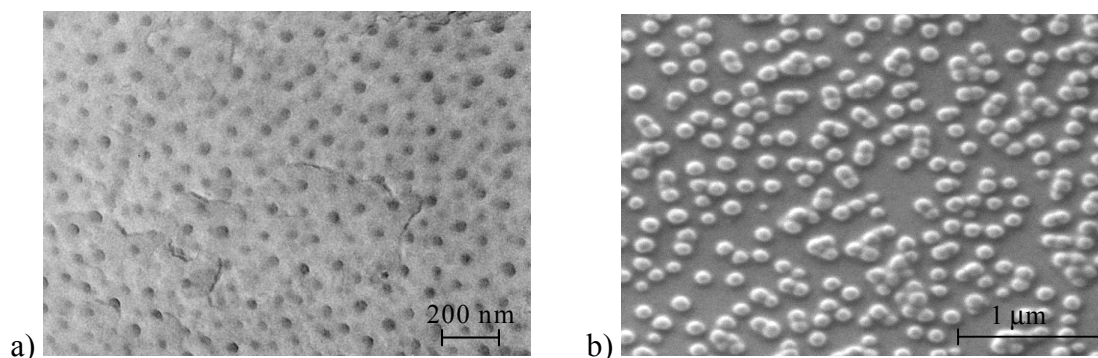
The free-radical polymerisation process is initiated by the decomposition of the initiator at elevated temperatures. The free radicals grow in the continuous phase by addition of monomeric units. With increasing concentration the radical concentration and, thus, the concentration of growing oligomer chains increases. Therefore, the time for the oligomers to reach the critical chain length is extended. This leads to a lower number of particles, but with larger size.<sup>25</sup> Figure 2.12a displays a very weak relationship between initiator concentration and particle size. Under the present circumstances, in all cases rather small particles were obtained with narrow size distributions. From Figure 2.13 a proportional increase of the polymerisation rate with the square root of the initiator concentration can be derived.



**Figure 2.13:** Total monomer conversion (according to GC) as a function of time for free-radical polymerisations with various initiator concentrations: ( $\blacklozenge$ )  $0.5 \text{ g.l}^{-1}$ ; ( $\triangle$ )  $2.5 \text{ g.l}^{-1}$ ; ( $\bullet$ )  $5.0 \text{ g.l}^{-1}$ . The broken lines are drawn to guide the eye.

### 2.3.5 Examples of the particle morphology

With dispersion polymerisation in *n*-heptane poly(methyl methacrylate-*co*-divinylbenzene) colloids were obtained with uniform sizes ranging from approximately 25 nm to 1.2  $\mu\text{m}$ . A few examples of particle morphologies are shown in Figure 2.14. In Table 2.5 the corresponding particle size characteristics are listed. Particle densities, which were estimated via gravimetrical analysis were generally found to be in between  $1.0$  and  $1.1 \text{ g.ml}^{-1}$ .



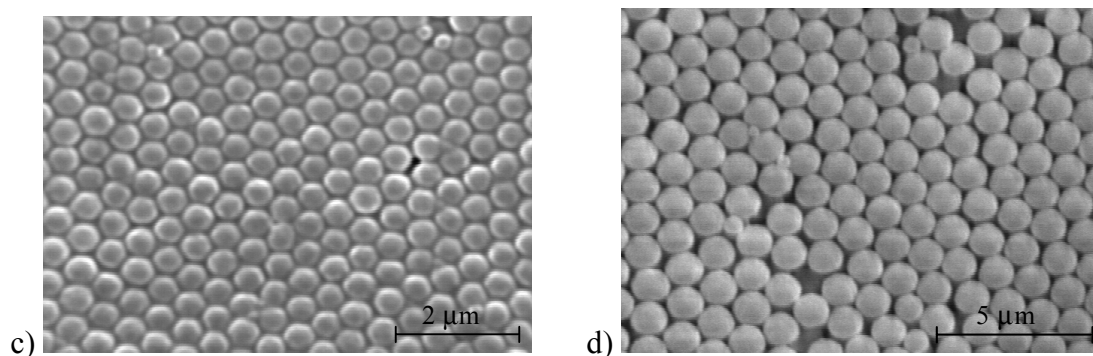


**Figure 2.14:** Some examples of the morphology of poly(methyl methacrylate-co-divinylbenzene) particles that were obtained by dispersion polymerisation in *n*-heptane according to the recipes listed in Table 2.5: (a) TEM micrograph of 27 nm sized particles; (b) ESEM micrograph of 100 nm sized particles; (c) SEM micrograph of 630 nm sized particles; (d) SEM micrograph of 1.2  $\mu\text{m}$  sized particles.

**Table 2.5:** Recipes for the preparation of refractive index matched poly(methyl methacrylate-co-divinylbenzene) colloids of Figure 2.14 together with the results of the particle sizing measurements.

Parameter	(a)	(b)	(c)	(d)
Monomer concentration [wt %]	1	10	20	15
Stabiliser concentration [ $\text{g}\cdot\text{l}^{-1}$ ]	20	8	3	1
Initiator concentration [ $\text{g}\cdot\text{l}^{-1}$ ]	0.5	0.5	0.5	0.5
Temperature [ $^{\circ}\text{C}$ ]	70	70	70	80
Mean particle diameter	27 <sup>a</sup>	100 <sup>a</sup>	630 <sup>a</sup>	1180 <sup>a</sup>
$\bar{d}$ [nm]	-	230 <sup>b</sup>	634 <sup>c</sup> (593) <sup>d</sup>	1231 <sup>c</sup> (1177) <sup>d</sup>
S.D. [nm]	-	35.1 <sup>b</sup>	143 <sup>c</sup>	259 <sup>c</sup>
C.V. [%]	-	15.2 <sup>b</sup>	22.6 <sup>c</sup>	21.0 <sup>c</sup>

<sup>a</sup> According to ESEM, SEM or TEM investigations

<sup>b</sup> Photon correlation spectroscopy

<sup>c</sup> Laser light scattering

<sup>d</sup> Surface area-weighted mean particle diameter (laser light scattering)

From Table 2.5 it is seen that the particle size data are in good agreement with the electron microscopy results. Only for the extremely small particles of Figure 2.14a a much larger diameter was obtained via the particle sizing measurements than via electron microscopy investigations, which again points to agglomeration in the organic medium. The smaller particles were produced by using extremely high loads of stabiliser in combination with a very low monomer concentration (Table 2.5a). It was commonly experienced that the production of particles with sizes smaller than 100 nm under this kind of extreme



polymerisation conditions was accompanied with several difficulties, such as low monomer conversions and extremely high medium viscosities. Moreover, the TEM photograph of Figure 2.14a visualises the appearance of ‘soft’ particles, which is an indication that the small particles mainly consist of stabiliser.

### 2.3.6 Emulsion polymerisation

To extend the range of available particle sizes to smaller sizes ( $< 100$  nm) with a high control over morphology, additional emulsion polymerisations were performed. The aim of the emulsion polymerisation was to generate small particles with the desired properties, e.g. non-swellable in an organic medium and compatible with an LC medium.

Via the recipe of Table 2.3, particles were successfully obtained with an average size of approximately 43 nm (Figure 2.15 and Table 2.6). The monomer conversion was measured in-situ during the polymerisation reaction by gravimetric analysis and was found to be equal to 92.5 % after 1 hour. After 2 hours of polymerisation the reaction was terminated and a conversion of 96.2 % was achieved. This high monomer conversion points to the formation of highly crosslinked particles.

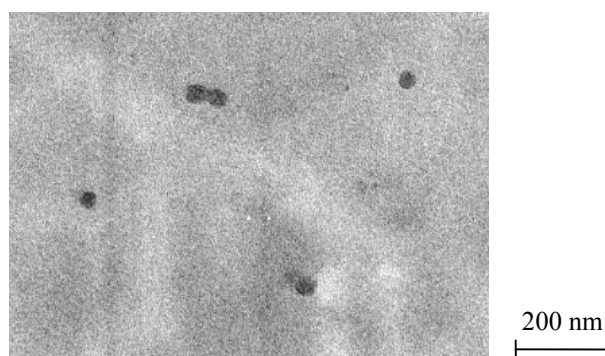


**Figure 2.15:** *TEM micrograph of poly(methyl methacrylate-co-divinylbenzene) particles that were obtained by emulsion polymerisation in aqueous medium according to the recipe listed in Table 2.3.*

**Table 2.6:** *Results of the particle sizing measurements by photon correlation spectroscopy.*

$\bar{d}$ [nm]	42.9
S.D. [nm]	10.8
C.V. [%]	25.2

## 2.4 Conclusions

For the free-radical dispersion polymerisation of MMA in *n*-heptane a fast polymerisation rate was found, which is indicative of a combination of solution

polymerisation in the continuous phase and micro-bulk polymerisation within the monomer-swollen particles. Upon the additional use of DVB55 as a crosslinker mixture the polymerisation kinetics was significantly slowed down, pointing to a shift in polymerisation locus from the particle phase towards the continuous phase. Consequently, growth of the densely crosslinked particles probably occurs through precipitation of oligomeric chains onto the existing particle surfaces. The incorporation of the crosslinkers preferentially takes place at the start of the copolymerisation reaction. This implies that the particle cores consist of more highly crosslinked material than the particle shells.

Via free-radical dispersion polymerisation in *n*-heptane 'hard', poly(styrene-*b*-[ethylene-*co*-propylene]) stabilised poly(methyl methacrylate-*co*-divinylbenzene) particles were successfully produced in uniform sizes ranging from 100 nm up to 1.2  $\mu$ m. It was demonstrated that within the free-radical dispersion polymerisation process the size of the particles is reasonably well controlled by an appropriate fine-tuning of polymerisation parameters. However, in case the dispersion polymerisation was performed under conditions that favoured the formation of larger particles, the particles formed usually exhibited a broader size distribution. This was attributed to the introduction of secondary nucleation phenomena. Under the more extreme polymerisation conditions such as high monomer or stabiliser concentrations, problems were encountered with, for instance, coagulation and extremely high medium viscosities.

Via emulsion polymerisation in aqueous media the range of available particle sizes was successfully extended to smaller particles sizes via the production of 43 nm sized, sterically stabilised particles.

## 2.5 References

- (1) Horak, D. *Acta Polym.*, **1996**, *47*, 20-28.
- (2) Gilbert, R.G., Russell, G.T. *Emulsion polymerization: a mechanistic approach*, Academic Press, London, **1995**.
- (3) Cheng, C.M., Micale, F.J., Vanderhoff, J.W., El-Aasser, M.S. *J. Polym. Sci., Part A*, **1992**, *30*, 235-244.
- (4) Kim, J.W., Ryu, J.H., Suh, K.D. *Colloid Polym. Sci.*, **2001**, *279*, 146-152.
- (5) Ogino, K., Sato, H., Tsuchiya, K., Suzuki, H., Moriguchi, S. *J. Chromatogr., A*, **1995**, *699*, 59-66.
- (6) Okubo, M., Katayama, Y., Yamamoto, Y. *Colloid Polym. Sci.*, **1991**, *269*, 217-221.
- (7) Shen, S., El-Aasser, M.S., Dimonie, V.L., Vanderhoff, J.W., Sudol, E.D. *J. Polym. Sci., Part A*, **1991**, *29*, 857-867.
- (8) Tuncel, A. *J. Appl. Pol. Sci.*, **1999**, *71*, 2291-2302.
- (9) Ugelstad, J., et al. *J. Polym. Sci.-Polym. Symp.*, **1985**, 225-240.
- (10) Barrett, K.E.J., Thomas, H.R. *J. Polym. Sci., Part A*, **1969**, *7*, 2621-2650.
- (11) Barrett, K.E.J. *Dispersion polymerization in organic media*, Wiley Interscience, London, **1975**.
- (12) Paine, A.J., Luymes, W., McNulty, J. *Macromolecules*, **1990**, *23*, 3104-3109.
- (13) Shen, S., Sudol, E.D., El-Aasser, M.S. *J. Polym. Sci., Part A*, **1993**, *31*, 1393-1402.
- (14) Almog, Y., Reich, S., Levy, M. *Br. Polym. J.*, **1982**, *14*, 131-136.

- (15) Lok, K.P., Ober, C.K. *Can. J. Chem.*, **1985**, *63*, 209-216.
- (16) Fitch, R.M., Kamath, Y.K. *J. Colloid Interface Sci.*, **1976**, *54*, 6-12.
- (17) Antl, L., et al. *Colloids Surf.*, **1986**, *17*, 67-78.
- (18) Lu, Y.Y., El-Aasser, M.S., Vanderhoff, J.W. *J. Polym. Sci., Part B*, **1988**, *26*, 1187-1203.
- (19) Tseng, C.M., Lu, Y.Y., El-Aasser, M.S., Vanderhoff, J.W. *J. Polym. Sci., Part A*, **1986**, *24*, 2995-3007.
- (20) Bamnolker, H., Margel, S. *J. Polym. Sci., Part A*, **1996**, *34*, 1857-1871.
- (21) Ober, C.K., Lok, K.P., Hair, M.L. *J. Polym. Sci., Part C*, **1985**, *23*, 103-108.
- (22) Paine, A.J., Deslandes, Y., Gerroir, P., Henrissat, B. *J. Colloid Interface Sci.*, **1990**, *138*, 170-181.
- (23) Williamson, B., Lukas, R., Winnik, M.A., Croucher, M.D. *J. Colloid Interface Sci.*, **1987**, *119*, 559-564.
- (24) Shen, S., Sudol, E.D., El-Aasser, M.S. *J. Polym. Sci., Part A*, **1994**, *32*, 1087-1100.
- (25) Bulmus, V., Tuncel, A., Piskin, E. *J. Appl. Pol. Sci.*, **1996**, *60*, 697-704.
- (26) Winnik, M.A., Lukas, R., Chen, W.F., Furlong, P., Croucher, M.D. *Makromol. Chem.-Macromol. Symp.*, **1987**, *10*, 483-501.
- (27) Baines, F.L., Dionisio, S., Billingham, N.C., Armes, S.P. *Macromolecules*, **1996**, *29*, 3096-3102.
- (28) Dawkins, J.V., Shakir, S.A., Croucher, T.G. *Eur. Polym. J.*, **1987**, *23*, 173-175.
- (29) Cowley, D.R., Price, C., Hardy, C.J. *Polymer*, **1980**, *21*, 1356-1357.
- (30) Dawkins, J.V., Maghami, G.G., Shakir, S.A., Higgins, J.S. *Colloid Polym. Sci.*, **1986**, *264*, 616-618.
- (31) Dawkins, J.V., Shakir, S.A. *Colloid Polym. Sci.*, **1987**, *265*, 329-335.
- (32) Stejskal, J., et al. *Polymer*, **1990**, *31*, 1816-1822.
- (33) Stejskal, J., Kratochvil, P., Konak, C. *Polymer*, **1991**, *32*, 2435-2442.
- (34) Dawkins, J.V., Taylor, G. *Polymer*, **1979**, *20*, 599-604.
- (35) Hattori, M., Sudol, E.D., El-Aasser, M.S. *J. Appl. Pol. Sci.*, **1993**, *50*, 2027-2034.
- (36) Tseng, C.M., Lu, Y.Y., El-Aasser, M.S., Vanderhoff, J.W. *J. Polym. Sci., Part A: Polym. Chem.*, **1986**, *24*, 2995-3007.
- (37) Li, K., Stover, H.D.H. *J. Polym. Sci., Part A*, **1993**, *31*, 2473-2479.
- (38) Thomson, B., Rudin, A., Lajoie, G. *J. Appl. Pol. Sci.*, **1996**, *59*, 2009-2028.
- (39) Thomson, B., Rudin, A., Lajoie, G. *J. Polym. Sci., Part A*, **1995**, *33*, 345-357.
- (40) Cheng, C.M., Vanderhoff, J.W., El-Aasser, M.S. *J. Polym. Sci., Part A*, **1992**, *30*, 245-256.
- (41) Okay, O., Kurz, M., Lutz, K., Funke, W. *Macromolecules*, **1995**, *28*, 2728-2737.
- (42) Malinsky, J., Klaban, J., Dusek, K. *J. Macromol. Sci., Chem.*, **1971**, *5*, 1067-1081.
- (43) Van den Brink, M., Pepers, M., Van Herk, A.M., German, A.L. *Macromol. Symp.*, **2000**, *150*, 121-126.
- (44) Wilderbeek, J.T.A., *Polymer filled nematics for electro-optical applications*, graduation thesis, Eindhoven University of Technology, Eindhoven, **1996**, 1-11.
- (45) Partington, J.R. *An advanced treatise on physical chemistry: physico-chemical optics*, Longmans, Green, London, **1960**.
- (46) Cao, K., Li, B.G., Pan, Z.R. *Colloids Surf., A*, **1999**, *153*, 179-187.
- (47) Pepers, M.L.H., *On-line monitoring and control of emulsion (co)polymerizations of styrene and butyl acrylate using raman spectroscopy*, graduation thesis, Eindhoven University of Technology, Eindhoven, **1999**, 1-47.
- (48) Downey, J.S., Frank, R.S., Li, W.H., Stover, H.D.H. *Macromolecules*, **1999**, *32*, 2838-2844.
- (49) Brandrup, J., Immergut, E.H. *Polymer handbook*, second ed., edited by Brandrup, J. Immergut, E.H., Wiley Interscience, New York, **1974**.
- (50) Walczynski, B., Kolarz, B.N., Galina, H. *Polym. Commun.*, **1985**, *26*, 276-280.
- (51) Leicht, R., Fuhrmann, J. *Polym. Bull.*, **1981**, *4*, 141-148.
- (52) Okay, O., Kaya, D., Pekcan, P. *Polymer*, **1999**, *40*, 6179-6187.

# Chapter 3

## Colloidal dispersions in a liquid crystal

### Phase behaviour, morphology and rheological properties\*

#### 3.1 Introduction

Classical colloidal dispersions in isotropic media show intriguing properties due to specific interactions between the colloids and have been well studied in the past.<sup>1</sup> By exchanging the isotropic dispersion medium by an anisotropic liquid crystal (LC) medium, the interactive behaviour of the dispersed particles is substantially modified. As a result, the particle dispersions in a nematic LC exhibit very distinctive features compared to their isotropic analogues. The peculiar behaviour of single particles immersed in an LC concerning topological defect phenomena has been subjected to a number of theoretical studies during the last years and is nowadays quite well understood.<sup>2-7</sup> Experimental studies that supported the theoretical predictions usually concerned emulsions of an isotropic fluid in a thermotropic LC.<sup>8-11</sup>

A few years ago the first experimental evidence has been brought up for the segregation of a lyotropic LC, doped with small 120 nm sized latex particles, into a particle-rich isotropic phase and a particle-poor nematic phase upon cooling below the isotropic-nematic phase transition.<sup>12</sup> In recent years, more detailed reports have appeared on this typical collective aggregation behaviour and the resulting interesting properties of colloidal dispersions in an LC.<sup>13-16</sup> Generally, these studies were focussed on dispersions of ~200 nm sized poly(methyl methacrylate) spheres in *n*-pentylcyanobiphenyl as LC medium.

This study is focussed on the use of internally crosslinked poly(methyl methacrylate-*co*-divinylbenzene) colloids, immersed in a nematic LC. These colloids distinguish themselves from those previous studies by a refractive index of the dispersed phase that can be adjusted to be equal to the ordinary refractive index ( $n_o$ ) of the LC. Upon electrical addressing of the liquid crystals complete refractive index matching occurs and the optical contrast ratio of these materials during electrical switching processes is improved. This makes these materials interesting candidates for electro-optical applications. Furthermore, it

---

\* Part of this work has been published: Van Boxtel, M.C.W., Broer, D.J., Bastiaansen, C.W.M. *Polym. Prepr.*, **1999**, *40*, 1156-1157; Van Boxtel, M.C.W., Janssen, R.H.C., Broer, D.J., Wilderbeek, J.T.A., Bastiaansen, C.W.M. *Adv. Mater.*, **2000**, *12*, 753-757; Van Boxtel, M.C.W., Janssen, R.H.C., Bastiaansen, C.W.M., Broer, D.J. *J. Appl. Phys.*, **2001**, *89*, 838-842.

is anticipated that the use of crosslinked polymer instead of linear polymer not only promotes the preparation of well-defined polymer/LC materials, but also allows a wide range of temperatures and the use of an additional solvent. This significantly facilitates the handling and processing of the materials.

In this chapter an overview is given of the existing theory on the typical behaviour of LC's doped with spherical particles. Subsequently, LC colloidal dispersions are studied based on internally crosslinked (sub-)micron sized polymer colloids that were synthesised as described in Chapter 2. Next, the LC colloidal dispersions are evaluated on their phase behaviour, morphology and rheological properties.

### 3.2 Theoretical background

When colloidal particles are immersed in a liquid crystal, the orientational order of the surrounding liquid crystal becomes distorted. The extent of this elastic distortion of the LC depends on (1) the bulk deformation energy or elastic distortion energy of the LC ( $F_d$ ), and on (2) the impact of the particle surface on the distortion of the nematic director via the anchoring energy, which arises from the interactions between the particle surface and the surrounding LC molecules ( $F_s$ ). Both contributions add to the one-constant Frank elastic energy as follows:<sup>2,4</sup>

$$F = F_d + F_s = \int \frac{1}{2} K \left[ (\text{div } \hat{\mathbf{n}})^2 + (\text{curl } \hat{\mathbf{n}})^2 \right] d^3 r - \oint \frac{1}{2} W (\hat{\mathbf{n}} \cdot \hat{\mathbf{v}})^2 dS \quad (3.1)$$

where  $\hat{\mathbf{n}}$  represents the nematic director field,  $\hat{\mathbf{v}}$  is the unit vector normal to the surface,  $K$  is the average Frank elastic constant of the LC, and  $W$  is the anchoring energy.

The first effect has a characteristic energy of the order  $KR$ , where  $R$  is the radius of the particle, while the second energy effect approximately equals  $WR^2$ . The ratio of these two energies is expressed by the dimensionless parameter  $WR/K$ .<sup>2-4,8,15</sup> The magnitude of this dimensionless parameter in principle determines the behaviour of the LC colloidal dispersions and one can distinguish between two extreme cases:

**(1)  $WR/K \gg 1$ :** The director anchoring energy is relatively high compared to the bulk deformation energy of the LC, and the director field will deform by the creation of topological defects in the LC matrix. Since the particle surface carries a topological charge of  $N = 1$ , the accompanying topological defect must have a compensatory charge of  $N = -1$ . The type of topological defect that is introduced must satisfy the topological restrictions that are imposed by the director field at infinity and the boundary conditions that apply at the particle surfaces.

For instance, if the LC is confined within a parallel cell, an immersed particle with radial boundary conditions will deform the director field around the particle into a so-called hyperbolic or radial hedgehog (Figure 3.1).<sup>6,8,9</sup> This topological defect includes a point defect at a certain distance separated from the particle.

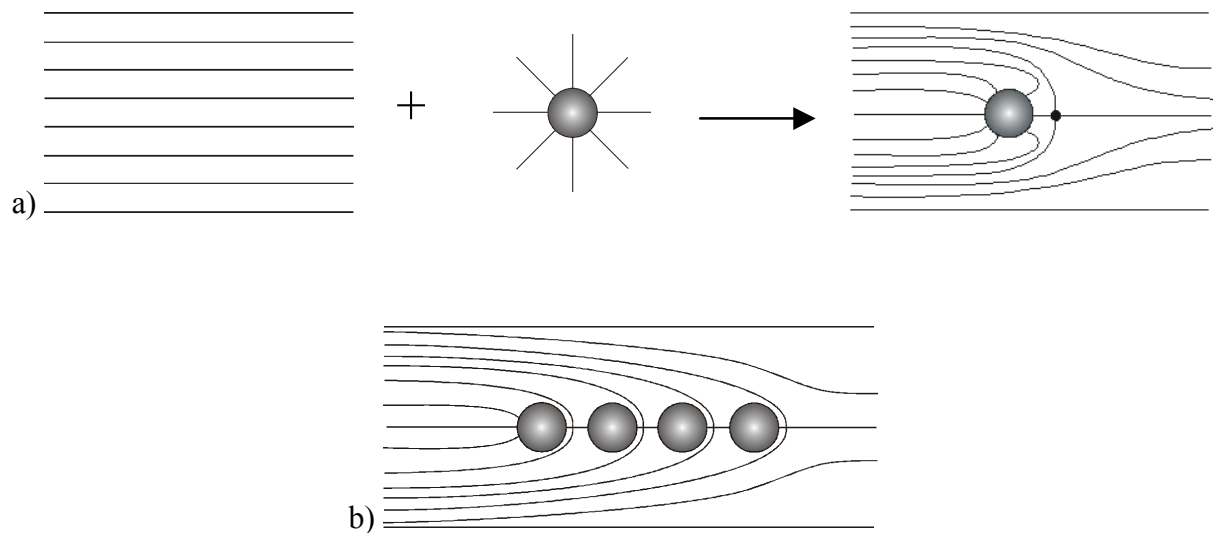


**Figure 3.1:** (a) Schematic representation of a particle with radial anchoring conditions in combination with a unidirectional nematic director field. The topological defect that is formed is known as a hyperbolic hedgehog; (b) the particles with radial anchoring conditions spontaneously assemble into linear chains, which are directed parallel to the alignment axis of the LC.

Another topological defect that also meets the boundary conditions imposed is the so-called Saturn ring, which, however, has been found to be much less stable.<sup>3,6,9</sup>

In case the spherical particle imposes planar orientational behaviour on the surrounding LC molecules, the particle will be accompanied with two point defects at the particle surface, known as boojums (Figure 3.2).<sup>2,8,17,18</sup>

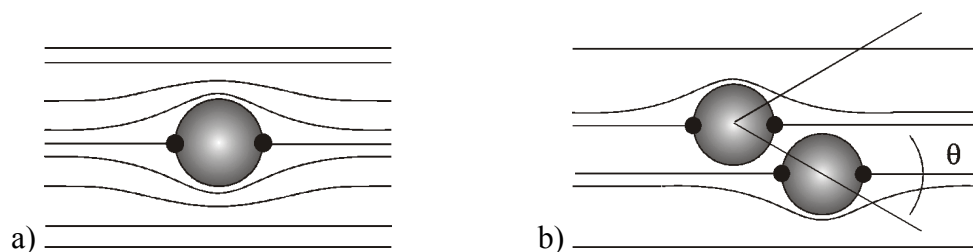


**Figure 3.2:** (a) Schematic representation of the deformed director field around a particle with planar anchoring conditions. Two surface defects, also called boojums, are situated opposite towards each other at the poles of the particle; (b) the particles with planar anchoring conditions feel a maximum attraction force under a specific oblique angle between 30 and 70°.

Although it would be expected that the addition of particles with rigid anchoring conditions causes the system to phase separate on a macroscopic scale into an LC and a colloidal phase, the supply of sufficient thermal or mechanical energy to the system might even enable the dispersion of a low number of particles.<sup>18</sup> The interactions between the resulting disclinations then lead to specific anisotropic interactions between the spherical particles. This causes the formation of peculiar colloidal structures in the LC, which have in fact a metastable character, but which can have a very long lifetime, due to the strong topological stabilisation.<sup>15,18</sup>

The collective behaviour of the colloidal dispersions in an LC is shown in Figures 3.1b and 3.2b. The dipolar character of the particle-defect assemblies as shown in Figure 3.1a causes the formation of linear chainlike colloidal structures (Figure 3.1b). The point defects in between neighbouring particles provide a short-range repulsion force and stabilise the colloids against coalescing.<sup>8-11</sup>

The particle-defect assemblies of Figure 3.2a experience quadrupolar-like interactions. Experimentally, it has been found that these defect structures form rather compact anisotropic colloidal clusters, with an angle of  $\pm 30^\circ$  between the neighbouring particles (Figure 3.2b).<sup>8,17</sup> Earlier, theoretical models predicted maximal attraction forces between the approaching particles for a characteristic angle between  $30$  and  $70^\circ$ .<sup>8</sup> The interparticle potential was predicted to be proportional to  $d^{-5}$ , where  $d$  is the separation between the particles.<sup>2,8,19</sup>

**(2)  $WR/K \ll 1$ :** The bulk deformation energy of the LC prevails over the director anchoring energy and, consequently, the particles only slightly perturb the director field. Thus, in this weak anchoring regime, no topological defects are supposed to be formed upon immersion of spherical particles in the LC. The low elastic energy cost of dispersing the particles in the LC can be easily overcome by the supply of sufficient thermal or mechanical energy to the system. However, in order to minimise the (weak) elastic deformation of the director, the particles are inclined to coalesce into larger clusters.<sup>12,18</sup> Also, whenever the isotropic phase is introduced locally, e.g. in the biphasic regime around the nematic to isotropic phase transition temperature of the LC,  $T_{NI}$ , the system is apt to reduce its free energy by expelling the particles within the coexisting isotropic phase and keeping them there. Consequently, when the system is cooled down from the isotropic phase below  $T_{NI}$ , nematic regions with low colloid concentration nucleate and grow by compacting the colloids in the isotropic phase (Figure 3.3).<sup>13,14</sup>

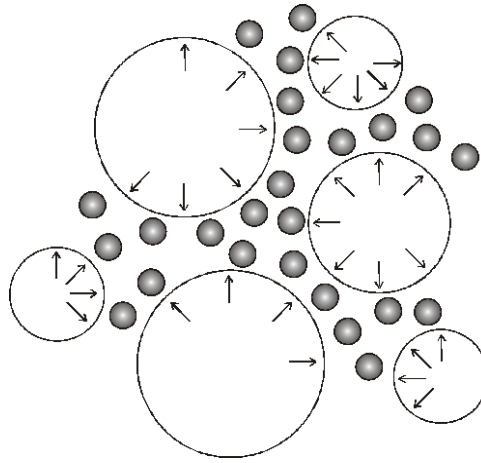


**Figure 3.3:** *During cooling down the isotropic-nematic phase transition the colloidal particles (black spheres) are expelled from the growing nematic phase (growth of the droplets is indicated by the arrows) into the coexisting isotropic phase in order to avoid the extra elastic cost of dispersing the particles in the nematic phase.*

Recent theoretical work has ascribed the occurrence of this phase separation to the fact that the dimensionless parameter  $WR/K$  changes its magnitude in the vicinity of the nematic-to-isotropic phase transition; As the nematic order parameter  $S(T)$  approaches zero, the Frank elastic constant  $K$  ( $\sim S^2$ ) approaches zero faster than the anchoring energy  $W$  ( $\sim S$ ), which may cause the dimensionless parameter  $WR/K$  ( $\sim S^{-1}$ ) to become very large.<sup>15</sup> In this way, even very small particles will enter the topological regime and, therefore, will strongly interfere with the orientational order of the surrounding LC matrix. However, if the material constants are chosen such, that the parameter remains small, even during the phase transition, the system is more likely to homogeneously disperse the spherical inclusions within the LC.

In case the dimensionless parameter remains large deep into the nematic phase, the aggregation behaviour depends on the colloid concentration. At low particle concentration, the particle alignment and the accompanying director profiles are formed as shown in Figures 3.1 and 3.2. At high concentration, the strong interaction forces between the particles promote a rapid aggregation of the particles into three-dimensional aggregates, while at intermediate concentrations the aggregates are bridged by disclinations of the LC. For the network of disclination lines, elastic moduli in the order of 0.01 Pa have been reported.<sup>20</sup>

For particles with weak radial anchoring, the small continuous deformation of the director field was previously described by the director rotation angle  $\beta$ , which was derived from Equation 3.1:<sup>4</sup>

$$\beta = \frac{WR}{4K} \left( \frac{R}{r} \right)^3 \sin 2\theta \quad (3.2)$$



where  $r$  and  $\theta$  are spherical co-ordinates. For the case of strong anchoring ( $WR/K \gg 1$ ) a similar expression can be derived for the more strongly deformed director field around a particle.<sup>2</sup> According to Equation 3.2 the director will indeed only slightly deviate from its uniform orientation ( $\beta \ll 1$ ) when  $WR/K \ll 4$ . Taking typical values for  $K \sim 10^{-11} \text{ J.m}^{-1}$ , then, even when high anchoring energies are presumed ( $W \geq 10^{-5} \text{ J.m}^{-2}$ ) colloidal particles with a radius  $R \ll 3\text{-}4 \mu\text{m}$  fall within the “weak anchoring regime” and can show typical behaviour as sketched in Figure 3.3.<sup>2</sup>

### 3.3 Experimental

#### 3.3.1 Materials

The liquid crystal material used was LC E7 ( $\epsilon'_{\perp} = 5.2$  and  $\epsilon'_{\parallel} = 19$ ,<sup>21</sup>  $n_e = 1.7462$ ,  $n_o = 1.5216$ )<sup>22</sup>, a liquid crystal mixture purchased from Merck Ltd. (Darmstadt, Germany or Poole, England) containing 51% *n*-pentylcyanobiphenyl (5CB), 25% *n*-heptylcyanobiphenyl (7CB), 16% *n*-octyloxycyanobiphenyl (80CB) and 8% *n*-pentylcyanoterphenyl (5CT) (see Figure 3.4).<sup>23-25</sup>

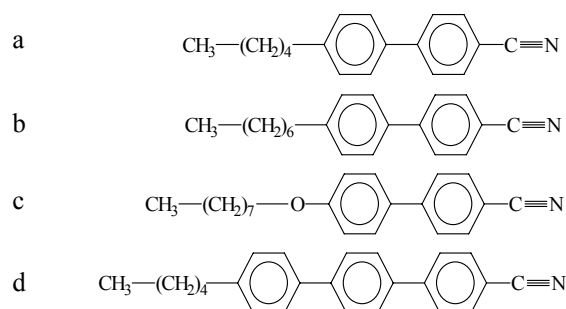


**Figure 3.4:** Chemical structure of LC E7, a mixture of: (a) 5CB; (b) 7CB; (c) 16CB; (d) 5CT.

According to the manufacturer, the density of the LC E7 is approximately equal to  $1.0 \text{ g.ml}^{-1}$ . The poly(methyl methacrylate-*co*-divinylbenzene) particles were prepared as described in Chapter 2.

#### 3.3.2 Preparation of the LC colloidal dispersions

Firstly, a pre-set amount of the LC E7 was added to a pre-set amount of dry poly(methyl methacrylate-*co*-divinylbenzene) colloids. Secondly, an organic solvent was added, usually chloroform. Homogeneous dispersion of the colloids in the medium was achieved via ultrasonic mixing. Then the chloroform was evaporated from the mixture by

drying the sample for 24 hours in a vacuum chamber at room temperature. Next, the dried material was heated into the isotropic phase at 120-150 °C to erase its history and to homogeneously disperse the colloids in the LC continuous phase. After cooling the sample down to room temperature, an LC colloidal dispersion was obtained with an opaque and soft solid-like appearance.

### **3.3.3 Electro-optical cell construction**

Electro-optical cells were prepared from indium tin oxide (ITO) coated glass (Merck, type 327 735 PO), cut into pieces of 3.0 x 3.0 cm. The glass slides were cleaned after which a polyimide precursor solution (AL 1051, JSR Electronics) was spincoated (5 s at 1000 rpm, 40 s at 3500 rpm) at the ITO-side of the glass substrates. After preheating for 10 minutes at 100 °C and 90 minutes baking at 170 °C under vacuum, the polyimide layers were softly rubbed in one direction with a velvet cloth. On one of the plates constituting a cell an ethanol solution containing 6 µm polystyrene spheres was spincoated (45 s at 1000 rpm) to ensure a fixed spacing of the plates. The cells were assembled by mounting two glass slides, of which one was provided with an ultraviolet (UV) curable sealant (UVS 91, Norland Products Inc.), on top of each other. Electro-optical cells with a twisted nematic (TN) configuration were prepared by placing the glass slides such, that the orientation layers on the two substrates were perpendicular. Electro-optical cells with (anti-)parallel aligning boundary conditions were prepared by mounting the glass slides with their orientation layers (anti-)parallel with respect to each other. The cell construction was fixed via UV curing. The constructed cells were filled with the preheated LC colloidal dispersions in the isotropic state by capillary action at 150 °C. After complete filling, the cells were cooled down to room temperature. As soon as the isotropic-nematic transition temperature was passed, the cell turned somewhat opaque, depending on the material composition.

The cells for the confocal laser scanning microscopy studies were prepared in a similar manner, except for the fact that at one side of the cell a thin, polyimide coated microscopy glass slide (without ITO coating) was used with a thickness of approximately 0.17 µm in order to obtain a sufficient resolution to depth ratio. For the other substrate a normal polyimide coated glass slide was used without an ITO coating. The constructed cells were placed on a hot-stage where the thin glass slide was positioned at the top. Subsequently, the cells were filled with the preheated LC colloidal dispersions in the isotropic state by capillary action at 150 °C. In order to promote a homogeneous colloid distribution over the sample thickness, the samples were held by a pair of tweezers and homogeneously cooled in air with the thin glass slide directed upwards.

### 3.3.4 Techniques

#### *Light microscopy (LM)*

The morphology of the LC colloids was examined at temperatures ranging from room temperature to 150 °C with the aid of a Zeiss Universal optical microscope, which was operated in transmission mode and equipped with a Linkam TMS 92 hot-stage. The ordering of the particle-defect assemblies in parallel electro-optical cells was visualised by use of a Zeiss Axioplan 2 optical microscope.

#### *Differential scanning calorimetry (DSC)*

The phase transition temperatures and the heat of fusion at the nematic-isotropic phase transition of the LC colloidal dispersions with different colloid concentrations were studied by use of a Perkin Elmer Pyris 1 DSC. The samples were measured over a temperature range of –110 to 100 °C using heating and cooling rates of 10 °C.min<sup>-1</sup>. Before measurement the filled sample pans were preheated at 140 °C for only a few seconds for homogeneous distribution of the sample materials and for restoring the structure of the composite material.

From the DSC thermographs obtained the change in enthalpy per unit mass at the nematic-isotropic transition temperature,  $\Delta H_{NI}$ , was determined by integrating the area under the peak via a properly selected baseline. The peaks of the transitions were used to detect the corresponding transition temperatures. The incremental specific heat at the glass transition temperature of LC E7,  $\Delta C_p$  (LC) was determined via extrapolation of two baselines from below and above the transition. The glass transition temperature was derived from the extrapolated half  $\Delta C_p$  (LC) value.

#### *Spectroscopy in the ultraviolet-visible (UV-VIS) light region*

The thickness of the constructed cells was measured by use of UV-VIS spectroscopy. From the interference pattern over the 400-800 nm wavelength range the cell thickness was calculated according to:<sup>26</sup>

$$d = \frac{k}{2} \cdot \frac{\lambda_1 \cdot \lambda_2}{(\lambda_1 - \lambda_2)} \quad (3.3)$$

where  $d$  denotes the cell thickness,  $k$  is the number of sequential maxima or minima counted minus 1,  $\lambda_1$  is the wavelength of the first counted maximum or minimum and  $\lambda_2$  is the wavelength of the last counted maximum or minimum.

### Confocal laser scanning microscopy (CLSM)

The morphology of the LC colloidal dispersions confined within cells with parallel or TN configuration was investigated in three dimensions by use of a Zeiss laser scanning microscope (LSM 510). This apparatus employed a pinhole to eliminate the out-of-focus light from planes above and below the focal plane (Figure 3.5). By moving the focal plane along the  $z$ -direction within the sample by pre-set steps of  $0.1\ \mu\text{m}$ , a three-dimensional stack was built up from the single optical slices. The microscope was operated in reflection mode, where the refractive index difference between the colloidal and the LC phase provided the optical contrast. Monochromatic laser light with a wavelength of  $540\ \text{nm}$  was used for illumination of the sample cells. For the focussing of the laser light a plan-apochromat  $63\times/1.4$  oil objective lens was used.

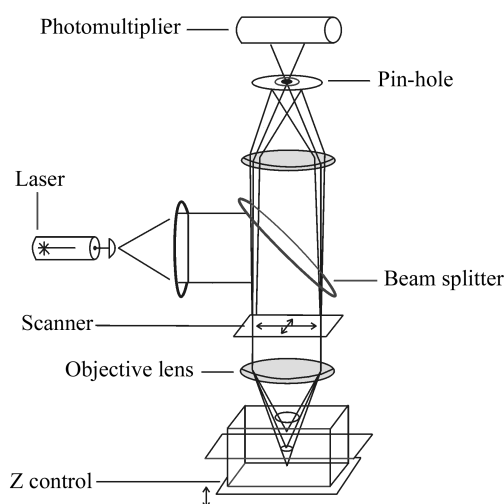


**Figure 3.5:** Operation principle of a confocal laser scanning microscope.

### Thermogravimetric analysis (TGA)

The thermal stability of the LC colloidal dispersions was examined by use of a Perkin Elmer TGA 7. The weight loss of LC colloidal dispersions with different colloid concentrations was measured during heating from  $40$  to  $700\ ^\circ\text{C}$  with a rate of  $10\ ^\circ\text{C}\cdot\text{min}^{-1}$  under an airflow of  $20\ \text{ml}\cdot\text{min}^{-1}$ . Before measurement the sample pans filled with the material were preheated at  $140\ ^\circ\text{C}$  for a few seconds in order to restore the structure of the composite material.

### Rheology

Stationary and dynamic rheological experiments were performed with an Ares Rheometric Scientific laboratory instrument, equipped with two circular, serrated parallel plates with diameters of  $25\ \text{mm}$ . The measurement geometry including the sample was locked up in a temperature-controlled oven. The material was homogenised at an elevated

temperature of  $\sim 140$  °C, was placed between the two plates and was subsequently cooled to 26 °C. The recorded temperature profile ensured that for every sample the isotropic-nematic transition of the LC was passed with a similar rate of  $10$  °C.min<sup>-1</sup>. During cooling, the normal force registered, exerted on the upper plate, was kept constant by carefully readjusting the distance between the plates. Finally, a rheological analysis was performed on the approximately 0.5 mm thick films after it was observed that the normal force remained constant in time. Before each measurement the material was reheated into the isotropic phase in order to erase its deformation history.

## 3.4 Results and discussion

### 3.4.1 Phase behaviour

The phase behaviour of the LC colloidal dispersions was examined with DSC. Figures 3.6 and 3.7 show the DSC thermographs of the LC E7 and LC dispersions based on various fractions of 630 nm sized colloids. Although it is not clearly seen from Figures 3.6 and 3.7, apart from the glass transition and the nematic-isotropic transition of the LC E7 another small peak was observed around  $-18$  °C. This peak is commonly ascribed to the crystalline-nematic transition,  $T_{CN}$ , of the LC E7.<sup>22</sup> The DSC thermographs exhibit two main features. Firstly, the nematic-isotropic transition temperature,  $T_{NI}$ , appears to vary only slightly with varying colloid concentration and shows a minimum at a colloid concentration around 20 wt %. Secondly, with increasing colloid concentration the peaks at  $T_{NI}$  tend to broaden somewhat, while the total area under the peaks (per unit of mass) becomes lower.

For liquid crystals in confined geometries a decrease of the transition temperature has been commonly observed and has previously been ascribed to a variation in director among confined LC domains<sup>27</sup> or to disordering of the LC molecules within the confined cavities under influence of the confining surfaces.<sup>28-30</sup> It has also been shown that the transition temperature is slightly raised in case the LC is conformed into a more highly ordered state at the vicinity of a confining surface.<sup>27</sup> Although here, the variation of the transition temperature is very subtle, possibly these two effects are competing with each other and can be related to the corresponding morphological features.

As would be expected, the transition temperature is initially shifted to slightly lower temperatures, due to the effect of the confining colloidal network onto the perturbation of the LC order. By an increase in the colloid concentration from 2.7 to 6.4 wt %, the LC mesh size becomes smaller, which shifts the  $T_{NI}$  to even lower temperatures. With increasing colloid concentration, however, apparently the surface anchoring effect starts to compete with the finite size effect. In advance of what will be discussed later in the morphology section, this might be attributed to the fact that the aggregated colloidal system becomes more irregular

with increasing colloid concentration. Possibly, due to compression of the nearly colloid-free LC regions between the densely packed colloid regions, the LC molecules collectively adopt themselves into a more highly ordered state. Evidently, at high colloid concentration the small-scale ordering of this bulk LC fraction dominates over the perturbation of the LC fraction within the highly concentrated regions, leading to an increase in transition temperature. Furthermore, it is anticipated that at higher colloid content the existence of a distribution of domains, with each domain having its own characteristic size and director, will become more pronounced. The separated LC domains will undergo the phase transition independently of each other, which manifests itself in a broadening of the peaks.<sup>27</sup>

Recently, the  $T_{NI}$  peak of this material was found to consist of two distinctive peaks, where the main peak was designated to the transition of the bulk LC. However, apart from the bulk LC also LC molecules are present within the swollen colloidal network, which have adopted a random (isotropic) orientation due to finite size effects. This fraction gives rise to a peak at somewhat lower temperature as, during cooling, this remaining isotropic liquid is expelled from the highly swollen colloidal regions by the ‘nematic pressure’ exerted by the coexisting nematic liquid.<sup>14</sup>

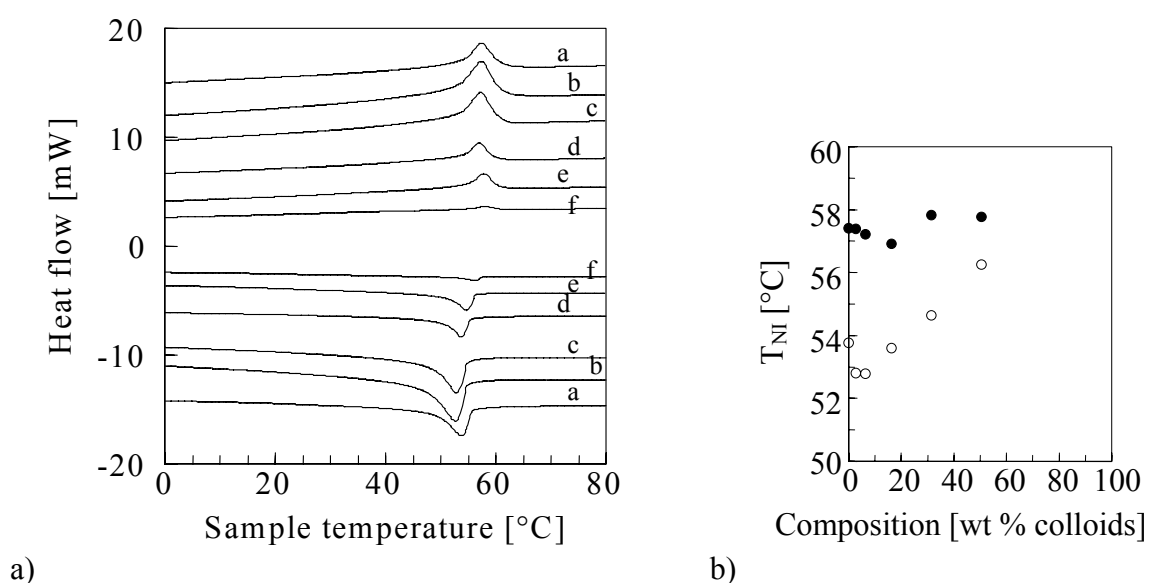


**Figure 3.6:** (a)  $T_{NI}$  of LC E7 in LC colloidal dispersions with various amounts of 630 nm sized colloids: (a) 0 wt %; (b) 2.7 wt %; (c) 6.4 wt %; (d) 16.9 wt %; (e) 31.4 wt %; (f) 50.6 wt %; (b)  $T_{NI}$  determined via the peaks of the clearing points as a function of colloid concentration: (●) Values obtained from the DSC heating runs; (○) values obtained from the DSC cooling runs.

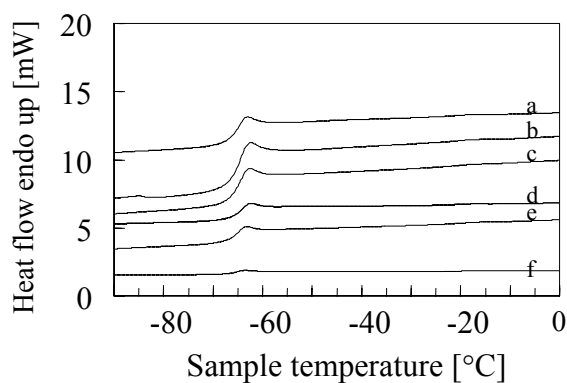


**Figure 3.7:** Glass transition temperatures of LC E7 in LC colloidal dispersions with various amounts of 630 nm sized colloids: (a) 0 wt %; (b) 2.7 wt %; (c) 6.4 wt %; (d) 16.9 wt %; (e) 31.4 wt %; (f) 50.6 wt %.

From the DSC thermographs the degree of phase separation between the polymer and LC phases can be evaluated. From Figures 3.6 and 3.7 it is seen that the transitions of the LC can be distinguished for each sample composition. Furthermore, no significant shifts are observed of these transition temperatures of the LC E7 in the colloidal dispersions, compared to the transition temperatures of the pure LC E7. These observations are indicative of the presence of non-contaminated LC domains and point to a complete exclusion of polymer chains from the LC regions and the absence of solute impurities in the LC regions.<sup>31-34</sup>

The solubility of the LC molecules in the polymer was deduced via two relevant quantities. The first one was the heat of fusion of the nematic-isotropic transition,  $\Delta H_{NI}$ . For each heating curve in Figure 3.6 the integrated area of the  $T_{NI}$  peak was determined and depicted as a function of the E7 weight content (Figure 3.8a).

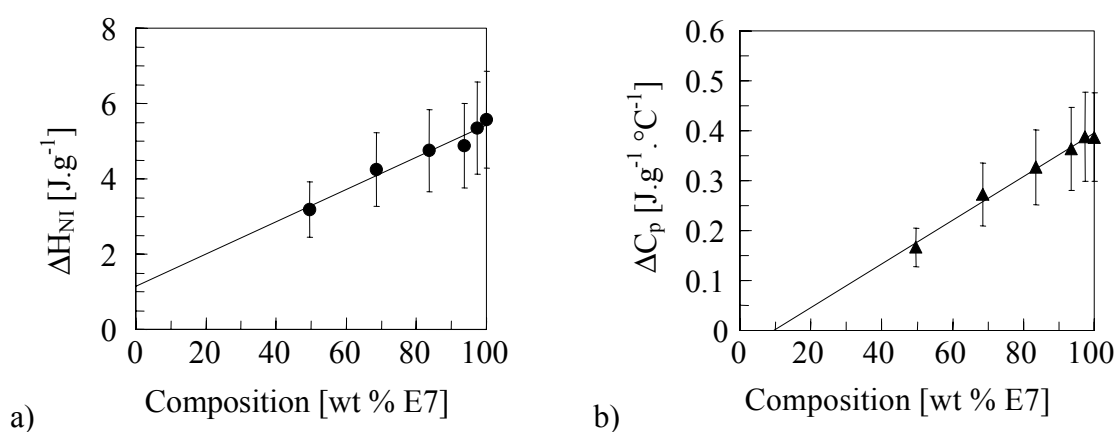


**Figure 3.8:** (a) Heat of the nematic-isotropic transition and (b) specific heat increment at the glass transition temperature of the LC E7 molecules in LC colloidal dispersions containing various amounts of colloids. The solid lines represent linear fits of the experimental data.

The second characteristic quantity was  $\Delta C_p$  (LC), representing the increase in specific heat per unit mass at the glass transition temperature,  $T_g$ , of the bulk LC. These quantities were derived from Figure 3.7 and are plotted versus the sample composition in Figure 3.8b. A third parameter that could be useful here is the  $T_g$  of the polymer material. However, due to the high crosslinking level of the colloids the  $T_g$  of the copolymer could not be observed.

Linear regression of the experimental data depicted in Figure 3.8, followed by calculation of the  $x$ -axis intercept, yields the LC solubility limit.<sup>33,35</sup> The large scattering in these numbers and the unreal outcome (i.e. negative values) suggest that experimental errors in the  $\Delta H_{NI}$  and  $\Delta C_p$  (LC) measurements are easily introduced, due to the small magnitude of both quantities. In spite of these experimental deviations, the first impression of Figure 3.8 is that a linear relation can be seen between both the  $\Delta H_{NI}$  and  $\Delta C_p$  (LC) and the sample composition going through the point (0,0), which suggests that virtually all the LC is present as bulk LC. This implies that, for the investigated composition range, solution of the LC in the polymer phase is more or less negligible and that the LC molecules are not extremely strongly bound to the colloidal network. The results from the DSC analysis are summarised in Table 3.1.

**Table 3.1:** *Characteristic values obtained from the DSC analysis (heating run) on LC colloidal dispersions with various colloid weight contents.*

Composition [wt % colloids]	$T_{NI}$ [°C]	$\Delta H_{NI}$ [J.g <sup>-1</sup> ]	$T_g$ (LC) [°C]	$C_p$ (LC) [J.g <sup>-1</sup> .°C <sup>-1</sup> ]	$T_{CN}$ [°C]
0	57.40	5.57	-65.65	0.387	-18.12
2.7	57.38	5.34	-65.57	0.388	-18.12
6.4	57.22	4.89	-65.65	0.364	-18.11
16.9	56.90	4.75	-65.12	0.327	-17.93
31.4	57.83	4.24	-66.03	0.272	-18.10
50.6	57.76	3.19	-66.17	0.166	-16.23

For anisotropic gels a more than proportional decrease of  $\Delta H_{NI}$  with increasing content of network molecules has been observed previously.<sup>36,37</sup> This has been ascribed to the presence of two populations of LC apart from the network molecules, namely (1) LC molecules that are so strongly bound to the network, that they do not undergo the nematic-isotropic phase transition and (2) LC molecules that are not strongly bound to the network. It was estimated that the size of the confined LC domains had to be smaller than 85 nm to completely suppress the nematic-isotropic transition.<sup>38,39</sup> The strongly bound LC population remained oriented at temperatures largely exceeding the  $T_{NI}$  and provided some residual birefringence.



In order to check the presence of LC molecules that remained oriented at temperatures above  $T_{NI}$ , parallel cells filled with the LC colloidal dispersions were examined by optical polarisation microscopy. It was observed that all samples, including the 50.6 wt % LC dispersion, became completely isotropic after heating above  $T_{NI}$ , which excludes the presence of a strongly bound LC fraction.

### 3.4.2 Morphology formation

According to previous theoretical studies on particles immersed in an LC (see Section 3.2 for a brief review) the “strong anchoring regime” with the topological defect formation is valid in case the condition  $WR/K \gg 1$  is satisfied. Figure 3.9 shows optical micrographs of a parallel cell capillary filled with LC E7 containing 5 wt % of 3.4  $\mu\text{m}$  poly(methyl methacrylate-*co*-divinylbenzene) colloids (contaminated with a small amount of much smaller colloids). The large particles have assembled into anisotropic colloidal clusters, with an angle of exactly  $\pm 30^\circ$  between the neighbouring particles. Obviously, these 3.4  $\mu\text{m}$  particles are able to perturb the nematic director to such an extent, that topological defects are created within the LC matrix. When viewed under crossed polarisers, the distorted LC orientation at the particle surface can be observed.

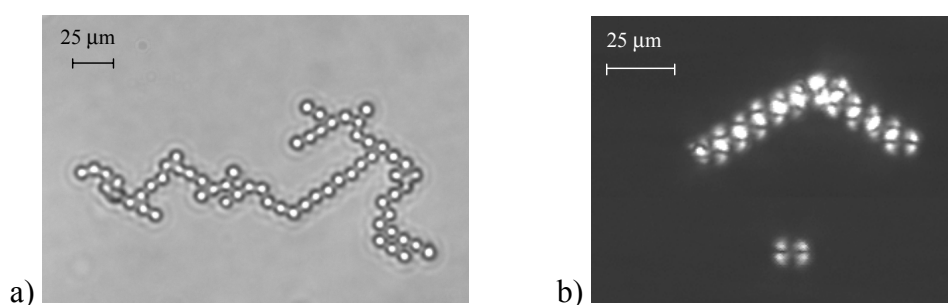


**Figure 3.9:** *Optical micrographs of a parallel electro-optical cell filled with a 5 wt % dispersion in LC E7 based on 3.4  $\mu\text{m}$  poly(methyl methacrylate-*co*-divinylbenzene) colloids: (a) Viewed without polarisers; (b) viewed under crossed polarisers.*

The formation of the quadrupolar-like particle-defect assembly points to the presence of planar anchoring conditions at the particle surface. This confirms the expectation that the rather high molecular weight steric stabiliser, which was used within the dispersion polymerisation reaction, provides a planar alignment of the LC around the immersed particles. In contrast to this, the use of low molecular weight surfactants is expected to induce a homeotropic alignment of the LC.<sup>8</sup>

The type of behaviour that is characteristic for the “weak anchoring regime” was observed for colloidal dispersions in LC E7 based on 1.2  $\mu\text{m}$  sized (see also Figure 2.14d)

and smaller poly(methyl methacrylate-*co*-divinylbenzene) colloids. Also, monodisperse 1.8  $\mu\text{m}$  sized poly(styrene-*co*-divinylbenzene) colloids, which were obtained via the same dispersion polymerisation procedure as described in the previous chapter, could be classified into this regime. From the crossover radius between the two distinctive regimes, which is at most equal to 1.7  $\mu\text{m}$ , the energy  $W$  that comes from the anchoring of the LC molecules onto the particle surfaces can be approximated. By taking  $R = 1.7 \cdot 10^{-6}$  m and  $K(\text{E7}) \sim 12.8 \cdot 10^{-12}$   $\text{J} \cdot \text{m}^{-1}$ ,<sup>40,41</sup> then it is estimated that the anchoring energy  $W \gg 7.5 \cdot 10^{-6}$   $\text{J} \cdot \text{m}^{-2}$ . This is a quite reasonable estimate, which will fall within the convention of “strong anchoring” in case  $W$  exceeds the limit of  $10^{-5}$   $\text{J} \cdot \text{m}^{-2}$ . Here, it has to be noticed that it’s assumed that, apart from the particle radius, other differences in particle features are not taken into account.

The general morphology development of the LC colloidal dispersions can be described by use of Figure 3.10. In order to distinguish between the separate particles at elevated temperatures, for this purpose the large 1.8  $\mu\text{m}$  sized particles were employed.

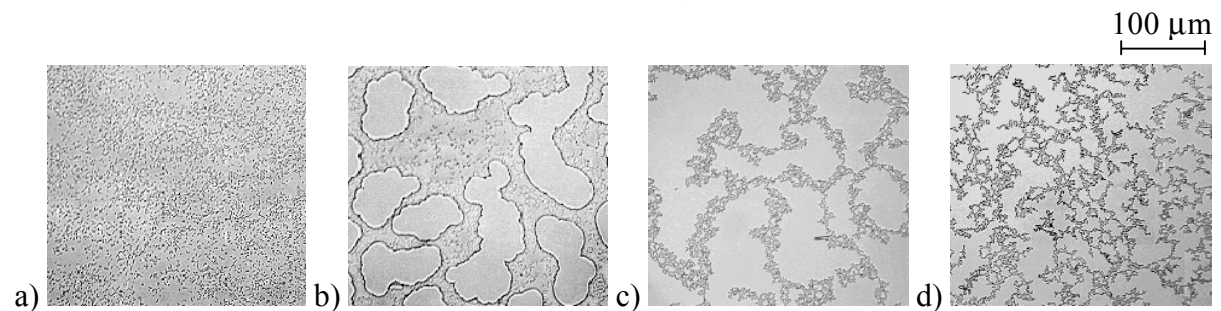


**Figure 3.10:** *Optical micrographs showing the general morphology formation process of an LC colloidal dispersion: (a) Homogenisation at 150 °C; (b) growth of nematic LC droplets at 60.1 °C during cooling with a rate of 0.2 °C.min<sup>-1</sup>; (c) morphology at room temperature, formed after cooling with a rate of 0.2 °C.min<sup>-1</sup>; (d) morphology at room temperature, formed after cooling with a rate of 50 °C.min<sup>-1</sup>.*

During heating to temperatures around 150 °C the aggregated structures were gradually broken down, due to the increased Brownian motion at elevated temperatures. This eventually led to the formation of homogeneous dispersions of the particles in the isotropic LC that showed no significant evidence of particle aggregation on length-scales accessible by optical microscopy (Figure 3.10a). After this homogenisation of the LC colloids, during cooling down to room temperature, it was observed that the inclusions remained nicely dispersed showing no pronounced signs of aggregation all the way down to the  $T_{\text{NI}}$  of LC E7. It was only upon passing the nematic-isotropic transition temperature that the growing nematic droplets, which appeared to be free of polymer inclusions, pushed aside the dispersed particles by their expanding interfaces (Figure 3.10b).<sup>12,15</sup> In this way, the polymer particles became finally trapped between the growing nematic droplets, resulting in the formation of the network structure, depicted in Figures 3.10c and d. After the phase transition, the

morphology instantaneously formed was frozen in and remained unchanged during further cooling to room temperature. The network formation process turned out to be fully reversible, although with increasing colloid content the time spans needed to fully homogenise the dispersions at elevated temperatures significantly increased.

The final morphology seemed to be influenced by the rate at which the isotropic-nematic transition was passed during cooling. During slower cooling, fewer nematic nuclei were formed, giving the nematic droplets more time to grow and to coagulate, resulting in somewhat larger LC domains and a polymer particle network with a larger mesh size (for comparison see Figure 3.10c and d). For higher cooling rates it was commonly observed that a more finely dispersed, but more irregularly structured network was formed.

The extension of the colloidal network in three dimensions was studied with CLSM. Figure 3.11 shows the variation of the morphology as a function of penetration depth for a TN cell filled with an LC colloidal dispersion based on 6.4 wt % of 630 nm sized colloids (see also Figure 2.14c).

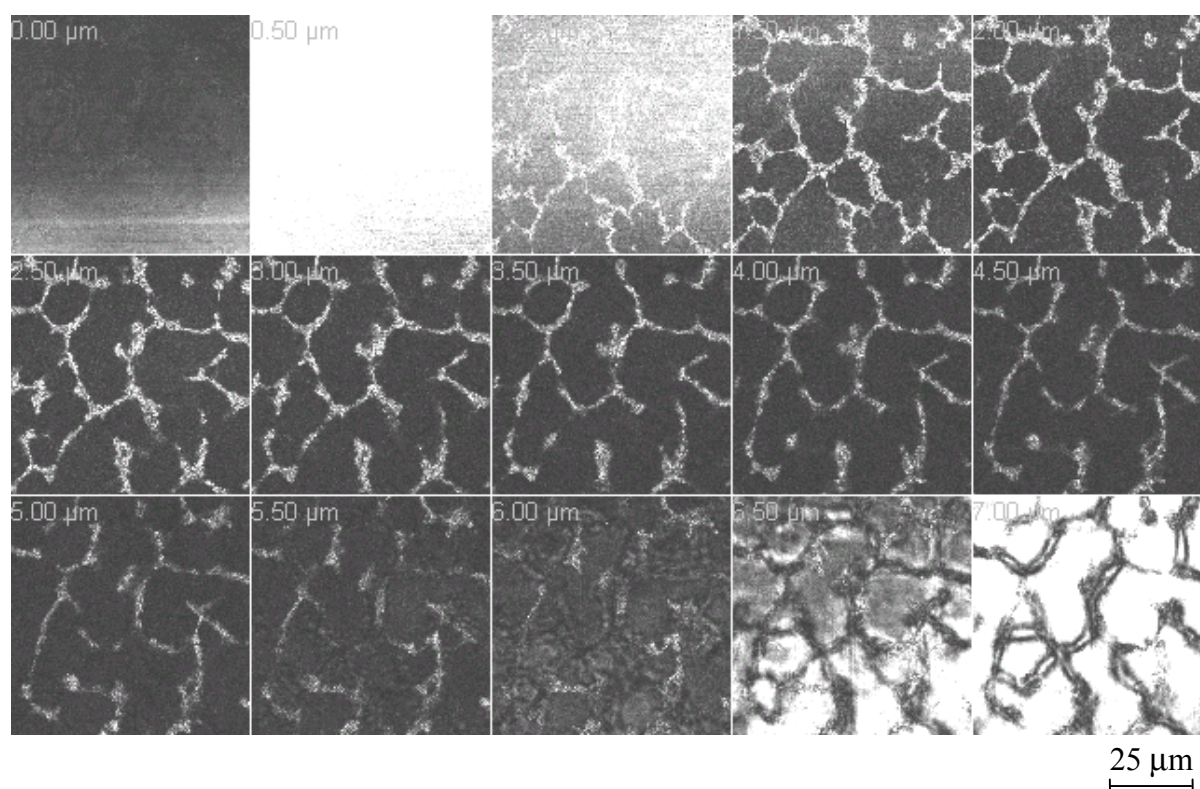


**Figure 3.11:** Reflection-mode confocal images of a 7  $\mu\text{m}$  thick TN cell filled with a 6.4 wt % LC dispersion of 630 nm sized colloids. The micrographs show cross-sections of the sample at increasing penetration depth.

Both the top and the bottom of the sample cell are marked by a broad, intensely light region, which comes from strong reflection of the laser light at the glass substrates. The light intensity of the collected images gradually decreases with increasing penetration depth going from the thin to the thick glass slide, as the light loss due to multiple scattering phenomena

becomes more significant with increasing path length of the laser light. The network structure seems to extend itself over the full thickness of the sample cell and varies only slightly in the third dimension. The confocal images suggest that no sedimentation of the colloids with a density of  $\sim 1.1 \text{ g.ml}^{-1}$  has occurred during the cell filling procedure, since in that case a higher colloid concentration would be expected in the vicinity of the thick glass substrates, at high penetration depths.

The absence of sedimentation phenomena during a typical time span of a few minutes needed to fill a cell was confirmed by stability tests. For these tests thin tubes with an inner diameter of 2 mm were filled via capillary action with the 2.7 wt % and 6.4 wt % LC dispersions of 630 nm colloids at a temperature of 150 °C. After cooling to room temperature, the tubes were placed vertically and sedimentation effects were studied over a period of two weeks. In both cases, the light scattering remained uniform over the whole length ( $l = 2 \text{ cm}$ ) of the tube during the whole investigation period, indicating that the network is stable and able to resist gravitational forces. In another set of experiments, the tubes were placed in an oven at 150 °C, directly after the filling process. In case of the 2.7 wt % LC colloidal dispersion, a macroscopic settling of the polymer particles could be detected after 20 minutes and in case of the 6.4 wt % composite material, sedimentation occurred after several hours.

### 3.4.3 Influence of colloid concentration on morphology

The influence of the colloid concentration on the morphology was studied by use of optical microscopy. In Figure 3.12 optical micrographs are shown of 17.8  $\mu\text{m}$  thick electro-optical cells filled with LC colloidal dispersions with concentrations of 630 nm sized colloids ranging from 2.7 to 16.9 wt %. At the lowest colloid concentration of 2.7 wt % the network structure is clearly visible. With increasing colloid concentration, the LC domain size gradually decreases until, at very high concentration, the LC domains cannot be distinguished anymore with the optical microscopy technique. Whereas in the lower concentration range the network is rather homogeneously dispersed within the LC continuum, in the higher concentration range aggregation phenomena become more pronounced and a more irregular network structure is observed.

At even higher concentrations of 31.4 wt %, the colloids appeared to have a strong tendency to aggregate within very dense, partly interconnected islands. These islands showed a fine, internal network structure, but between neighbouring islands also LC regions could be distinguished, which seemed to be nearly free of colloids.

Optical polarisation microscopy on these parallel cells and other (parallel and TN) cells with different cell gaps visualised that the orientation of the LC molecules in the near

vicinity of the colloidal network was always highly distorted. In general, the bulk LC was always still aligned according to the direction of the orientation layers of the cell.

From all observations, it was concluded that the distorting effect of the dispersed colloids strongly competes with the aligning effect of the orientation layers and becomes more dominating with increasing cell gap and, usually, with increasing colloid concentration.

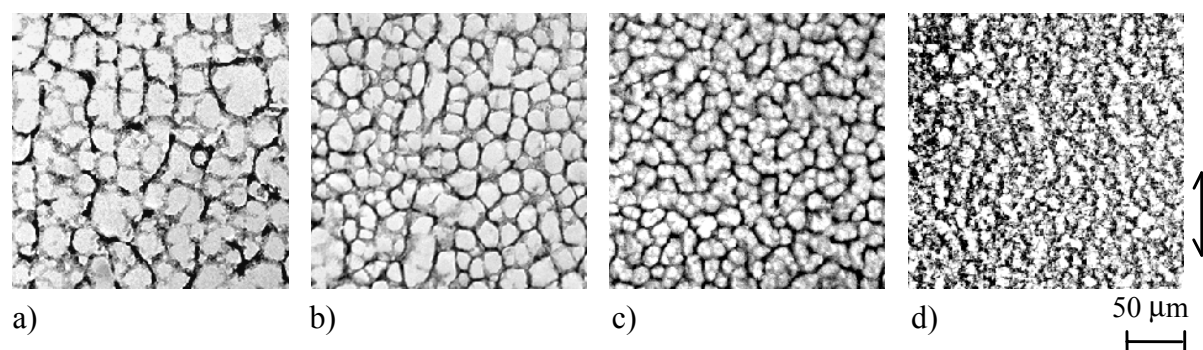


**Figure 3.12:** *Optical micrographs of 17.8  $\mu\text{m}$  thick parallel cells filled with LC dispersions with various fractions of 630 nm sized colloids: (a) 2.7 wt %; (b) 4.5 wt %; (c) 6.4 wt %; (d) 16.9 wt %. The arrow indicates the direction of the orientation layers.*

#### 3.4.4 Influence of colloid size on morphology

In order to determine the effect of colloid size on morphology of the LC colloidal dispersions, the following colloids were used as the disperse phase for the LC: (1) the 630 nm sized colloids, (2) much smaller colloids of 43 nm (Section 2.3.6) and (3) the much larger colloids of 1.2  $\mu\text{m}$ .

The LC dispersions based on 6.4 wt % colloids were confined within 7  $\mu\text{m}$  thick cells with TN configuration and studied with CLSM. Figure 3.13 shows the three-dimensional images that were gathered for the three different colloid sizes, compressed as orthogonal images. The middle area represents one optical slice of the three-dimensional stack of collected images in the  $x$ - $y$  plane. The side views show the morphology development in the  $z$ -direction there, where the intersecting lines in the  $x$ - $y$  plane slice the sample. When comparing the morphologies of the three different samples, it is evident that the size of the LC domains that are confined within the polymer network significantly decreases with decreasing colloid size, at constant colloid weight fraction. The overall structure gradually coarsens with increasing colloid size or, one might also say, with decreasing number of particles. Especially for the largest colloids, it is clearly visualised that the colloids have assembled into larger aggregates that are partly interconnected to form a three-dimensional network. The more pronounced aggregation of the larger particles, induced by cooling down the isotropic-nematic phase transition after the cell filling process at elevated temperatures, can be interpreted in terms of the dimensionless parameter  $WR/K$  (see Section 3.2). Figures

3.12 and 3.13 nicely illustrate that the material properties and composition influence the aggregation behaviour of the colloids in a very subtle manner and, therefore, need to be tuned very carefully in order to get the desired morphology development of the LC colloidal dispersions.

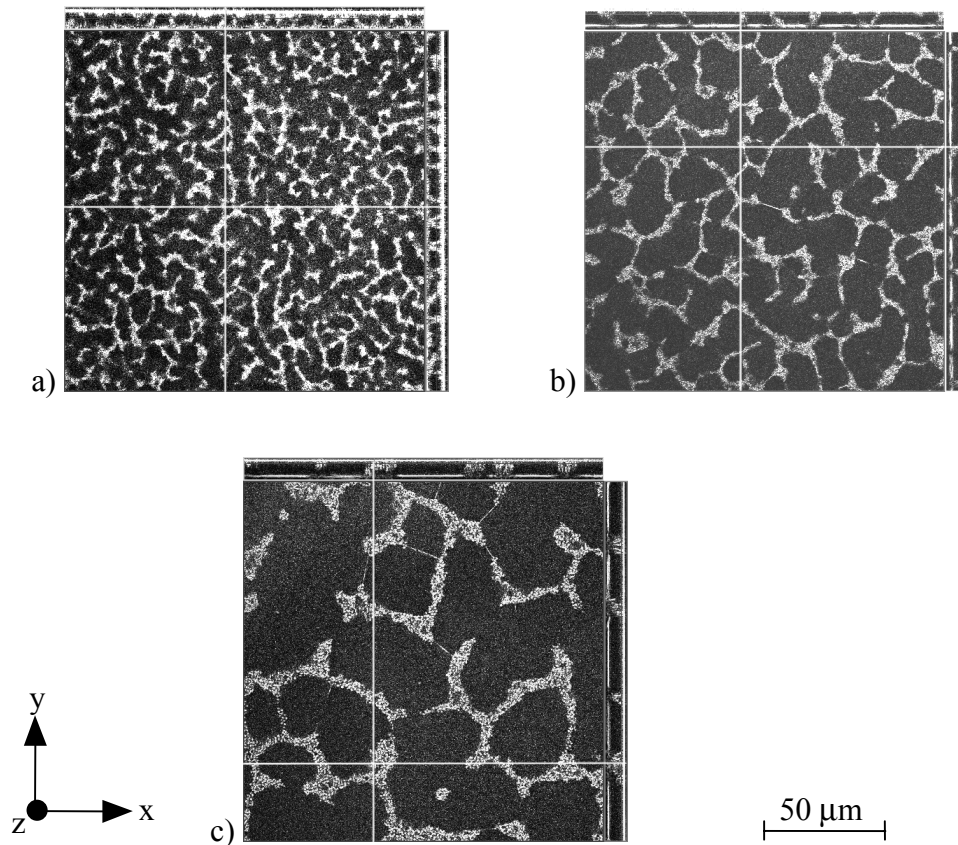


**Figure 3.13:** *Confocal orthogonal images of approximately 7  $\mu\text{m}$  thick TN cells filled with LC dispersions based on 6.4 wt % poly(methyl methacrylate-co-divinylbenzene) colloids with different diameters: (a) 43 nm; (b) 630 nm; (c) 1.2  $\mu\text{m}$ . One cross-section of the sample is shown in the large area, while the two side views show the extension of the sample morphology in the z-direction.*

Figure 3.14 gives a detailed view on the aggregate network of the 1.2  $\mu\text{m}$  colloidal particles. The image clearly visualises that the aggregated colloids in the TN cell are not only interconnected via bridging colloid structures, but also via extremely straight disclination lines. Under the microscope it was observed that, by imposing an instantaneous pressure onto the cell, the line defects were bent due to the LC flow, while the particle structures remained at their initial position. For these TN cells a small variation in colour was observed between neighbouring LC regions, which were confined within the colloidal network or the disclination lines, which pointed to a small variation in director between the various LC domains. For LC colloidal dispersions confined within parallel cells the presence of the disclination lines was less obvious (although present). Therefore, it is assumed that the

twisted configuration of the cell in combination with the polymer network promotes the division of the twisted LC into domains and the introduction of the line defects.

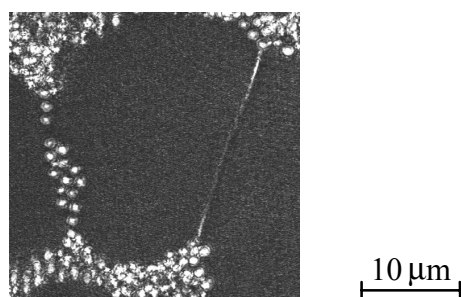


**Figure 3.14:** Detailed confocal image of a TN cell filled with an LC dispersion based on 6.4 wt % 1.2  $\mu\text{m}$  poly(methyl methacrylate-co-divinylbenzene) colloids.

### 3.4.5 Thermal stability

The weight loss of the LC colloidal dispersions during heating was studied with TGA and compared to the weight loss as a function of temperature for the pure LC E7 and the colloids (Figure 3.15).

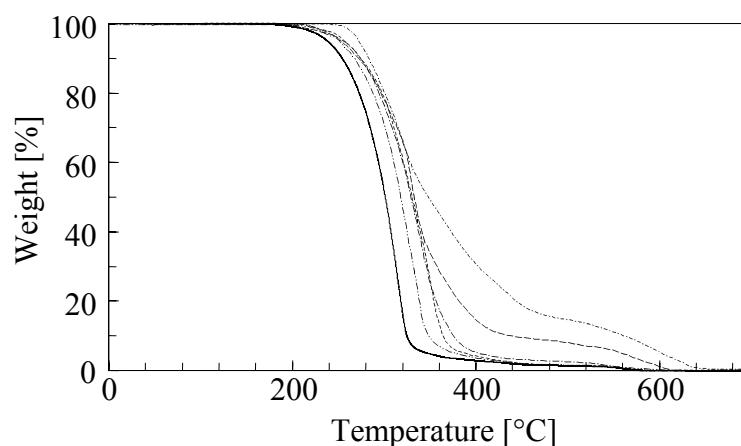


**Figure 3.15:** Sample weight as a function of temperature for the LC dispersions based on various fractions of 630 nm sized poly(methyl methacrylate-co-divinylbenzene) colloids: (—) 0 wt % (pure E7); (---) 2.7 wt %; (- -) 6.4 wt %; (-.-) 16.4 wt %; (- -) 50.4 wt %; (-.-) 100 wt %.

Significant weight loss of the LC E7 starts to occur at temperatures  $\sim 150$ - $160$   $^{\circ}\text{C}$  and at  $350$   $^{\circ}\text{C}$  most of the LC has gone. The internally crosslinked colloids show a higher thermal stability, as degradation phenomena are absent during heating up to  $250$   $^{\circ}\text{C}$ . At  $500$   $^{\circ}\text{C}$  their weight has been largely diminished and complete thermal degradation of the colloids has been accomplished at  $630$   $^{\circ}\text{C}$ . From Figure 3.15 it is seen that the degradation behaviour of

the LC colloidal dispersions is intermediate to the behaviour of the single constituents. With increasing colloid content the thermal stability of the materials is slightly improved.

### 3.4.6 Rheological properties

In order to study the impact of the colloidal network on the flow behaviour of the LC material, stationary rheological measurements were conducted on E7 and on a 6.4 wt % colloidal dispersion in E7. For a gradually increasing shear rate the viscosity and stress were measured (Figure 3.16).

For the pure LC E7 shear thinning behaviour is observed (Figure 3.16a), which is associated with gradual changes in texture and a decrease in the domain size.<sup>42</sup> After the viscosity has levelled off, another shear thinning region (not seen in Figure 3.16a) is expected, arising from a further homogenisation of the sample. Obviously, the viscosity of the material is significantly increased by the presence of a colloidal network in the LC. At a certain strain rate the viscosity instantaneously starts to decrease, which is associated with a breakdown of the colloidal network. The strong decrease of the viscosity with a slope smaller than minus one is expressed in Figure 3.16b by a maximum in the stress-rate curve. The curve indicates that, as soon as the maximum in the stress is reached for a stress-driven flow, the rate will instantaneously jump to a much higher value, which is found by extrapolation of the broken line. For processing conditions (rate  $> \sim 10 \text{ s}^{-1}$ ) the viscosity becomes of the same order of magnitude as is found for the pure LC.

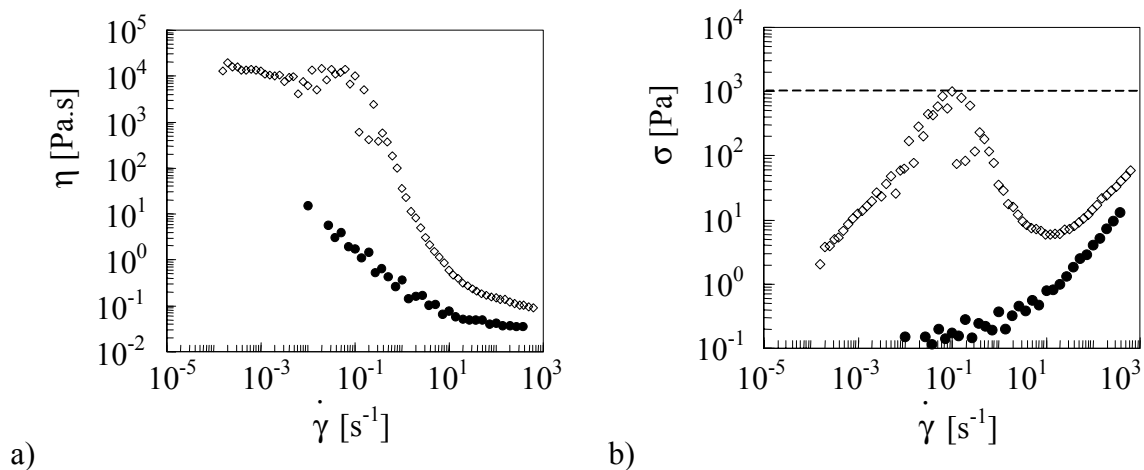


**Figure 3.16:** (a) Viscosity  $\eta$  and (b) stress  $\sigma$  as a function of the applied shear rate  $\dot{\gamma}$  for (●) E7 and (◇) a 6.4 wt % LC colloidal dispersion.

It is noticed that for the realisation of a continuous process as envisaged by Figure 1.7 this peculiar flow behaviour can easily be circumvented by coating the material in the



homogeneously dispersed, isotropic state. This isotropic state is accomplished (1) by the use of an additional solvent or (2) by heating the material at temperatures above  $T_{NI}$ . After application of the coating the added solvent is evaporated or the material is cooled below  $T_{NI}$ , respectively, during which the colloidal network is formed within the LC. Therefore, for the realisation of a continuous process, the flow stability and mechanical strength of the material in rest is of more importance here. In this respect, the rise in viscosity points to a significant improvement in rheological stability of the LC colloidal dispersions with respect to the pure LC through the presence of the colloidal network.

In addition to the stationary measurements, dynamic mechanical experiments were performed to evaluate the mechanical strength of the materials for small deformations. Figure 3.17a shows that at an angular frequency  $\omega = 1 \text{ rad.s}^{-1}$  for low strains  $\gamma$  the LC dispersions containing 2.7 and 6.4 wt % of 630 nm colloids both exhibit linear visco-elastic behaviour.

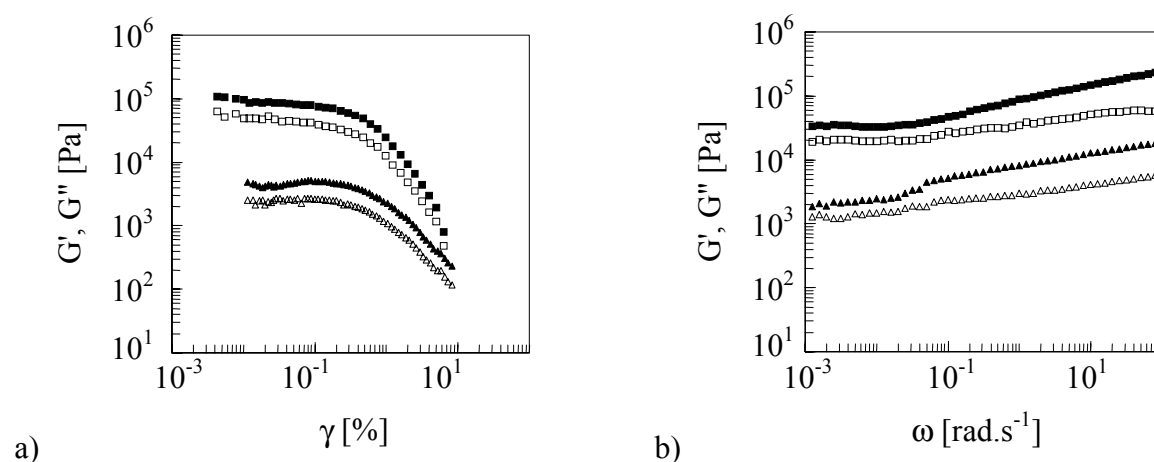


**Figure 3.17:** The elastic storage modulus  $G'$  (closed symbols) and loss modulus  $G''$  (open symbols) for LC dispersions based on 2.7 wt % (triangles) and 6.4 wt % (squares) of 630 nm colloids: (a)  $G'$  and  $G''$  depicted as a function of the applied strain  $\gamma$ , at angular frequency  $\omega$  of  $1 \text{ rad.s}^{-1}$ ; (b)  $G'$  and  $G''$  for frequencies ranging from  $10^{-3}$  to  $10^2 \text{ rad.s}^{-1}$  at a fixed  $\gamma$  of 0.25 %.

In the linear range the 6.4 wt % LC colloidal dispersion possesses a stiffness of  $G' \sim 10^5 \text{ Pa}$  and complex viscosity  $\eta^* = (G'^2 + G''^2)^{1/2} / \omega \sim 10^5 \text{ Pa.s}$ . For the pure LC E7 no linear range was observed within the applied range of strains. Instead, a continuously decreasing trend was observed over the whole strain range. The values that were recorded for the moduli of the LC were several orders of magnitude lower than those obtained for the colloidal dispersions and, consequently, less reliable, strongly scattered data points were collected. Thus, the presence of the colloidal network provides an increased mechanical stiffness of the material.

As shown in Figure 3.17b the basic characteristics of the material are maintained over five frequency decades. The data condensed in Figure 3.17 are commensurate with the

presence of a "dynamic network structure in an LC matrix". Obviously, upon linear deformation of the composite material, the particle network does exhibit elastic energy storage. However, the relatively high  $G''$ -value points to reorganisations (break and subsequent build-up) within the network, associated with viscous flow. At higher frequencies this reorganisation effect is, relative to the elastic energy storage, less pronounced, as may be explained by the smaller time-span at which a reorganisation has to take place. At increasing strain, at some point the moduli instantaneously collapse. This is associated with a breakdown of the colloidal network.

In literature, several possible explanations have been put forward in order to describe the origin of the anomalously high elastic moduli of the LC colloidal dispersions in a rest situation.<sup>13,14,16</sup> Plausible arguments have ascribed the manifestation of the high rigidity to a combination of depletion interactions between neighbouring colloids and the presence of locally melted LC within the closely packed colloid-rich regions. The latter contribution accounts for the gradual rise of the modulus with decreasing temperature below  $T_{NI}$ , as the 'nematic pressure' and thus the colloid compaction continues to increase with decreasing temperature.<sup>14</sup> The contribution of the LC depletion between neighbouring polymer spheres accounts for the dependence of  $G'$  on particle size, as will be discussed in the following part.

To look into the influence of colloid size on mechanical properties, the same dynamic mechanical analysis was performed with 6.4 wt % dispersions based on 43 nm, 630 nm and 1.2  $\mu\text{m}$  sized colloids. Figure 3.18 shows that for a colloid content of 6.4 wt % the 630 nm sized colloids provide the highest moduli, while lower moduli are found for the 43 nm and the 1.2  $\mu\text{m}$  sized colloids.

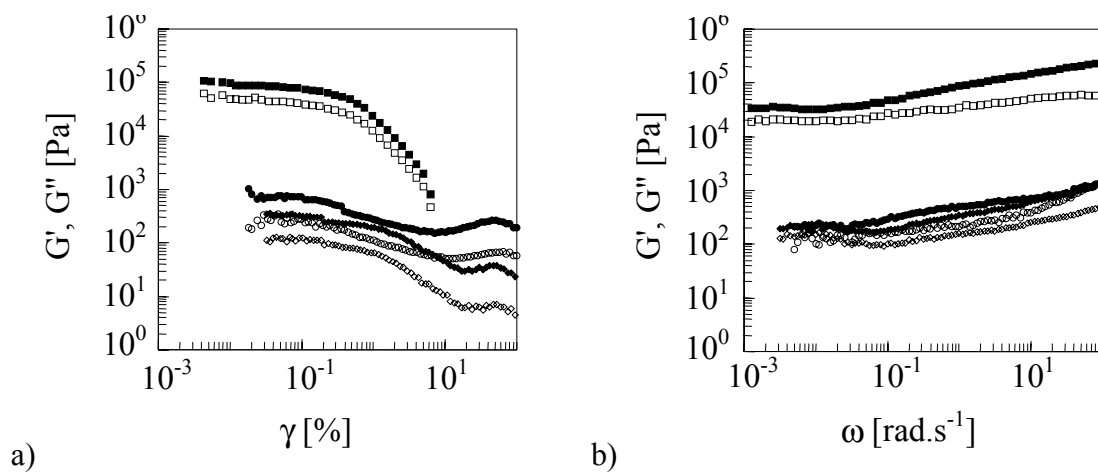


**Figure 3.18:** The elastic storage modulus  $G'$  (closed symbols) and loss modulus  $G''$  (open symbols) for LC dispersions based on 6.4 wt % colloids of 43 nm (circles), 630 nm (squares) and 1.2  $\mu\text{m}$  (diamonds): (a)  $G'$  and  $G''$  depicted as a function of the applied strain, at angular frequency of  $1 \text{ rad}\cdot\text{s}^{-1}$ ; (b)  $G'$  and  $G''$  for frequencies ranging from  $10^{-3}$  to  $10^2 \text{ rad}\cdot\text{s}^{-1}$  at a fixed  $\gamma$  of 0.15 %, 0.25 % and 0.2 % for the 43 nm, 630 nm and 1.2  $\mu\text{m}$  colloidal dispersions, respectively.

The elastic force upon stretching of the colloidal network is thought to arise from attempts of the system to maintain the particles in direct contact with each other in order to reduce the surface energy. In considering the occurrence of these depletion effects, it is expected that the elastic modulus increases with decreasing colloid size. This trend is found for the 630 nm and 1.2  $\mu\text{m}$  sized colloids. In agreement with other findings the exceptional behaviour of the 43 nm sized colloids might be attributed to their deformable, 'soft' surface.<sup>14,43</sup> Secondly, as discussed before, with decreasing colloid size a weaker elastic energy becomes involved. This could ultimately lead to a homogeneous mixing of the particle inclusions with the LC, cf. molecular mixtures. Thus, in case of the small 43 nm sized colloids, the phase separation that leads to the formation of the network structure is probably not very strong, which could cause the levels of the corresponding moduli to be significantly lower than expected.

### 3.5 Conclusions

Polymer/LC blends were prepared by dispersing highly crosslinked poly(methyl methacrylate-*co*-divinylbenzene) colloids within a liquid crystal, LC E7. It was demonstrated that, within the presented route for the preparation of LC dispersions based on internally crosslinked polymer colloids, the introduction of all kinds of intermixing phenomena is circumvented and ultimately results in complete phase separation between the polymer and the LC phase.

Furthermore, it was established that the resulting LC colloidal dispersions can be homogenised in the isotropic phase at temperatures around 140 °C. During subsequent cooling below the isotropic-nematic transition temperature, the colloids tend to aggregate into a three-dimensional network within the LC matrix. The multidomain structure of the composite materials became more pronounced with increasing colloid content and decreasing colloid size, at constant colloid weight content. Particle sedimentation phenomena were not detected during and after the capillary filling of electro-optical cells

Rheology measurements indicated that the LC colloids have a strongly enhanced flow stability in rest when compared to the pure LC E7, depending on colloid concentration and size. This might be exploited for the production of liquid crystal displays using cost-effective, continuous coating processes.

### 3.6 References

- (1) Lekkerkerker, H.N.W., Dhont, J.K.G., Verduin, H., Smits, C., Van Duijneveldt, J.S. *Physica A*, **1995**, *213*, 18-29.
- (2) Ruhwandl, R.W., Terentjev, E.M. *Phys. Rev. E*, **1997**, *55*, 2958-2961.
- (3) Ruhwandl, R.W., Terentjev, E.M. *Phys. Rev. E*, **1997**, *56*, 5561-5565.

- (4) Kuksenok, O.V., Ruhwandl, R.W., Shiyonovskii, S.V., Terentjev, E.M. *Phys. Rev. E*, **1996**, *54*, 5198-5203.
- (5) Lavrentovich, O.D. *Liq. Cryst.*, **1998**, *24*, 117-125.
- (6) Lubensky, T.C., Pettey, D., Currier, N., Stark, H. *Phys. Rev. E*, **1998**, *57*, 610-625.
- (7) Raghunathan, V.A., Richetti, P., Roux, D. *Langmuir*, **1996**, *12*, 3789-3792.
- (8) Poulin, P., Weitz, D.A. *Phys. Rev. E*, **1998**, *57*, 626-637.
- (9) Poulin, P., Stark, H., Lubensky, T.C., Weitz, D.A. *Science*, **1997**, *275*, 1770-1773.
- (10) Loudet, J.C., Barois, P., Poulin, P. *Nature*, **2000**, *407*, 611-613.
- (11) Loudet, J.C., Poulin, P., Barois, P. *Europhys. Lett.*, **2001**, *54*, 175-181.
- (12) Poulin, P., Raghunathan, V.A., Richetti, P., Roux, D. *J. Phys. II*, **1994**, *4*, 1557-1569.
- (13) Meeker, S.P., Poon, W.C.K., Crain, J., Terentjev, E.M. *Phys. Rev. E*, **2000**, *61*, R6083-R6086.
- (14) Petrov, P.G., Terentjev, E.M. *Langmuir*, **2001**, *17*, 2942-2949.
- (15) Anderson, V.J., Terentjev, E.M., Meeker, S.P., Crain, J., Poon, W.C.K. *Eur. Phys. J. E*, **2001**, *4*, 11-20.
- (16) Anderson, V.J., Terentjev, E.M. *Eur. Phys. J. E*, **2001**, *4*, 21-28.
- (17) Poulin, P., Frances, N., Mondain-Monval, O. *Phys. Rev. E*, **1999**, *59*, 4384-4387.
- (18) Poulin, P. *Curr. Opin. Colloid Interface Sci.*, **1999**, *4*, 66-71.
- (19) Ramaswamy, S., Nityananda, R., Raghunathan, V.A., Prost, J. *Mol. Cryst. Liq. Cryst. Sci. Technol., Sect. A*, **1996**, *288*, 175-180.
- (20) Zapotocky, M., Ramos, L., Poulin, P., Lubensky, T.C., Weitz, D.A. *Science*, **1999**, *283*, 209-212.
- (21) Drzaic, P.S., Muller, A. *Liq. Cryst.*, **1989**, *5*, 1467-1475.
- (22) Kim, B.K., Kim, S.H., Choi, C.H. *Mol. Cryst. Liq. Cryst. Sci. Technol., Sect. A*, **1995**, *261*, 605-616.
- (23) Bahadur, B., Sarna, R.K., Bhide, V.G. *Mol. Cryst. Liq. Cryst.*, **1982**, *72*, 139-145.
- (24) Lovinger, A.J., Amundson, K.R., Davis, D.D. *Chem. Mater.*, **1994**, *6*, 1726-1736.
- (25) Zhong, Z.Z., Schuele, D.E., Gordon, W.L., Adamic, K.J., Akins, R.B. *J. Polym. Sci., Part B*, **1992**, *30*, 1443-1449.
- (26) Demus, D., Goodby, J., Gray, G.W., Spiess, H.W., Vill, V. *Handbook of liquid crystals, volume 2A: low molecular weight liquid crystals*, Wiley-VCH, Chichester, **1998**.
- (27) Dadmun, M.D., Muthukumar, M. *J. Chem. Phys.*, **1993**, *98*, 4850-4852.
- (28) Abd-El-Messieh, S.L., Werner, J., Schmalfluss, H., Weissflog, W., Kresse, H. *Liq. Cryst.*, **1999**, *26*, 535-539.
- (29) Corvazier, L., Zhao, Y. *Liq. Cryst.*, **2000**, *27*, 137-143.
- (30) Haga, H., Garland, C.W. *Phys. Rev. E*, **1997**, *56*, 3044-3052.
- (31) Ahn, W., Kim, C.Y., Kim, H., Kim, S.C. *Macromolecules*, **1992**, *25*, 5002-5007.
- (32) Carpaneto, L., Ristagno, A., Stagnaro, P., Valenti, B. *Mol. Cryst. Liq. Cryst. Sci. Technol., Sect. A*, **1996**, *290*, 213-226.
- (33) Roussel, F., Buisine, J.M., Maschke, U., Coqueret, X. *Phys. Rev. E*, **2000**, *62*, 2310-2316.
- (34) Vaz, N.A., Smith, G.W., Montgomery, G.P. *Mol. Cryst. Liq. Cryst.*, **1987**, *146*, 17-34.
- (35) Smith, G.W., Vaz, N.A. *Mol. Cryst. Liq. Cryst. Sci. Technol., Sect. A*, **1993**, *237*, 243-269.
- (36) Hikmet, R.A.M. *Mol. Cryst. Liq. Cryst.*, **1991**, *198*, 357-370.
- (37) Hikmet, R.A.M. *Liq. Cryst.*, **1991**, *9*, 405-416.
- (38) Hikmet, R.A.M., Zwerver, B.H. *Liq. Cryst.*, **1991**, *10*, 835-847.
- (39) Hikmet, R.A.M., Zwerver, B.H. *Liq. Cryst.*, **1992**, *12*, 319-336.
- (40) Polak, R.D., Crawford, G.P., Kostival, B.C., Doane, J.W., Zumer, S. *Phys. Rev. E*, **1994**, *49*, R978-R981.
- (41) Buttsworth, D.R., Elston, S.J., Jones, T.V. *Meas. Sci. Technol.*, **1998**, *9*, 1856-1865.
- (42) Larson, R.G. *Constitutive equations for polymer melts and solutions*, edited by Larson, R.G., Butterworth Publishers, London, **1988**.
- (43) Frith, W.J., Mewis, J., Strivens, T.A. *Powder Technol.*, **1987**, *51*, 27-34.



# Chapter 4

## Colloidal dispersions in a liquid crystal

### Dielectric and electro-optical properties\*

#### 4.1 Introduction

In the previous chapter LC colloidal dispersions were prepared and characterised with respect to their phase behaviour and mechanical properties. Intermixing phenomena appeared to be virtually completely absent within the heterogeneous materials, implying that the morphology and properties of the two-phase materials can be well controlled. A surprising quasi-solid behaviour was revealed for the two-phase materials at zero flow, which has been found to significantly facilitate the handling and processing of these so-called soft-solid materials compared to a pure LC. Here, it is anticipated that the rotational mobility of the LC on a molecular scale is still (partly) maintained, in spite of the solid-like behaviour of the LC phase, confined within a colloidal network, on a macroscopic scale. In view of this, the application of these materials for electro-optical switches produced via continuous processing methodologies may be feasible.

The influence of confinement of liquid crystals on physical properties, such as orientational order and phase transitions, has been addressed by various studies.<sup>1</sup> Due to the high surface to volume ratio the physical properties of liquid crystals are strongly altered with respect to the behaviour of bulk LC, dependent on the size and size distribution of the confining cavities. For instance, while surface induced alignment effects tend to increase the nematic order and shift the nematic-isotropic phase transition to higher temperatures, finite size effects have a tendency to reduce the nematic order and shift the phase transition to lower temperatures.<sup>2,3</sup> A broad LC domain size distribution is expressed by a strong broadening of the phase transition.<sup>3,4</sup> In the ultimate case, the prominent presence of a confining surface leads to such substantial spatial inhomogeneities in the director order that the phase transition is completely suppressed.<sup>5,6</sup> These confinement studies were usually concerned with liquid crystals in random porous media like silica aerosils<sup>6</sup> or glassy materials,<sup>3,5,7</sup> in polymer matrices (PDLC's),<sup>4,8</sup> in anisotropic gels<sup>9</sup> or in silica filled

---

\* Part of this work has been published: Van Boxtel, M.C.W., Janssen, R.H.C., Broer, D.J., Wilderbeek, J.T.A., Bastiaansen, C.W.M. *Adv. Mater.*, **2000**, *12*, 753-757; Van Boxtel, M.C.W., Janssen, R.H.C., Bastiaansen, C.W.M., Broer, D.J. *J. Appl. Phys.*, **2001**, *89*, 838-842. Part of this work will be published: Van Boxtel, M.C.W., Wübbenhorst, M., Van Turnhout, J., Bastiaansen, C.W.M., Broer, D.J., manuscript in preparation.

nematics.<sup>2,10,11</sup> In most cases, the LC molecular ordering and phase behaviour was probed with differential scanning calorimetry (DSC)<sup>2,6</sup> or with nuclear magnetic resonance (NMR).<sup>4,12</sup> In recent years, dielectric relaxation spectroscopy (DRS) has been employed as another tool to assess the behaviour of LC's in confined geometries.<sup>7-9,13,14</sup> Apart from modification of phase transitions and spatial inhomogeneities in director order, this technique also reveals information about the impact of the surface on the dynamics of the LC molecules.

Within this chapter dielectric relaxation spectroscopy experiments are performed in order to gain more insight into the molecular ordering and dynamics of the LC confined within the colloidal network. Furthermore, the LC colloidal dispersions are evaluated for their electro-optical switching behaviour. The materials will be used for two types of display principles: (i) conventional twisted nematic (TN) display principle, and (ii) display principle based on light scattering. It is emphasised that, in case of the TN configuration, the colloids are solely utilised to enhance the mechanical strength of the LC. In case of the light-shutter application an efficient light scattering is pursued, in addition to the mechanical stabilisation.

## 4.2 Experimental

### 4.2.1 Materials and sample preparation

For details on the liquid crystal LC E7 used see Section 3.3.1. The poly(methyl methacrylate-*co*-divinylbenzene) filler particles used were prepared via dispersion and emulsion polymerisation, according to the procedures described in Section 2.2. For details on the preparation of the LC colloidal dispersions see Section 3.3.2. Electro-optical cells were constructed and filled with the LC colloidal dispersions as described in Section 3.3.3.

### 4.2.2 Techniques

#### *Electro-optical characterisation*

The electro-optical characteristics of electro-optical cells were recorded using a Display Measuring System DMS 703 obtained from Autronic Melchers GmbH equipped with a voltage amplifier. Transmittance-voltage characteristics of TN cells were measured by applying AC voltages of 1 kHz square waves, which were increased in steps of 0.05 V at a rate of 1 V.s<sup>-1</sup>. The cells were illuminated with a 100 W halogen light source provided with a diffuser plate. The electro-optical cells were held between crossed polarisers in an aluminium sample holder, which was placed directly on the diffuser plate. The absolute transmittance through the two polarisers, which were positioned mutually parallel, was determined to be approximately equal to 26 % in the absence of a sample.

Transmittance-voltage characteristics of parallel (light-scattering) electro-optical cells were measured by applying AC voltages of 1 kHz square waves, which were increased in steps of 0.5 V at a rate of 5 V.s<sup>-1</sup>. The memory state was determined as a function of the applied voltage by measuring the transmittance 2 s after removal of the corresponding voltage.

For illumination a light source was used from Oriel Instruments equipped with a 500 W Hg(Xe) lamp in combination with a light-transporting fibre system and a 442 nm coloured glass filter for absorption of light in the low wavelength region. The cells were held in an aluminium sample holder and positioned on the plate (without diffuser plate) at a height of approximately 10 cm.

For all measurements a detector opening of 0.2 mm was used and the sample-detector distance was set in focus before measurement. All measurements were referenced against air.

#### *Dielectric relaxation spectroscopy (DRS)*

The dielectric properties of the LC colloidal dispersions were studied by means of a broadband dielectric spectrometer covering a total frequency range from 10<sup>-2</sup> Hz to 10<sup>6</sup> Hz. This spectrometer utilises a combination of two measurement systems with overlapping frequency ranges: 1) a frequency response analyser (Schlumberger 1260) equipped with a custom made dielectric interface (developed by TNO) for frequencies between 10<sup>-2</sup> and 10<sup>4</sup> Hz, and 2) a Hewlett-Packard 4284A precision LCR-meter for frequencies between 10<sup>2</sup> and 10<sup>6</sup> Hz.

For the dielectric experiments 17.8 μm parallel electro-optical cells were used, filled with the LC colloidal dispersions with various colloid contents. For reference purposes, also a 5.0 μm electro-optical cell filled with pure E7 was used. These glass cells were clamped between solid gold plated circular electrodes of the dielectric sample cell and placed in a nitrogen cryostat (Novocontrol), which regulated the temperature with a stability better than ± 0.05 °C. In order to provide an electrical contact between the inner conductive indium tin oxide (ITO) layers of the electro-optical cells and the (outer) sample electrodes, conductive paths around the glass edges were made by means of silver paint.

The linear (dynamic) dielectric response of the samples was probed with a low AC voltage, usually 0.3 V for 17.8 μm cells, well below the Frederiks transition in order to prevent changes in the director order due to the probe field. In case an electric field induced homeotropic alignment was examined, the weak AC field was superimposed by an additional bias voltage of up to 40 V. If necessary, the dielectric measurements were properly corrected for the (ITO) contact resistance using an equivalent circuit model.



## 4.3 Results and discussion

### 4.3.1 Determination of the director order parameter

A director parameter,  $S_d$ , is a measure for the degree of director orientation with respect to an arbitrarily chosen reference axis and is defined as:<sup>15</sup>

$$S_d = \frac{3(\cos^2 \theta) - 1}{2} \quad (4.1)$$

where  $\theta$  represents the angle between the director and the reference axis. Thus, for angles  $\theta$  ranging from 0 to 90 °,  $S_d$  varies between values of  $-0.5$  and 1.

Since dielectric spectroscopy enables the determination of the director order parameter  $S_d$  from the dielectric frequency spectra, this method is particularly suitable to quantify the impact of the colloidal network on the orientational order of the LC. Three schematic spectra of the permittivity  $\epsilon'(f)$  are displayed in Figure 4.1, referring to the planar state ( $\epsilon'_{s\perp}$ , static dielectric constant), the homeotropic state ( $\epsilon'_{s//}$ ) and the randomly aligned (isotropic) state ( $\epsilon'_{s, \text{average}}$ ).

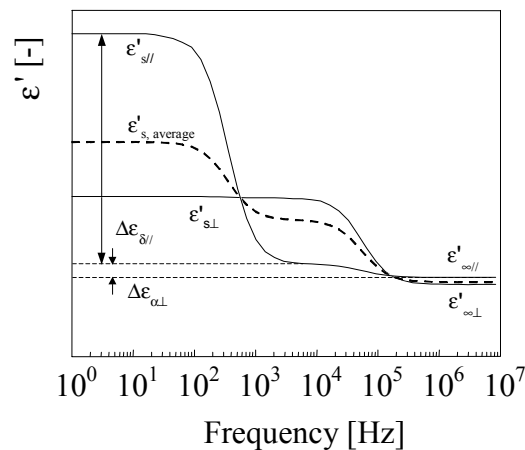


**Figure 4.1:** Schematic representations of dielectric spectra  $\epsilon'(f)$  of a liquid crystal in the planar, randomly aligned and homeotropic state.

From the figure two principal relaxation processes,  $\alpha$  and  $\delta$ , can be distinguished. Here, the slow  $\delta$ -relaxation process is related to flip motions of the rod-like LC molecules over their short molecular axis. The faster  $\alpha$ -relaxation process is usually related to the rotation of the molecules around their long molecular axis.<sup>14,16,17</sup>

According to Attard et al.,<sup>18</sup> the complex dielectric constant  $\varepsilon^*$  of an uniaxial liquid crystal, which is assumed to be built up of many domains, can be linked to the director order parameter  $S_d$  via:

$$\varepsilon_z^* = \varepsilon_{//}^*(1 + 2S_d)/3 + 2\varepsilon_{\perp}^*(1 - S_d)/3 \quad (4.2)$$

and

$$\varepsilon_x^* = \varepsilon_y^* = \varepsilon_{//}^*(1 - S_d)/3 + \varepsilon_{\perp}^*(2 + S_d)/3 \quad (4.3)$$

where  $\varepsilon_{\perp}^*$  and  $\varepsilon_{//}^*$  are the reference complex permittivities in the planar and homeotropic state, respectively, and  $\varepsilon_x^*$ ,  $\varepsilon_y^*$  and  $\varepsilon_z^*$  denote the complex permittivities measured in the direction of the electric field  $x$ ,  $y$  or  $z$ . For a parallel plate capacitor, where the electric field is in parallel to the plane normal direction  $z$ , Equation 4.2 can be solved for  $S_d$  which yields, using the real part of the complex dielectric constant:

$$S_d = \frac{3\varepsilon_z' - (\varepsilon_{//}' + 2\varepsilon_{\perp}')}{2(\varepsilon_{//}' - \varepsilon_{\perp}')} \quad (4.4)$$

The dielectric spectra of pure E7 as well as the colloidal mixtures with 2.7 and 6.4 wt % filler particles were recorded at  $-40$  °C, where both principal relaxation processes  $\alpha$  and  $\delta$  (see Figure 4.1) could conveniently be measured in the accessible experimental frequency range. The results are given in Figures 4.2a and b, which show the dielectric spectra in the non-addressed ( $p$ -aligned) state as well as in the addressed ( $h$ -aligned) state after correction for the volume fraction of the colloidal filler. These corrections were done by assuming that the spectra, "cleaned" from the influence of the filler on the dielectric spectra, should match each other in the isotropic phase. For this purpose, a rule of mixtures for heterogeneous two-phase systems known as the generalised Looyenga equation was used:<sup>19</sup>

$$\varepsilon^{*(1-2n)} = \phi_m \varepsilon_m^{*(1-2n)} + \phi_f \varepsilon_f^{*(1-2n)} \quad (4.5)$$

where  $\varepsilon_m^*$ ,  $\varepsilon_f^*$  and  $\varepsilon^*$  represent the complex dielectric constants of the continuous medium (LC E7), filler particles and the composite, respectively,  $\phi_m$  and  $\phi_f$  are the volume fractions of the matrix material and filler particles, respectively, and  $n$  is the shape or depolarisation factor of the dispersed phase ( $= 1/3$  for spherical particles). The volume fractions were approximated by the corresponding weight fractions, as the densities of both phases are

approximately equal. For the crosslinked PMMA colloids a dielectric permittivity,  $\epsilon'_f$ , of 3.5 was assumed.

Furthermore, for a quantitative data analysis of the spectra the frequency dependencies  $\epsilon'(f)$  and/or  $\epsilon''(f)$  were fitted by a sum of two empirical Havriliak-Negami (HN) relaxation functions,<sup>20</sup> which account for the (possibly broadened)  $\alpha$ - and  $\delta$ -relaxation process:

$$\epsilon'(\omega, T) = \epsilon'_\infty + \sum_{k=1}^2 \Re \left\{ \frac{\Delta\epsilon_k}{\left[1 + (i\omega\tau_k)^{a_k}\right]^{b_k}} \right\} \quad (4.6)$$

$$\epsilon''(\omega, T) = \sum_{k=1}^2 \Im \left\{ \frac{\Delta\epsilon_k}{\left[1 + (i\omega\tau_k)^{a_k}\right]^{b_k}} \right\} + \frac{\sigma}{\epsilon_o\omega} \quad (4.7)$$

In Equations 4.6 and 4.7, the parameters  $\Delta\epsilon_k$ ,  $\tau_k$ ,  $a_k$  and  $b_k$  denote the  $k^{\text{th}}$  relaxation strength, relaxation time as well as the shape parameters  $a$  and  $b$ ,  $\Re$  indicates the real part and  $\Im$  indicates the imaginary part. The 2<sup>nd</sup> term in Equation 4.7 accounts for the ohmic conduction  $\sigma$ . Note that all these parameters, and thus  $\epsilon'$  and  $\epsilon''$ , depend on  $\phi_f$ . A major advantage of the fit procedure is that it allows to obtain the static permittivity  $\epsilon'_s$  by the sum  $\epsilon'_s = \epsilon'_\infty + \Delta\epsilon_1 + \Delta\epsilon_2$  even from spectra which do not show a clear plateau value of the permittivity at the lowest frequency (cf. Figure 4.2a) yet. The fit results corresponding to Figures 4.2a and b are listed in Table 4.1 together with the order parameters  $S_d$  for three sample compositions. Note that  $\epsilon'_\perp$  and  $\epsilon''_{//}$  were taken as the reference permittivities from  $p$ - and  $h$ -aligned E7, while  $\epsilon'_z$  is the permittivity of E7 confined within the colloidal network in the absence or presence of an electric field. For each sample the reference permittivities of E7 were corrected for the colloid volume fraction.

The results displayed in Table 4.1 indicate that the colloidal dispersions show an obvious switching effect between the unaddressed ( $p$ -aligned) state and the addressed ( $h$ -aligned) state. As would be expected, the E7 becomes less perfectly oriented with increasing colloid content in both orientational states, due to local perturbation of the orientational ordering of the LC molecules that are in the direct surroundings of the immersed colloids. Thus, with increasing colloid content the multidomain formation of the confined E7 becomes more significant. The variation in director order with blend composition is nicely illustrated via a change in the ratio of the relaxation strengths of the  $\alpha$  and  $\delta$  peaks (see also Figure 4.2b).

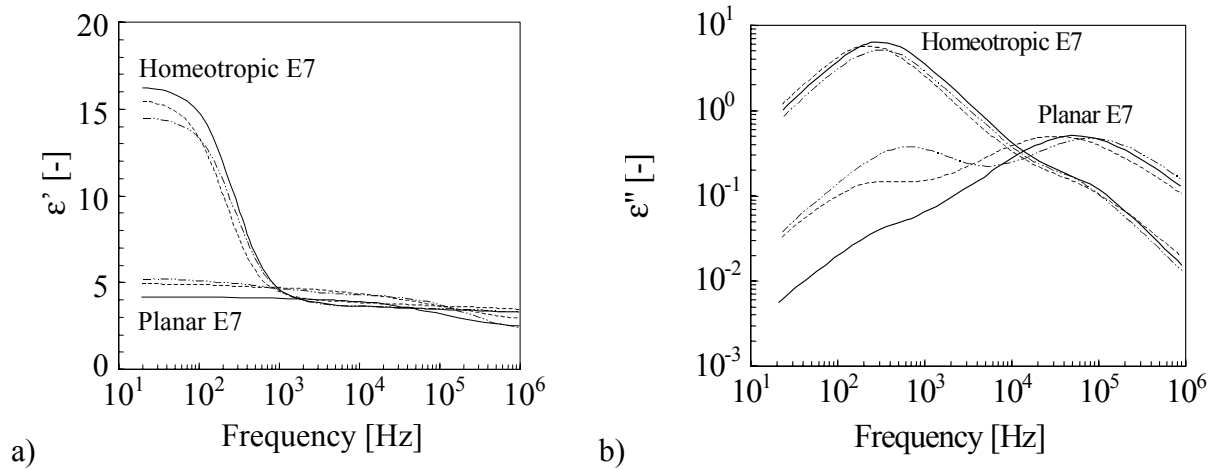


**Figure 4.2:** *Havriliak-Negami fits of (a) the dielectric permittivity  $\epsilon'$  and (b) the corresponding dielectric loss  $\epsilon''$  as a function of frequency at  $T = -40$  °C for E7/colloid mixtures with various colloid contents: (—) 0 wt % (pure E7); (---) 2.7 wt %; (-.-) 6.4 wt %. For a fair comparison between the  $\epsilon'$  spectra, the curves were properly normalised with respect to the reference spectrum of pure E7 (overlap of  $\epsilon'$  average).*

**Table 4.1:** *Director order parameters ( $S_d$ ) and relaxation strengths of the fitted  $\alpha$  and  $\delta$  peaks for E7 with various colloid contents in the unaddressed and addressed state. The  $S_d$  applies to the lowest frequency of 20 Hz.*

Colloid content [wt %]	$\Delta\epsilon$ ( $\delta$ )	$\Delta\epsilon$ ( $\alpha$ )	$\Delta\epsilon$ ( $\delta$ )	$\Delta\epsilon$ ( $\alpha$ )	$S_d$	
	[-]	[-]	[-]	[-]	[-]	
	0 V	0 V	40 V	40 V	0 V	40 V
0	0.0498	1.37	12.9	0.173	-0.5	1
2.7	0.248	1.42	11.6	0.226	-0.402	0.927
4.5	0.565	1.32	-	-	-0.395	-
6.4	0.771	1.19	10.5	0.176	-0.378	0.787
8.6	0.540	1.19	-	-	-0.387	-

### 4.3.2 The interlayer model

For the E7 being in the isotropic phase, both the continuous LC medium and the LC molecules in the direct neighbourhood of the inclusions adopt a random orientation. In this situation, a two-phase model, such as the generalised *Looyenga* model,<sup>19</sup> is sufficiently adequate to describe the mean dielectric properties of the matrix-inclusion type heterogeneous material. In the nematic state of E7, however, three distinct phases with different dielectric permittivities have to be considered: (i) The crosslinked colloids as the dispersed phase, (ii) the aligned, bulk LC as the continuous medium and, additionally, a shell

around the particles that consists of LC molecules with a distorted orientation. To this situation, when neglecting the anisotropy of the matrix phase, the so-called *interlayer* model that uses an asymmetrical effective medium approach can be satisfactorily applied. This model accounts for the presence of an additional interfacial layer in matrix-inclusion type heterogeneous materials (Figure 4.3).<sup>21</sup>

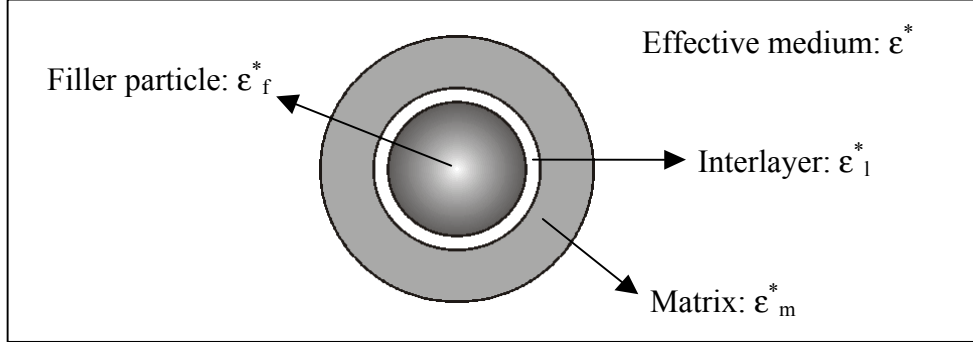


**Figure 4.3:** Schematic representation of the nematic LC E7 filled with colloidal particles according to the interlayer model. The interfacial layer accounts for the LC molecules with random orientation, confined within a shell around the particles.

The interlayer model describes the dielectric behaviour of the inhomogeneous system as follows:

$$\epsilon^* = \frac{\epsilon_f^* \cdot \phi_f + \epsilon_l^* \cdot \phi_l \cdot Y + \epsilon_m^* \cdot \phi_m \cdot Z}{\phi_f + \phi_l \cdot Y + \phi_m \cdot Z} \quad (4.8)$$

with:

$$Y = \frac{[(1-n)\epsilon_l^* + n\epsilon_f^*]}{\epsilon_l^*} \quad (4.9)$$

$$Z = \frac{[n\epsilon_l^* + (1-n)\epsilon_m^*] \cdot [n\epsilon_f^* + (1-n)\epsilon_l^*] + d \cdot n \cdot (1-n) (\epsilon_l^* - \epsilon_m^*) (\epsilon_f^* - \epsilon_l^*)}{\epsilon_l^* \cdot \epsilon_m^*} \quad (4.10)$$

$$d = \frac{\phi_f}{\phi_f + \phi_l} \quad (4.11)$$

where  $\epsilon_l^*$  and  $\phi_l$  are the complex dielectric constant and the volume fraction of the interfacial layer. The filler dependent static dielectric constants of Figure 4.2a were modelled by use of

Equation (4.8), with  $\phi_1$  as the fitting parameter. Here,  $\epsilon'_1$  was approximated by the dielectric constant of randomly aligned E7,  $\epsilon'_{\text{average}}$ , which was calculated via  $\epsilon'_{\text{average}} = (2\epsilon'_{\perp} + \epsilon'_{\parallel})/3$ .<sup>22</sup> The values for  $\epsilon'_{\perp}$  and  $\epsilon'_{\parallel}$  were taken from the fits of the experimental curves for *p*- and *h*-aligned E7. For the colloid filled LC samples the thickness of the interfacial layer,  $D_1$ , was calculated from the corresponding volume fractions. The results are listed in Table 4.2 for the samples containing various amounts of colloids.

**Table 4.2:** *Results of the interlayer model applied to the fits of the Looyenga-corrected static dielectric constants of colloid/E7 mixtures in the unaddressed and addressed state.*

$\phi_f$ [-]	$\phi_1$ [-]	$\phi_1$ [-]	$D_1$ [nm]	$D_1$ [nm]
	0 V	40 V	0 V	40 V
0.027	0.208	0.070	337	164
0.045	0.220	-	254	-
0.064	0.231	0.150	216	156
0.086	0.180	-	145	-

It is noteworthy that the interfacial layer thickness decreases with increasing particle content. This suggests that agglomeration phenomena become more significant with increasing colloid content in the E7. The remaining shell of perturbed LC during application of a bias voltage is indicative of an incomplete homeotropic alignment of the LC.

### 4.3.3 Quasi-static field-induced changes of the director order

Whereas the previous sections have focussed on the ultimate planar and homeotropic order that is achievable in E7 and in the related colloidal mixtures, in this section the switching process from the initial off-state to the homeotropically aligned on-state will be discussed in more detail. For this purpose, dielectric spectra were taken while the samples were exposed to a constant bias voltage in order to ensure a quasi-static, i.e. almost time-independent, state of alignment during the acquisition of an individual spectrum. In this way, by step-wise increasing the DC voltage between 0 and 40 V, a gradual change from *p*-alignment to *h*-alignment was induced, which resulted in gradual changes in the dielectric spectra as shown in Figure 4.4. With increasing bias voltage, all materials reveal a competitive behaviour between the amplitude of the  $\delta$ -relaxation peak (gradually increasing) and the amplitude of the  $\alpha$ -relaxation peak (gradually decreasing).

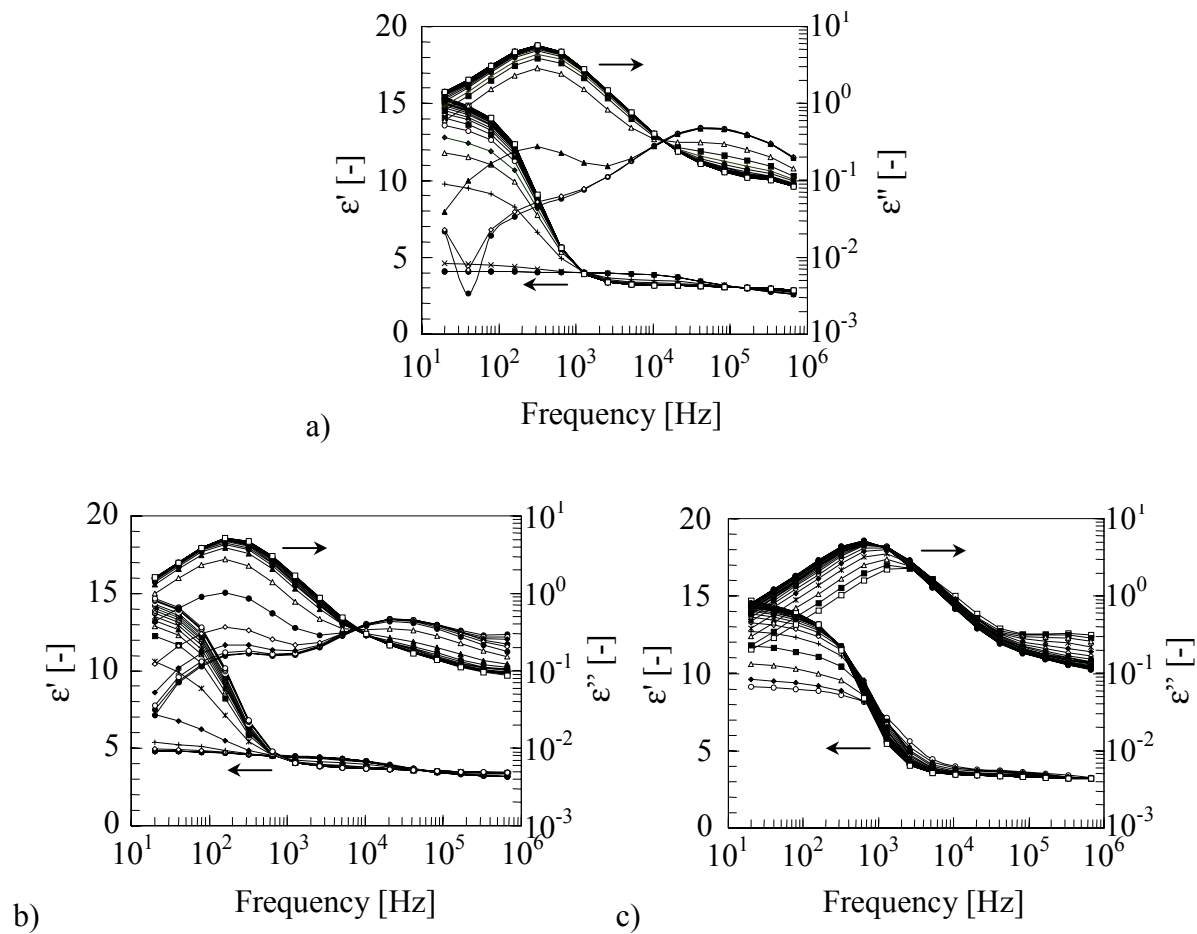


**Figure 4.4:** Dielectric spectra of E7/colloid mixtures with various colloid contents: (a) 0 wt % (pure E7); (b) 2.7 wt %; (c) 6.4 wt %. The spectra were recorded at  $-40$  °C during the application of a bias voltage, which was gradually increased from 0 to 40 V by steps of 2 V.

Figure 4.4a shows a striking feature of pure E7, the existence of isosbestic points, i.e. frequencies at which either  $\epsilon'$  or  $\epsilon''$  are virtually independent on the state of alignment. Upon addition of colloids to the E7, these isosbestic points become less obvious or even disappear as the  $\delta$ -relaxation peak gradually shifts with increasing bias voltage.

For a quantitative analysis of these phenomena, the spectra were fitted to Equation 4.7. Here, the slow  $\delta$  relaxation can fairly be described as a single relaxation time process (Debye relaxation). In contrast, the fast  $\alpha$  process is the manifestation of (at least) two indistinguishable different molecular relaxation modes, causing a natural peak broadening as well as a combined (averaged) relaxation time depending on the angle between the electric field and the nematic director.<sup>17</sup> Hence, the analysis was restricted to the  $\delta$  process. The results are displayed in Figure 4.5, showing the relaxation strength  $\Delta\epsilon_\delta$  as well as the peak relaxation frequency  $f_{\max}$ , which corresponds to the relaxation time  $\tau_\delta$ .

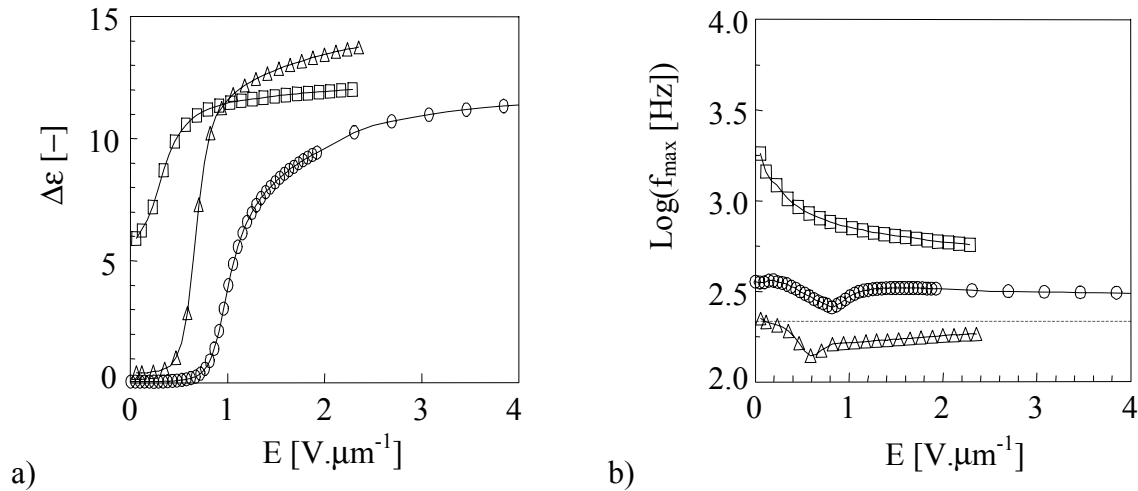


**Figure 4.5:** (a) Dielectric relaxation strength  $\Delta\epsilon$  and (b) peak relaxation frequency  $f_{\text{max}}$  of the  $\delta$  process for E7 and E7/colloid mixtures obtained from the dielectric spectra at  $-40^\circ\text{C}$  as a function of the bias field: (○) E7; (△) 2.7 wt % colloid/E7; (□) 6.4 wt % colloid/E7.

Figure 4.5a shows the (quasi-static) switching characteristics in terms of a field-dependent relaxation strength,  $\Delta\epsilon_\delta$ . Surprisingly, the pure liquid crystal exhibits the highest threshold field. Addition of 2.7 wt % colloidal filler results in a lowering of the threshold voltage while maintaining the switching range between full  $p$ - and  $h$ -alignment. Further increase of the filler content further reduces the threshold field, but shows no recovery of the planar state on the time-scale of the experiment at  $-40^\circ\text{C}$ .

The reduction of the threshold field upon addition of a second phase to the LC has been reported earlier for anisotropic thermoreversible gels within TN cells.<sup>23-25</sup> In agreement with the explanation given for these physical gels, it is thought here that this effect comes from the anchoring of the LC domains to the colloidal network. This anchoring interaction will (locally) dominate over the interaction between the LC and the rubbed polyimide orientation layers, resulting in elastic director deformations. As a consequence, parts of the LC domains are able to switch between *two metastable* orientation states, which might lower the elastic energy to be overcome by the electric field. In addition, local field enhancements due to the dielectric heterogeneities are also likely to contribute to the low-field switching characteristics. It has to be emphasised, however, that the experiments were carried out at an unusually low temperature. This might give other switching characteristics, e.g. a relatively high threshold field for the pure E7.

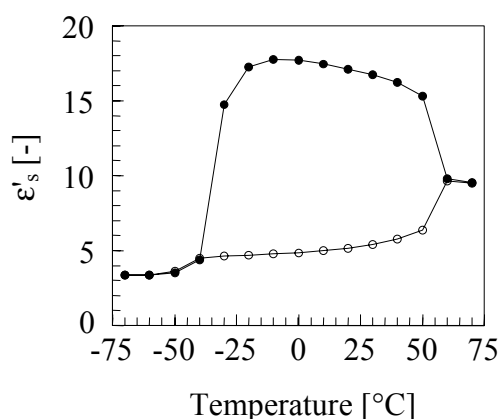
According to Figure 4.5b, the peak relaxation frequency of pure E7 indeed shows only a marginal dependence on the state of alignment (see also Figure 4.4a). The small local minimum corresponds to the transition range between  $p$ - and  $h$ -alignment, where a planarly aligned surface layer coexists with an oriented bulk fraction, possibly causing a slight peak shift due to the dielectric inhomogeneity in that transition region. However, much larger peak



shifts were found for the colloidal mixtures. Both these considerable peak shifts and the disappearance of the isosbestic points can be ascribed to the existence of different LC fractions in the colloidal dispersions with specific molecular mobilities.<sup>7,10,12-14</sup> One possible reason for altering the molecular dynamics can be a change in anchoring from a weak to a strong anchoring regime affecting particularly the mobility on internal surfaces. In addition, changes in the relaxation time of the  $\delta$ -relaxation process are also likely to occur as a result of elastic director deformations of the LC domains. A detailed modelling of these phenomena is given elsewhere.<sup>26</sup>

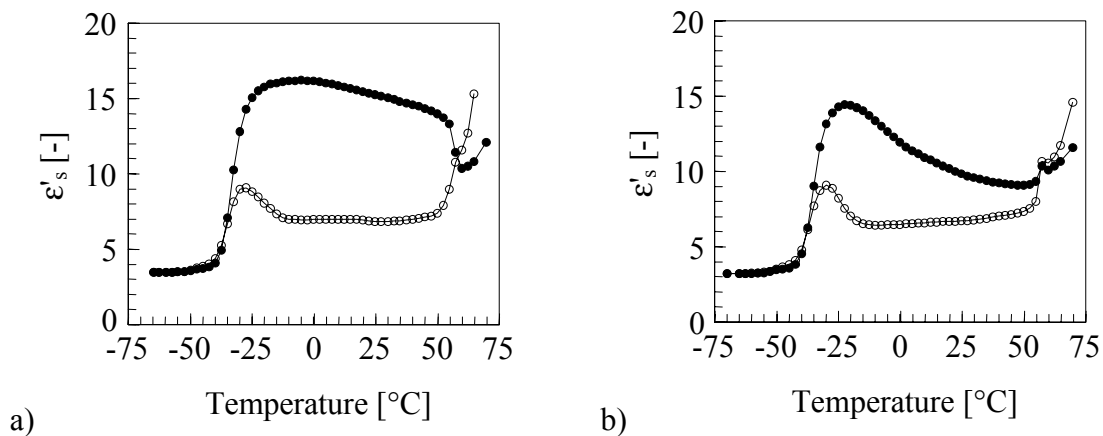
#### 4.3.4 Temperature- and time-dependent orientational order

The temperature-dependent alignment of the LC E7 is illustrated by Figure 4.6. The figure shows the initial static dielectric permittivities of E7 in the planar state together with the permittivities that were collected at the end of a voltage scan from 0 to 40 V, as a function of temperature and at a frequency of 1 kHz. At temperatures above  $\sim 60$  °C the E7 is in the isotropic phase and does not align anymore in the presence of the DC field. As expected, at temperatures well below  $-40$  °C (close to the  $T_g$  of E7) also no response is observed, indicating that molecular motions ( $\alpha$  and  $\delta$  process) have been frozen in.



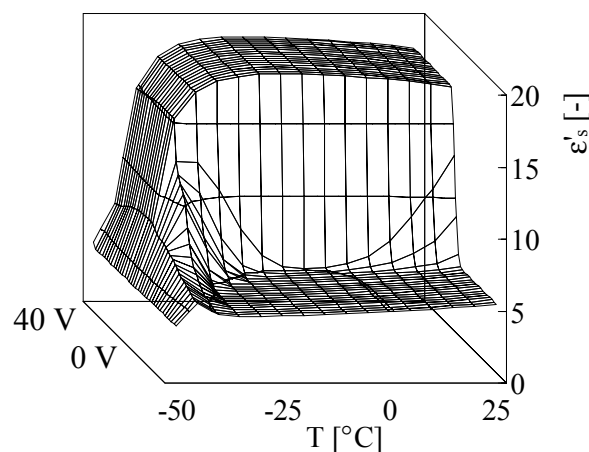
**Figure 4.6:** *Static dielectric permittivity as a function of temperature obtained from scans at 1 kHz for pure E7 in the 0 V unaddressed state (○) and the 40 V addressed state (●).*

Figure 4.7 shows the (Looyenga-corrected) static dielectric permittivities of the 2.7 and 6.4 wt % colloid/E7 samples as a function of temperature for the unaddressed and addressed state. With increasing colloid content, a less perfectly planarly aligned and homeotropically aligned state is achieved. For the initial static dielectric constants an additional (remaining) orientation is visible at low temperatures. In case of the highest filler content (6.4 wt %) the bias field applied is obviously too low to achieve an effective homeotropic orientation of the E7 bulk fraction, due to the large cell thickness of 17.8  $\mu\text{m}$ .



**Figure 4.7:** Static dielectric permittivity as a function of temperature obtained from scans at 1 kHz for (a) 2.7 wt % and (b) 6.4 wt % colloid/E7 samples in the 0 V unaddressed state ( $\circ$ ) and the 40 V addressed state ( $\bullet$ ).

The switching kinetics of E7 was investigated by subjecting the E7 to a step-voltage sequence  $0 \rightarrow 40 \text{ V} \rightarrow 0 \text{ V}$ , at temperatures ranging from 25 to  $-50 \text{ }^\circ\text{C}$  and at a fixed frequency of 110 Hz (Figure 4.8). Here, each voltage level was continued for two minutes. In this way, the *retardation* behaviour to the homeotropic state, driven by the electric field, and the *relaxation* behaviour of the nematic director to the planar (ground) state, controlled by elastic restoration forces, is addressed separately.



**Figure 4.8:** Relaxation of the static dielectric permittivity for temperatures ranging from 25 to  $-50 \text{ }^\circ\text{C}$  obtained at 110 Hz for the pure E7 in the 40 V addressed state (curves at the back) and the 0 V unaddressed state (curves at the front). The time interval between the curves is 2 s.

When focussing on the switching to the on-state it is seen from Figure 4.8 that, on the time-scale of the experiment, the LC molecules show an instantaneous switching behaviour to the homeotropic state even for temperatures as low as  $-40 \text{ }^\circ\text{C}$ . In contrast, the relaxation of

the nematic director to the planar state after removal of the bias voltage shows some slow-down at both the highest and the lowest temperatures.

The increasing relaxation time for the decay of the nematic order with decreasing temperature is plausible since the restoration of the planar order is directly linked to the viscosity of the nematic crystal, which in turn scales with the relaxation times of the two principal molecular relaxations.<sup>27</sup> Hence, at sufficiently high temperatures we find an instantaneous decay on the time-scale of the experiment (time interval  $\Delta t = 2\text{s}$ ).

In contrast, the delayed relaxation behaviour at higher temperatures is obviously of different nature, most likely associated with an increase in conductivity as ionic impurities start to respond to the biasing DC field. This effect is known especially from dielectric liquids as electrode polarisation, caused by accumulation of ionic charge carriers at the ion-blocking liquid/electrode interface. In this way, an internal field is built-up at a time constant  $\tau_{\text{EP}}$  (EP: electrode polarisation) which is given by the cell bulk resistance,  $R$ , and the two double layer capacitances,  $C_d$ , in series to  $R$  according to  $\tau_{\text{EP}} = RC_d/2$ . A detailed treatment of this problem is given elsewhere.<sup>28</sup> Electrode polarisation can easily be identified in the frequency spectra  $\epsilon'(f)$  as a huge increase of the dielectric constant beyond the static permittivity of the LC. Since the time constant  $\tau_{\text{EP}}$  usually also scales with the molecular relaxations, electrode polarisation only manifests itself at elevated temperatures, if the time-scale of the experiment approaches the order of  $\tau_{\text{EP}}$ . Summarising the features seen in Figure 4.8, one has to be aware that the apparent switching characteristics might reflect both molecular reorientation processes and electric charge redistribution effects.

Upon addition of non-conductive particles to the LC, an additional interfacial charge build-up between the particles and the LC matrix might occur due to a difference in conductivity between the two phases, which is known as the Maxwell-Wagner effect.<sup>29,30</sup> Figure 4.9 shows the retardation and relaxation behaviour of the (mean) nematic director of the LC/colloid mixtures as a response to a step-up ( $0 \rightarrow 40\text{ V}$ ) and step-down ( $40 \rightarrow 0\text{ V}$ ) bias change. For both colloidal mixtures, two distinct slow decay processes relaxation phenomena can be identified at low temperatures. While the decay process at  $-30\text{ }^\circ\text{C}$  corresponds reasonably well to that of pure E7, the other relaxation phenomenon around  $-10\text{ }^\circ\text{C}$  indicates that charge phenomena could be involved in this anomalous switching response. This idea is supported by Figure 4.9b showing an overshoot in the permittivity around  $-10\text{ }^\circ\text{C}$  just after switching off the DC voltage, indicating the presence of a strong internal field.<sup>31,32</sup>

On the basis of the Maxwell-Wagner effect, it could be anticipated that the charge polarisation effects become stronger upon addition of non-conductive colloids to the LC medium,<sup>29,30</sup> and are present at much lower temperatures for the colloid filled LC than for the pure LC. In order to rationalise the shift of charge polarisation phenomena towards such low temperatures one has to assume that the colloidal mixtures exhibit a dramatically higher conductivity than pure E7.

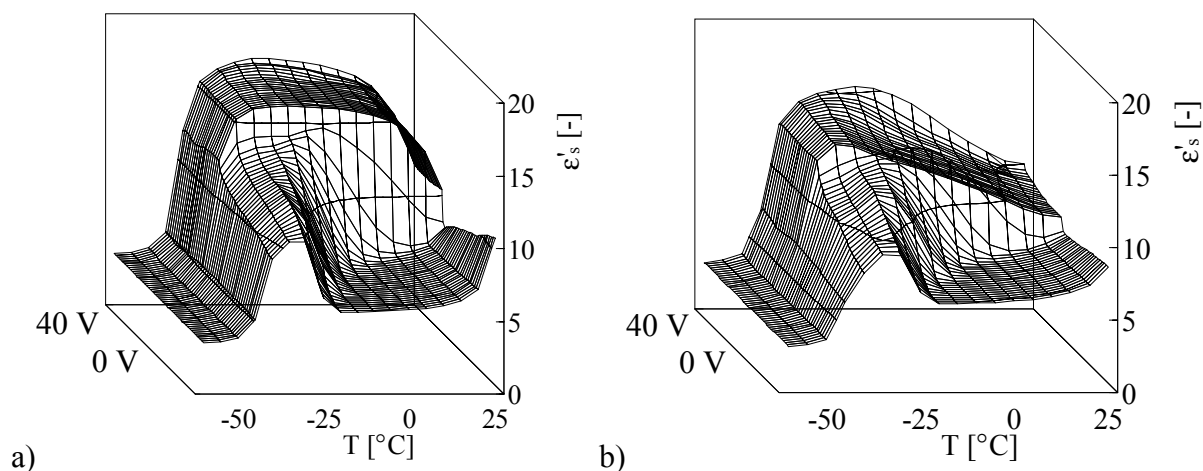


**Figure 4.9:** Relaxation of  $\epsilon'_s$  for temperatures ranging from 25 to  $-60$  °C obtained at 110 Hz for (a) 2.7 wt % and (b) 6.4 wt % colloid/E7 samples in the 40 V addressed state (curves at the back) and the 0 V unaddressed state (curves at the front). The time interval between the curves is 2 s.

Figure 4.10, which displays the temperature dependence of the conductivity as obtained from the dielectric spectra, indeed reveals a substantial increase of the conductivity for colloidal filled LC at all temperatures. As a consequence, the temperature at which the conductivity amounts to a certain value of e.g.  $10^{-10}$  S.m $^{-1}$  shifts down by almost 60 °C between pure E7 and E7 with 6.4 wt % filler, which is in fair agreement with the temperature shifts noticed in Figure 4.9 before.

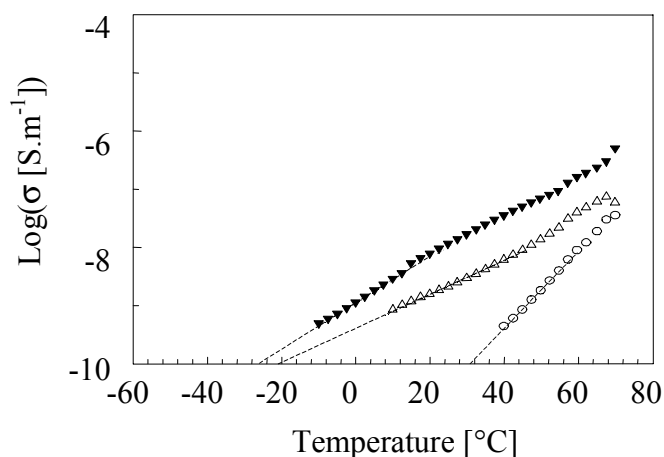


**Figure 4.10:** Temperature dependent conductivity of E7/colloid mixtures with various colloid contents: (○) 0 wt % (pure E7); (△) 2.7 wt %; (▼) 6.4 wt %.

Possible reasons for the surprising increase in conductivity could be extra ionic impurities originating from the polymer filler phase, an intrinsic surface conductivity along the colloidal network or a significant increase of the conductivity of bulk E7 due to elastic distortions of the director order and/or a high number of disclinations.

### 4.3.5 Electro-optical properties of the LC colloidal dispersions in TN displays

#### 4.3.5.1 Transmittance-voltage characteristics

TN cells filled with various colloidal dispersions in E7 were characterised with respect to their electro-optical performance. In Figure 4.11, the transmittance is shown as a function of the voltage applied for TN cells filled with E7 and various 630 nm sized colloid fractions. From Figure 4.11 and Table 4.3 it is deduced that the transmittance in the off-state decreases with increasing colloid concentrations, which is attributed to light loss due to light scattering. For the rather low colloid concentrations the absolute transmittance in the off-state is only slightly reduced by the colloidal network, when compared to the conventional cell filled with the pure LC E7. Furthermore, Figure 4.11 shows that the colloid materials are reversibly switched from a transparent to a dark state. This indicates that the particle network does not prevent the LC matrix to be organised in a twisted fashion by the weak external forces exerted by the polyimide orientation layers, as was also confirmed by optical polarisation microscopy. The appearance of a highly black on-state implies that the refractive index matching of the polymeric inclusions and LC matrix is reasonably successful.

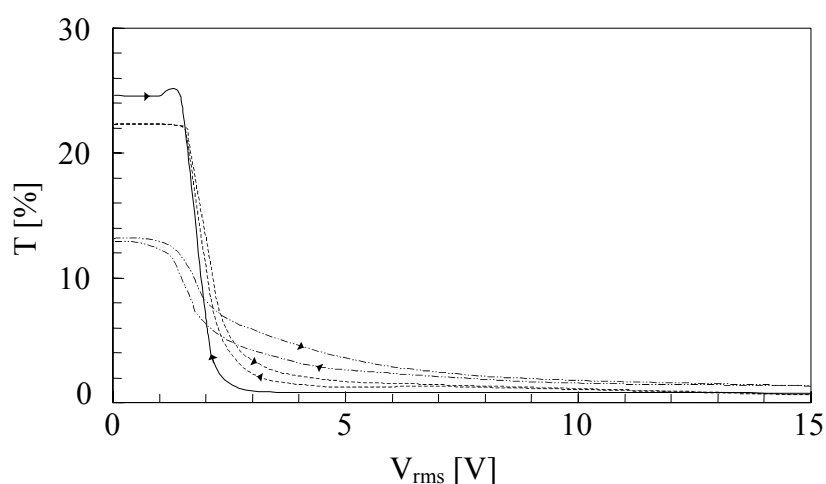


**Figure 4.11:** *Transmittance as a function of the applied AC voltage of 1 kHz square wave for 7  $\mu\text{m}$  TN electro-optical cells filled with LC colloidal dispersions with various fractions of 630 nm sized colloids: (—) 0 wt % (pure E7); (--) 2.7 wt %; (-.-) 11.7 wt %.*

In Figure 4.12 the transmittance-voltage characteristics are shown for LC dispersions based on different colloid sizes (see also Table 4.3). The electro-optical characteristics of the TN cells based on the small 43 nm colloids clearly distinguish themselves from the switching behaviour of the cells based on the larger colloids. This is attributed to the pronounced polydomain structure of the LC dispersion based on the 43 nm colloids, which strongly enhances the light-scattering phenomenon and significantly hampers the LC director to be oriented into a twisted state.

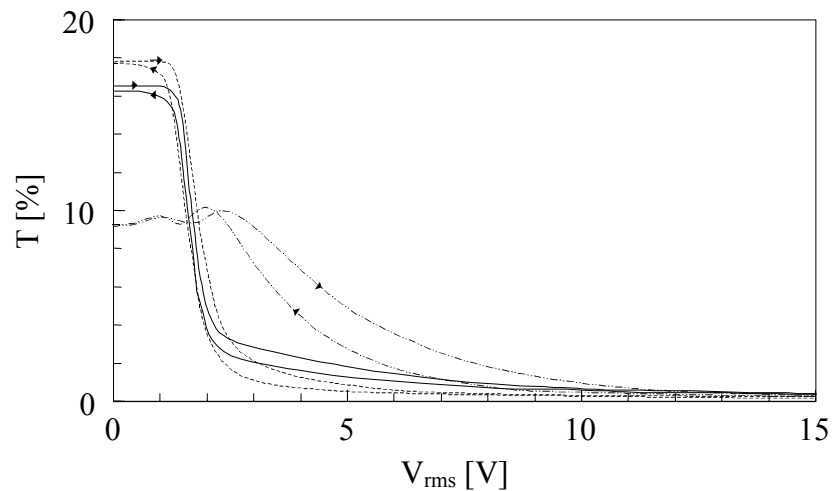


**Figure 4.12:** *Transmittance as a function of the applied voltage for 7  $\mu\text{m}$  TN electro-optical cells filled with 6.4 wt % colloid/LC dispersions based on various colloid sizes: (---) 43 nm; (--) 630 nm; (—) 1.2  $\mu\text{m}$ .*

The impact of colloid size and colloid concentration on the threshold voltage  $V_{90}$ , defined here as the voltage needed to switch from 100 to 10 % of the relative transmission, is summarised in Figure 4.13a. The figure reflects an increase in switching voltage with increasing colloid concentration. Additionally, it is seen that the LC filled with the small 43 nm colloids needs much higher voltages to switch to a homeotropic state. Both these observations are consistent with the expectation that smaller LC domains require higher switching voltages, as the anchoring interaction of LC molecules with the particle surfaces becomes more significant.<sup>33-35</sup> In spite of this, Figures 4.11 and 4.12 reveal that upon addition of 630 nm or 1.2  $\mu\text{m}$  colloids to the E7 the switching process is initiated at voltages similar to the one needed for the pure E7. For high amounts of 630 nm sized colloids the switching process is initiated at even lower voltages than required for the pure E7, as was also observed for the switching experiments at  $-40\text{ }^{\circ}\text{C}$  (see Figure 4.5a). To illustrate this, in Figure 4.13b the corresponding  $V_{10}$  is shown, which is defined as the voltage needed to switch from 100 to 90 % of the relative transmission. Obviously, the initial fast switching is shielded by a significant transmission-"tail", which implies a decreasing steepness of the T-V curve in the intermediate voltage regime. This continuous decay of the transmittance with increasing voltage is commonly related to the existence of a distribution of LC domain sizes.<sup>36</sup> Optical polarisation microscopy was used to verify that LC molecules in the vicinity of the polymeric aggregates reorient into the homeotropic state at somewhat higher voltages than the 'free' LC, which also explains the higher  $V_{10}$  that is observed for the LC filled with the 43 nm sized colloids.

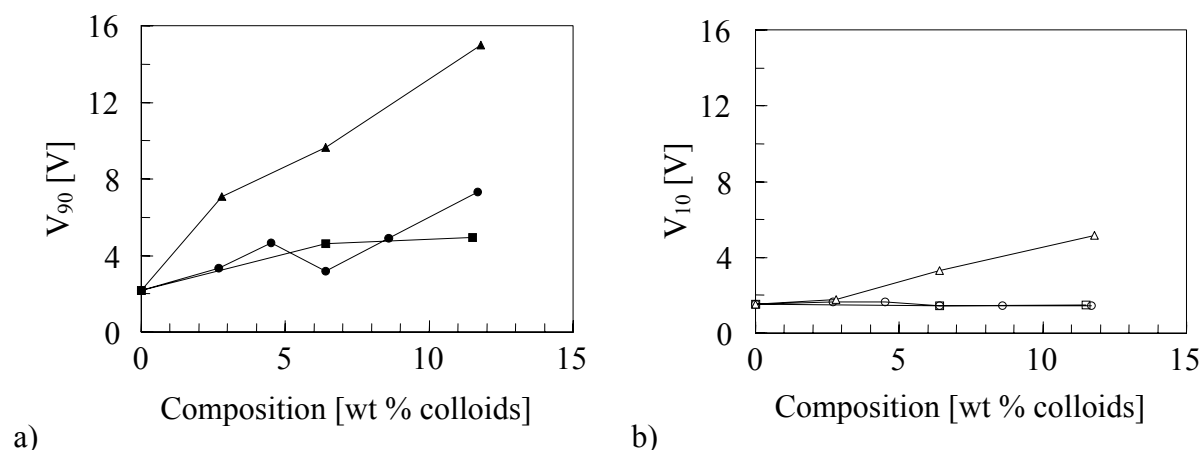


**Figure 4.13:** (a)  $V_{90}$  and (b)  $V_{10}$  for TN electro-optical cells filled with LC colloidal dispersions as a function of colloid concentration for various colloid sizes: ( $\blacktriangle$ ,  $\triangle$ ) 43 nm; ( $\bullet$ ,  $\circ$ ) 630 nm; ( $\blacksquare$ ,  $\square$ ) 1.2  $\mu\text{m}$ .

**Table 4.3:** Transmittance in the 0 V unaddressed and 10 V addressed state together with the corresponding contrast ratio for TN cells (equipped with crossed polarisers) filled with various LC colloidal dispersions.

Composition [colloids wt %]	$T_{\text{off}}$ [%]	$T_{\text{on}}$ [%]	$\text{CR}^1$ [-]
0	24.42	0.083	294
2.8 (43 nm)	14.41	0.111	130
6.4 (43 nm)	9.30	0.111	84
11.8 (43 nm)	9.34	1.111	8.4
2.7 (630 nm)	22.06	0.195	113
4.5 (630 nm)	20.45	0.225	91
6.4 (630 nm)	17.81	0.111	160
8.6 (630 nm)	17.56	0.281	62
11.7 (630 nm)	13.14	0.613	21
6.4 (1.2 $\mu\text{m}$ )	16.52	0.251	66
11.5 (1.2 $\mu\text{m}$ )	15.51	0.306	51

<sup>1</sup>CR = Optical contrast ratio

#### 4.3.5.2 Switching kinetics

Figure 4.14 demonstrates the effect of colloid size and concentration on the switching times, which were monitored at an applied voltage of 10 V. The results are summarised in Table 4.4. Here, the rise time,  $\tau_r$ , represents the time between 100 and 10 % of the relative transmission. The decay time,  $\tau_d$ , represents the time between 0 and 90 % (relative)

transmission. Again, it appears that the results are strongly related to the morphology of the materials. For instance, for the 43 nm sized colloids it is deduced from Table 4.4 that the addition of the colloids to the LC E7 initially leads to both a faster response and a faster relaxation. Upon addition of more colloids longer response times are found. Similar behaviour was previously observed for LC physical gels with finely dispersed molecular networks.<sup>25</sup> In agreement with those findings, it is anticipated that the existence of finely dispersed aggregates within the LC efficiently weakens the interaction between the LC and the rubbed polyimide layers, thereby accelerating the response behaviour towards applied electric fields. However, at a too high concentration of the dispersed phase the anchoring interaction between colloids and LC will prevail, resulting in longer rise times.

At the same time, an increased anchoring interaction between the finely dispersed phase and the LC leads to a faster relaxation after removal of the external electric field. Previously, for anisotropic networks a decrease in  $\tau_d$  and an increase in both  $\tau_r$  and  $V_{90}$  were associated with an increase in the elastic constant.<sup>37</sup> For closed and open pore type PDLC's these shifts were accounted for by a decrease in the LC cavity size or a more pronounced ellipticity of the LC domains according to:<sup>33-35,38</sup>

$$V_{on} \approx \frac{1}{c} \frac{d}{R} \left[ \frac{K(L^2 - 1)}{\epsilon_o \Delta \epsilon} \right]^{\frac{1}{2}} \quad (4.12)$$

$$\tau_r = \frac{\gamma_1}{\epsilon_o \Delta \epsilon E^2 - \frac{K(L^2 - 1)}{R^2}} \quad (4.13)$$

$$\tau_d = \frac{\gamma_1 R^2}{K(L^2 - 1)} \quad (4.14)$$

where  $c^{-1}$  is a prefactor that corrects for the dielectric mismatch between the dispersed and continuous phase,  $d$  the film thickness,  $R$  a characteristic drop radius,  $L$  the droplet aspect ratio and  $\gamma_1$  a rotational viscosity coefficient. Note that  $\tau_r$  and  $\tau_d$  of Equations 4.13 and 4.14 do not correspond to a 90 % change in transmittance and do not account for charge storage and backflow phenomena.

In contrast with these observations for the 43 nm colloids/LC mixture with respect to  $\tau_r$  and  $\tau_d$ , the LC's filled with the 630 nm and 1.2  $\mu\text{m}$  sized colloids show an opposite trend. This might suggest the existence of an optimum LC domain size with respect to switching kinetics, determined by the competition between colloid-LC and polyimide-LC interaction forces. Apart from switching times, it is observed from the change in optical bounce in Figure 4.14 that the so-called backflow effect<sup>39,40</sup> becomes less pronounced upon immersion of



colloids in the LC. This is presumably the direct result of the presence of the polymeric network, which restricts macroscopic flow within the electro-optical cell.

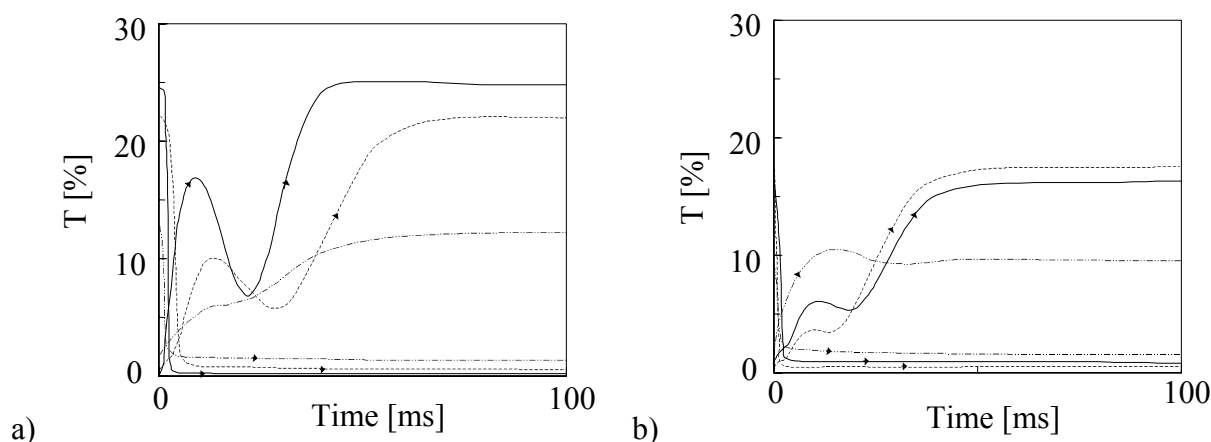


**Figure 4.14:** *Transmittance in time during switching between the 0 V non-addressed and 10 V addressed state for 7  $\mu\text{m}$  TN electro-optical cells filled with various LC colloidal dispersions: (a) (—) 0 wt % (pure E7); (---) 2.7 wt % 630 nm sized colloids; (···) 11.7 wt % 630 nm sized colloids; (b) 6.4 wt % colloids with a size of (···) 43 nm; (---) 630 nm; (—) 1.2  $\mu\text{m}$ .*

**Table 4.4:** *Rise and decay times for TN cells (equipped with crossed polarisers) filled with various LC colloidal dispersions, obtained for 10 V addressing.*

Composition [colloids wt %]	$\tau_r$ [ms]	$\tau_d$ [ms]
0	2.79	36.5
2.8 (43 nm)	2.01	24.3
6.4 (43 nm)	7.16	5.98
11.8 (43 nm)	22.7	1.23
2.7 (630 nm)	5.13	38.9
4.5 (630 nm)	5.37	58.5
6.4 (630 nm)	1.54	38.1
8.6 (630 nm)	2.23	42.6
11.7 (630 nm)	2.41	52.3
6.4 (1.2 $\mu\text{m}$ )	2.46	39.4
11.5 (1.2 $\mu\text{m}$ )	2.34	41.7

In Figure 4.15 the switching times are shown as a function of the voltage applied. According to Equations (4.13) and (4.14) the rise times are expected to be reduced upon application of higher electric fields, while the fall times are expected to be independent of the electric field applied. Figure 4.15a shows a rapid decrease of  $\tau_r$  in the transition region. Figure

4.15b shows only marginal variations of  $\tau_d$  over the voltage regime, both for the pure E7 as well as for the E7 filled with the colloidal particles.

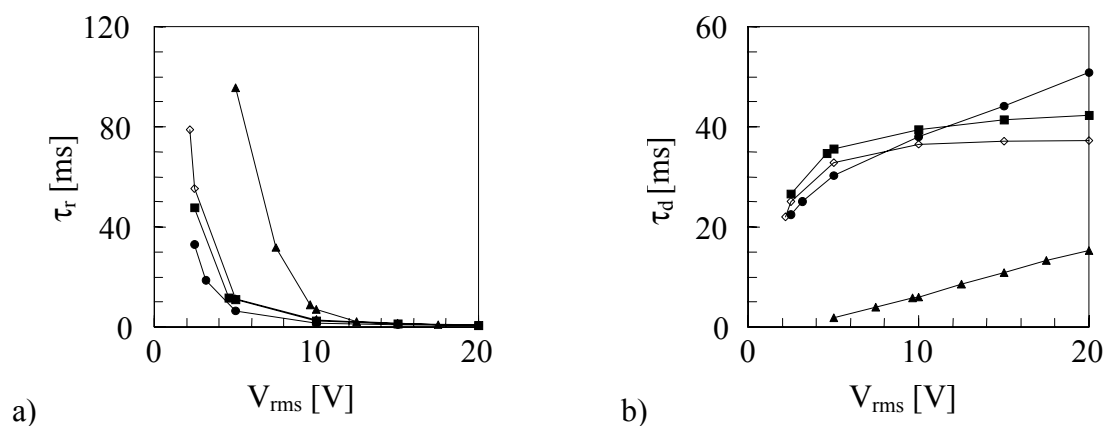


**Figure 4.15:** (a) Rise and (b) decay times as a function of the applied voltage for ( $\diamond$ ) LC E7 (pure) and for 6.4 wt % LC colloidal dispersions based on colloids with different diameters: ( $\blacktriangle$ ) 43 nm; ( $\bullet$ ) 630 nm; ( $\blacksquare$ ) 1.2  $\mu m$ .

### 4.3.6 Electro-optical properties of the LC colloidal dispersions for light-scattering electro-optical switches

#### 4.3.6.1 Transmittance-voltage characteristics

The LC colloidal dispersions were tested for their applicability in optical light-shutters. In Figure 4.16 the absolute transmittance is shown as a function of the applied voltage for a reference PDLC cell and for parallel cells filled with various colloidal dispersions in the on-state and in the off-state, measured 2 s after removal of the voltage applied. In order to avoid an already present memory in the initial state, these measurements were performed with freshly prepared cells. Figure 4.16a shows that the colloidal dispersions efficiently scatter light in the unaddressed state, due to refractive index mismatches between LC domains and/or between polymer and LC phase. Upon application of an external electric field the materials are switched to a more transparent state, which indicates that refractive index differences within the two-phase material largely disappear upon homeotropic alignment of the LC. Part of the incident light ( $\sim 15$ -20 %) is lost due to reflections and absorptions via the glass/ITO layers of the electro-optical cell. From Figure 4.16a it is seen that an increase in the concentration of the dispersed phase is generally accompanied by an increase in the threshold voltage, a more efficient light scattering in the off-state and a less transparent on-state. As with the TN configuration, also here a continuous increase in transmittance with voltage is observed. Especially in the high voltage regime the memory effects appear to be considerable, which points to a slower relaxation of the highly anchored LC molecules with respect to the bulk LC molecules.

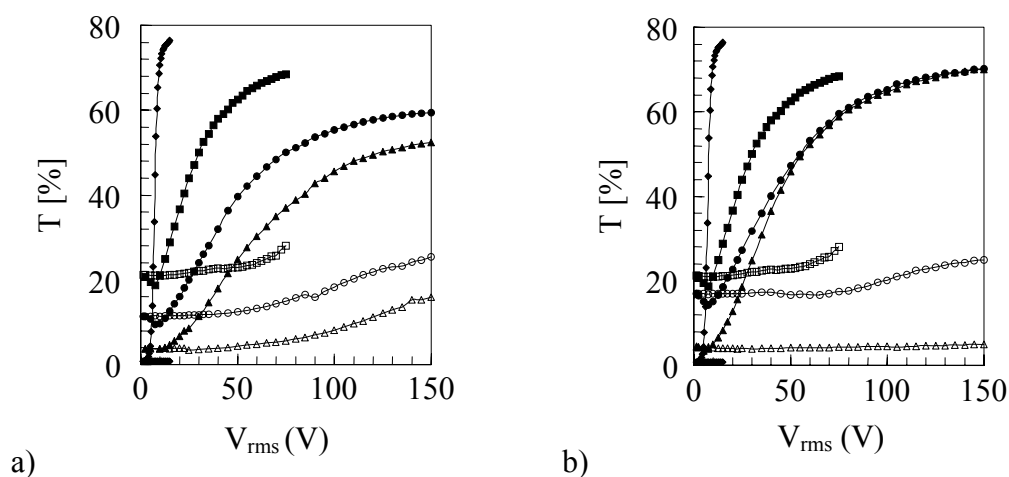


**Figure 4.16:** *Transmittance as a function of the applied voltage in the on-state (closed symbols) and memory state after 2 s (open symbols) for (♦) a 7  $\mu\text{m}$  reference PDLC and 17.8  $\mu\text{m}$  parallel electro-optical cells filled with various LC colloidal dispersions: (a) (■) 11.7 wt % 1.2  $\mu\text{m}$  sized colloids; (●) 16.9 wt % 1.2  $\mu\text{m}$  sized colloids; (▲) 30.7 wt % 1.2  $\mu\text{m}$  sized colloids; (b) 11.7 wt % colloids with a size of (■) 1.2  $\mu\text{m}$ ; (●) 630 nm; (▲) 43 nm.*

The influence of colloid size on the shape of the transmittance-voltage characteristics is visualised in Figure 4.16b. A striking feature is that, in case of the 43 nm colloids, no remaining orientation is seen in the 2 s memory state, while the memory effects are quite significant for the larger colloids. In all cases hysteresis was observed, also for the most rapidly relaxing material, as illustrated by Figure 4.17.

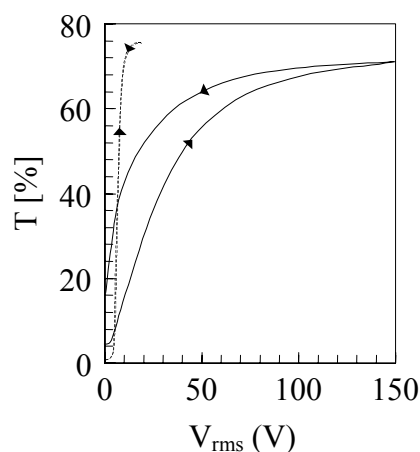


**Figure 4.17:** *Up and down transmittance-voltage scans for (---) a 7  $\mu\text{m}$  reference PDLC cell and (—) a 17.8  $\mu\text{m}$  parallel electro-optical cell filled with an 11.7 wt % LC dispersion based on 43 nm sized colloids.*

Previously, the occurrence of this hysteresis has been attributed to the random orientation of the LC molecules within the two-phase system.<sup>41</sup> In case the influence of the orientation layers is largely lost and no preferential orientation is imposed by the dispersed phase, the LC molecules become frustrated during their reorientation process and are free to choose different orientation routes during the voltage-up and voltage-down scan.

In Figure 4.18 the threshold voltage  $V_{90}$  is shown for the various colloid sizes and concentrations. In general,  $V_{90}$  increases with increasing concentration of the dispersed phase. Only in case of the 630 nm colloids this proportionality does not persist, most probably due to network irregularities at high colloid concentration. In case of the smaller and larger colloids, for all concentrations homogeneous films were obtained.

Since for the high colloid concentrations the degree of interaction between the network and the LC is considerable, also the  $V_{90}$  is considerable for all LC colloidal dispersions.

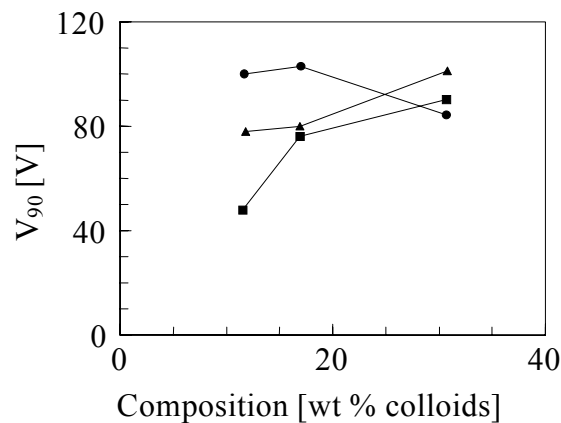


**Figure 4.18:** Threshold voltage ( $V_{90}$ ) for parallel electro-optical cells filled with LC colloidal dispersions as a function of colloid concentration for various colloid sizes: ( $\blacktriangle$ ) 43 nm; ( $\bullet$ ) 630 nm; ( $\blacksquare$ ) 1.2  $\mu\text{m}$ .

#### 4.3.6.2 Switching kinetics

In Figure 4.19 the dependence of rise and decay times on applied voltage is illustrated. It is seen that with increasing voltage  $\tau_r$  becomes shorter, while  $\tau_d$  becomes longer. The rather long decay times that are observed in Figure 4.19b might point to a tendency of the particles to form linear particle chains upon application of a 1 kHz AC electric field, via dipolar polarisation. Since at higher voltages the dipolar alignment becomes more perfect, the decay times increase with increasing voltage. In addition, the occurrence of chaining phenomena explains the shorter decay times which are found for the smaller particles, since the electric dipole moment of a single particle of radius  $R$  scales with  $R^3$ .<sup>42</sup> After removal of the AC electric field, both the reorientation of the particle dipoles and the LC molecular dipoles contribute to the decay times observed.

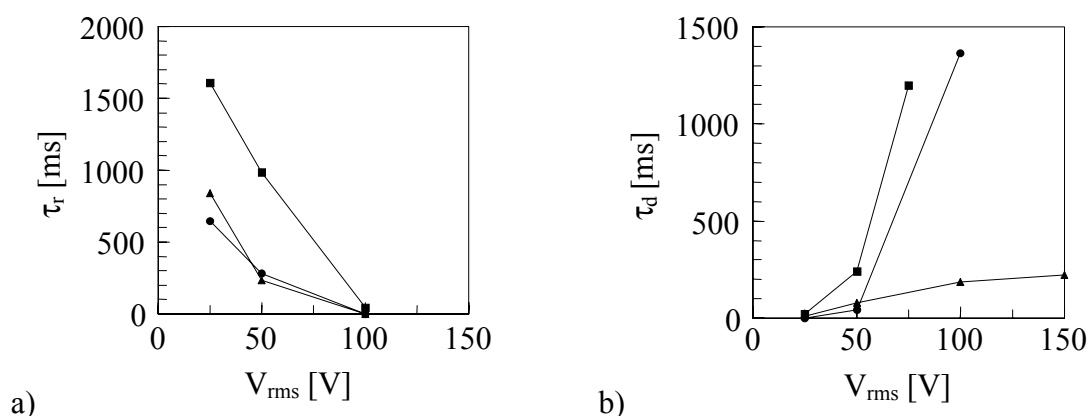


**Figure 4.19:** (a) Rise and (b) decay times as a function of the applied voltage for 11.7 wt % LC colloidal dispersions based on colloids with different diameters: (▲) 43 nm; (●) 630 nm; (■) 1.2  $\mu$ m.

Finally, it is noticed that the (temporary) transparent ‘memory state’, which was obtained for large particles after removal of the voltage, could immediately be switched back to the initial light-scattering state by heating the sample cell just above the clearing temperature of the LC.

#### 4.4 Conclusions

Dielectric experiments indicated that the LC order in the unaddressed and addressed state becomes more distorted upon addition of colloids. The degree of LC order was quantified by use of a director order parameter and by use of the interlayer model.

Switching experiments at  $-40$  °C revealed a reduction of the threshold field in case colloids were added to the LC. With increasing colloid fraction also a tremendous increase in conductivity was found. This caused a slow relaxation of the LC molecules after removal of a biasing field, especially at lower temperatures around  $-10$  °C.

Furthermore, the colloidal dispersions in LC were evaluated for their application as electro-optical switches. Firstly, the materials were confined within TN electro-optical cells equipped with crossed polarisers. Especially for low colloid concentrations and rather large colloid sizes ( $\gg 50$  nm) the electro-optical characteristics of the colloid/LC mixtures were found to be comparable to the characteristics of the pure LC. For low-concentrated and finely dispersed colloidal networks the response of the LC molecules towards application or removal of a biasing field was accelerated with respect to the response of the pure LC.

Secondly, the filled LC’s were tested for their applicability as light-shutters. It was demonstrated that the materials are electrically switched between a light-scattering and a

transparent state, using voltages in the order of 80 V. In this case, a considerable hysteresis was observed, independent of colloid size.

## 4.5 References

- (1) Crawford, G.P., Zumer, S. *Liquid crystals in complex geometries: formed by polymer and porous networks*, edited by Crawford, G.P. Zumer, S., Taylor and Francis, London, **1996**.
- (2) Haga, H., Garland, C.W. *Phys. Rev. E*, **1997**, *56*, 3044-3052.
- (3) Dadmun, M.D., Muthukumar, M. *J. Chem. Phys.*, **1993**, *98*, 4850-4852.
- (4) Golemme, A., Zumer, S., Allender, D.W., Doane, J.W. *Phys. Rev. Lett.*, **1988**, *61*, 2937-2940.
- (5) Werner, J., et al. *Liq. Cryst.*, **2000**, *27*, 1295-1300.
- (6) Bellini, T., et al. *Phys. Rev. Lett.*, **1992**, *69*, 788-791.
- (7) Arndt, M., Stannarius, R., Gorbatschow, W., Kremer, F. *Phys. Rev. E*, **1996**, *54*, 5377-5390.
- (8) Jadzyn, J., Czechowski, G., Mucha, M., Nastal, E. *Liq. Cryst.*, **1999**, *26*, 453-456.
- (9) Hikmet, R.A.M., Zwerver, B.H. *Liq. Cryst.*, **1991**, *10*, 835-847.
- (10) Aliev, F.M., Sinha, G.P., Kreuzer, M. *Mol. Cryst. Liq. Cryst.*, **2001**, *359*, 537-550.
- (11) Abd-El-Messieh, S.L., Werner, J., Schmalfluss, H., Weissflog, W., Kresse, H. *Liq. Cryst.*, **1999**, *26*, 535-539.
- (12) Cramer, C., Cramer, T., Kremer, F., Stannarius, R. *J. Chem. Phys.*, **1997**, *106*, 3730-3742.
- (13) Batalla, B., Sinha, G., Aliev, F. *Mol. Cryst. Liq. Cryst. Sci. Technol., Sect. A*, **1999**, *331*, 1981-1988.
- (14) Sinha, G.P., Aliev, F.M. *Phys. Rev. E*, **1998**, *58*, 2001-2010.
- (15) Williams, G., *Dielectric relaxation behaviour of liquid crystals* in *Molecular dynamics of liquid crystals*, edited by Luckhurst, G.R., Veracini, C.A., Kluwer Academic Publishers, **1994**, 431-450.
- (16) Jadzyn, J., Legrand, C., Czechowski, G., Bauman, D. *Liq. Cryst.*, **1998**, *24*, 689-694.
- (17) Jadzyn, J., Czechowski, G., Douali, R., Legrand, C. *Liq. Cryst.*, **1999**, *26*, 1591-1597.
- (18) Attard, G.S., Araki, K., Williams, G. *Br. Polym. J.*, **1987**, *19*, 119-127.
- (19) Steeman, P.A.M., *Interfacial phenomena in polymer systems; a dielectric approach*, dissertation, Delft University of Technology, Delft, **1992**, 1-214.
- (20) Havriliak, S., Negami, S. *Polymer*, **1967**, *8*, 161-205.
- (21) Steeman, P.A.M., Maurer, F.H.J. *Colloid Polym. Sci.*, **1990**, *268*, 315-325.
- (22) Kresse, H., *Dielectric properties of nematic liquid crystals* in *Handbook of Liquid Crystals*, edited by Demus, D., Goodby, J.W. Gray, G.W., et al., Wiley-VCH, Chichester, **1998**, 91-112.
- (23) Kato, T., Mizoshita, N., Katsuna, T., Kondo, G., Hanabusa, K. *Abstr. Pap. Am. Chem. Soc.*, **1999**, *218*, 364-365.
- (24) Mizoshita, N., Hanabusa, K., Kato, T. *Adv. Mater.*, **1999**, *11*, 392-394.
- (25) Mizoshita, N., Hanabusa, K., Kato, T. *Displays*, **2001**, *22*, 33-37.
- (26) Van Boxtel, M.C.W., Wübbenhorst, M., Van Turnhout, J., Bastiaansen, C.W.M., Broer, D.J. *manuscript in preparation*.
- (27) De Jeu, W.H. *Physical properties of liquid crystalline materials*, edited by Gray, G.W., Gordon and Breach Science Publishers, London, **1980**.
- (28) Wübbenhorst, M., Van Turnhout, J. *accepted for publication in J. Non-cryst. Solids*.
- (29) Rout, D.K., Jain, S.C. *Jpn. J. Appl. Phys., Part 1*, **1992**, *31*, 1396-1398.
- (30) Zhong, Z.Z., Schuele, D.E., Gordon, W.L., Adamic, K.J., Akins, R.B. *J. Polym. Sci., Part B*, **1992**, *30*, 1443-1449.
- (31) Hikmet, R.A.M., Zwerver, B.H. *Liq. Cryst.*, **1992**, *12*, 319-336.

- 
- (32) Craighead, H.G., Cheng, J., Hackwood, S. *Appl. Phys. Lett.*, **1982**, *40*, 22-24.
- (33) Amundson, K. *Phys. Rev. E*, **1996**, *53*, 2412-2422.
- (34) Wu, B.G., Erdmann, J.H., Doane, J.W. *Liq. Cryst.*, **1989**, *5*, 1453-1465.
- (35) Carter, S.A., LeGrange, J.D., White, W., Boo, J., Wiltzius, P. *J. Appl. Phys.*, **1997**, *81*, 5992-5999.
- (36) Andreau, A., Farhi, R., Tarascon, J.M., Gisse, P. *Liq. Cryst.*, **2000**, *27*, 1-4.
- (37) Hikmet, R.A.M., Higgins, J.A. *Liq. Cryst.*, **1992**, *12*, 831-845.
- (38) Amundson, K., Van Blaaderen, A., Wiltzius, P. *Phys. Rev. E*, **1997**, *55*, 1646-1654.
- (39) Berreman, D.W. *J. Appl. Phys.*, **1975**, *46*, 3746-3751.
- (40) Van Doorn, C.Z. *J. Appl. Phys.*, **1975**, *46*, 3738-3745.
- (41) Hikmet, R.A.M., Boots, H.M.J. *Phys. Rev. E*, **1995**, *51*, 5824-5831.
- (42) Jones, T.B., Saha, B.J. *J. Appl. Phys.*, **1990**, *68*, 404-410.

# Chapter 5

## Dendrimer filled nematics\*

### 5.1 Introduction

Dendrimers are highly branched macromolecules with a regularly shaped, three-dimensional architecture. The dendrimers have a layered structure, which originates from the either divergent<sup>1,2</sup> or convergent<sup>3,4</sup> approach that is used in the synthesis of these molecules. With increasing number of layers, commonly denoted as generations, the number of endgroups incorporated at the periphery of the dendritic molecule increases exponentially.

The ability to provide a single nanometer-sized molecule with a well-defined number of functionalities and specific functions via an appropriate design of the external and internal chemical structure has given the dendrimer its versatile nature. Since the introduction of these extraordinary molecules, numerous studies have evaluated these polyfunctionalised molecules on their application as e.g. extractants,<sup>5-8</sup> homogeneous catalysts<sup>9,10</sup> or host-guest systems.<sup>11-14</sup>

Although the dendrimers are often represented as perfectly spherically shaped, rigid molecules, the conformational shape and assembly behaviour of the molecule has been found to be highly dependent on the chemical surroundings. Previous reports have described a flattening of the dendrimer shape on solid surfaces with increasing interaction strength between the dendrimer functionalities and surface and with increasing number of interaction sites per molecule.<sup>9</sup> The type of interactions that exists between the individual molecules themselves and between molecules and surface significantly influences the organisation of the monomolecular structures and can give rise to the formation of various types of highly ordered monolayers or multilayers. Amphiphilic poly(propylene imine) dendrimers functionalised with hydrophobic alkyl chains have been found to adopt a completely deformed conformational shape when brought in contact with an air-water interface.<sup>15-17</sup> Due to preferential interaction of the polar interior with the polar water medium, the dendritic core resembles a floating 'pancake' with all attached alkyl chains directed upwards in the air.

The surprisingly high flexibility of the dendritic molecules has also become apparent for dendrimers modified with mesogenic endgroups.<sup>18-21</sup> This special class of dendrimers is

---

\* Part of this work has been published: Baars, M.W.P.L., Van Boxtel, M.C.W., Bastiaansen, C.W.M., Broer, D.J., Söntjens, S.H.M., Meijer, E.W. *Adv. Mater.*, **2000**, *12*, 715-719; Van Boxtel, M.C.W., Broer, D.J., Bastiaansen, C.W.M., Baars, M.W.P.L., Janssen, R.H.C. *Macromol. Symp.*, **2000**, *154*, 25-36.



able to form mesophases through rigorous deformation of the dendrimer interior, thereby enabling the assembly of the rigid, rodlike mesogenic units. The coupling of cyanobiphenyl mesogenic units to a poly(propylene imine) skeleton via the use of alkyl spacers previously yielded smectic A ( $S_A$ ) phases with an interdigitated bilayer, independent of generation.<sup>22</sup> Longer spacers were found to provide a more efficient stabilisation of the liquid crystal phases, due to a more efficient decoupling of the mesogenic groups from the dendritic skeleton.

Although the dispersion of dendrimers in isotropic media has been a subject of many studies in the past,<sup>9,15</sup> the immersion of highly branched molecules in an LC medium has merely been suggested and received less attention.<sup>19,23</sup> In this chapter poly(propylene imine) dendrimers are dispersed in a nematic LC in order to obtain novel two-phase materials for potential use in LCD's.

In the previous chapter the application of LC colloidal dispersions for electro-optical switches has been discussed. These materials were based on polymer colloids with dimensions ranging from ~40 nm to 1.2  $\mu\text{m}$ . Via an extension of the range of sizes of the dispersed phase down to 2-3 nm for the monomolecular dendrimers,<sup>5</sup> it is attempted to design (alternative) electro-optical switches which show a new combination of relevant properties with respect to e.g. light scattering power, switching kinetics, hysteresis, coatability, mechanical stiffness, etcetera. In order to gain more insight into the behaviour of the dendrimer filled LC's, in the following sections the materials are evaluated on their phase behaviour, morphology, flow behaviour, electro-optical and dielectric properties.

## 5.2 Experimental

### 5.2.1 Materials

The dendrimer filled nematics were prepared starting from LC E7 (see Section 3.3.1 for details) and fifth generation poly(propylene imine) dendrimers, functionalised with apolar alkyl chains. Three types of poly(propylene imine) dendrimers were used, which differed from each other in the length of the attached hydrophobic alkyl chains (Figure 5.1). These modified dendrimers were synthesised via reaction of fifth generation amine-terminated poly(propylene imine) dendrimers, denoted as *DAB-dendr*-( $\text{NH}_2$ )<sub>64</sub>, (DAB: denotation for the diaminobutane core) with the corresponding alkyl acid chloride.<sup>24\*</sup>

---

\* The modified dendrimers were kindly supplied by Bas de Waal and Maurice Baars, group of Macromolecular and Organic Chemistry (SMO) headed by Prof. dr. E.W. Meijer, Eindhoven University of Technology.

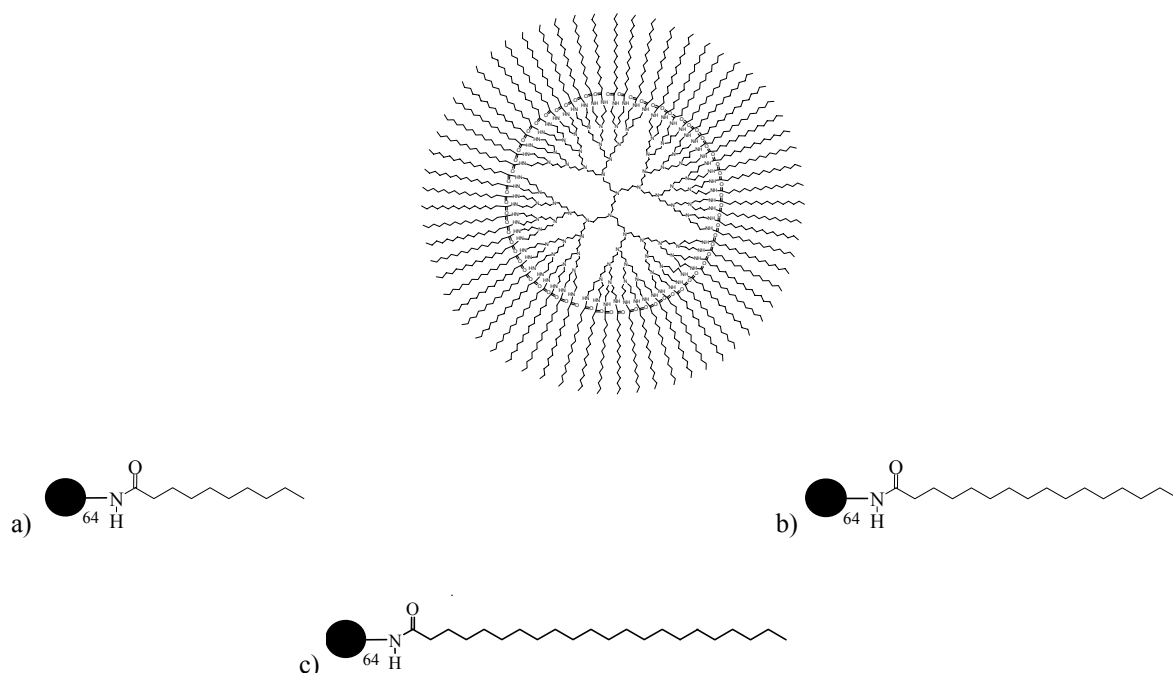


**Figure 5.1:** Schematic representations of poly(propylene imine) dendrimers modified with various alkyl chains: (a) DAB-dendr-(NHCO-C<sub>9</sub>H<sub>19</sub>)<sub>64</sub>, **1**; (b) DAB-dendr-(NHCO-C<sub>15</sub>H<sub>31</sub>)<sub>64</sub>, **2**; DAB-dendr-(NHCO-C<sub>21</sub>H<sub>43</sub>)<sub>64</sub>, **3**. The molecular structure is illustrated in more detail for the palmitoyl-modified dendrimer, **2** (top).

## 5.2.2 Preparation of the dendrimer filled nematics

A pre-set amount of the LC E7 was added to a pre-set amount of the dendrimer together with a small amount of chloroform. Homogeneous dispersion of the dendrimers in the LC/chloroform medium was achieved via ultrasonic mixing. Then the chloroform was evaporated from the mixture by drying the sample for 24 hours in a vacuum chamber at room temperature. Next, the dried material was heated into the isotropic phase at 100-120 °C to ensure homogeneous dispersion of the dendrimer in the LC, after which the samples were cooled down to room temperature.

## 5.2.3 Electro-optical cell construction

Electro-optical cells with (anti-)parallel aligning boundary conditions were constructed as described in Section 3.3.3. The cells were filled with the preheated dendrimer filled LC's in the isotropic state by capillary action at ~120 °C. After complete filling the cells were quenched below the clearing point of the LC E7.

## 5.2.4 Techniques

### *Differential scanning calorimetry (DSC)*

The peak temperatures of the phase transitions of the various dendrimer/LC mixtures were measured with DSC by use of a Perkin Elmer Pyris 1 DSC. The samples were measured over a temperature range of  $-20$  to  $140$  °C using heating and cooling rates of  $5$  °C.min<sup>-1</sup>. Before measurement the filled sample pans were preheated at  $\sim 140$  °C for a few seconds for homogeneous distribution of the sample materials.

### *Light microscopy (LM)*

The morphology of the dendrimer filled LC's in electro-optical cells was examined with the aid of a Zeiss Universal optical microscope operated in transmission mode.

### *Rheology*

For details on the rheology experiments, see Section 3.3.4.

### *Electro-optical characterisation*

The electro-optical characteristics of electro-optical cells were recorded using a display measuring system DMS 703 obtained from Autronic Melchers GmbH equipped with a voltage amplifier. Transmittance-voltage characteristics were measured by applying AC voltages of  $1$  kHz square waves, which were increased in steps of  $0.5$  V at a rate of  $5$  V.s<sup>-1</sup>. For illumination a  $100$  W halogen light source was used. The cells were held in an aluminium sample holder and positioned on the plate at a height of approximately  $10$  cm. A detector opening of  $0.2$  mm was used and the sample-detector distance was set in focus before measurement. All measurements were referenced against air.

### *Dielectric relaxation spectroscopy (DRS)*

For details on the dielectric measurement set-up see Section 4.2.2. The dielectric analysis was performed with  $17.7$   $\mu\text{m}$  parallel electro-optical cells filled with dendrimer/LC mixtures. For reference purposes, a  $5.0$   $\mu\text{m}$  parallel electro-optical cell filled with pure E7 was used. If necessary, the dielectric measurements obtained were corrected for the (ITO) contact resistance.

## 5.3 Results and discussion

### 5.3.1 Phase behaviour

DSC experiments were conducted in order to study the phase behaviour of dendrimer filled LC's based on E7 and the poly(propylene imine) dendrimers **1**, **2** and **3**. The peak temperatures of the nematic-isotropic phase transition of E7 and the crystalline-isotropic transition of the dendrimers **1**, **2** and **3** were used to construct the phase diagrams of the **1**/E7, **2**/E7 and **3**/E7 mixtures (Figure 5.2). In the (partial) phase diagrams of Figure 5.2 the expected single- and two-phase regions at both sides of the phase diagram are omitted, as these (small) regions were not revealed by the DSC experiments.

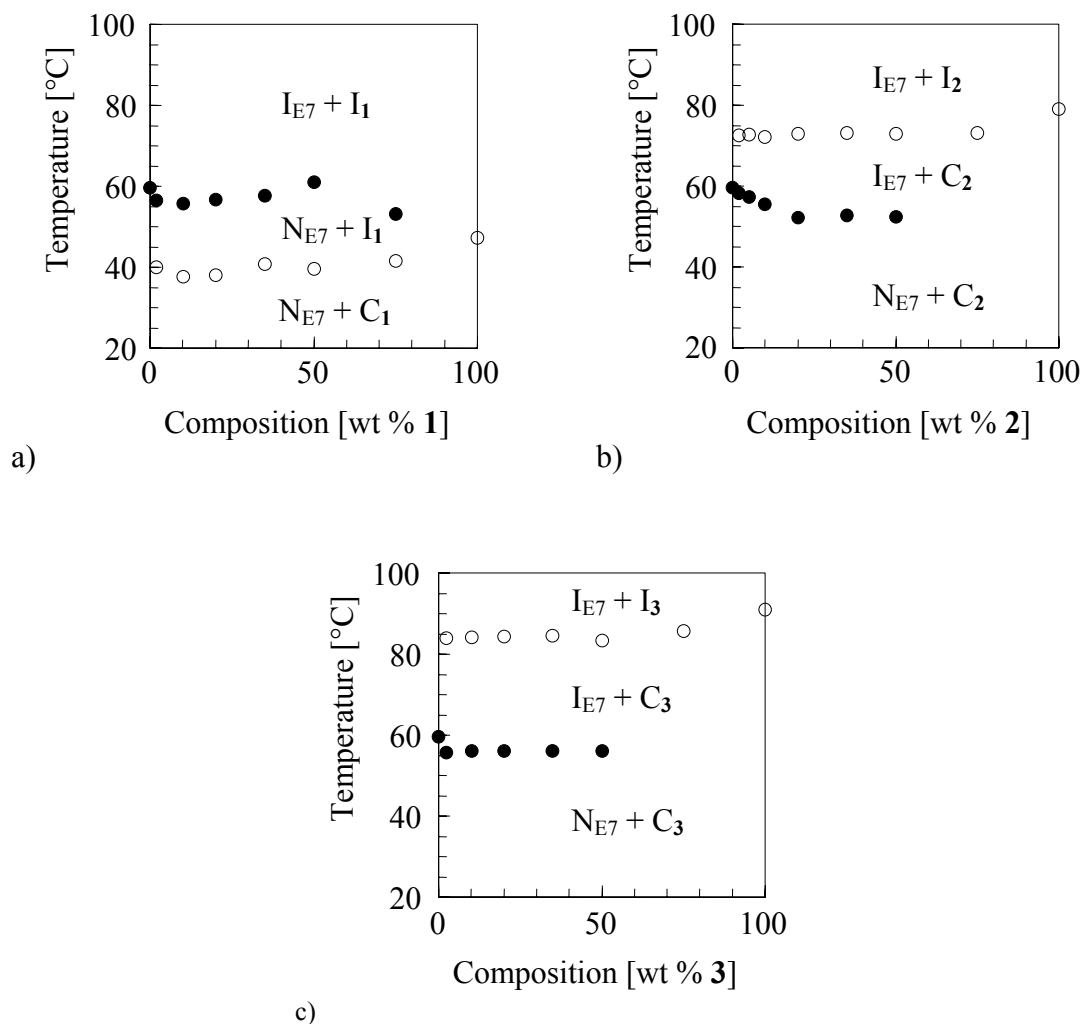


**Figure 5.2:** Phase diagrams of mixtures of LC E7 and various dendrimers: (a) **1**; (b) **2**; (c) **3**. The phase diagrams show the nematic-isotropic transition temperature of LC E7 (●) and the crystalline-isotropic transition temperature of the dendrimers (○), obtained from the second DSC heating run.

From Figure 5.2 it is seen that, independent of the length of the alkyl chain at the periphery of the dendrimer, the clearing temperature of E7 shifts to lower values with increasing fraction of dendrimer. Whereas in case of the LC colloidal dispersions the  $T_{NI}$  (nematic-isotropic transition temperature) shift was restricted to less than  $0.5\text{ }^{\circ}\text{C}$ , the shifts that are observed here are quite considerable. Especially for the **2**/E7 mixtures large shifts are apparent, reaching up to  $\sim 8\text{ }^{\circ}\text{C}$ . This indicates an efficient distortion of the LC order via the presence of the dendrimer aggregates.<sup>25,26</sup> This suggests that the dendrimers are highly capable of acting as nucleating agents for the formation of a polydomain structure, where the LC molecules become confined within finite LC domains with a corresponding loss of orientational order.

For the dendrimers a strong depression in the melting point is observed upon addition of the LC. This is also seen from Figure 5.3, which shows the corresponding DSC thermographs of the pure LC E7 and **2**/E7 mixtures with various fractions of **2**. The melting point depression is indicative of a distortion of the dendrimer alkyl chain ordering via the presence of LC molecules. For a 75 wt % **2**/E7 mixture two peaks can be distinguished, indicating both the presence of a perturbed dendrimer phase and a largely undistorted dendrimer phase.

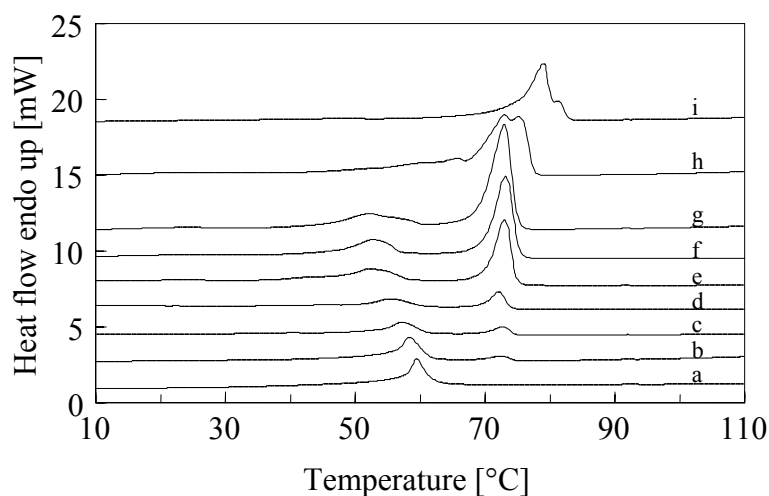


**Figure 5.3:** Second DSC heating scans for **2**/E7 mixtures with various amounts of **2**: (a) 0 wt % (pure E7); (b) 2 wt %; (c) 5 wt %; (d) 10 wt %; (e) 20 wt %; (f) 35 wt %; (g) 50 wt %; (h) 75 wt %; (i) 100 wt % (pure **2**).

Furthermore, Figure 5.3 clearly illustrates a significant broadening of the peaks at  $T_{NI}$  with increasing fraction of **2**. It is expected that, dependent on the LC domain size, each LC cluster undergoes the isotropisation at a characteristic temperature. Therefore, the strong broadening of the  $T_{NI}$  peak points to the existence of a broad LC domain size distribution within the dendrimer filled LC's.<sup>27,28</sup> Due to partial overlapping of the two peaks in the DSC

thermographs after peak broadening no conclusive remarks are made about the degree of phase separation between the dendrimer and LC phase.

### 5.3.2 Morphology

Figure 5.4 shows optical micrographs of parallel electro-optical cells with a gap of 5  $\mu\text{m}$ , which were capillary filled at elevated temperatures with the isotropic 2/E7 mixture. After complete filling, the cells were cooled down to a specific temperature. Figure 5.4a shows the morphology of the 2/E7 mixture after quenching to room temperature. It appears that the dendrimer molecules have assembled themselves into larger spherical aggregates with a diameter of  $\sim 20 \mu\text{m}$ . When viewed under crossed polarisers (Figure 5.4b), it is found that the LC molecules in the direct surroundings of the dendrimer aggregates have lost their uniform orientation and, instead, adopt a random orientation. The bulk E7 still has a uniform unidirectional alignment in agreement with the orientation direction that is imposed by the rubbed polyimide layers of the cell.

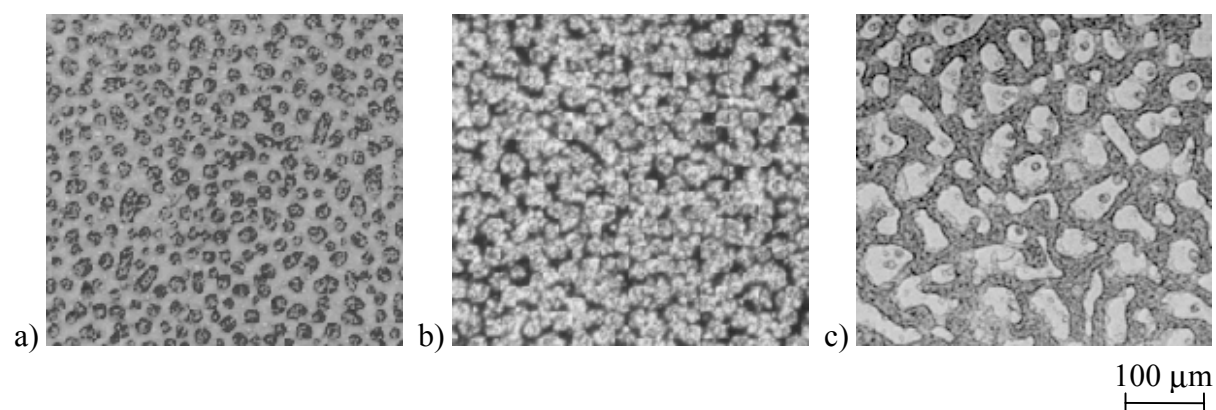


**Figure 5.4:** *Optical micrographs of 5  $\mu\text{m}$  parallel cells filled with a 20 wt % 2/E7 mixture: (a) Quenched to room temperature directly after filling and viewed without polarisers; (b) quenched to room temperature directly after filling and viewed with crossed polarisers; (c) quenched to  $-15 \text{ }^\circ\text{C}$  directly after filling and viewed without polarisers.*

In order to investigate the influence of quenching temperature on morphology, another cell was quenched to  $-15 \text{ }^\circ\text{C}$  directly after the capillary filling procedure. Figure 5.4c shows that the dendrimers have now organised themselves into a network of interconnected aggregates, thereby dividing the LC in domains with sizes in the order of 50  $\mu\text{m}$ . The dependence of morphology on quenching rate indicates that, like the LC colloidal systems, also the dendrimer filled nematics undergo a type of phase segregation during cooling down the  $T_{\text{NI}}$  of the LC.<sup>29-32</sup> Due to the smaller (molecular) size of the dendrimers, however, the dendrimers are expected to deform the nematic director to a much less extreme extent, resulting in a less strong phase separation.<sup>30,33-35</sup> The differences in morphology (Figures

5.4a and c) are attributed to the differences in cooling rate with which the isotropic-nematic transition of the LC is passed. In case of the lower quenching temperature the isotropic-nematic transition of the E7 is passed at a higher rate. In this way, more nematic nuclei are instantaneously formed, which have less time to grow and to coalesce. Therefore, the LC in Figure 5.4c is confined within a dendrimer network, while the LC in Figure 5.4a is present as a continuum.

### 5.3.3 Rheological properties

In order to study the flow behaviour of the dendrimer filled nematics, dynamic mechanical measurements were performed. Over the whole accessible range of applied strains ( $\gamma$ ) no linear visco-elastic behaviour was detected in the form of linear regime for  $G'(\gamma)$  and  $G''(\gamma)$ . Instead, the moduli showed a continuous decrease as soon as the experiment was started, even with a low sinusoidal strain amplitude.

As an alternative, stationary rheological measurements were conducted with the 2/E7 mixtures in order to measure the viscosity as a function of the shear rate (Figure 5.5). For reference purposes the same experiment was performed for the pure LC E7. The two-phase materials were found to exhibit thixotropic behaviour, due to a breaking down and building up of the dendrimer aggregates during flow and in rest, respectively. In order to perform reproducible measurements, the materials were heated into the isotropic phase just before each measurement, thereby erasing their deformation history.

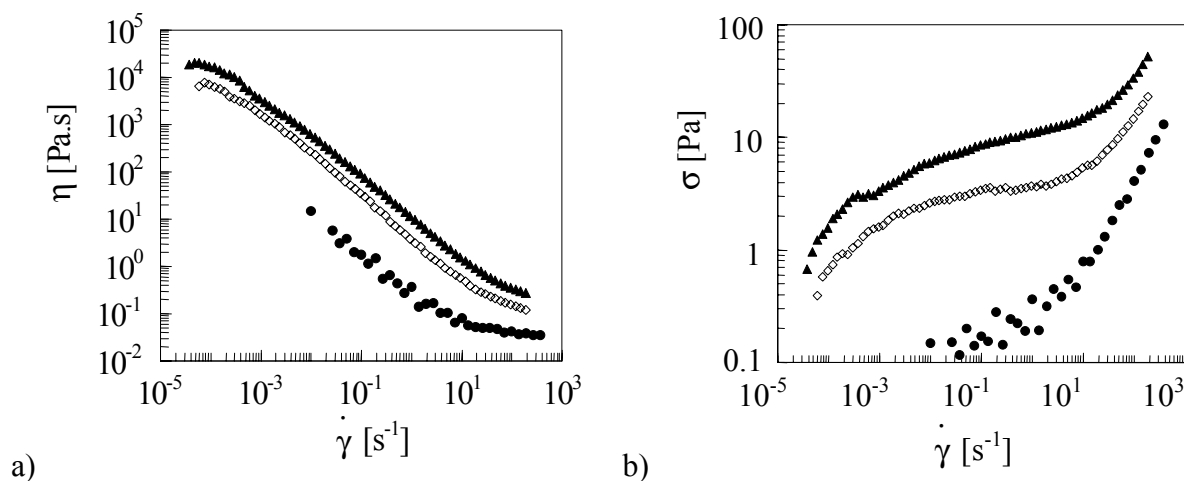


**Figure 5.5:** (a) Viscosity  $\eta$  and (b) stress  $\sigma$  as a function of the applied shear rate  $\dot{\gamma}$  for 2/E7 blends with various fractions of 2: (●) 0 wt %; (◊) 10 wt %; (▲) 20 wt %.

The shear thinning behaviour of the LC of Figure 5.5a has already been discussed in Section 3.4.6. Figure 5.5a nicely illustrates an enormous increase in viscosity upon

immersion of a dendrimer phase in the E7. The high viscosities that are seen for very low deformation rates are ascribed to the interconnection of the LC domains around the dendrimer aggregates, comprising LC molecules with a highly distorted orientation (see also Figure 5.4b). Although a plateau is visible in the viscosity at very low rates, the strong decrease in the viscosity (with a slope closely approaching minus one) might be interpreted as an apparent yield stress. The decrease in viscosity is associated with a breakdown of the interconnected LC domains and homogenisation of the LC alignment in the flow field. The shift in (apparent) yield stress with increasing fraction of dendrimer in the LC is indicative of an increased flow stability of the dendrimer filled nematics with respect to the pure LC in a rest situation. In this respect, Figure 5.5b demonstrates that, if one would define an apparent yield stress, its value would be in the order of 1-10 Pa, depending on the filler content. Furthermore, it is observed from Figure 5.5b that with increasing strain rate the measured stress increases over the whole deformation range. In contrast to what was found for the LC colloidal dispersions (see Figure 3.16) this points to a stable coating behaviour, which might be exploited in a continuous coating process as described in Figure 1.7.

### 5.3.4 Dielectric behaviour

Dielectric spectroscopy experiments were performed in order to gain more insight into the orientational and relaxation behaviour of the LC molecules within the dendrimer/LC blends. Figure 5.6 shows the Havriliak-Negami fits (see Equation 4.6 and 4.7) of the dielectric permittivity and loss of the pure E7 and a 10 wt % 2/E7 blend, recorded as a function of the frequency at  $-40\text{ }^{\circ}\text{C}$ .

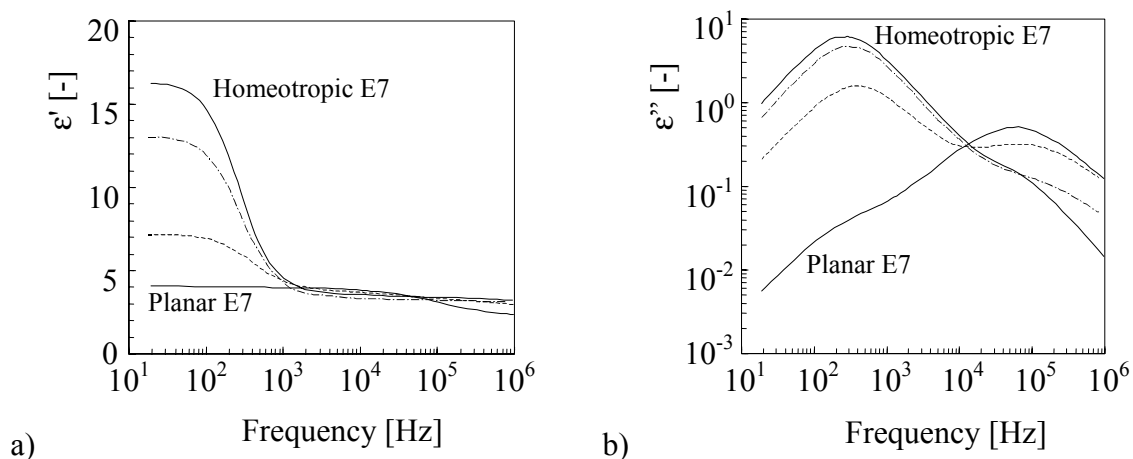


**Figure 5.6:** *Havriliak-Negami fits of (a) the dielectric permittivity  $\epsilon'$  and (b) the dielectric loss  $\epsilon''$  as a function of frequency ( $T = -40\text{ }^{\circ}\text{C}$ ) for the pure E7 and for a 10 wt % 2/E7 blend in  $17.7\text{ }\mu\text{m}$  parallel cells: (—) 0 wt % (pure E7) in the unaddressed and 40 V addressed state; (- -) 10 wt % 2/E7 in the unaddressed state; (-.-) 10 wt % 2/E7 in the 40 V addressed state.*



Figure 5.6a clearly shows that, in case no electric field is applied, the pure E7 is in a perfectly planarly aligned state within the parallel cell. In the 40 V biased state the pure LC E7 molecules are aligned in a homeotropic manner. The static dielectric constant of the 2/E7 blend in the off-state more closely approximates  $\epsilon'_{s, \text{average}} = (2\epsilon'_{s\perp} + \epsilon'_{s\parallel})/3$ ,<sup>36</sup> which is indicative of a more random, isotropic-like LC orientation, or, in other words, an LC polydomain structure. Evidently, the presence of **2** within the E7 highly suppresses the influence of the orientation layers within the parallel electro-optical cell in the unaddressed state. The 2/E7 blend shows an incomplete reorientation to the homeotropic state, which indicates that the threshold voltage in the smaller domains exceeds 40 V.

From Figure 5.6a it is calculated that the director order parameter  $S_d$  of the 10 wt % 2/E7 sample changes its value from  $-0.115$  to  $+0.606$  during switching from the off- to the 40 V on-state (Equation 4.4).

**Table 5.1:** Director order parameters ( $S_d$ ) and dielectric strengths of the fitted  $\alpha$  and  $\delta$  peaks for E7 (in a  $5.0 \mu\text{m}$  parallel cell) and for a 10 wt % 2/E7 mixture (in a  $17.7 \mu\text{m}$  parallel cell) in the unaddressed and addressed state (see Figure 5.6b). The  $S_d$  applies to the lowest frequency of 20 Hz.

2 content [wt %]	$\Delta\epsilon$ ( $\delta$ )	$\Delta\epsilon$ ( $\alpha$ )	$\Delta\epsilon$ ( $\delta$ )	$\Delta\epsilon$ ( $\alpha$ )	$S_d$	
	[-]	[-]	[-]	[-]	[-]	
	0 V	0 V	40 V	40 V	0 V	40 V
0	0.0498	1.37	12.9	0.173	-0.5	1
10	3.46	0.877	9.65	0.296	-0.115	0.606

Via the interlayer model (Equations 4.8-4.11) the fraction of randomly aligned LC around the immersed dendrimers,  $\phi_l$ , is estimated to be approximately equal to 0.8 for the off-state and 0.2 for the 40 V on-state, based on estimations for  $\epsilon'_2$ . From these values the thickness of the layer of randomly oriented LC around the immersed dendrimers is estimated, thereby neglecting density differences between the LC and dendrimer phase. In case it is assumed that the dendrimers are dispersed as  $\sim 20 \mu\text{m}$  spherical aggregates in the E7 (Figure 5.4), the estimated values for  $\phi_l$  correspond to a layer thickness of  $10.8$  and  $4.4 \mu\text{m}$  for the unaddressed and 40 V addressed state, respectively.

The dielectric loss spectra of Figure 5.6b exhibit two peaks. The  $\delta$ -relaxation peak in the low frequency regime originates from the slow molecular wiggling of the LC molecules around their short molecular axis, while the  $\alpha$ -relaxation peak in the high frequency regime is usually related to the rotation of the molecules around their long molecular axis. Figure 5.6b nicely illustrates the differences in LC orientation via the ratio of the dielectric strengths of the two peaks.

The switching between the 0 V unaddressed state and the 40 V addressed state is shown in more detail in Figure 5.7 for a 10 wt % 2/E7 blend (see Figure 4.4a for the dielectric behaviour of the pure E7).

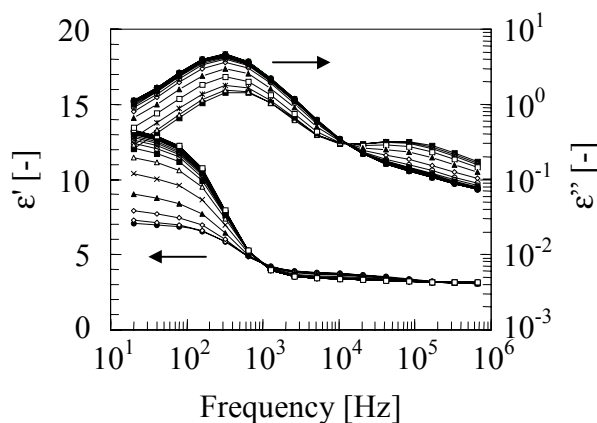


**Figure 5.7:** *Variation in dielectric permittivity and loss for a 10 wt % 2/E7 mixture confined within a 17.7  $\mu\text{m}$  parallel cell during application of a bias voltage, which was gradually increased from 0 to 40 V in steps of 2 V. The spectra were recorded at  $-40^\circ\text{C}$ .*

With increasing bias voltage the LC alignment along the electric field lines becomes more perfect. This is expressed by a gradual increase in the ratio between the dielectric strengths of the  $\delta$ - and  $\alpha$ -relaxation peak and by a gradual increase in static dielectric permittivity. The figure visualises the existence of an isosbestic point in between the  $\delta$ - and  $\alpha$ -relaxation peak. As already discussed in the previous chapter, the presence of this isosbestic point is indicative of the fact that the rotational mobility of the LC molecules is not affected by the application of an electric field.

The temperature-dependent orientation of the LC in the 0 and 40 V biased state is shown in Figure 5.8. When comparing the orientational behaviour of the LC molecules surrounding the dendrimer phase with the behaviour of the pure E7 (see Figure 4.6), it is evident that the orientation of the LC molecules is highly affected by the presence of the dendrimer phase over the complete temperature range. Above the  $T_{\text{NI}}$  and close to the  $T_{\text{g}}$  (glass transition temperature) of the E7 the LC molecules do not respond anymore to the electric field, due to isotropisation and a freezing in of the molecular motion, respectively. In the high temperature regime, electrode polarisation phenomena start to interfere with the measurement.

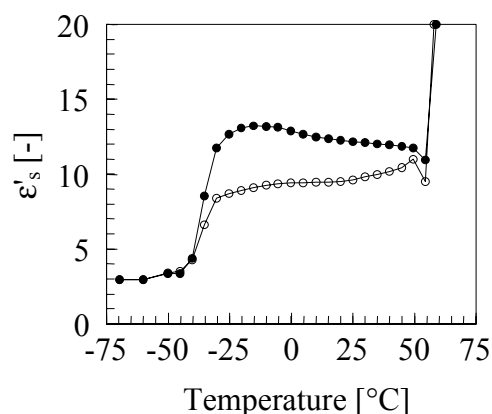


**Figure 5.8:** *Static dielectric permittivity versus temperature obtained from scans at 1 kHz for a 10 wt % 2/E7 blend in a 17.7  $\mu\text{m}$  parallel cell ( $\circ$ ) in the 0 V state and ( $\bullet$ ) in the 40 V addressed state.*

The time and temperature dependence of the relaxation behaviour of the dendrimer filled nematics was studied by subjecting the 2/E7 blend to a step-voltage sequence from 0 to 40 V and back to 0 V (Figure 5.9). Both the 40 V and 0 V states were continued for 2 minutes. Figure 5.9 illustrates the relaxation behaviour of the LC molecules within the LC/dendrimer blends directly after application and removal of the bias voltage at time intervals of 2 s.

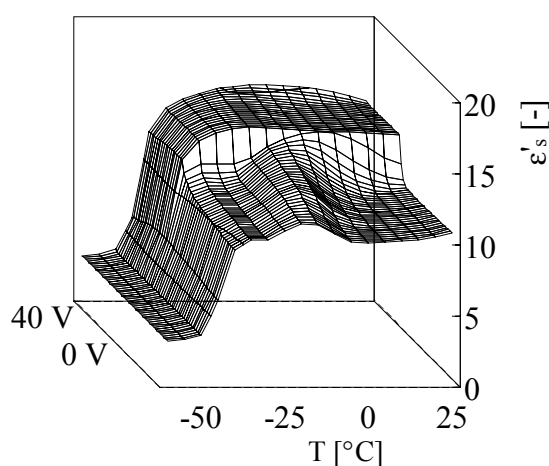


**Figure 5.9:** *Relaxation of the static dielectric permittivity for temperatures ranging from 25 to  $-60$   $^{\circ}\text{C}$  obtained at 110 Hz for 17.7  $\mu\text{m}$  parallel cells filled with a 10 wt % 2/E7 blend in the 40 V addressed state (curves at the back) and the 0 V unaddressed state (curves at the front).*

As far as the time-scales of the experiment allow, the LC molecules immediately respond to the bias voltage by aligning themselves in the direction of the external electric field. The occurrence of charge separation upon application of the step-up voltage is expressed by a gradual decrease of  $\epsilon'_s$  in time and is indicative of the build-up of an internal electric field. The surface plot expresses the occurrence of two different temperature-dependent relaxation phenomena after removal of the biasing DC voltage, as was also

observed for the pure E7 and the LC colloidal dispersions (Figures 4.8 and 4.9). The slower molecular dynamics in the low temperature regime hamper the relaxation of the material around  $-35\text{ }^{\circ}\text{C}$ , while charge polarisation effects interfere with the relaxation process at intermediate temperatures around  $-15\text{ }^{\circ}\text{C}$ . At temperatures around room temperature a rapid relaxation of the LC molecules is observed. As over the complete temperature range no overshoot in  $\epsilon'$  is observed upon instantaneous removal of the bias voltage, the introduced internal electric field is expected to be limited in magnitude. The 3-D plot visualises the presence of a remaining LC orientation at the end of the 0 V step in the low temperature regime, as a result of the slowed down reorientation processes.

### 5.3.5 Electro-optical properties of the dendrimer filled nematics for light-scattering electro-optical switches

#### 5.3.5.1 Transmittance-voltage characteristics

For the dendrimer filled LC's it was observed that the polydomain structure gives rise to a strong light scattering. By the application of an electric field the differences in refractive indices between the LC domains are reduced due to a more homogeneous LC alignment, resulting in a more transparent state. The transmission as a function of the applied voltage during voltage-up and -down scans was measured for 1/E7, 2/E7 and 3/E7 mixtures based on 5 wt % dendrimer confined within  $17.7\text{ }\mu\text{m}$  parallel electro-optical cells (Figure 5.10a).

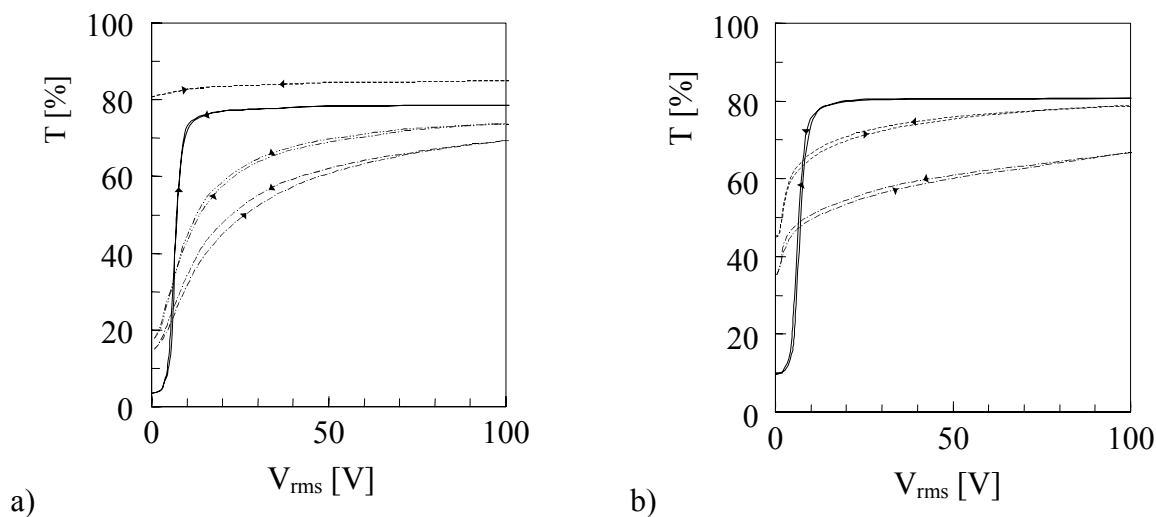


**Figure 5.10:** (a) Transmission as a function of the applied AC voltage of 1 kHz square wave for  $17.7\text{ }\mu\text{m}$  parallel electro-optical cells filled with 5 wt % mixtures of E7 and various dendrimers: (---) 1; (---) 2; (-.-) 3; (b) transmission as a function of the applied AC voltage for  $7.6\text{ }\mu\text{m}$  parallel electro-optical cells filled with a 20 wt % 2/E7 mixture, quenched to different temperatures after the cell filling: (---)  $20\text{ }^{\circ}\text{C}$  (room temperature); (-.-)  $-15\text{ }^{\circ}\text{C}$ . As a reference the  $T$ - $V$  characteristic of an optimised  $7\text{ }\mu\text{m}$  PDLC cell is shown: (—).

The most striking feature of this figure is that the **1**/E7 sample material has an extremely high transparency in the off-state. On the other hand, it is seen that both the **2**/E7 and the **3**/E7 blends scatter the incident light more efficiently. These differences in light-scattering capability are related to the phase behaviour of the two-phase materials, as portrayed by Figure 5.2. Dendrimer **1** undergoes a phase transition from a semi-crystalline state to an isotropic state at a temperature below the  $T_{NI}$  of the LC E7. In this way, during cooling from the completely isotropic state to room temperature, firstly the E7 undergoes its isotropic-nematic transition and, secondly, the dendrimer crystallises. Due to this particular sequence with which the two transitions are passed, the LC molecules are still able to orient themselves along the orientation layers of the electro-optical cell and the distortion of the nematic LC order is kept to a minimum.<sup>37</sup> As opposed to this, in case of **2** and **3** the dendrimer crystallises before the E7 gains its nematic nature. As a result, the adopted orientation of the LC molecules is highly affected by the presence of the semi-crystalline additive. As the interaction between dendrimer and LC now interferes with or even dominates over the interaction between the polyimide layers and LC, a more pronounced polydomain structure results.<sup>38,39</sup> Also, during the voltage step-up scan the transmission increases with voltage in a continuous manner. This confirms the presence of a broad distribution of LC domain sizes, as was also concluded from the DSC experiments.

Figure 5.10b shows the impact of morphology on the shape of the T-V characteristics obtained. Apparently, the network-type morphology of the dendrimer filled nematics (see Figure 5.4c) more efficiently scatters incident light than the spherical aggregate-type morphology (Figure 5.4a). Note, however, that the lower light transmittance in the off-state is accompanied with a less transparent on-state.

The influence of dendrimer concentration and cell thickness on the shape of the T-V characteristic is displayed in Figure 5.11. Figure 5.11a shows the electro-optical behaviour of **2**/E7 mixtures with various concentrations of **2**, confined within 17.7  $\mu\text{m}$  parallel electro-optical cells. Here, the same trend is seen as was observed for the LC colloidal dispersions. With increasing fraction of the additive the transmission in the off-state decreases, while the transmission in the on-state at equal voltage also decreases.

Figure 5.11b illustrates the effect of the cell gap on the electro-optical characteristics. The use of a larger cell gap is accompanied by a lower transmittance in the off-state, but also by a lower transmittance in the on-state. In general, the contrast ratio between the off- and on-state seems to be better for larger cell gaps.

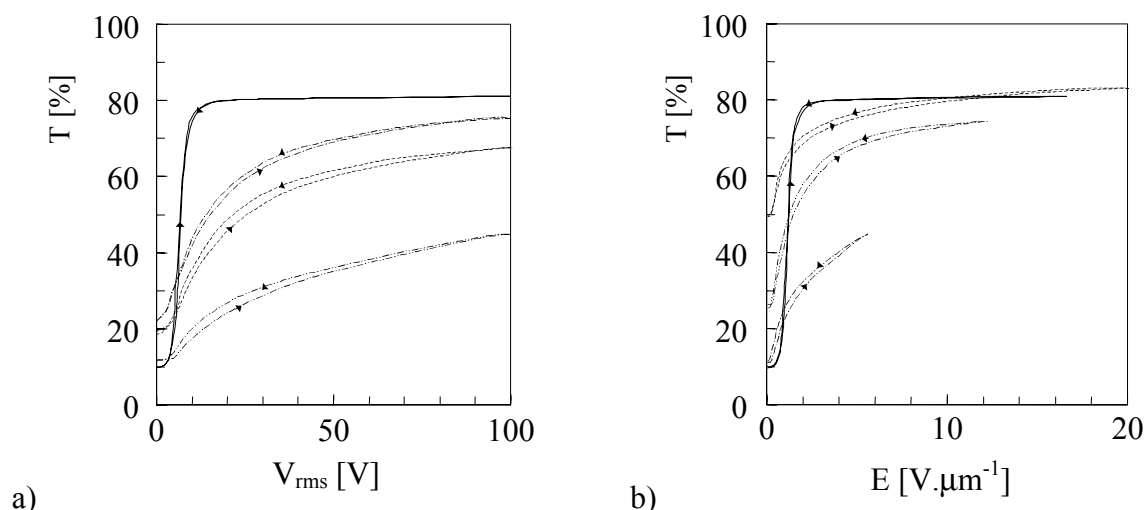


**Figure 5.11:** (a) Transmission as a function of the applied voltage for 17.7  $\mu m$  parallel electro-optical cells for various fractions of **2** in 2/E7 mixtures: (---) 5 wt %; (- -) 10 wt %; (- . .) 20 wt %; (b) transmission as a function of the applied electric field for parallel electro-optical cells filled with a 20 wt % 2/E7 mixture for various cell gaps: (- -) 4.9  $\mu m$ ; (- . .) 8.1  $\mu m$ ; (- - -) 17.7  $\mu m$ . As a reference the T-V characteristic of an optimised 7  $\mu m$  PDLC cell is shown: (—).

A general, remarkable feature of the dendrimer filled nematics is that the hysteresis in the electro-optical curves is limited, i.e. the transmittance during the voltage-down scan almost equals the transmittance during the voltage-up scan. The absence of hysteresis is an indication that the LC molecules follow the same orientational route during application of the voltage as during removal of the voltage.<sup>40</sup> In order to force LC molecules in the absence of a second phase to follow one specific route, the LC molecules must have a strong interaction with the orientation layers of the electro-optical cell. In case a second phase is added to the LC, the anchoring interaction between the LC and the additive may start to dominate. Here, it seems to be very likely that the dendrimer additive is able to impose a highly preferential orientational route to the LC, thereby taking over the function of the orientation layers and suppressing the occurrence of hysteresis phenomena.

### 5.3.5.2 Switching kinetics

The dependence of rise and decay times,  $\tau_r$  and  $\tau_d$ , on applied voltage is demonstrated by use of Figure 5.12. As is generally predicted by equations for  $\tau_r$  (see for instance Equation 4.13), the response of the LC molecules is strongly accelerated with increasing magnitude of the external electric field (Figure 5.12a).<sup>41,42</sup> The relation between rise time and applied voltage appears to be unaffected by the concentration of the dendrimer in the two-phase mixtures.

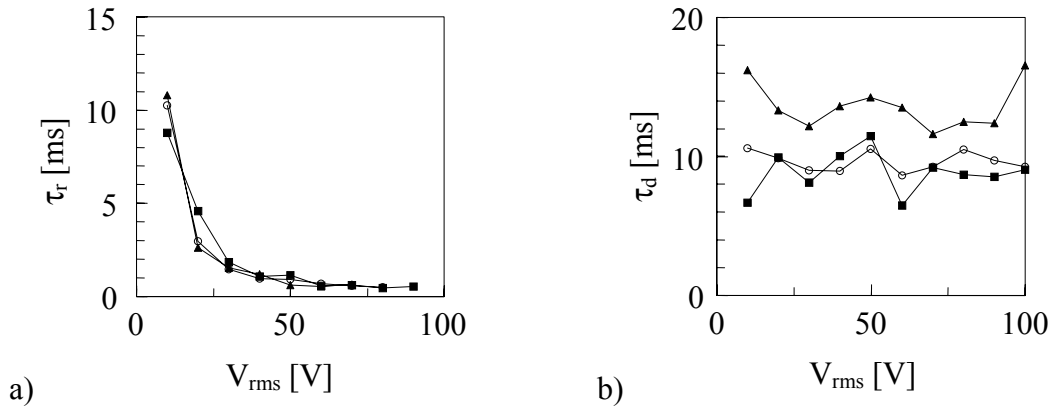


**Figure 5.12:** (a) Rise and (b) decay times as a function of the applied voltage for 17.7  $\mu\text{m}$  parallel cells filled with 2/E7 mixtures with various amounts of 2: (▲) 5 wt %; (○) 10 wt %; (■) 20 wt %.

Figure 5.12b shows that the decay times are independent of the applied voltage. This is in agreement with reported equations for  $\tau_d$  (see for instance Equation 4.14).<sup>43,44</sup> Here, higher dendrimer concentrations seem to lead to a somewhat faster relaxation of the LC molecules. Although the differences are very small, this may indicate that an increased interaction between the LC and the dendrimer phase promotes a faster relaxation of the LC molecules to their initial orientation state.<sup>45</sup>

The influence of the chosen cell gap on the switching times is demonstrated by Figure 5.13. As expected, larger cell gaps correspond to longer rise times.<sup>46</sup> Figure 5.13b suggests a decrease in decay time with increasing cell gap. Thus, as the interaction between the LC and the dendrimer phase starts to dominate over the interaction between the LC and the orientation layers of the cell, the relaxation of the LC is accelerated upon removal of the electric field. This confirms the idea that the dendrimer phase provides a ‘memory’ for the orientation of the LC via anchoring forces.

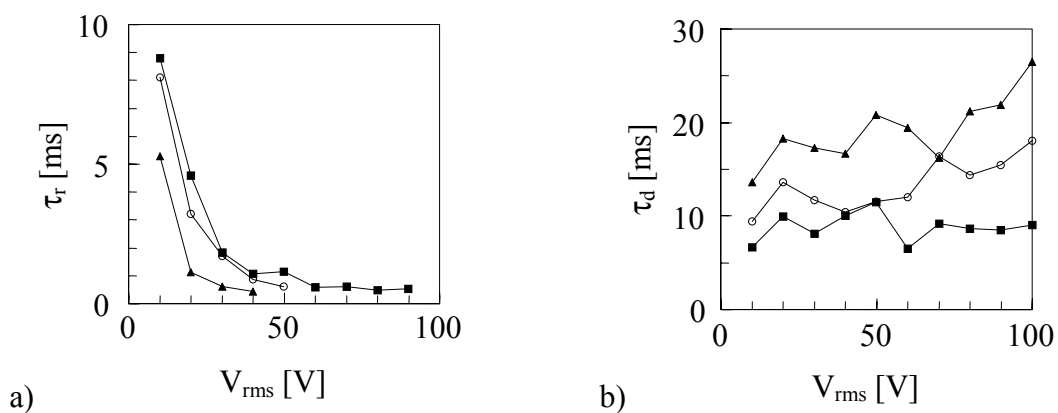


**Figure 5.13:** (a) Rise and (b) decay times as a function of the applied voltage for 20 wt % 2/E7 mixtures in parallel cells with various cell gaps: (▲) 5  $\mu\text{m}$ ; (○) 8.1  $\mu\text{m}$ ; (■) 17.7  $\mu\text{m}$ .

## 5.4 Conclusions

Dendrimer filled nematics were prepared based on LC E7 and poly(propylene imine) dendrimers, which were modified with alkyl chains at the periphery. In order to investigate the relation between phase behaviour of the dendrimer/LC blends and electro-optical characteristics, three types of dendrimers were used that differed from each other in alkyl chain length. In case the dendrimer had a transition from the semi-crystalline state to the isotropic state at a temperature below the nematic-isotropic transition of the E7, rather transparent materials were obtained. Dendrimer/LC mixtures with a reversed sequence of the phase transitions were found to exhibit an efficient light scattering in the off-state due to the formation of an LC polydomain structure. Upon application of a bias voltage, the two-phase materials switch in a continuous manner from the light-scattering state to a more transparent state. Hysteresis appears to be nearly absent, and this can be ascribed to the presence of a 'memory' within the material, as provided by the dendrimer phase.

Rheology experiments on the dendrimer filled nematics showed that upon addition of dendrimer to the E7 the viscosity significantly increases and that the deformation rate gradually increases with increasing stress. Both these features make these light-scattering, modified LC's suitable for processing via a continuous coating process.

Dielectric spectroscopy experiments confirmed the presence of an LC polydomain structure within the dendrimer filled nematics over a wide temperature range. Upon removal of a biasing DC field a rapid relaxation of the LC molecules was observed at temperatures around room temperature. At lower temperatures longer relaxation times were observed, due to the interference of charge polarisation effects and due to a slowing down of the molecular dynamics.

## 5.5 References

- (1) De Brabander-van den Berg, E.M.M., Meijer, E.W. *Angew. Chem., Int. Edit. Engl.*, **1993**, *32*, 1308-1311.
- (2) Tomalia, D.A., et al. *Polym. J.*, **1985**, *17*, 117-132.
- (3) Hawker, C.J., Frechet, J.M.J. *J. Am. Chem. Soc.*, **1990**, *112*, 7638-7647.
- (4) Xu, Z.F., Moore, J.S. *Angew. Chem., Int. Ed. Engl.*, **1993**, *32*, 246-248.
- (5) Stevelmans, S., et al. *J. Am. Chem. Soc.*, **1996**, *118*, 7398-7399.
- (6) Baars, M.W.P.L., Froehling, P.E., Meijer, E.W. *Chem. Commun.*, **1997**, 1959-1960.
- (7) Stephan, H., Spies, H., Johannsen, B., Klein, L., Vogtle, F. *Chem. Commun.*, **1999**, 1875-1876.
- (8) Chechik, V., Zhao, M.Q., Crooks, R.M. *J. Am. Chem. Soc.*, **1999**, *121*, 4910-4911.
- (9) Bosman, A.W., Janssen, H.M., Meijer, E.W. *Chem. Rev.*, **1999**, *99*, 1665-1688.
- (10) Knapen, J.W.J., et al. *Nature*, **1994**, *372*, 659-663.
- (11) Watkins, D.M., Sayed-Sweet, Y., Klimash, J.W., Turro, N.J., Tomalia, D.A. *Langmuir*, **1997**, *13*, 3136-3141.
- (12) Baars, M.W.P.L., Kleppinger, R., Koch, M.H.J., Yeu, S.L., Meijer, E.W. *Angew. Chem., Int. Ed.*, **2000**, *39*, 1285-1288.



- (13) Jansen, J., De Brabander-van den Berg, E.M.M., Meijer, E.W. *Science*, **1994**, 266, 1226-1229.
- (14) Boas, U., Karlsson, A.J., De Waal, B.F.M., Meijer, E.W. *J. Org. Chem.*, **2001**, 66, 2136-2145.
- (15) Schenning, A., et al. *J. Am. Chem. Soc.*, **1998**, 120, 8199-8208.
- (16) Schenning, A., Peeters, E., Meijer, E.W. *J. Am. Chem. Soc.*, **2000**, 122, 4489-4495.
- (17) Weener, J.W., Meijer, E.W. *Adv. Mater.*, **2000**, 12, 741-746.
- (18) Percec, V., Chu, P.W., Ungar, G., Zhou, J.P. *J. Am. Chem. Soc.*, **1995**, 117, 11441-11454.
- (19) Lorenz, K., Holter, D., Stuhn, B., Mulhaupt, R., Frey, H. *Adv. Mater.*, **1996**, 8, 414-416.
- (20) Cameron, J.H., Facher, A., Lattermann, G., Diele, S. *Adv. Mater.*, **1997**, 9, 398-403.
- (21) Barbera, J., Marcos, M., Serrano, J.L. *Chem.-Eur. J.*, **1999**, 5, 1834-1840.
- (22) Baars, M.W.P.L., Söntjens, S.H.M., Fischer, H.M., Peerlings, H.W.I., Meijer, E.W. *Chem.-Eur. J.*, **1998**, 4, 2456-2466.
- (23) Chen, F.L., Jamieson, A.M., Kawasumi, M., Percec, V. *J. Polym. Sci., Part B*, **1995**, 33, 1213-1223.
- (24) Baars, M.W.P.L., *Dendritic macromolecules; host-guest chemistry and self-assembly by design*, dissertation, Eindhoven University of Technology, Eindhoven, **2000**, 1-185.
- (25) Bellini, T., et al. *Phys. Rev. Lett.*, **1992**, 69, 788-791.
- (26) Mukherjee, P.K. *Liq. Cryst.*, **1997**, 22, 239-243.
- (27) Dadmun, M.D., Muthukumar, M. *J. Chem. Phys.*, **1993**, 98, 4850-4852.
- (28) Corvazier, L., Zhao, Y. *Liq. Cryst.*, **2000**, 27, 137-143.
- (29) Petrov, P.G., Terentjev, E.M. *Langmuir*, **2001**, 17, 2942-2949.
- (30) Anderson, V.J., Terentjev, E.M., Meeker, S.P., Crain, J., Poon, W.C.K. *Eur. Phys. J. E*, **2001**, 4, 11-20.
- (31) Anderson, V.J., Terentjev, E.M. *Eur. Phys. J. E*, **2001**, 4, 21-28.
- (32) Meeker, S.P., Poon, W.C.K., Crain, J., Terentjev, E.M. *Phys. Rev. E*, **2000**, 61, R6083-R6086.
- (33) Poulin, P., Raghunathan, V.A., Richetti, P., Roux, D. *J. Phys. II*, **1994**, 4, 1557-1569.
- (34) Kuksenok, O.V., Ruhwandl, R.W., Shiyankovskii, S.V., Terentjev, E.M. *Phys. Rev. E*, **1996**, 54, 5198-5203.
- (35) Poulin, P. *Curr. Opin. Colloid Interface Sci.*, **1999**, 4, 66-71.
- (36) Demus, D., Goodby, J., Gray, G.W., Spiess, H.W., Vill, V. *Handbook of liquid crystals, volume 2A: low molecular weight liquid crystals*, Wiley-VCH, Chichester, **1998**.
- (37) Janssen, R.H.C., et al. *Jpn. J. Appl. Phys., Part 1*, **2000**, 39, 2721-2726.
- (38) Janssen, R.H.C., et al. *Macromol. Symp.*, **2000**, 154, 117-126.
- (39) Janssen, R.H.C., et al. *J. Appl. Phys.*, **2000**, 88, 161-167.
- (40) Hikmet, R.A.M., Boots, H.M.J. *Phys. Rev. E*, **1995**, 51, 5824-5831.
- (41) Amundson, K. *Phys. Rev. E*, **1996**, 53, 2412-2422.
- (42) Doane, J.W., Golemme, A., West, J.L., Whitehead, J.B., Wu, B.G. *Mol. Cryst. Liq. Cryst.*, **1988**, 165, 511-532.
- (43) Andreau, A., Farhi, R., Tarascon, J.M., Gisse, P. *Liq. Cryst.*, **2000**, 27, 1-4.
- (44) Wu, B.G., Erdmann, J.H., Doane, J.W. *Liq. Cryst.*, **1989**, 5, 1453-1465.
- (45) Mizoshita, N., Hanabusa, K., Kato, T. *Displays*, **2001**, 22, 33-37.
- (46) Hikmet, R.A.M. *J. Appl. Phys.*, **1990**, 68, 4406-4412.

# Chapter 6

## Anisotropic thermoreversible gels\*

### 6.1 Introduction

A number of low molecular weight compounds has been found to gel various common organic solvents via a self-organisation into supramolecular structures, primarily through intermolecular hydrogen bonding interactions.<sup>1-3</sup> Through a three-dimensional extension of the hydrogen bonded network the organic solvent is subdivided into smaller cavities, in which the solvent molecules become confined. The interaction between the two phases separated on a microscopic scale causes a macroscopic immobilisation or, in other words, physical gelation of the solvent phase. As the self-assembly of the functional molecules involves non-covalent interactions, the supramolecular structure is able to form and break in a thermoreversible manner.

In recent years, Kato et al. have reported on anisotropic thermoreversible gels formed through the gelation of cyclohexane diamide or amino acid derivatives within a nematic<sup>4-7</sup> or smectic<sup>8</sup> LC medium. Until now, the nematic liquid crystalline physical gels have been applied within twisted nematic cells in order to achieve an acceleration of the response speed as compared to the pure LC. In this respect, the response behaviour of the anisotropic gels to electric fields has been found to be highly dependent on the morphology of the microphase-separated gels and thus on the nature of the hydrogen bonding gelling agent and on its concentration in the LC matrix.<sup>9,10</sup> A faster response was achieved in case the (fibrous) aggregates of the gelling agent were finely dispersed in the LC. Also, a not too high thermal stability of the anisotropic gel appeared to have a positive effect on the electro-optical response. Via an additional appropriate tuning of the concentration of finely dispersed microphase-separated aggregates within the LC, the LC-network and LC-polyimide interaction forces seemed to be subtly balanced, ultimately leading to improved threshold voltages and rise times.<sup>9-11</sup>

Within this chapter physical anisotropic gels are described based on 12-hydroxyoctadecanoic acid (HOA) and *n*-hexylcyanobiphenyl (LC K18). A practical advantage of this gel system with respect to the above-mentioned anisotropic gels is that the gelling agent, HOA, is commercially available. Here, in the preparation of light-scattering

---

\* Similar work on an LC E7 based gel system has been published: Janssen, R.H.C., Stümpflen, V., Van Bostel, M.C.W., Bastiaansen, C.W.M., Broer, D.J., Tervoort, T.A., Smith, P. *Macromol. Symp.*, **2000**, *154*, 117-126.

gels, the LC K18 was chosen as the LC medium for its appropriate, rather low nematic-isotropic transition temperature. The HOA/K18 anisotropic gels are assessed for their potential use as electrically switchable, light-scattering systems by studying their phase behaviour, morphology, dynamic mechanical, and electro-optical properties.

## 6.2 Experimental

### 6.2.1 Materials

Racemic 12-hydroxyoctadecanoic acid (HOA) was purchased from Aldrich (12-hydroxystearic acid, 99 % pure) and used as received. The liquid crystal K18 (*n*-hexylcyanobiphenyl,  $\Delta\epsilon = 10.8$ ,<sup>12</sup>  $T_{CN} = 15$  °C,  $T_{NI} = 29$  °C<sup>13</sup>) was purchased from Merck (Poole, England).

### 6.2.2 Preparation of the thermoreversible gels

A pre-set amount of the solid HOA powder was added to a pre-set amount of the LC K18. Next, the HOA was dissolved in the LC by heating the mixture into the isotropic phase at approximately 120 °C. Subsequently, the sample was cooled down to room temperature, resulting in the formation of materials with an opaque and soft solid-like appearance.

### 6.2.3 Electro-optical cell construction

Electro-optical cells with (anti-)parallel configuration were constructed as described in Section 3.3.3. The cells were filled with the preheated HOA/K18 gels in the isotropic state by capillary action at  $\sim 120$  °C. After filling the cells were quenched to room temperature.

### 6.2.4 Techniques

#### *Differential scanning calorimetry (DSC)*

Calorimetric analysis was performed by use of a Perkin Elmer Pyris 1 DSC. The samples were measured over a temperature range of  $-30$  to  $150$  °C using a scanning rate of  $10$  °C.min<sup>-1</sup>. Before sealing the filled capsules, their contents were homogenised at  $120$  °C for a few seconds.

#### *Transmission electron microscopy (TEM)*

The structure of the HOA network was examined with transmission electron microscopy (TEM) using a JEOL 2000 FX microscope, which was operated at 80 kV. For a

better visualisation of the structure of the HOA aggregates, HOA samples were prepared where the LC medium was replaced by volatile toluene. For the TEM samples carbon coated grids were used. The samples were prepared by applying a droplet of the heated, isotropic specimen on a sample holder. Subsequently, the material was cooled at ambient temperature to allow gelation of the material. To minimise damage of the samples during irradiation with the electron beam, a relatively low magnification was used ( $< 10^3 \times$ ).

#### *Wide angle X-ray scattering (WAXS)*

Integrated patterns were obtained via the use of a Rigaku Geigerflex equipped with a monochromator in order to obtain X-rays with a Cu/K-alpha 1 wavelength of 1.54 Å. During measurement the angle was incremented in steps of 0.01°. Here, the measurement time per angle was equal to 2 s (in case of K18, 10 wt % HOA/K18) or 12 s (for pure HOA).

Alternatively, 2-D WAXS patterns of the samples were recorded on a photographic plate under vacuum. A Cu/K-alpha wavelength of 1.54 Å was used in combination with a Philips generator. For calibration purposes, a HDPE standard was employed.

#### *Dynamic mechanical analysis*

A dynamic mechanical analysis was performed as described in Section 3.3.4.

#### *Electro-optical characterisation*

For details on the electro-optical characterisation see Section 5.2.4.

## **6.3 Results and discussion**

### **6.3.1 Phase behaviour**

The phase transitions of the HOA/K18 system were determined via DSC experiments and plotted as a function of the composition as shown in Figure 6.1. The (partial) phase diagram of Figure 6.1 does not show the expected single and two-phase regions at low and high concentrations of HOA, as these (small) regions were not detected by the performed DSC analysis. The phase diagram reveals that at high temperature the mixture is present as an isotropic liquid. During cooling of the isotropic liquid first the HOA molecules undergo the sol-gel transition ( $T_{SG}$ ) and crystallise, while the coexisting LC remains in the isotropic phase. In this region the mixture exists as a (highly viscous) isotropic gel. During further cooling the LC reaches the isotropic-nematic phase transition temperature, indicated by  $T_{NI}$ , and an anisotropic gel is formed. It is anticipated that, when brought in a glass cell provided with rubbed polyimide interfaces, the presence of the dispersed HOA network significantly weakens the influence of the rubbed polyimide layers on the orientation of the LC molecules

below their clearing temperature. In this way the network is able to prevent the LC molecules to align in a unidirectional manner and will, instead, strongly promote the introduction of spatial inhomogeneities in the nematic director field. This is expected to lead to an enhanced light scattering with respect to the pure K18. It was noticed that the formation of the isotropic or anisotropic gel is fully thermally reversible, due to the reversibility of the formation and break of hydrogen bonds.<sup>9</sup> When the gelled material was heated above the gel melting transition, a fluid isotropic liquid was again obtained. According to Figure 6.1, at low temperatures both the LC and the HOA exist as a crystalline phase.

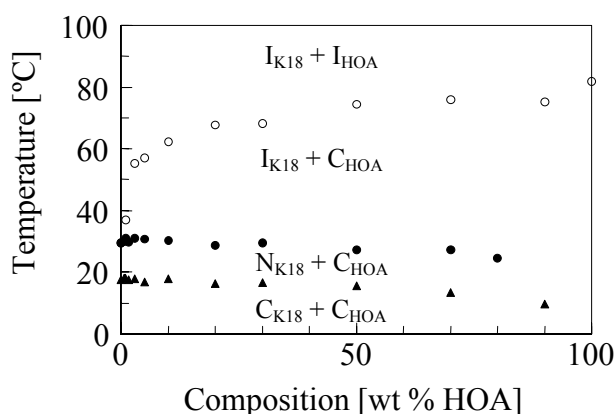


**Figure 6.1:** Phase diagram of the HOA/LC K18 system: (▲) crystalline-nematic transition of K18; (●) nematic-isotropic transition of K18; (○) gel melting transition. The (peak) transition temperatures were determined from the second heating run.

Furthermore, Figure 6.1 reveals that the melting temperature of the HOA,  $T_m$ , is strongly depressed due to the presence of the LC K18, similar to what was previously observed for anisotropic gels.<sup>7,9</sup> Also, both the  $T_{NI}$  and the  $T_{CN}$  (crystalline-nematic transition temperature) of K18 show a shift to lower temperature at high HOA concentrations, which is attributed to finite size effects. At low weight fractions of the gelling agent only small variations in transition temperature are observed.<sup>7,9</sup> In Figure 6.2 DSC thermographs are shown of the bulk LC K18 and HOA/K18 mixtures with various weight fractions of HOA.

The DSC curves of Figure 6.2 clearly illustrate the increase in the enthalpy of gel melting,  $\Delta H_m$ , and the shift of  $T_m$  to higher temperatures with increasing concentration of HOA in the gel. The relationship between  $T_m$  and the concentration of HOA in the gel is described by the Eldridge-Ferry equation:<sup>14</sup>

$$\log(c_{HOA}) = \frac{\Delta H_m^{EF}}{RT_m} + \text{constant} \quad (6.1)$$

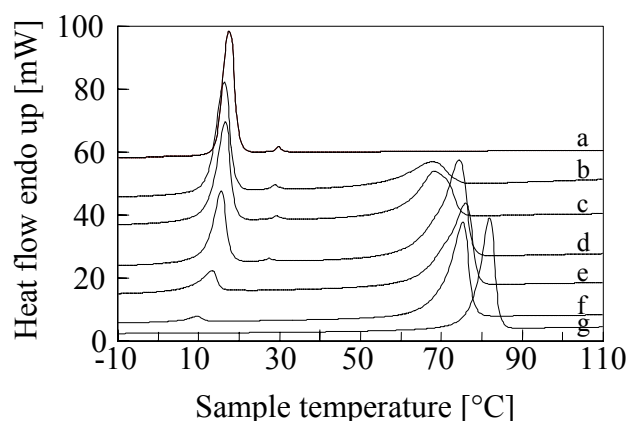


**Figure 6.2:** Heating DSC curves for HOA/LC K18 gels with various concentrations of HOA: (a) 0 wt % (pure K18); (b) 20 wt %; (c) 30 wt %; (d) 50 wt %; (e) 70 wt %; (f) 90 wt %; (g) 100 wt %.

where  $c_{\text{HOA}}$  is the HOA concentration (wt %) and  $\Delta H_{\text{m}}^{\text{EF}}$  is the heat absorbed when forming a mole of junction points within the HOA crystalline network. Thus, while  $\Delta H_{\text{m}}$  reflects all the interactions within the gel,  $\Delta H_{\text{m}}^{\text{EF}}$  only reflects the interactions at the junction points of the aggregate network. For the HOA/K18 system the Eldridge-Ferry plot gives a value for  $\Delta H_{\text{m}}^{\text{EF}}$  of  $58.3 \text{ kJ}\cdot\text{mol}^{-1}$ , which is in the appropriate order of magnitude (Figure 6.3).<sup>15</sup>

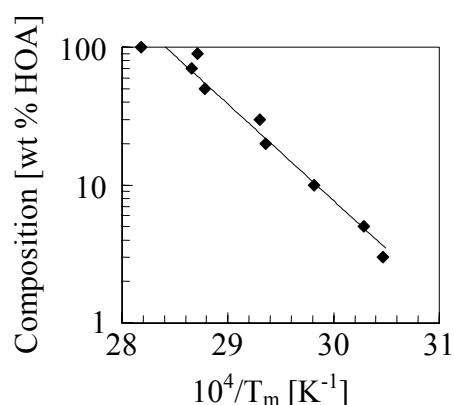


**Figure 6.3:** Eldridge-Ferry plot for HOA/K18 gels showing the relationship between  $1/T_{\text{m}}$  and  $\log(c_{\text{HOA}})$ . The solid line represents a fit through the experimental data points.

From the DSC curves, a non-linear weakening of the peaks at  $T_{\text{NI}}$  with increasing concentration of the gelling agent is observed (Figure 6.4). This phenomenon indicates the presence of a fraction of LC molecules that is so strongly bound to the dispersed network that it is completely immobilised and does not participate in the nematic-isotropic transition.<sup>16,17</sup> Further investigation by use of optical polarisation microscopy confirmed the remaining presence of a highly birefringent LC phase after heating into the isotropic phase. From the heat of the nematic to isotropic transition of the mobile (bulk) LC molecules the fraction of

physically adsorbed K18 was calculated and this was found to increase with increasing weight fraction of the dispersed HOA phase (see also Figure 6.4).

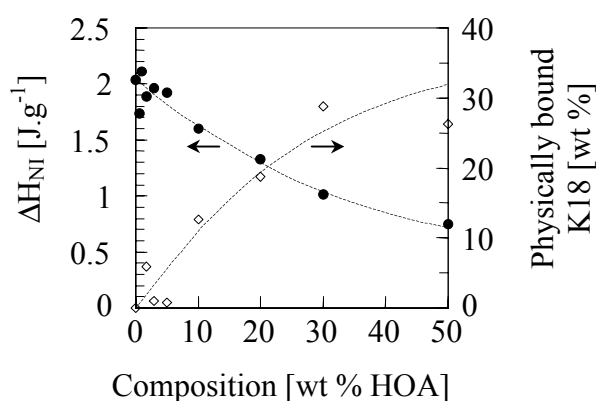


**Figure 6.4:** Heat of nematic to isotropic transition for K18 molecules and the fraction of physically bound K18 molecules versus gel composition. The broken lines are drawn to guide the eye.

### 6.3.2 Morphology

Figures 6.5 and 6.6 show the integrated and non-integrated WAXS diffraction patterns of the pure LC K18, the solid HOA powder and a 10 wt % HOA/K18 gel. The nematic LC shows a diffuse band around  $2\theta = 19.5^\circ$  corresponding to a periodicity  $d$  perpendicular to the director of  $\sim 0.46$  nm. At low angles  $2\theta$  around  $3.4^\circ$  ( $d \sim 2.6$  nm) another (very weak) broad band might be distinguished from the pattern of Figure 6.5, originating from a (local) periodic arrangement parallel to the director.

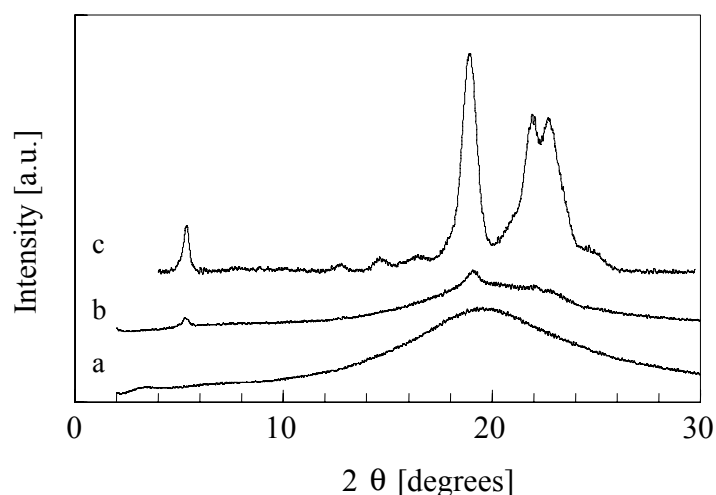


**Figure 6.5:** Integrated wide angle X-ray patterns of: (a) K18; (b) 10 wt % HOA/K18; (c) (grinded) HOA powder. All three patterns were recorded at room temperature.

The WAXS recordings for the HOA solid show intense reflections that are indicative of a crystalline organisation. For the 10 wt % gel these reflections have become less resolved due to the diffuse scattering of the LC solvent. Elsewhere, a detailed structural model for the organisation of racemic HOA molecules within the aggregates has been proposed.<sup>18</sup> Within this model the HOA molecules are arranged “head to head” through dipolar interactions between the carboxylic groups. The assembly of two molecules gives rise to a long spacing  $d \sim 4.6$  nm, which is expressed by a strong (001) Bragg reflection (not seen in Figure 6.5). Through the formation of long hydrogen bond sequences via the hydroxyl groups on the C<sub>12</sub> position filaments are grown, as will be shown later.

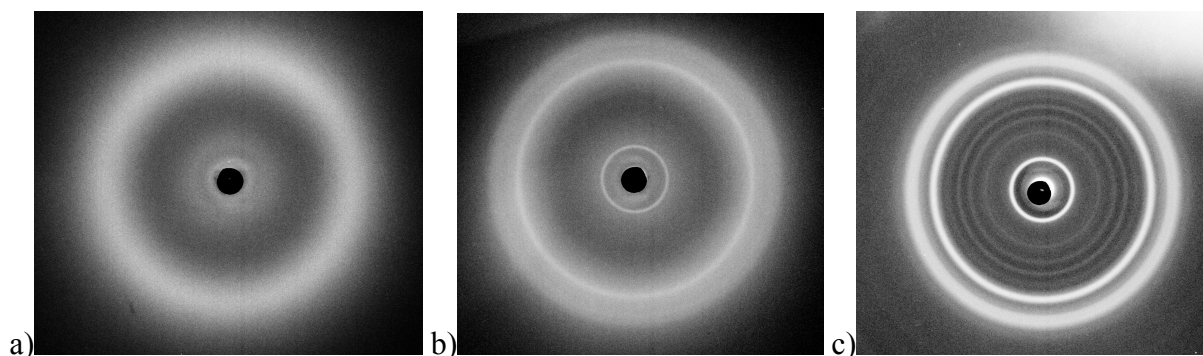


**Figure 6.6:** 2-D WAXS patterns of: (a) K18; (b) 10 wt % HOA/K18; (c) (grinded) HOA powder. All three patterns were recorded at room temperature.

The morphology of the HOA aggregates was visualised via the TEM technique. The TEM images of Figure 6.7 demonstrate the presence of fibrous aggregates after evaporation of the solvent in the electron microscope. In earlier publications it was claimed that racemic compounds are not able to form filaments.<sup>19</sup> It was thought that steric hindrance effects prevented the linking of the molecules through the development of long hydrogen bond sequences. In contrast with this, more recently it was demonstrated that both racemic and chiral HOA are indeed able to associate into filaments via intermolecular hydrogen bonding.<sup>18</sup> Moreover, no differences between the chiral and racemic HOA were detected with respect to e.g. their gel forming ability with a variety of solvents and properties of the corresponding gels.

Figure 6.7c shows that the racemate HOA molecules assemble into helically twisted filaments with a width of about 100 nm. Previously, a left-handed twist was found for the *R*-acid and a right-handed twist for the *S*-acid.<sup>20</sup> For the racemic mixture, here, both left-handed and right-handed helices were observed. When looking at Figure 6.7b it seems to be reasonable to believe that the shape of the junction zones resembles bundles of fibres, as was proposed earlier.<sup>18</sup> The overall network structure as shown in Figure 6.7a strongly suggests that, when dispersed in an LC, the interconnected fibrous aggregates are able to subdivide the



LC matrix in smaller domains. This is expected to lead to an enhanced light scattering as compared to the pure LC.

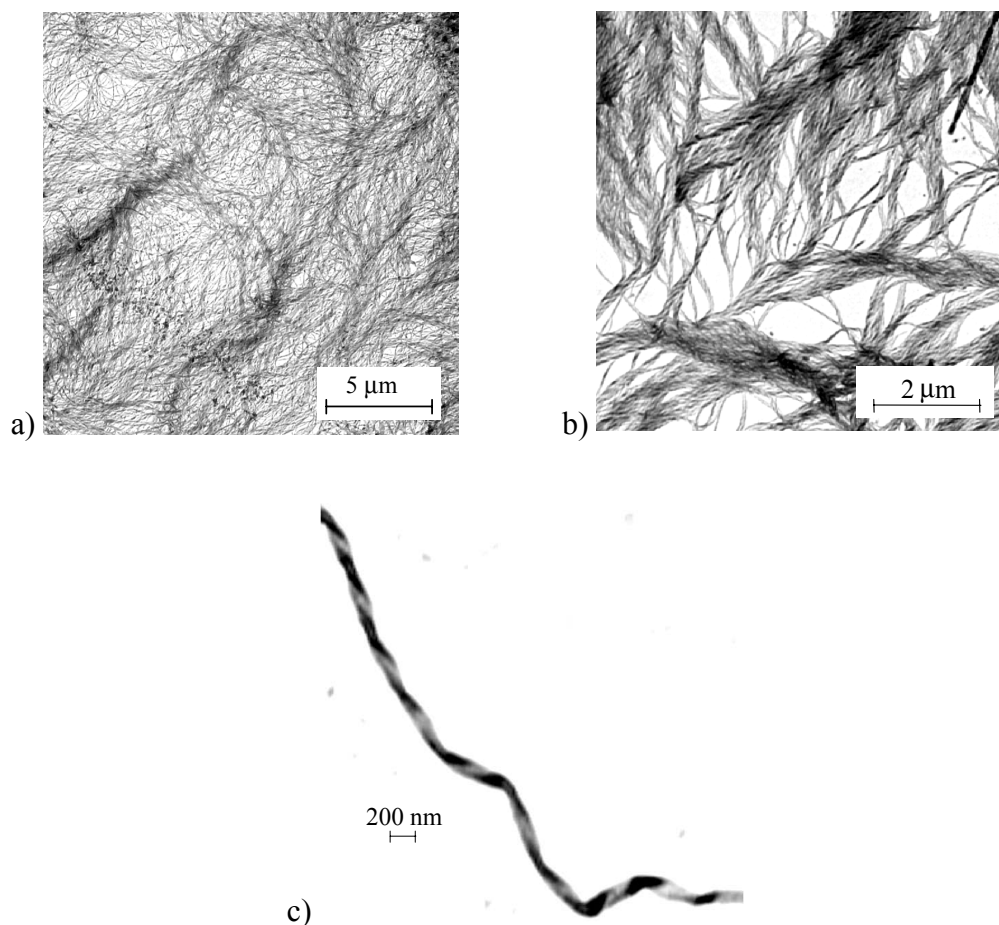


**Figure 6.7:** *Transmission electron micrographs of fibrous HOA aggregates within K18 (a) or toluene (b,c), showing several aspects of the aggregates: (a) Overall network structure; (b) unravelling of bundles of fibres into single filaments; (c) single filament showing a helical twist. The concentration of HOA in all samples was around 0.5 wt %.*

### 6.3.3 Dynamic mechanical properties

Dynamic mechanical measurements were conducted in order to study the elastic and viscous response of the anisotropic thermoreversible gels. Figure 6.8a shows a typical measurement performed with a 1 wt % HOA/K18 gel. Similar to the LC colloidal dispersions also here a linear regime is observed for the moduli at low strains. However, whereas in case of the LC colloidal dispersions the value for  $G'$  in the linear regime was approximately a factor 2 times the  $G''$  value, the anisotropic gels exhibit a  $G'$  that is more like a factor 10 times the  $G''$  value. This indicates that the occurrence of structural reorganisation during a deformation is less pronounced within the HOA gels. In Figure 6.9 the  $G'$  values detected within the linear regime are plotted as a function of the weight fraction HOA in the gel. As

expected, the mechanical stability of the gels improves upon addition of higher amounts of the gelling agent to the LC K18 (see also Figure 6.8b). The high moduli are indicative of solid-like behaviour and suggest the formation of microcrystalline nodes instead of entangled nodes.<sup>18</sup>

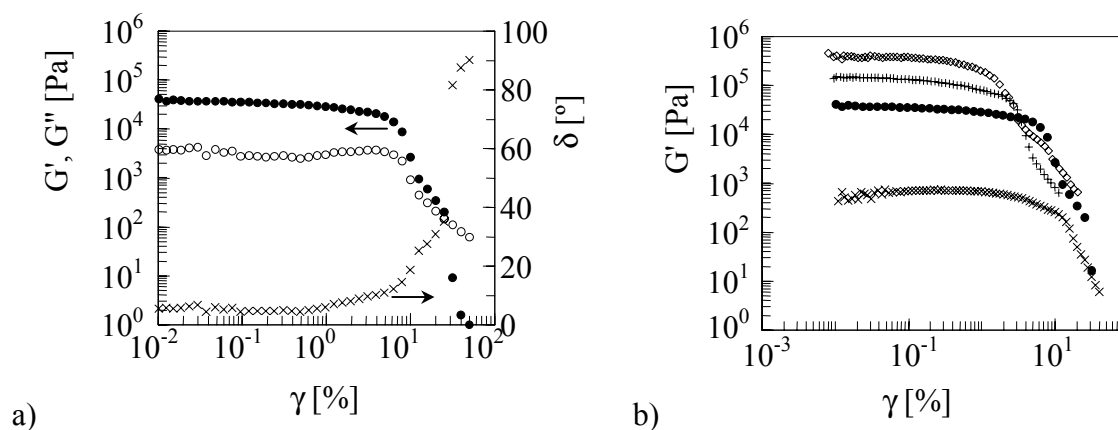


**Figure 6.8:** (a) Storage  $G'$  ( $\bullet$ ) and ( $\circ$ ) loss  $G''$  moduli together with the loss angle  $\delta$  versus the applied strain  $\gamma$  for a 1 wt % HOA/K18 gel at an angular frequency  $\omega$  of  $1 \text{ rad.s}^{-1}$ ; (b) storage modulus versus the applied strain for gels with various concentrations of HOA: ( $\diamond$ ) 3 wt %; (+) 1.5 wt %; ( $\bullet$ ) 1 wt %; ( $\times$ ) 0.5 wt %.

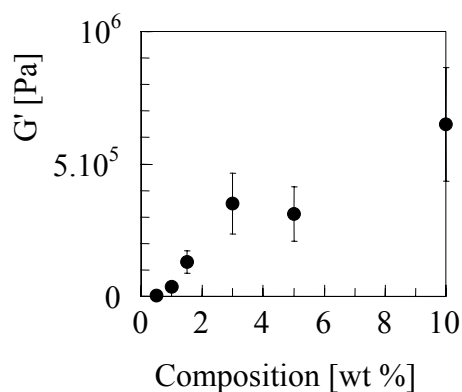


**Figure 6.9:** Storage modulus taken from the linear regime of a  $G'$  versus  $\gamma$  plot as a function of the gel composition.

Because of this solid-like behaviour in rest, it is expected that coatings of the gels are able to carry other layers on top of themselves. Therefore, apart from the LC colloidal dispersions and the dendrimer filled nematics, also these materials are interesting candidates for the fabrication of LCD's via a film-based continuous production process. It is anticipated that, like in case of the colloidal gels (Figure 3.16), also here the presence of a three-dimensional physical network will introduce an instable deformation behaviour during

application of a sufficiently high stress. In spite of this, in agreement with the discussion around the colloid filled LC's it is anticipated that the application of coatings of these gels would then still be possible by coating from the isotropic state.

In another experiment, the evolution of the dynamic moduli during formation of the fibrous HOA network was examined by subjecting a HOA/K18 mixture to a temperature sweep (Figure 6.10). Figure 6.10 illustrates that at high temperature moduli are undetectable for the isotropic liquid. At a certain time (or temperature) of the kinetic curve a steep rise in  $G'$  and  $G''$  is observed. Elsewhere, it has been demonstrated that the settling of  $G'$  is shifted to higher temperature with increasing concentration of racemic HOA.<sup>18</sup> After the steep rise the strengthening of the material is still gradually continued and, eventually, a constant rigidity is obtained for the gel at equilibrium.

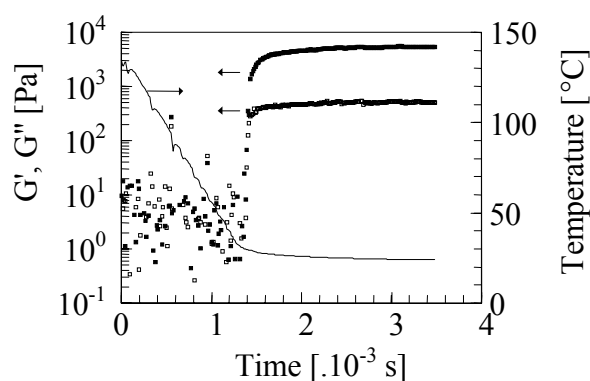


**Figure 6.10:** Evolution of the storage ( $\blacksquare$ ) and loss ( $\square$ ) moduli measured at  $\omega = 1 \text{ rad.s}^{-1}$  for a 0.75 wt % HOA/K18 gel during cooling from 140 to 26 °C with an (initial) cooling rate of  $5 \text{ °C.min}^{-1}$ .

### 6.3.4 Electro-optical properties of the thermoreversible gels for light-scattering electro-optical switches

#### 6.3.4.1 Transmittance-voltage characteristics

The HOA/K18 gel system was assessed for its potential use as light-scattering display system. For this purpose, gels with various weight fractions of HOA were brought within 18  $\mu\text{m}$  electro-optical cells with parallel orientation layers. Subsequently, voltage-up and -down scans were applied to the cells. In Figure 6.11a the electro-optical behaviour is depicted for gels based on 0.75, 1.5 and 1.9 wt % of gelling agent. The low transmittance in the off-state points to an efficient light scattering caused by the confinement of the LC molecules within smaller domain through the presence of the 3-D fibrous HOA aggregate network (Figure 6.7a). The impressive light-scattering capability of the gels is an inherent property of these two-phase materials and arises from their phase diagram, as was demonstrated earlier in the preparation of both light-scattering and transparent LC physical gels.<sup>21-23</sup>

Figure 6.11b displays the influence of cell gap on the shape of the T-V characteristic. The use of a larger cell gap is accompanied by a lower transmittance in the off-state, while the transmittance in the on-state is only slightly affected. In general, larger cell gaps provide for a better contrast ratio at a similar threshold electric field.

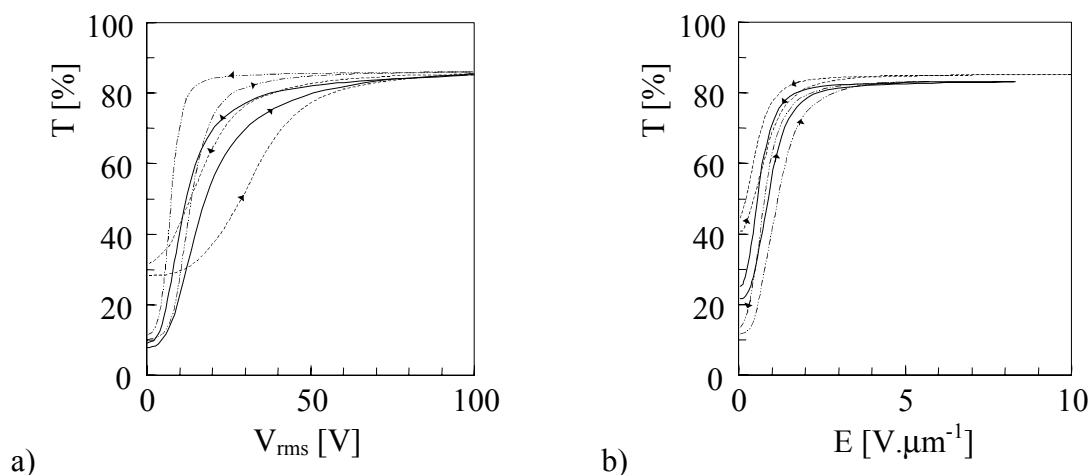


**Figure 6.11:** (a) Transmission as a function of the applied voltage for 18  $\mu\text{m}$  parallel electro-optical cells filled with HOA/K18 gels based on various fractions of HOA: (---) 0.75 wt %; (---) 1.5 wt %; (—) 1.9 wt %; (b) transmission as a function of the applied electric field for parallel electro-optical cells filled with a 1 wt % HOA/K18 gel for various cell gaps: (---) 5  $\mu\text{m}$ ; (—) 9  $\mu\text{m}$ ; (---) 13  $\mu\text{m}$ . For a reference measurement on a PDLC, see Figure 5.10.

Upon application of an increasing voltage, the LC gradually becomes homogeneously aligned in the direction of the field. It is a striking feature that, although the anisotropic gel resembles a soft solid on a macroscopic scale, the LC molecules obviously maintain their rotational mobility on a microscopic scale. The significantly high transparency in the on-state is indicative of a perfect LC monodomain, showing no influence of the small fraction of physically bound LC (if present, see Figure 6.4). Moreover, light-scattering effects due to refractive index mismatches between the continuous and dispersed phase are largely absent because of the small cross-sectional size of the finely dispersed aggregates ( $\sim 100$  nm, see Figure 6.7c). Further evidence in this was found when heating a HOA/K18 gel into the isotropic phase; a perfectly transparent material was obtained.

When looking at the effect of HOA concentration in the LC K18 on the T-V electro-optical curve, it is seen that there appears to be an optimum in concentration with respect to the threshold voltage (Figure 6.12). An increase from 0.75 to 1.5 wt % HOA initially shifts the electro-optical response to lower voltages. By further increasing the gelling agent concentration up to 1.9 wt % the threshold voltage,  $V_{90}$ , becomes higher again. Like in case of the LC colloidal dispersions and the dendrimer filled nematics, also here it is thought that this peculiar behaviour originates from the existence of a subtle balance between the LC-

dispersed phase and LC–polyimide interaction. This is also in agreement with previous findings on similar gel systems.<sup>9–11</sup> The increasing anchoring between the K18 molecules and the fibrous network with increasing fraction of the network might also explain the apparent decrease of the hysteresis with increasing network fraction by providing a ‘memory’.<sup>24</sup> In addition, it is seen from Figure 6.12 that the contrast ratio continues to increase with increasing HOA fraction, mainly through an increasing light-scattering efficiency arising from the LC polydomain structure.

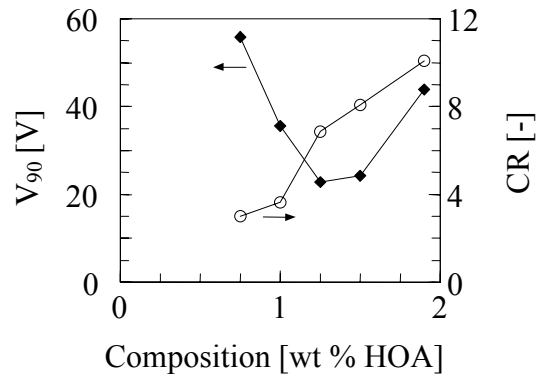


**Figure 6.12:** *Threshold voltage and contrast ratio for 18  $\mu\text{m}$  parallel electro-optical cells filled with HOA/K18 gels versus gel composition.*

#### 6.3.4.2 Switching kinetics

The dependence of rise and decay times,  $\tau_r$  and  $\tau_d$ , on applied voltage is demonstrated for 0.75, 1.5 and 1.9 wt % gels by use of Figure 6.13.

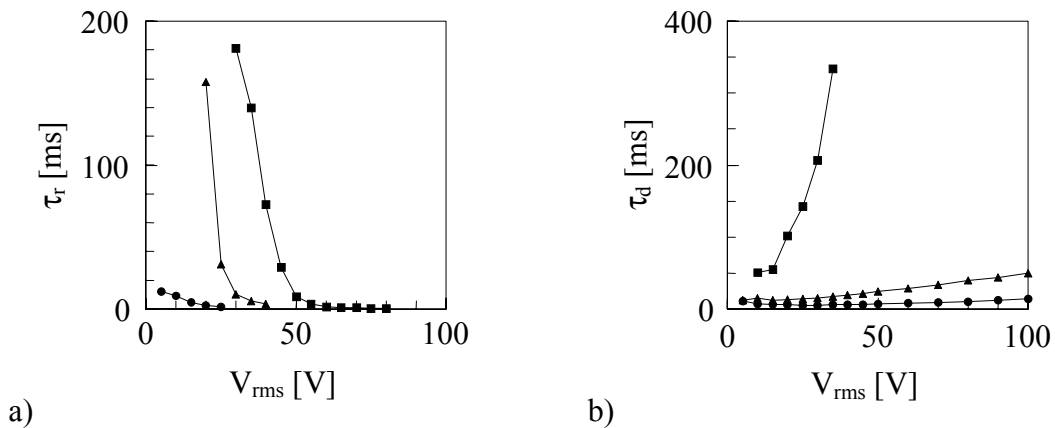


**Figure 6.13:** *(a) Rise and (b) decay times versus applied voltage for 18  $\mu\text{m}$  parallel cells filled with HOA/K18 gels based on various amounts of HOA: (■) 0.75 wt %; (▲) 1.5 wt %; (●) 1.9 wt %.*

As would be expected, the response of the LC molecules is strongly accelerated with increasing magnitude of the external electric field.<sup>25,26</sup> For each curve in Figure 6.13a rise

times of 0.5-1 ms are achieved at the highest voltages. For even higher voltages the rise times became so small, that they could not be measured anymore by the experimental set-up.

When looking into the influence of HOA concentration on  $\tau_r$  and  $\tau_d$ , it is very striking to see a significant acceleration of the response in both the rise and decay process upon addition of higher amounts of the gelling agent to the LC. For instance, for the 1.9 wt % gel the smallest decay times are found in the order of 5-10 ms. This feature has been observed before<sup>11</sup> and illustrates the fine balance of interaction forces for the gel confined within an electro-optical cell. Apparently, the finely dispersed fibrous network is able to fulfil two functions: (i) It efficiently weakens the interaction between the LC and the polyimide layers within the cell, and (ii) it provides the LC molecules with a memory via (not too strong) anchoring forces.

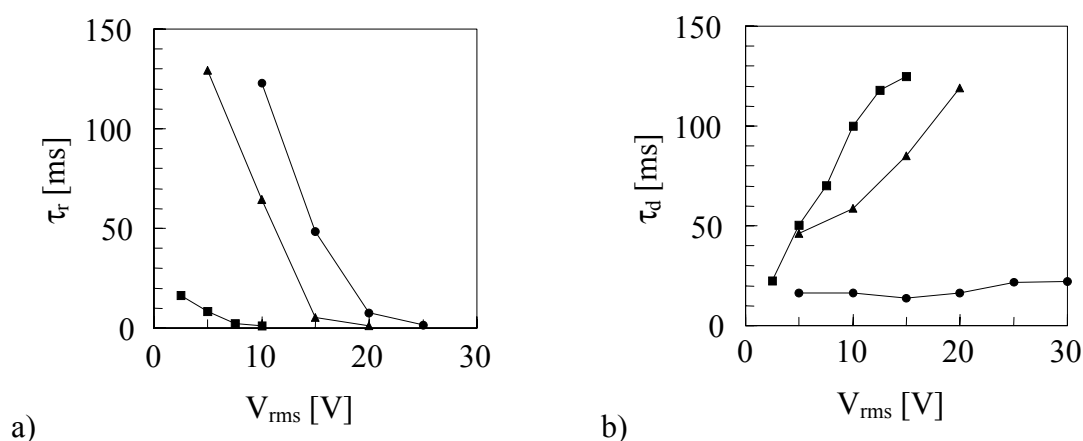


**Figure 6.14:** (a) Rise and (b) decay times as a function of the applied voltage for 1 wt % HOA/K18 gel in parallel cells with various cell gaps: (■) 5  $\mu\text{m}$ ; (▲) 9  $\mu\text{m}$ ; (●) 13  $\mu\text{m}$ .

The influence of the chosen cell gap on the switching times is demonstrated via Figure 6.14. According to Figure 6.14a, larger cell gaps correspond to longer rise times, as is predicted by equations for  $\tau_r$ .<sup>27</sup> Figure 6.14b suggests a decrease in decay time with increasing cell gap, which is indicative of an accelerated relaxation of the LC molecules upon removal of the electric field via the increased interaction between the LC and the dispersed phase.

## 6.4 Conclusions

Thermoreversible physical gels were prepared based on 12-hydroxyoctadecanoic acid (HOA) and LC K18. Transmission electron microscopy shows that the dispersed HOA compound associates into interconnected, helically twisted filaments via intermolecular hydrogen bonding. Dynamic mechanical analysis indicated that the finely dispersed, fibrous

HOA network within the LC provides a significant mechanical stabilisation of the LC matrix. This makes these materials interesting candidates for the production of light-scattering LCD's via the use of a continuous coating process.

The pronounced LC polydomain structure within the soft-solid HOA/K18 gels is expressed by strong light scattering. Upon application of a voltage, the microphase-separated material switches to a highly transparent state. Here, the contrast ratio of the gels was found to increase with increasing HOA concentration over the studied 0.75-1.9 wt % HOA range. Additionally, an increase in the concentration of the gelling agent was found to promote a faster response both in the rise and decay process, while an optimum was observed in the threshold voltages versus the gel composition.

## 6.5 References

- (1) Terech, P., Weiss, R.G. *Chem. Rev.*, **1997**, *97*, 3133-3159.
- (2) Hanabusa, K., Shimura, K., Hirose, K., Kimura, M., Shirai, H. *Chem. Lett.*, **1996**, 885-886.
- (3) Hafkamp, R.J.H., et al. *Chem. Commun.*, **1997**, 545-546.
- (4) Kato, T., Kutsuna, T., Hanabusa, K., Ukon, M. *Adv. Mater.*, **1998**, *10*, 606-608.
- (5) Kato, T., Kondo, G., Hanabusa, K. *Chem. Lett.*, **1998**, 193-194.
- (6) Kato, T., et al. *Abstr. Pap. Am. Chem. Soc.*, **1999**, *218*, 301-302.
- (7) Kato, T., Kutsuna, T., Hanabusa, K. *Mol. Cryst. Liq. Cryst. Sci. Technol., Sect. A*, **1999**, *332*, 2887-2892.
- (8) Mizoshita, N., Kutsuna, T., Hanabusa, K., Kato, T. *Chem. Commun.*, **1999**, 781-782.
- (9) Mizoshita, N., Hanabusa, K., Kato, T. *Adv. Mater.*, **1999**, *11*, 392-394.
- (10) Kato, T., Mizoshita, N., Katsuna, T., Kondo, G., Hanabusa, K. *Abstr. Pap. Am. Chem. Soc.*, **1999**, *218*, 364-365.
- (11) Mizoshita, N., Hanabusa, K., Kato, T. *Displays*, **2001**, *22*, 33-37.
- (12) Yamamoto, R., Ishihara, S., Hayakawa, S., Morimoto, K. *Phys. Lett. A*, **1978**, *69A*, 276-278.
- (13) Jadzyn, J., Czechowski, G., Mucha, M., Nastal, E. *Liq. Cryst.*, **1999**, *26*, 453-456.
- (14) Eldridge, J.E., Ferry, J.D. *J. Phys. Chem.*, **1954**, *58*, 992-995.
- (15) Watase, M., Itagaki, H. *Bull. Chem. Soc. Jpn.*, **1998**, *71*, 1457-1466.
- (16) Hikmet, R.A.M. *Mol. Cryst. Liq. Cryst.*, **1991**, *198*, 357-370.
- (17) Hikmet, R.A.M. *Liq. Cryst.*, **1991**, *9*, 405-416.
- (18) Terech, P., Rodriguez, V., Barnes, J.D., McKenna, G.B. *Langmuir*, **1994**, *10*, 3406-3418.
- (19) Tachibana, T., Yoshizumi, T., Hori, K. *Bull. Chem. Soc. Jpn.*, **1979**, *52*, 34-41.
- (20) Tachibana, T., Mori, T., Hori, K. *Bull. Chem. Soc. Jpn.*, **1980**, *53*, 1714-1719.
- (21) Janssen, R.H.C., et al. *Macromol. Symp.*, **2000**, *154*, 117-126.
- (22) Janssen, R.H.C., et al. *J. Appl. Phys.*, **2000**, *88*, 161-167.
- (23) Janssen, R.H.C., et al. *Jpn. J. Appl. Phys., Part 1*, **2000**, *39*, 2721-2726.
- (24) Hikmet, R.A.M., Boots, H.M.J. *Phys. Rev. E*, **1995**, *51*, 5824-5831.
- (25) Hikmet, R.A.M. *J. Appl. Phys.*, **1990**, *68*, 4406-4412.
- (26) Doane, J.W., Golemme, A., West, J.L., Whitehead, J.B., Wu, B.G. *Mol. Cryst. Liq. Cryst.*, **1988**, *165*, 511-532.
- (27) Hikmet, R.A.M., Higgins, J.A. *Liq. Cryst.*, **1992**, *12*, 831-845.

# Chapter 7

## A continuous process for the production of liquid crystal displays

### 7.1 Introduction

In the previous chapters new materials have been presented based on low molecular weight liquid crystals modified via the addition of a filler compound. It has been demonstrated that through a self-assembling of the filler compound new combinations of rheological and electro-optical properties are achieved. In view of this, these materials are considered to be particularly interesting for the introduction of new production processes for liquid crystal displays.

An example of a mass-production technology, and therefore very cost-effective process was shown in Chapter 1. It is based on so-called bottom-up stacking of the various layers that are needed for the operation of a display. For practical reasons, as long as solvent coatable electrodes of sufficient quality are not available, the display is designed as an in-plane switch by using interdigital electrodes. The interdigital electrodes can be applied on a polymer base material by sputter coating followed by a lithographic structuring. By applying an in-plane electric field, the liquid crystal (LC) molecules are reoriented in the plane parallel to the plane of the substrate along the electric field-lines (Figure 7.1). The in-plane switch is switched between a dark and a transparent state in case two polarisers are installed.<sup>1-3</sup>

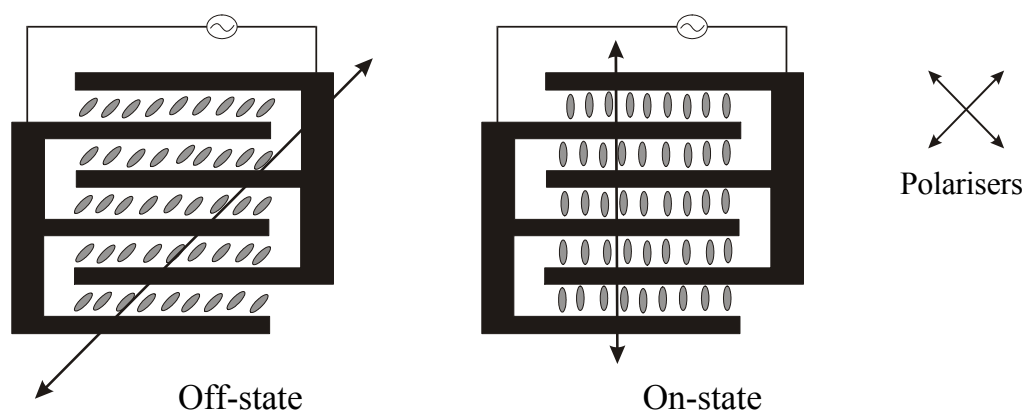


**Figure 7.1:** Schematic representation of the on- and off-states of an in-plane switch (top view) based on a liquid crystal with positive anisotropy.



For light-scattering materials the in-plane electric field results in switching between a light-scattering and a completely transparent state in case the dimensions of the dispersed phase are much smaller than the wavelength of visible light. For larger dimensions of the dispersed phase only one polarisation direction of the incident light is transmitted via an appropriate refractive index matching of the dispersed phase to one refractive index of the LC. The other polarisation direction of the light is scattered as it experiences different refractive indices.

In Chapter 3 colloid filled LC's have been described and evaluated for their rheological and electro-optical performance. For rather high colloid fractions these materials exhibit an impressive stiffness in combination with a strong light scattering (see Figure 7.2). It is expected that the presence of the colloidal network hinders the direct coating of these materials (see Figure 3.16). To circumvent this problem, the coating of the colloid/LC materials might be performed at elevated temperatures where the LC is in its isotropic liquid state and where the colloidal network has not been formed yet. After application of the coating the nematic phase is then automatically reintroduced upon cooling to room temperature and the physical network is formed simultaneously. The network provides the mechanical stabilisation necessary for further processing.

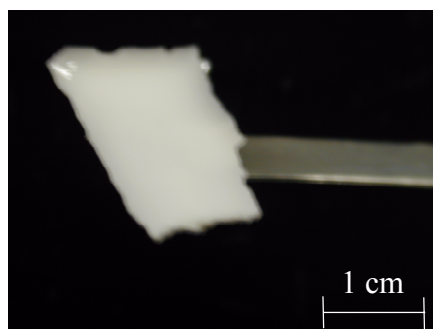


**Figure 7.2:** *Photograph of an aggregated 15 wt % LC E7 dispersion based on 630 nm sized poly(methyl methacrylate-co-divinylbenzene) colloids showing its white appearance and its soft solid-like nature.*

In this chapter the practical realisation of a continuous process for the production of liquid crystal displays is investigated into some more detail. In order to demonstrate the validity of the new display manufacturing process, two issues have to be solved: (1) the stabilised LC formulation should be able to form homogeneous films of controlled thickness by means of current coating technologies, and (2) the films should be assessable for overcoating, such that the other optical components can be applied and that the LC layer can be protected against touch and other exterior influences. The emphasis of this first proof of principle has been laid on the application process of the LC layer.

## 7.2 Experimental

### 7.2.1 Materials

For details on the liquid crystal LC E7 used see Section 3.3.1. For the experiments described in this chapter 630 nm sized poly(methyl methacrylate-*co*-divinylbenzene) filler particles were used, which were prepared via dispersion polymerisation according to the procedures described in Section 2.2 (see Figure 2.14c for a SEM image).

### 7.2.2 Sample preparation

The LC colloidal dispersions were prepared as described in Section 3.3.2. For the coating experiments in some cases toluene was added to LC colloidal dispersions. Subsequently, the colloids were homogeneously dispersed in the (isotropic) medium via ultrasonic mixing. In case no additional solvent was used for the coating experiments, the LC colloidal dispersions were preheated and homogenised directly before use at 140 °C.

### 7.2.3 Techniques

#### *Doctor blading*

The LC colloidal materials were applied on 2.5 x 2.5 cm glass substrates by use of a Coatmaster 509/MC-I purchased from Erichsen GmbH equipped with a temperature controller and a film applicator (Erichsen multicat model 411) (see Figure 7.3). The glass substrates were provided with a rubbed polyimide layer according to the procedure described in Section 3.3.3.

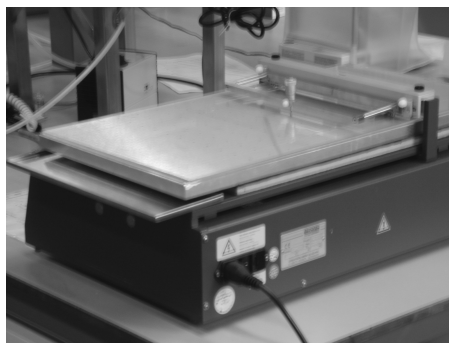


**Figure 7.3:** *Photograph of the experimental set-up that was used for the preparation of coatings of the LC colloidal dispersions.*

In most cases, toluene was used as an additional solvent for the LC colloidal dispersions in the coating process. In order to minimise edge effects the polyimide coated

glass substrate was positioned on the Coatmaster in between two other glass substrates of similar thickness. The glass pieces were placed on a paper substrate and were held in position via vacuum. Next, a few droplets of a homogenised dispersion of the colloids in the E7/toluene medium were applied on the first glass substrate. The film was formed by a controlled movement of the blade with a speed of  $2.5 \text{ mm.s}^{-1}$ . After application of the coating, the remaining toluene was evaporated from the coated, middle glass substrate at room temperature for a few days.

Alternatively, the LC colloidal dispersions were applied in the isotropic state by heating the material well above the  $T_{\text{NI}}$  of the E7 at  $140 \text{ }^\circ\text{C}$ . The substrate holder of the Coatmaster was heated at  $75 \text{ }^\circ\text{C}$ . The polyimide coated glass substrate was placed against a pre-cut glass plate in order to keep it in position. Directly after positioning of the droplets of preheated LC material the film was formed at a speed of  $2.5 \text{ mm.s}^{-1}$ . After the doctor blading process, the coated glass substrate was removed from the machine and cooled down to room temperature.

Before each coating experiment the gap between the doctor blade and the glass substrate was determined via the use of a set of metal blades of known thickness. In all cases the shearing direction was chosen parallel to the rubbing direction of the polyimide layers.

### *Light microscopy (LM)*

The morphology and thickness of the coatings were examined with the aid of a Zeiss Axioplan 2 optical microscope equipped with crossed polarisers.

## **7.3 Results and discussion**

### **7.3.1 Influence of processing parameters**

Initial experiments were directed towards the preparation of homogeneous coatings with a thickness in the order of a few micrometer made from LC colloidal dispersions. For this purpose, the influence of processing parameters, such as toluene concentration and blade gap, on the film homogeneity and thickness was investigated. To evaluate the impact of toluene concentration on homogeneity of the resulting films, coatings were prepared from 15 wt % LC colloidal dispersions in the absence and in the presence of toluene. From Figure 7.4 it is seen that, in case no toluene is used during processing, coatings are obtained which are inhomogeneous on a microscopic scale (Figure 7.4a). Generally, it was found that for sufficiently thin films these inhomogeneities are also apparent on a macroscopic scale.

Upon addition of small amounts of toluene to the colloid/LC mixture homogeneous coatings are obtained after evaporation of the toluene, even when observed on a microscopic scale (Figure 7.4b).

Obviously, the use of only a small amount of solvent already enables a perfect homogenisation of the colloid/LC/toluene mixture before application.

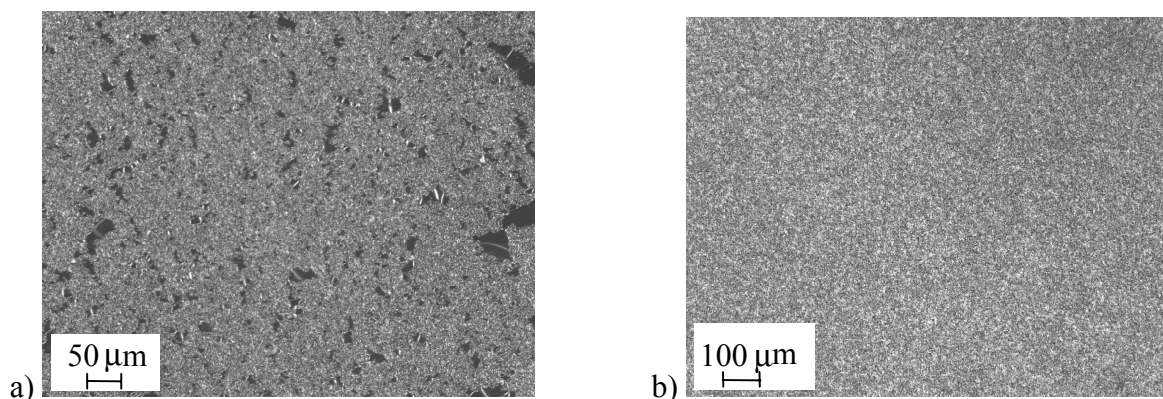


**Figure 7.4:** *Optical polarisation micrographs of coatings made from LC colloidal dispersions based on 15 wt % 630 nm colloids to which different amounts of toluene were added: (a) 0 % w/w; (b) 20 % w/w toluene/(E7+colloids). The blade gap was set on 124  $\mu\text{m}$ . The black areas in the micrographs of (a) are free of both LC and colloids.*

The thickness of the film shown in Figure 7.4b was measured via microscopy on the freeze-broken sample and was found to be equal to approximately 9.2  $\mu\text{m}$ . For the same blade gap a coating with a reduced film thickness of 4-6  $\mu\text{m}$  was obtained by starting the coating experiment from a 10 wt % LC colloidal dispersion dispersed in 40 wt % toluene. For the latter coating, however, a larger variation in film thickness was found. This phenomenon was generally observed in case toluene concentrations were used exceeding approximately 30 wt % and is ascribed to an uncontrolled spreading of the liquid crystal material due to the extremely low viscosities involved.

In order to obtain a completely isotropic colloidal dispersion in E7/toluene a minimum amount of toluene is required, which corresponds to a concentration of approximately 10 wt %. In conclusion, the optimum concentration of toluene for obtaining homogeneous films is in the order of 10-20 wt %.

In Table 7.1 the results are summarised concerning the measured film thickness as a function of the toluene concentration and blade gap used. As expected, the thickness of the film obtained after evaporation of the toluene decreases with increasing concentration of toluene used.

Usually, the film thickness was found to increase with increasing blade gap, although this is not so obvious from Table 7.1. In general, thin films of the 15 wt % colloid/E7 mixtures with a thickness of  $\sim 5$   $\mu\text{m}$  are obtained by using toluene concentrations of the order of 20 wt % (see also Figure 7.5). The achieved film thickness is much lower than the blade gap used, due to the evaporation of toluene after application of the mixture and due to a spreading of the mixture during application.

**Table 7.1:** *Dependence of film thickness (in micrometers) on toluene concentration and blade gap. The coatings were made from LC colloidal dispersions based on 15 wt % colloids.*

Toluene concentration [% w/w (E7+colloids)]	Blade gap [ $\mu\text{m}$ ]		
	124	146	167
13	11	8.9	8.9
17	-	4.4	7.8
20	9.2	4.6	7.8
25	-	4.2	5.0
40	4-6	-	-

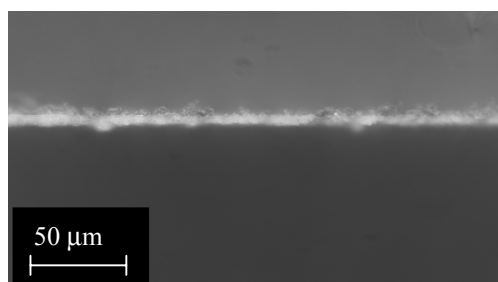


**Figure 7.5:** *Cross-section of a freeze-broken coating (middle) on a glass substrate (top side) based on a 15 wt % LC colloidal dispersion mixed with 25 wt % toluene. The coating was applied on the glass substrate using a blade gap of 167  $\mu\text{m}$ .*

To evaluate the influence of the film applicator gap on homogeneity of the films, various coatings were prepared from a 10 wt % colloid/LC mixture dispersed in 17 wt % toluene. Here, the gap in between the doctor blade and the polyimide coated glass substrates was increased from 124 up to 189  $\mu\text{m}$ .

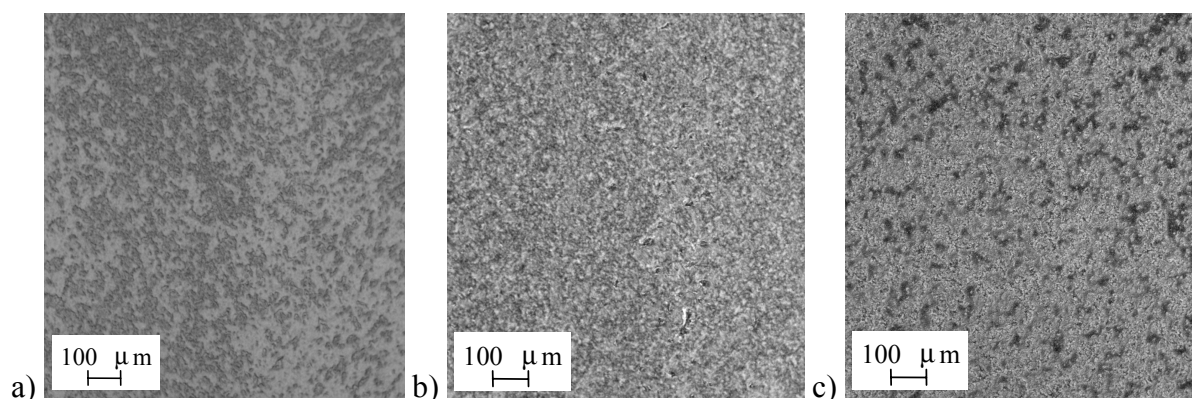


**Figure 7.6:** *Optical polarisation micrographs of coatings made from LC colloidal dispersions based on 10 wt % 630 nm colloids dispersed in 17 % w/w toluene/(E7+colloids), using various gaps for the film applicator: (a) 124  $\mu\text{m}$ ; (b) 167  $\mu\text{m}$ ; (c) 189  $\mu\text{m}$ . The dark areas in the micrographs of (a) and (c) are aligned LC-rich regions.*

In case the gap was chosen too low, the resulting films were obviously so thin, that microscopic inhomogeneities became apparent (Figure 7.6a). Usually, these microscopic inhomogeneities also persisted on a macroscopic scale. In case the gap was chosen too large, significant variations in film thickness were visible on a macroscopic scale, which is attributed to flow of the material after application of the film. This inhomogeneous distribution of the material can also be extracted from the optical micrograph of Figure 7.6c.

The optical micrographs of Figure 7.6 illustrate that for the particular mixture composition used the homogeneity of the coatings is optimised for an intermediate film applicator gap around 150  $\mu\text{m}$ . Figure 7.7 shows an example of the visual appearance of a colloid/E7 coating corresponding to the film shown in Figure 7.6b. The thickness of this film was found to be equal to approximately 6.7  $\mu\text{m}$ .

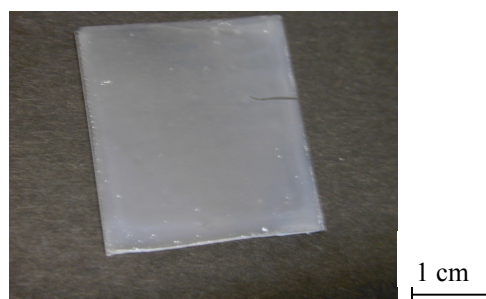


**Figure 7.7:** *Photograph of polyimide coated glass substrate provided with a coating made from a LC colloidal dispersion based on 10 wt % 630 nm colloids dispersed in 17 % w/w toluene/(E7+colloids). The gap of the film applicator was set at 167  $\mu\text{m}$ .*

It is anticipated that the optimum applicator gap is highly dependent on the viscosity of the material and, thus, on the composition of the material with respect to e.g. solvent type, solvent concentration, and colloid concentration. It is emphasised that every combination of desired film properties requires an accurate fine-tuning of processing parameters.

Usually, it was observed that LC molecules in LC-rich regions have the tendency to align in the shearing direction, independent of the direction of the rubbed polyimide layers. This LC alignment enables the generation of a contrast between the electrically unaddressed and addressed state. For the real application of these films in e.g. TN displays, more practical work is needed to find the optimum processing parameters for the production of films with optimised electro-optical and mechanical properties.

A final remark concerns the application of a protective layer on top of the applied colloid/LC layer. This overcoat should enhance the mechanical stability and enables the application of additional layers needed for the operation of the display, such as colour filters, optical retardation layers and the polariser. Initial experiments have demonstrated that the LC E7 with its intermediate polarity very easily mixes with bulky or rather polar monomers, such as bornyl or hydroxymethyl methacrylate. In view of this, the use of reactive monomers for

the top layer, which are polymerised after application, does not seem to be very promising. Alternatively, appropriate materials for the top coating might comprise a polymer solution. After application of the polymer solution the medium is evaporated, giving rise to the formation of a polymer film. Since the LC E7 was found to mix very well with both apolar and rather polar solvents, including ethanol, water was selected as the medium in combination with a water-soluble polymer, polyvinylpyrrolidone (PVP). A first problem that was encountered during the application of these materials on an LC layer was a limited wetting. Although the use of a surfactant substantially improved the wetting, it is assumed that it also promotes the occurrence of intermixing phenomena. However, at this point no quantitative or conclusive data are available with regard to this mixing issue. A second problem observed was the formation of macroscopic cracks in the LC layer during or after evaporation of the aqueous medium at the edge round the transparent PVP film.

Evidently, more work in this field is necessary to select the appropriate materials for the top coating which should provide an appropriate balance between wetting and mixing phenomena, in combination with appropriate application processes. Alternatively, the application of a top layer might be effected through lamination of a solid, polymer film.

## 7.4 Conclusions

The LC colloidal dispersions can be successfully applied on a substrate by starting the coating process from homogeneously dispersed, isotropic colloidal dispersions with fluid-like rheological properties. After application of the isotropic liquid the colloidal network is restored, providing a mechanical stabilisation of the LC coating. This result is considered to be important, rationalising the project results presented in the previous chapters such that the set of new LC properties can lead to completely new display manufacturing concepts.

It was demonstrated that, in case the coating experiment is performed at elevated temperature in the absence of an additional solvent, the resulting films exhibit microscopic inhomogeneities, pointing to an inefficient breakdown of the colloidal network before application of the material. For sufficiently thin films, these inhomogeneities are also distinguished on a macroscopic level. As opposed to this, the use of a small amount toluene already enables a complete breakdown of the colloidal aggregates before application. In this way, via an appropriate combination of processing parameters, such as toluene concentration and blade gap, homogeneous films are gained with a thickness in the order of 5-10  $\mu\text{m}$ .

## 7.5 References

- (1) Ohe, M., Kondo, K. *Appl. Phys. Lett.*, **1995**, *67*, 3895-3897.
- (2) Yoneya, M., Kondo, K. *Appl. Phys. Lett.*, **1999**, *74*, 3477-3479.
- (3) Ohe, M., Kondo, K. *Appl. Phys. Lett.*, **1996**, *69*, 623-625.

## Technology assessment

Conventional flat panel liquid crystal displays are fabricated via expensive and rather inefficient batch-wise fabrication methods. In order to meet the rapidly increasing demand for flat panel displays new, continuous fabrication processes are required, which are significantly more cost-effective than the established step-by-step, batch-wise methods. Moreover, the existing processes are rather rigid with respect to display size and shape. The introduction of a new fabrication technology for liquid crystal displays (LCD's) is, however, hindered by the rheological properties of the low molecular weight liquid crystals used. This problem was dealt with by considering two criteria that need to be fulfilled by the liquid crystal (LC) material. Firstly, the LC material must allow processing via a continuous coating process for obtaining homogeneous films of the LC material on a substrate. Secondly, the materials must have sufficient mechanical strength to resist the stresses that are exerted during, for instance, the application of a top layer. In this research a low molecular weight LC (E7) was tailor-made for continuous processing by mixing the LC with functional additives, such as (i) polymer colloids, (ii) dendrimers or (iii) gelling agents. Via specific interactions, the dispersed phase assembles itself into larger aggregates within the LC matrix, thereby strongly modifying the rheology of the LC material.

In case of the LC colloidal dispersions and the thermoreversible gels a three-dimensional network is present, which imposes a significant stiffness to the LC material. This enables these materials to resist quite large stresses in the order of  $10^2$ - $10^3$  Pa for fractions of the dispersed phase in the 1-10 wt % range. Additionally, it has been shown that the LC colloidal dispersions can be processed via a continuous process, such as doctor blading, by using a small amount of an additional solvent. By an appropriate combination of processing parameters macroscopically homogeneous coatings are obtained with a film thickness in the order of 5-10  $\mu\text{m}$ . For in-plane electro-optical switches, the thickness of the film needs to be further reduced via an adjustment in processing parameters. One also might consider replacing the highly birefringent LC E7 by another LC with a lower birefringence, thereby allowing the use of thicker LC films. It is anticipated that the processing of the network-type thermoreversible gels can be performed in a similar manner, i.e. via the use of an additional solvent. In view of their coating behaviour and favourable mechanical strength both the LC colloidal dispersions and the thermoreversible gels are considered to be suitable for processing via continuous technologies.

In case of the dendrimer filled LC's a three-dimensional network is absent. These materials flow very easily under an applied stress and might be coated on a substrate without the use of an additional solvent. Unfortunately, these materials are able to bear only small stresses in the order of 1-10 Pa before flow sets in. Probably, this mechanical stiffness is not sufficient to allow the application of a top layer. Therefore, with respect to the LC colloidal



dispersions and the thermoreversible gels these dendrimer modified LC's are less suitable for use in a continuous fabrication process.

Before a continuous LCD manufacturing process can become reality, several other problems have to be solved concerning the other constituent layers of the LCD. For instance, after the application of the LC layer on an ITO coated substrate a protecting top coating needs to be applied. The materials for the top coating need to be carefully selected on the basis of their compatibility with the LC. In order to provide a good wetting of the LC layer, a sufficient compatibility with the LC material is required. On the other hand, however, the compatibility must be kept to a minimum since intermixing between the top coating and the LC layer needs to be avoided. Alternatively, one might consider application of a top layer by use of a lamination process. In this case, sufficient mechanical coherence between the LC layer and the laminated top layer has to be established. Finally, also the materials selected for the implemented polarisers have to meet several criteria with respect to e.g. coatability and polarising efficiency.

Apart from the introduction of new production processes for LCD's, the modified LC materials were also explored with the aim to introduce new or improved electro-optical properties via an appropriate tuning of their morphology and additive structure.

For high colloid filler content the LC colloidal dispersions show a strong light scattering and are electrically switched to a more transparent state. Their electro-optical features are similar to the electro-optical characteristics that are generally observed for polymer dispersed liquid crystals (PDLC's),<sup>1,2</sup> including for instance a significant hysteresis in the electro-optical curves and rather high switching voltages. These materials are suitable for low-end, large-area commercial applications, such as traffic signs or switchable windows, although a further improvement or fine-tuning of their performance might be necessary. Since the preparation of the LC colloidal dispersions involves a mixing step, this is rather easily achieved via a modification of the chemical and physical properties of the individual phases of the LC colloidal dispersions.

Alternative light-scattering systems are based on the addition of dendrimers or gelling agents to an LC. These systems allow morphology control predominantly via the weight fraction of the dispersed phase in the LC. For the dendrimer filled nematics fast switching kinetics are found, while hysteresis phenomena are largely absent in their transmittance-voltage curves. Although the dendrimer systems can be optimised with respect to their light-scattering off-state or transparent on-state, their contrast ratio remains largely unaffected and might require further improvements via, for instance, an appropriate tuning of the refractive indices of the LC. Practical advantages of the thermoreversible gels presented in this thesis are that the molecular additive is commercially available and that a refractive index matching is not required due to the small, sub-VIS wavelength dimensions of the dispersed phase. In summary, the thermoreversible gels show the best combination of switching voltage, switching kinetics, contrast ratio and mechanical stiffness. However, in view of subtle

differences in properties between the three light-scattering systems investigated, the choice for one particular light-scattering system would probably need to be made on the basis of the requirements that are set for a particular application.

The same two-phase materials are in principle also suitable for use in the production of modified twisted nematic (TN) LCD's.<sup>3</sup> Elsewhere, it has been shown that, compared to conventional TN-LCD's, TN displays based on thermoreversible gels show deterioration in switching voltage and contrast ratio.<sup>4,5</sup> It is anticipated that dendrimer filled nematics do not offer any advantage with respect to properties or processes of conventional TN displays. Consequently, these materials were not considered for this particular application. In this thesis predominantly LC colloidal materials were evaluated for their application in TN-LCD's. It was attempted to minimise light-scattering effects and to maintain or improve the inherently excellent switching characteristics of a pure LC by using only low weight fractions of the filler component. Although, with respect to conventional TN-LCD's, the contrast ratio of TN-LCD's based on the colloid filled LC's is somewhat reduced, switching times and threshold voltages are largely maintained in the presence of the colloids. When comparing the LC colloidal dispersions with the transparent thermoreversible gels, the best combinations of switching voltage, contrast ratio and rheological properties are achieved for LC colloidal dispersions based on low fractions of colloids with sizes around 600 nm. In view of this, the LC colloidal dispersions are proposed to be the most suitable materials for the production of TN-LCD's where contrast is not an issue, but which might benefit from the freedom in shape, size, higher production speed and lower costs.

In conclusion, new materials have become available for the production of liquid crystal displays. The favourable combination of their rheological and electro-optical performance gives access to new manufacturing methods and applications for displays.

## References

- (1) Coates, D. *Displays*, **1993**, *14*, 94-103.
- (2) Doane, J.W., Vaz, N.A., Wu, B.G., Zumer, S. *Appl. Phys. Lett.*, **1986**, *48*, 269-271.
- (3) Schadt, M., Helfrich, W. *Appl. Phys. Lett.*, **1971**, *18*, 127-128.
- (4) Janssen, R.H.C., et al. *J. Appl. Phys.*, **2000**, *88*, 161-167.
- (5) Janssen, R.H.C., et al. *Macromol. Symp.*, **2000**, *154*, 117-126.



# Summary

Flat panel displays based on organic liquid crystals (LC's) have become very widely used because of their flatness and portability and are nowadays increasingly incorporated in advanced electronic systems, such as mobile phones, personal digital assistants, laptop computers, desktop computers and televisions. This recent explosive growth in applications of liquid crystal displays (LCD's) is mainly due to the spectacular progress in performance with regard to light efficiency and viewing angle of LCD's.

Most modern flat panel displays are based on a twisted nematic (TN) liquid crystal mode. These TN-LCD's employ electrical addressing to switch the polarisation direction of linearly polarised light through reorientation of the LC and are in this way switched between a transparent and a dark state. Alternatively, other display types generate contrast between an on- and an off-state via electrically modulated light scattering. This light scattering is usually introduced by the use of two-phase materials through refractive index mismatches within the material. In the presence of an electric field the refractive index mismatches are cancelled out via alignment of the LC molecules and, consequently, these materials are switched between a light-scattering (white) off-state and a transparent on-state. An advantage of these light-scattering systems over TN-LCD's is an improved light efficiency, since no polarisers are required. A disadvantage of most of the presently available two-phase systems is that control over the morphology and properties of these materials is lacking, since the morphology is fixed in-situ during a phase separation process. Another disadvantage of both the TN displays and the light-scattering systems is that the fabrication of these devices involves the use of very laborious and expensive batch-wise processes.

In the research presented in this thesis it is attempted to circumvent the above-mentioned problems of conventional electro-optical switches by the generation of an experimental route for the preparation of new materials of which the morphology can be well controlled. Moreover, it is attempted to make these materials suitable for use in a continuous process for the production of classical TN displays and/or light-scattering electro-optical switches. For these purposes, materials are developed based on low molecular weight LC's and functional additives, where the additives are used to introduce new or improved combinations of electro-optical and rheological properties via self-organisation. Here, three types of model systems are investigated, namely nematic LC's modified with (1) crosslinked polymer colloids, (2) dendrimers and (3) gelling agents.

In the first part of this thesis LC colloidal dispersions are described which are composed of two individually prepared phases. This ensures that the morphology of these two-phase materials is in principle well controlled with respect to, for instance, dimension and refractive index of the disperse phase. Through the utilisation of a crosslinker in the synthesis of the polymer particles, the morphology is preserved during post-processing.

Furthermore, it is demonstrated that the polymer colloids dispersed in the LC self-assemble into a three-dimensional network during cooling from the isotropic state to temperatures below the phase transition temperature of the LC. The average orientation of the LC and the interaction between the LC and the assembled colloids strongly depend on the set particle size and composition of the mixture. This opens the possibility to tune electro-optical properties via the morphology of these LC colloidal dispersions. It is demonstrated that, via an appropriate choice of polymer weight fractions and dimensions, these modified LC's are suitable both for application in classical TN display configurations and for application as light-scattering electro-optical switches.

In the second part of this thesis the possibilities with regard to material properties are extended by reducing the typical dimension of the dispersed phase to nanometer scale. This is realised through the use of highly branched molecules, so-called dendrimers, which are functionalised with apolar alkyl endgroups. These dendrimers are able to perturb the ordering of the LC molecules to such an extent, that a polydomain morphology is formed. On a macroscopic scale this results in an efficient light scattering, which makes these materials suitable for the fabrication of LCD's that switch between a light-scattering and a transparent state. Through specific interactions between the dendritic molecules and the LC surroundings, hysteresis appears to be largely absent in the electro-optical curve and fast switching kinetics are realised.

Finally, in the third part of this thesis the polydomain concept is further extended by the development of electro-optical switches based on LC's and low molecular weight gelling agents. For this study 12-hydroxyoctadecanoic acid is selected as the gelling agent. Via hydrogen bonding interactions these molecules assemble into fibrous aggregates, which are interconnected to form a three-dimensional network. The finely dispersed network provides a pronounced polydomain structure in combination with an acceleration of the reorientation process of the LC molecules after application or removal of an electric field. Moreover, by an appropriate tuning of the morphology of these so-called thermoreversible gels high contrast ratios and relatively low switching voltages are obtained.

For all three investigated materials it is shown that the rheological properties of the low molecular weight LC are strongly modified by the presence of the additive. The presence of a three-dimensional, physical network in both the LC colloidal dispersions and the thermoreversible gels enables these materials to resist quite high mechanical stresses in the order of  $10^2$ - $10^3$  Pa. For equal weight fractions of the additive, the thermoreversible gels are able to resist somewhat higher mechanical stresses than the LC colloidal dispersions. For the application of these materials with soft-solid behaviour on a substrate, the network has to be temporarily suppressed. This can be effected via the use of a small amount of solvent, such as toluene. For the LC colloidal dispersions it is demonstrated that in this way homogeneous and very thin films (layer thickness  $< 10$   $\mu\text{m}$ ) are generated via the use of conventional coating processes.

In case of the dendrimer filled LC's the dispersed phase organises itself in spherical aggregates instead of a three-dimensional network. Because of the absence of a dispersed network the dendrimer filled nematics are able to bear much lower mechanical stresses than the LC colloidal dispersions and the thermoreversible gels. In spite of this, a possible advantage of the absence of a network is that these easily deformable dendrimer systems are directly coated on a substrate without the use of an additional solvent. A remarkable feature is that the dendrimer/LC mixtures exhibit extremely high viscosities at low deformations. This resistance against flow is ascribed to the strongly perturbed orientation of the LC molecules surrounding the dendrimer aggregates, which can be interpreted in terms of a physical network of LC domains.

Summarising, the examined modified LC materials offer the possibility to generate a broad range of new and desired properties via an appropriate tuning of morphology. The advantageous combinations of rheological and electro-optical properties can be exploited for the introduction of new manufacturing processes and applications of LCD's.



# Samenvatting

Platte beeldschermen gebaseerd op laagmoleculaire, organische vloeibare kristallen (liquid crystals, LC's) zijn erg populair geworden vanwege hun gering volume en draagbaarheid en worden inmiddels in toenemende mate gebruikt in geavanceerde elektronische systemen zoals mobiele telefoons, elektronische zakagenda's, laptop computers, desktop computers en televisies. Deze recente explosieve groei van de toepassingen van vloeibare kristal schermen (liquid crystal displays, LCD's) is hoofdzakelijk te danken aan de spectaculaire technologische vooruitgang inzake helderheid, lichtefficiëntie en kijkhoek van LCD's.

Op dit moment worden platte beeldschermen hoofdzakelijk vervaardigd op basis van getwiste, nematische (twisted nematic, TN) vloeibare kristallen. Door elektrische schakeling van de polarisatie-richting van lineair gepolariseerd licht via het vloeibare kristal worden deze TN-LCD's geschakeld tussen een transparante en een donkere toestand. Een geheel andere wijze om contrast tussen de aan- en de uittoestand van een display te realiseren berust op het principe van elektrisch gemoduleerde lichtverstrooiing. Deze lichtverstrooiing wordt doorgaans bewerkstelligd door het gebruik van tweefasen materialen, waardoor brekingsindexverschillen geïntroduceerd worden in het materiaal. Op macroscopische schaal resulteert dit in een witte toestand. In aanwezigheid van een elektrisch veld worden de brekingsindexverschillen opgeheven door uitlijning van de LC moleculen en wordt een transparante toestand verkregen. Een voordeel van deze lichtverstrooiende materialen is dat men, in tegenstelling tot de TN-LCD's, niet gebonden is aan het gebruik van polarisatoren, waardoor een hogere lichtefficiëntie gegenereerd kan worden. Een belangrijk nadeel van de meeste huidige tweefasen mengsels is dat de morfologie in-situ tijdens een fasescheidingsproces gevormd wordt, waardoor controle over de morfologie en eigenschappen ontbreekt. Een ander nadeel van zowel de TN-LCD's als de huidige lichtverstrooiende systemen is dat beide momenteel noodzakelijkerwijs gefabriceerd worden via batchwijze processen, hetgeen zeer arbeids- en kapitaalintensief is.

In het hier beschreven onderzoek wordt getracht bovengenoemde nadelen van conventionele elektro-optische schakelaars op te lossen door een alternatieve experimentele route te volgen voor de ontwikkeling van nieuwe materialen met een goed in te stellen morfologie. Bovendien wordt getracht om deze materialen geschikt te maken voor toepassing in klassieke TN displayconfiguraties en/of voor toepassing als elektrisch schakelbare lichtverstrooiende systemen en daarbij de mogelijkheid te creëren om continue processen aan te wenden in de productie van deze displays. Binnen dit promotieonderzoek zijn hiervoor materialen ontwikkeld gebaseerd op laagmoleculaire vloeibare kristallen en functionele additieven, waarbij de additieven worden gebruikt om nieuwe of verbeterde combinaties van elektro-optische en reologische eigenschappen te introduceren middels zelforganisatie. Een



drietal verschillende modelsystemen is onderzocht, namelijk nematische LC's waaraan respectievelijk (1) polymere colloïden, (2) dendrimeren en (3) organische verbindingen zijn toegevoegd.

In het eerste deelonderzoek wordt het aanmaken van de disperse, colloïdale fase en de bereiding van de LC colloïdale dispersies in twee gescheiden stappen uitgevoerd, waardoor de morfologie van deze tweefasen materialen in principe goed controleerbaar is met betrekking tot bijvoorbeeld dimensie en brekingsindex van de disperse fase. Door gebruik van een crosslinker in de synthese van de polymere deeltjes blijft de morfologie van de deeltjes behouden gedurende nabehandelingen. Aangetoond is dat de polymere deeltjes in het LC materiaal zich ordenen in een driedimensionaal netwerk tijdens een afkoelprocedure, waarbij de faseovergang van het LC gepasseerd wordt. De gemiddelde oriëntatie van het LC en de interactie tussen LC en de geordende disperse fase blijken in sterke mate afhankelijk te zijn van de ingestelde deeltjesgrootte en de samenstelling van het mengsel. Hierdoor is het mogelijk een scala aan electro-optische eigenschappen te behalen. Het is gedemonstreerd dat, door een juiste keuze van polymeergewichtsfracties en dimensies, deze gemodificeerde LC's zowel benut kunnen worden voor toepassing in klassieke TN displays alsook voor toepassing als elektrisch schakelbare, lichtverstrooiende systemen.

In het tweede deelonderzoek worden de mogelijkheden qua materiaaleigenschappen uitgebreid door de dimensie van de disperse fase te verlagen naar nanometer schaal. Hierbij wordt gebruik gemaakt van hoogvertakte moleculen, zogenaamde dendrimeren, die gefunctionaliseerd zijn met apolaire alkyl eindgroepen. Deze dendrimeren blijken in staat te zijn de ordening van de vloeibaar kristallijne moleculen zodanig te verstoren, dat een polydomein morfologie gevormd wordt. Op macroscopische schaal resulteert dit in een efficiënte lichtverstrooiing, wat deze materialen geschikt maakt voor de vervaardiging van LCD's, die schakelen tussen een lichtverstrooiende en een transparante toestand. Door een specifieke interactie tussen de dendritische moleculen en de vloeibaar kristallijne omgeving blijkt hysteresis in de schakelcurve grotendeels afwezig te zijn en wordt een hoge schakelsnelheid bewerkstelligd.

Tenslotte wordt in het derde deelonderzoek het polydomein concept verder uitgewerkt door schakelbare systemen te vervaardigen op basis van vloeibare kristallen en laagmoleculaire netwerkvormers. In dit onderdeel van het proefschrift wordt de nadruk gelegd op de additie van 12-hydroxystearinezuur aan een LC. Middels waterstofbrugvorming assembleren deze organische verbindingen (zogenaamde gelling agents) tot fibrillaire aggregaten, die onderling met elkaar verbonden zijn tot een driedimensionaal netwerk. Het fijn-gedispergeerde netwerk geeft aanleiding tot een uitgesproken polydomein structuur tezamen met een verrassend schakelgedrag van de LC moleculen, waarbij het netwerk de reoriëntatie van de LC moleculen na het opleggen of verwijderen van een elektrisch veld versnelt. Door een juiste instelling van de morfologie van deze systemen worden bovendien hoge contrastverhoudingen en relatief lage schakelvoltages verkregen.

Voor alle onderzochte materialen is vastgesteld dat de reologische eigenschappen van het laagmoleculaire LC materiaal sterk gemodificeerd worden door de aanwezigheid van het additief. De aanwezigheid van een driedimensionaal, fysisch netwerk in zowel de LC colloïdale dispersies als de thermoreversibele gellen, maakt deze materialen bestand tegen vrij hoge mechanische spanningen in de orde van  $10^2$ – $10^3$  Pa. Onderlinge vergelijking van deze twee materialen op basis van gelijke gewichtspercentages van het additief laat zien dat de thermoreversibele gellen in staat zijn iets hogere spanningen te verdragen. Voor het aanbrengen van deze materialen met vaste-stof gedrag op een substraat is het noodzakelijk dat het netwerk tijdelijk opgeheven wordt. Dit kan bewerkstelligd worden door bij het aanbrengen gebruik te maken van een kleine hoeveelheid oplosmiddel, zoals toluen. Voor de LC colloïdale dispersies is aangetoond dat op deze manier met behulp van conventionele filmvormende processen homogene en zeer dunne lagen (laagdikte  $< 10 \mu\text{m}$ ) verkregen kunnen worden

In geval van de dendrimeer gevulde LC's organiseert de disperse fase zichzelf in bolvormige aggregaten in plaats van in een driedimensionaal netwerk. Door de afwezigheid van een gedispergeerd netwerk kunnen de dendrimeer gevulde LC's veel lagere mechanische spanningen verdragen dan bovengenoemde materialen. Een mogelijk voordeel van de afwezigheid van een netwerk is echter, dat deze gemakkelijk vloeiende dendrimeer gevulde LC's door middel van een filmvormend proces direct aangebracht kunnen worden op een substraat zonder gebruik te maken van een oplosmiddel. Opmerkelijk is dat de dendrimeer/LC mengsels zeer hoge viscositeiten vertonen onder niet al te hoge spanningen. Deze weerstand tegen vloeit wordt toegeschreven aan de sterk verstoorde oriëntatie van de LC moleculen rondom de aggregaten, waardoor in feite een fysisch netwerk van LC domeintjes aanwezig is.

Samenvattend, de onderzochte gemodificeerde LC materialen bieden de mogelijkheid om een breed scala aan nieuwe, gewenste eigenschappen te behalen middels een juiste instelling van morfologie. De gunstige combinaties van reologische en electro-optische eigenschappen kunnen benut worden voor de introductie van nieuwe fabricageprocessen en toepassingen van LCD's.



# Dankwoord

Mijn promotietijd was voor mij een erg leerzame periode. Soms zat het mee, soms zat het tegen, maar al met al waren het voor mij vier fantastische jaren die me altijd bij zullen blijven. Ik wil dit boekje dan ook niet afsluiten zonder de mensen te bedanken die mij in deze tijd hebben bijgestaan op wetenschappelijk en persoonlijk vlak.

In de eerste plaats wil ik prof. Dick Broer, dr. Cees Bastiaansen en prof. Piet Lemstra bedanken voor het feit dat ze mij vier jaar geleden de mogelijkheid hebben geboden om mijn afstudeeronderzoek voort te zetten met een promotieonderzoek. Dick, ik wil je tevens met name bedanken voor je enthousiaste betrokkenheid bij het onderzoek en voor je deskundige en kritische kijk op de dingen. Cees, mijn hartelijke dank voor je inzet voor het onderzoek, de dagelijkse begeleiding van het project, het ‘alles even op een rijtje zetten’ tijdens ons overleg en je hulp bij het naar buiten brengen van de onderzoeksresultaten.

Tijdens mijn promotieonderzoek heb ik het genoeg gehad om te mogen samenwerken met een aantal mensen op verschillende onderwerpen. In chronologische volgorde gaat allereerst mijn dank uit naar voormalig post-doc Rob Janssen voor onze twee jaar durende samenwerking, voornamelijk op het gebied van anisotrope thermoreversibele gelen. Rob, ik heb erg veel van je geleerd, ook van jouw typisch nuchtere, doch wetenschappelijke manier van denken. Maurice Baars en prof. Bert Meijer wil ik bedanken voor hun enthousiaste medewerking om de dendrimeren toe te passen in lichtverstrooiende electro-optische schakelaars. Maurice, zoals je zelf al eerder genoemd hebt, uiteindelijk zijn er erg leuke dingen gekomen uit de experimenten waaraan we samen begonnen zijn. Ook een woord van dank gericht aan Michel Pepers van de polymeerchemie groep SPC voor zijn bereidwilligheid om zijn expertise op het gebied van Raman spectroscopie met mij te delen. Michel, ik vond het erg plezierig om met je samen te werken. Vanwege de complexiteit van de monomeersystemen verliepen de experimenten moeilijker dan verwacht, maar ik hoop dat je er net als ik veel van hebt opgestoken. Ik ben enorm veel dank verschuldigd aan Michael Wübbenhorst en prof. Jan van Turnhout van de TU Delft voor de prettige en vruchtbare samenwerking met betrekking tot de diëlektrische karakterisering van de mengsels en voor de hulp bij de interpretatie en modellering van de experimenten. Tevens bedankt voor jullie interesse in hoofdstuk 4 en de input voor het artikel. Piet Droppert, bedankt voor het helpen met de praktische uitvoering van de diëlektrische metingen.

Naast deze personen wil ik ook enkele mensen van Philips Research bedanken voor hun bijdrage. Cristiane de Witz wil ik graag bedanken voor haar hulp en uitleg bij het construeren van nette displaycellen in de cleanroom. Een bijzonder woord van dank aan Steve Klink en Roel Penterman voor hun interesse in mijn onderzoek en hun ideeën en experimentele ondersteuning met betrekking tot de laatste fase van mijn onderzoek, gericht op de praktische verwezenlijking van een continu productieproces voor LCD's.

Reologie expert Gerrit Peters van de faculteit werktuigbouwkunde wil ik hartelijk danken voor zijn ‘simpele’ uitleg met betrekking tot de interpretatie van de reologie experimenten. Gerrit, ik stel jouw bijdrage aan dit boekje middels het doornemen en corrigeren van de betreffende geschreven stukken erg op prijs. Naast mijn promotoren en copromotor ben ik tevens prof. Stephen Picken van de TU Delft en prof. Alfons van Blaaderen van de Universiteit Utrecht zeer erkentelijk voor hun bereidwilligheid om als lid van mijn leescommissie dit manuscript door te lezen en van correcties te voorzien.

De studenten Mark Antkowiak en Eric van den Dungen wil ik bedanken voor hun pogingen om mijn promotieonderzoek tot een mooi einde te brengen. Uiteindelijk hebben jullie toch veelbelovende resultaten behaald, die nog op het laatste moment in beknopte vorm terechtgekomen zijn in een afsluitend hoofdstuk 7.

De afgelopen jaren heb ik met veel plezier doorgebracht in de SKT groep. Ik wil alle collegae dan ook ontzettend bedanken voor hun bijdragen tot het creëren van een prettige en gezellige werksfeer. Anne, Joachim en Pauline, een speciaal bedankje voor al jullie hulp met het microscopiewerk. Ex-kamergenootjes Tosca en Michael, bedankt voor de leuke tijd die ik bij jullie op de kamer heb gehad. Mijn huidige kamergenootjes, Dennis en Francesco, en naaste (ex-)buren Isabelle, Vid, Martijn, Domenico, Pit, David, Fons en Henri, bedankt voor de alledaagse gezelligheid binnen (en buiten) de universiteit gedurende de afgelopen jaren en de plezierige gesprekken tijdens het koffiedrinken elke ochtend. Henri, Dennis en Vid, bedankt dat jullie mijn conditie op peil hebben gehouden middels de vele ‘ontspannende’ squashpartijtjes.

Mijn ouders wil ik graag hartelijk bedanken voor hun steun en belangstelling. Tot slot, Leon, de afgelopen maanden waren voor ons beiden een drukke tijd. Omdat we alles tegelijkertijd doormaakten, hebben we ook alles met elkaar kunnen delen. Bedankt dat je me altijd het gevoel hebt gegeven dat ik er niet alleen voor stond.

Marysia

# Curriculum Vitae

Marysia van Boxtel was born in Sint-Oedenrode on Februari 3<sup>rd</sup>, 1974. After she finished secondary school (VWO) at the Zwijsen College in Veghel she started with a study Chemical Engineering at the Eindhoven University of Technology in 1992. She finished her study in August 1997 with a masterclass graduation project in the Polymer Technology group under supervision of prof.dr. P.J. Lemstra and dr. C.W.M. Bastiaansen.

From October 1997 until January 2002 she was employed by the Netherlands Organisation for Scientific Research. During this period of time she worked as a Ph.D. student at the Eindhoven University of Technology within the group of Polymers for Information and Communication Technology headed by prof.dr. D.J. Broer and dr. C.W.M. Bastiaansen. In the year 2000 she was awarded for her research work with the DSM price for Chemistry and Technology (runner-up). During her Ph.D. study she completed all six modules of the “Registered Polymer Technologist” course (RPK, “Register Polymeerkundige”), organised by the “National Dutch Graduate School of Polymer Science and Technology” (PTN, “Polymeertechnologie Nederland”).